WYLE LABORATORIES
SCIENTIFIC SERVICES AND SYSTEMS GROUP
EASTERN OPERATIONS
FACILITIES LOCATED IN
HUNTSVILLE, ALA. AND HAMPTON, VA.

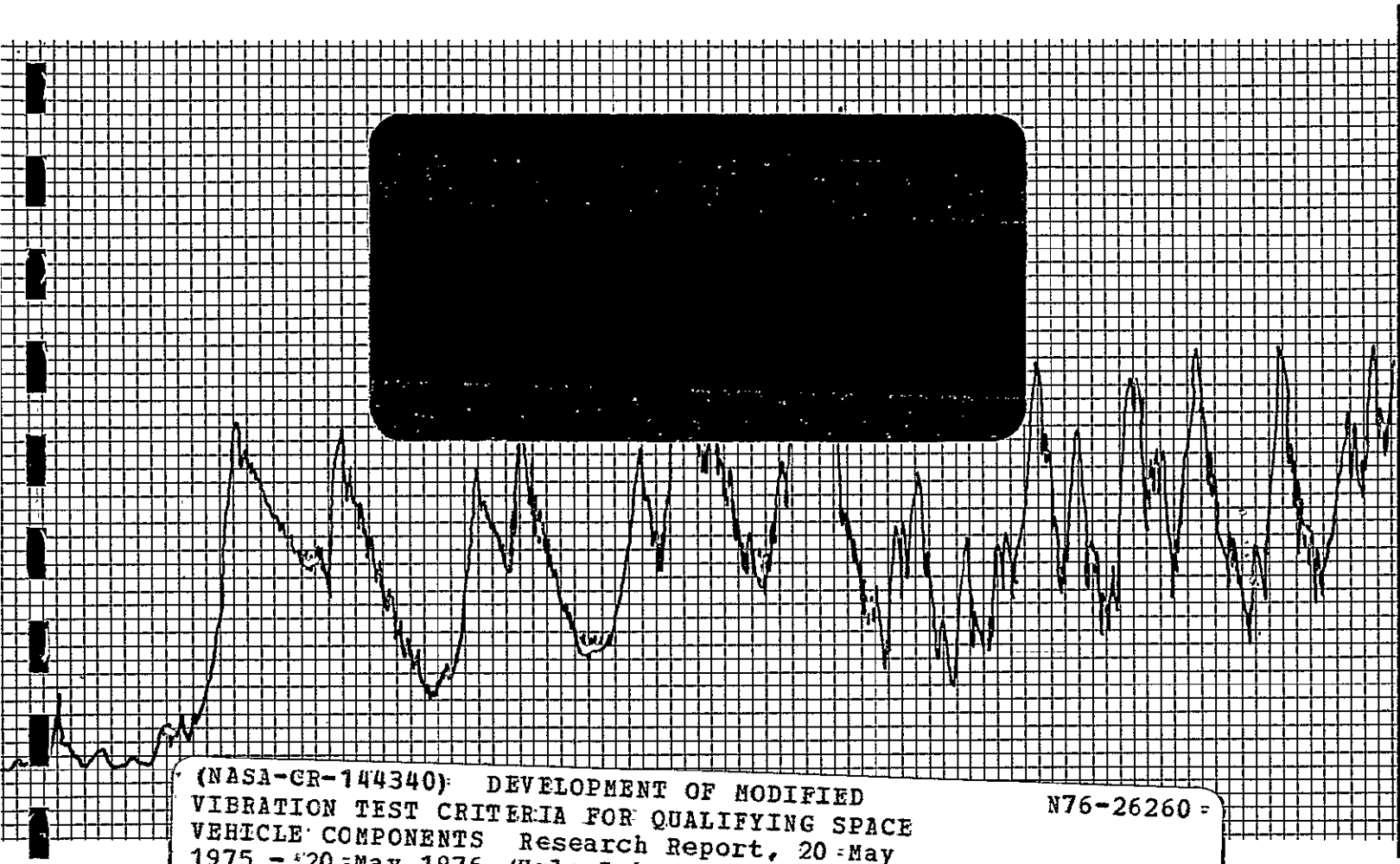

research REPORT

WYLE LABORATORIES — RESEARCH STAFF
REPORT WR 76-4

DEVELOPMENT OF MODIFIED VIBRATION TEST CRITERIA FOR QUALIFYING SPACE VEHICLE COMPONENTS

By

K.Y. Chang
G.C. Kao

Work Performed Under Contract NAS8-31414

May 1976

COPY NO. 2

FOREWORD

The work reported herein was supported by the National Aeronautics and Space Administration, Marshall Space Flight Center, under Contract No. NAS8-31414, and performed during the period of May 20, 1975, through May 20, 1976. Technical monitoring of the program was provided by Mr. J. Herring of the Aeroelastic and Acoustic Response Branch, Structural Dynamics Division, System Dynamics Laboratory, Marshall Space Flight Center, Huntsville, Alabama. The Principal Investigator was Dr. Kurng Y. Chang, Senior Research Specialist, Wyle Laboratories, Huntsville, Alabama.

The work performed consisted of evaluating structural responses obtained by the impedance ratio method and the constant mass attenuation method by means of experimentally measured data. The computation of input impedances of component and primary structure were based on nomograms and design charts developed under Contract Nos. NAS8-25811 and NAS8-30630.

ABSTRACT

This report presents the results of the evaluation of two response prediction methods relating to the prediction of structural responses of stiffened shell structures with or without attached components, subjected to broadband acoustic excitations. The methods under evaluation were the constant mass attenuation method and the impedance ratio method. Example problems were used to illustrate the application procedures of these two methods and to compare their predicted results with the experimentally measured data. It was found that more realistic estimates of the structural response can be obtained by the impedance ratio method.

TABLE OF CONTENTS

LIST OF FIGURES

LIST OF FIGURES (CONCLUDED)

1.0 INTRODUCTION

Research in seeking practical techniques or methods for predicting vibration environments of space vehicles subjected to random acoustic pressure has gained considerable attention in recent years. As a result, several methods and techniques have been developed for use in dynamic environment predictions. Of these methods, Barrett (ref. 1) used a standardized approach to predict vibro-acoustic environments with sufficient conservatism to meet design and test requirements. This approach, or so-called constant mass attenuation method, is based upon the fact that similar structures have similar response characteristics, but does not account for the component-primary structure coupling effects and the characteristics of frequency variations. However, it does provide a means to estimate the response of highly complex structures with only a few simple computations. The other methods, as described in references 2 and 3, utilize mechanical impedance concepts to predict broad frequency range vibration criteria. The impedance method was derived from a one-dimensional mathematical model, and the prediction equation is expressed in terms of four basic parameters at component mounting locations. These parameters consist of input impedance of the primary structure, input impedance of the component package, acoustic mobility, and blocked pressure spectrum. The impedance method indicates that the attenuation factor is based on a frequency-dependent ratio of the mechanical impedance of both the component and primary structures. Significant differences were observed in a comparison of the predicted vibration environments by these two methods. In order to validate the predicted results, an experimental testing program was conducted to obtain a data base for the evaluation of predicted responses. The objective of this report is to compare the predicted responses of these two methods with the experimentally measured data.

A description of the prediction methods is presented in Section 2.0, and the approximate equations used to compute responses are described. The approximate equations are further converted into nomograms and computation charts, and the results together with application guidelines are all included in this section. A detailed description of the experimental program, along with the test results, is presented in Section 3.0. In Section 4.0, example problems are used to demonstrate the computation procedures and to compare the differences between these two methods and their accuracy based on the measured experimental data. Finally, a summary of the advantages and limitations in terms of the accuracy of each method is discussed and the concluding remarks are contained in Section 5.0. The results of experimental measurements are presented in the Appendix.

2.0 METHODS FOR PREDICTING ENVIRONMENTS

2.1 Constant Mass Attenuation Method

The equation for predicting the vibration environment of acoustically susceptible structures is (ref. 1):

$$G_n = G_r \left(\frac{p_n}{p_r}\right)^2 \left(\frac{\rho_r h_r}{\rho_n h_n}\right)^2 F \qquad (1)$$

where:

G_n = the vibration response of the new vehicle structure at a particular location. The term G is the acceleration due to cyclic motion divided by the acceleration of gravity. Since rocket vehicle vibrations contain many frequencies, the response magnitude, G, is specified in mean square spectral form.

G_r = the known vibration response of a reference vehicle structure. This value has been determined by previous measurements and is shown in Figure 1 and 2.

h_r = the thickness of the skin associated with G_r.

ρ_r = the skin weight density of the reference structure.

p_r = the impinging acoustic pressure which is driving the reference structure.

h_n = the skin thickness associated with G_n.

ρ_n = the skin weight density associated with G_n.

p_n = the acoustic pressures impinging upon the new vehicle structure

F = a factor which accounts for the attenuation effects produced by incorporating additional mass into the existing system.

The above equation applies to random rms composite values or to sinusoidal values. The concept used to derive this equation is based on the assumption that a similar structure exhibits similar dynamic characteristics. Once the frequency and amplitude characteristics of a typical type of structure have been adequately defined, these results may then be utilized as a basis for predicting the vibration environment of like structures.

The foregoing equation is applicable to localized vibratory environments and is valid for all materials. It is invalid when considering large sections of a vehicle structure (i.e., the entire cylindrical tank). However, static loading of these large sections is generally the critical design factor, and localized dynamics thereby produce only negligible effects.

In Equation (1) the expression indicates that for a constant driving power, the structural response decreases as the weight density increases. Thus, when a component item is mounted on a structure in which the vibration environment has previously been defined, the resulting vibration responses will be decreased by a factor F. Therefore, the loaded response spectra, G_c, of the structure with a component attached can be expressed as:

$$G_c = G_n \left(\frac{W_n}{W_n + W_c} \right) \tag{2}$$

where: W_n = effective weight of the primary (support) structure.

W_c = component weight.

When determining the effective weight of structures, the circumferential distance should not exceed three times the distance between rings. This is because the dynamic characteristics of thin plates remain essentially constant above aspect ratios of three. In the preliminary development period, the weight of the basic structure or component may not be known and the attenuation factor is considered as unity. This will result in an estimate of the vibration environment which may tend to be conservative.

2.2 Impedance Ratio Method

The response prediction equation is derived based on a one-dimensional structural model. By applying Thevenins' and Norton's theorems to this model, the relationship between the unloaded and loaded response spectra is obtained and can be shown to have the following expression (refs. 2 and 3):

$$\Phi'_{\alpha}(\omega) = \Phi_{\alpha}(\omega) \cdot \left| \frac{Z_s(\omega)}{Z_s(\omega) + Z_L(\omega)} \right|^2 \tag{3}$$

where: $\Phi'_{\alpha}(\omega)$ = power spectral density (PSD) of loaded response spectrum.

$\Phi_{\alpha}(\omega)$ = PSD of unloaded structural response spectrum.

$Z_s(\omega)$ = input impedance of primary support structures.

$Z_L(\omega)$ = input impedance of component package.

ω = frequency parameter.

The equation to compute the unloaded response spectrum is given as follows (reference 4):

$$\Phi_\alpha(\omega) = \Phi_p(\omega) \cdot \left| \alpha(\omega) \right|^2 \tag{4}$$

where: $\Phi_p(\omega)$ = blocked sound pressure spectrum.

$\alpha(\omega)$ = acoustic mobility of the structure.

Equation (3) shows that the loaded response spectrum is equal to the response spectrum of the unloaded structure multiplied by the ratio of the impedances. The term $\left| Z_s(\omega) / Z_s(\omega) + Z_L(\omega) \right|$ represents a magnification factor for both the unloaded and the corresponding loaded spectra and its value will approach unity when the structural impedance, $Z_s(\omega)$, becomes infinite. The impedances expressed in Equation (3) can be obtained directly from measurements on the actual structure or through analytical prediction techniques. The equations and guidelines for predicting the input impedance and the unloaded response spectra of structures are presented in the subsequent sections. A flowchart indicating the computation sequence is shown in Figure 3.

2.2.1 Prediction of Structural Impedances. — Input impedances, $Z_L(\omega)$ and $Z_s(\omega)$, in the impedance ratio equation are specified in terms of the "force/velocity" format. The input impedance of the component package, $Z_L(\omega)$, is defined as an ideal damping, spring and mass system. The primary support structures considered herein consist of basic cylindrical shells, longitudinal stringers and ring frames. The cylindrical shells are stiffened by stringers in the axial direction, and ring frames are attached inside the shell wall. The direction of vibratory response under consideration is assumed to be normal to the skin which is excited by impinging acoustic pressures. The stiffeners are not directly excited by acoustic forces but are driven by the motion of attached panels. The approximate equations for predicting the input impedance of these three structural components are given in Table I in three different frequency ranges as defined below (references 4 and 5):

- Low frequency range, or frequencies below the fundamental frequency of the shell.
- Intermediate frequency range.
- High frequency range, or frequencies above the ring frequency of the shell.

TABLE I. SUMMARY OF INPUT-IMPEDANCE EQUATIONS OF BEAMS, RINGS AND SHELLS

Structure \ Frequency	Low Frequency Range $(f \le f_L)$	Fundamental Frequency, f_L	Intermediate Frequency Range $(f_L < f \le f_R)$	Ring Frequency, f_R	High Frequency Range $(f > f_R)$
Beam	$K_B = \frac{48\,EI}{\ell^3}$	$\frac{1}{2\pi}\left(\frac{\pi}{\ell}\right)^2 \sqrt{\frac{EI}{\rho A}}$	$Z_B = 2(1+i)\ \rho A \left[\frac{EI}{\rho A}\right]^{1/4} \sqrt{\omega}$		Same as Intermediate
Ring	$K_R = \frac{EI}{0.15R^3}$	$\frac{0.427}{R^2} \sqrt{\frac{EI}{\rho A}}$	$Z_R = 12\sqrt{2}\ \rho A \left[\frac{EI}{\rho A}\right]^{1/4} \sqrt{\omega}$		Same as Intermediate
Shell	$K_S = 2.5\,Eh \left(\frac{R}{L}\right)^{1/2} \left(\frac{h}{R}\right)^{1.25}$	$\frac{0.375}{L} \sqrt{\frac{Eh}{\rho R}}$	$\lvert Z_S \rvert = \frac{4}{\sqrt{3}}\ \rho h^2 \sqrt{\frac{E}{\rho R}} \left(\frac{E}{\rho}\right)^{1/4} \frac{1}{\sqrt{\omega}}$	$\frac{1}{2\pi R} \sqrt{\frac{E}{\rho}}$	$Z_S = \frac{4}{\sqrt{3}}\ h^2 \sqrt{E\rho}$
Stiffened Shell	$K = K_S + \sum K_B$ (or $+ \sum K_R$) $\lvert Z \rvert = K/\omega$		$Z = Z_S + \sum Z_B + \sum Z_R$		$Z = Z_S$, $Z = Z_B$, $Z = Z_R$

The evaluation of the stiffened shell impedances, $Z_s(\omega)$, is then obtained for the above three frequency ranges as follows:

Low Frequency Impedances: The static stiffness is the predominant factor which influences the input impedance. Due to the lack of theoretical expressions for input impedances of stiffened cylindrical shells, it is assumed that at low frequencies the input impedance at any location follows the stiffness line, this stiffness being equal to the summation of the stiffness of the individual structural elements that are present in that location. Two cases are considered in this frequency range, namely:

- If the stiffness of the ring is small in comparison to the stiffness of the stringer or the unstiffened shell, the overall stiffness can be computed by adding the stiffness of the properly modeled structural elements that are present at the input location as follows:

$$K = K_s + \sum K_B + \sum K_R \tag{5}$$

where:

K_s = static stiffness of shells

K_B = static stiffness of beams or stringers

K_R = static stiffness of rings.

Thus the input impedance of a stiffened cylindrical shell at low frequency follows a stiffness line whose value can be computed from the sum of stiffnesses of structural elements at that point.

- For a stiffened cylindrical shell, if the rings are sufficiently stiff in comparison with the entire shell, these rings act like the boundary of structural panels. Then the characteristic impedance of the shell can be determined from the length of the spacing between two adjacent rings.

$$K = K_s + \sum K_B \tag{6}$$

The characteristic impedance represents the impedance of a structure of such a length that reflections from the boundaries are negligible. In other words, the resonance modes of a structure with any nondissipative boundary conditions are identical to the resonance modes of a supported structure whose length is equal to the distance between the node lines.

Intermediate Frequency Impedances: Within the intermediate frequency range, which extends from the fundamental frequency to the ring frequency, the input impedances of the test specimens can be evaluated as the combination of the characteristic impedances of the primary structural components. The equation is written as:

$$Z = Z_s + \sum Z_B + \sum Z_R \tag{7}$$

where: Z_s = characteristic impedance of shells

Z_B = characteristic impedance of stringers

Z_R = characteristic impedance of rings.

High Frequency Impedances: The input impedance of a stiffened shell at high frequencies depends on the location of a measurement point and is evaluated by the following rules:

- Unstiffened (skin) point — The input impedance approaches that of an infinite plate of the same thickness.
- Stiffened point — The skin and the stiffener(s) decouple dynamically at high frequencies, therefore the input impedance approaches that of the stiffener(s).
- Stiffened intersection point — The input impedance at the centers of short stiffener segments are generally higher than those of longer stiffener segments, and the impedance at an intersection of the stiffener(s) is approximately equal to the sum of the individual impedances of the two stiffeners—the ring impedance and stringer impedance.

All equations in Table II contain a frequency-dependent and a frequency-independent term. Therefore, by evaluating the frequency-independent term and later combining with the frequency-dependent term, the impedance curve can be easily constructed. In order to minimize manual efforts in performing impedance computations, the derived equations described in Table I are converted into the form of nomographs and/or charts. A nomograph, in its simplest and most common form, is a chart on which one can draw a straight line that will intersect three or more scales at values that satisfy an equation or a given set of conditions. The frequency-independent terms in the equations of Table I were converted into nomographic terms, and are shown in Figures 4 through 9 . The driving-point impedance for beams and rings, based on the equations of Table I, were represented by two sets of intersecting lines varying with the frequency as shown in Figure 10. In this figure, the line representing the proper stiffness value is obtained either from the results of Figure 4 or 5 for rings and beams, respectively, the the Z_r line defining the proper value of the structural rigidity is determined from Figure 6. The stiffness lines represent the impedance at low frequencies and the Z_r lines represent the impedance at high frequencies. The intersection of

TABLE II. SUMMARY OF TEST PROGRAM

Test Identification	Test No.	Test Specimens	Location of Components	Transducer Locations									Test Level (dB)
				MC	M1	M2	M3	M4	A1	A2	A3	A4	
Unloaded Tests	P-1	Aluminum Cylinder	--	10 ft above the floor	Four Microphones Near the Surface of the Cylinder.				P1	P2	P3	P4	145
	R-1		--						R1	R2	R3	R4	
	S-1		--						S1	S2	S3	S4	
Loaded Test	P-2	Aluminum Cylinder and Component Plate	P						P1	P2	P3	P4	
	R-2		R						R1	R2	R3	R4	
	S-2		S						S1	S2	S3	S4	

these two lines determines the fundamental resonant frequency of the structural system. In this figure and the following figures, a scale factor is used to obtain correct scale values for the standard diagrams.

The driving-point impedance for unstiffened cylindrical shells is shown in Figure 11, where the Z_r lines are replaced by the Z_f lines. The Z_f lines, which represent the proper value of the structural flexibility and infinite-plate impedance, are obtained from Figures 7, 8 and 9, respectively. At low frequencies, the impedance of cylinders follows a stiffness line, and, at high frequencies, the impedance is equal to the impedance of an infinite plate which has a constant value. Within the intermediate frequency range, the input impedance may be represented by the Z_f line. The fundamental frequency and the ring frequency of cylinders are determined by the intersection of these three characteristic lines.

The impedance of the stiffened cylinder is equal to the linear summation of these component curves and is obtained in the following manner:

- The logarithmic summation chart (LSC) shown on the upper portion of these charts will be used to compute the linear summation of two impedance curves.
- At any frequency point, measure the difference of two impedance values and use this length as the abscissa value in the LSC.
- The ordinate corresponding to the abscissa in the LSC is the resulting value for these two curves in logarithmic summation.
- Add the length of the ordinate to the upper impedance curve; the resulting curve denotes the linear combination of these two impedances.

Figure 12 represents the impedance lines for the component package which is defined as an ideal damping, spring and mass system. The graph shown on the upper portion of this computational chart will be used to compute the logarithmic ratio of two impedance curves. The application of the LSC is similar to the procedure described before except that the length of the ordinate obtained from the LSC is subtracted from the lower impedance curve. The usage of the LSC is demonstrated in Section 4.0.

2.2.2 Prediction of Acoustic Mobility. — Acoustic mobility, $\alpha(\omega)$, is defined as the ratio of the mean-square spectral density of the velocity to the mean-square spectral density of the fluctuating pressure driving the structure. This quantity is expressed by Equation (8) as follows:

$$\alpha(\omega) = \frac{S_{\dot{U}}(\omega)}{S_p(\omega)} \tag{8}$$

where $S_{\dot{u}}(\omega)$ has units of $(\text{in./sec})^2/\text{Hz}$, and $S_p(\omega)$ is the blocked pressure spectral density having units of $(\text{psi})^2/\text{Hz}$. The blocked pressure includes the effects of reflection and thus accounts for the pressure doubling effect when an object is immersed in a random pressure field.

Generally, the acoustic mobility for a given structure would be calculated based upon modal analysis or statistical energy analysis. However, for the purposes of presenting simplified design techniques, empirical curves may be used for defining acoustic mobility. The development of these empirical curves from a broad range of available vibro-acoustic data is described in detail in Appendix C of reference 4. Relevant results relating to the present study will be presented in this report. The basic design curves for acoustic mobility are shown in Figure 13 for two values of damping: Q = 20 and Q = 200. In this figure, the normalized acoustic mobility derived from the measurements is expressed as:

$$\alpha'(\omega) = \frac{S_{\dot{u}}}{S_p} \left(\frac{m}{D}\right)^2 \tag{9}$$

and has units of $(\text{in./sec})^2/\text{in}^2$. The bascissa of this figures is fD, i.e., frequency times cylinder diameter in units of Hz-in.

In order to use the empirical curves of Figure 13, an estimate of the structural damping, Q, must first be made. Then by substituting for vehicle diameter, D, and surface weight, m, the acoustic mobility $S_{\dot{u}}/S_p$ (or α) may be determined as a function of frequency, Hz. For structural Q values other than those shown in Figure 13, the acoustic mobility term may be interpolated since an increase in Q by a factor of 10 results in an increase in the acoustic mobility term of one decade.

2.2.3 Evaluation of Blocked Pressure. — The blocked pressure spectrum, $\Phi_p(\omega)$, is defined as the effective acoustic pressure acting on a primary structure. The pressure is equivalent to that acting on a rigid cylinder which has identical geometrical dimensions as the primary structure. This pressure can be determined from the far-field sound pressure measurement and is given by (refs. 6 and 7):

$$\beta = \frac{\left[p^2_{\text{block}}\right]}{\left[p^2_{\text{far}}\right]} = 4(\pi kR)^{-2} \sum_{m=0}^{\infty} \epsilon_m \left| H'_m(kR) \right|^{-2} \tag{10}$$

where:

$\left[p_{far}\right]$ = measured sound pressure levels without the presence of flexible structures

k = wave number $= 2\pi f/c$

c = speed of sound in acoustic medium; for air $c = 13{,}400$ in./sec

R = radius of cylinder $= D/2$

ϵ_m = Neumann factor $= 1$ for $m = 0$, 2 for $m > 0$

$H'_m(kR)$ = derivative of Hankel function of order, m

The foregoing equation is derived from an infinite panel and does not account for diffraction effects of structures with finite length. However, the error due to diffraction effects is considered insignificant and will not influence the final results. In the frequency range of interest, the rms blocked sound pressure is approximately 40 percent higher than the measured sound pressure, and therefore the conversion from the free-field sound pressure to the blocked pressure is needed in order to provide conservative estimates of the force spectra.

The conversion of a free-field sound pressure spectrum into a corresponding blocked pressure spectrum is achieved by multiplying the far-field pressure spectrum by the correction coefficient, β, as shown in Figure 14. To obtain the $\sqrt{\beta}$-coefficient for a particular cylinder in the frequency scale, it is accomplished by shifting the fD scale in Figure 14 to the left for the amount corresponding to the cylinder diameter, D.

2.2.4 Computation of Response Spectrum. — The unloaded response spectrum is obtained by the product of the blocked pressure spectrum, and the velocity acoustic mobility. The normalized acoustic mobility curves shown in Figure 13 must be converted to $|\alpha^2|$ versus frequency format for use in response computations. The conversion can be accomplished graphically by shifting the abscissa scale to the left, corresponding to the diameter of a cylinder, D; and shifting the ordinate scale upward or downward, corresponding to the quantity $(m/D)^2$. The unloaded velocity response spectrum is obtained by logarithmically summing up the velocity acoustic mobility curve and the blocked pressure spectrum from a computation chart.

The impedance ratio and the unloaded response spectrum obtained previously are again plotted on the same computation chart for final computation. The sum of these two curves at a given frequency, as shown on the chart, is the resulting loaded response spectrum for the structural system. To illustrate this simplified technique, example problems to predict vibration environments for space vehicles are explained in detail in Section 4.0.

2.3 Measurement Approaches

To verify the predicted equations experimentally, a total of four types of measurements are required, namely:

- p_n = sound pressure levels
- Φ_p = blocked sound pressure spectrum
- Φ_α or G_n = unloaded structural response spectrum
- Φ'_α or G_c = loaded structural response spectrum

The sound pressure levels are defined by measuring the sound pressure levels within the reverberation room and in the free-field.

The blocked sound pressure is defined as the effective acoustic pressure load acting on a flexible structure and is defined by measuring the pressure at the surface of a cylinder. The measurement of structural responses is achieved by employing accelerometers and their associated electronic measurement systems. The unloaded structural responses are measured at the specified locations on the surface of the cylinder, and the loaded structural responses are defined as the measurements at the mounting locations between the component and the cylinder. The locations of the accelerometers are determined to be at the intersection of a ring and stringer, stringer and stringer, and the mid-point of an individual panel bay.

More detailed experimental approaches to acquire, reduce and analyze the data for computing force are presented in the subsequent sections.

3.0 EXPERIMENTAL PROGRAM

3.1 Introduction

The objective of the program was to acquire the needed experimental data to verify the accuracy of the analytical responses as defined in the previous section. For this purpose, considerable effort was exercised on the design of the measurement program for acquiring accurate response data from cylindrical type structure subjected to broadband acoustic excitation.

Test specimens used in the tests consisted of a stiffened aluminum cylinder, which was used as the support structure, and a simulated component package. The verification of test data was accomplished by employing multiple response measurements at similar locations on test structures so that, by comparing the characteristics of acquired response data at these locations, erroneous signals could be detected and appropriate corrections could be made during the tests.

3.2 Description of Test Specimens

3.2.1 Support Structure. — The support structure used in the experiment was a stiffened aluminum cylinder, as shown in Figure 15. The cylinder's dimensions were 36" (diameter) x 36" (length) x 0.2" (thick).* Its structural configuration is shown in Figure 16. The cylinder consisted of five aluminum rings spaced at 6 inches in the longitudinal direction and twenty-four longitudinal stringers spaced at 4.7 inches in the circumferential direction. The structural details of the stringers and ring frames are shown in Figures 17 and 18, respectively. All stiffeners were attached to the cylinder wall by rivets. The dimensions of the curved panels formed by the stiffeners were 6" x 4.75". Two steel rings of 1" x 1" x 1/8" angle section were riveted at both ends and two circular sandwich plates were bolted to the end rings by 1/4-inch diameter hex bolts and nuts. Each circular plate consisted of two steel end plates of 1/8-inch thickness with 1/2-inch plywood at its center core. The cylinder was suspended in the air by means or Bungee chords.

Three component mounting positions were used in the experiments and were designated as follows:

- Positions P1, P2, P3, P4: Centers of curved panels
- Positions R1, R2, R3, R4: Centers of ring frame segments
- Positions S1, S2, S3, S4: Centers of longutidinal stiffener segments.

3.2.2 Simulated Component Package. — The simulated component package was designed to represent a typical payload component package of a space vehicle. The design drawing is shown in Figure 19. This component package consisted of a 1/2-inch aluminum

*The test cylinder was originally fabricated by Republic Aviation Corporation in 1964.

plate with lateral dimensions of 8" x 8". The plate was supported by a set of leaf springs at each corner. The bottom of each spring was fitted with a mounting assembly, as shown in Figure 20. Each assembly was constructed of the top clamping strip and an aluminum stud. These two elements were held together by a center bolt. The total weight of the component package was 3.81 pounds; the resonances of the package were measured at 115 Hz and 350 Hz, respectively. The fundamental resonant frequency of the 1/2-inch plate was found to be 1,200 Hz.

3.3 Vibro-Acoustic Testing

The vibro-acoustic experiments were conducted in a 100,000 cubic foot reverberation facility with approximate dimensions of 60 ft (length) by 46 ft (width) by 37 ft (height), as shown in Figure 21. The aluminum cylinder was placed near the center of the room with the longitudinal axes parallel to the ground and a control microphone used to acquire the reference sound pressure was located near the cylinder and 10 feet above the floor level. A random acoustic excitation with an overall sound pressure level of 145 dB and a frequency range of 20 to 2,000 Hz was applied to the specimen. The transducers used in the test consisted of the following:

- One control microphone to measure free-field acoustic data.
- Four microphones placed 1/4-inch from the surface of the cylinder to measure blocked pressure.
- Four accelerometers attached to or near the component mounting positions.

The location of the transducers are shown in Figure 22.

The test specimen was subjected to a total of six tests. The first series of acoustic tests were performed without the simulated component attachment. Response measurements were acquired for the "P", "R" and "S" locations, together with sound pressure measurements. Following the unloaded response tests, the second series of tests were conducted at the same sound pressure levels as used in the first series of tests but with the component specimen attached in turn to the support locations "P", "R" and "S". Figure 23 represents a typical test set-up for the second series of tests. The acceleration responses obtained from these tests provided the load responses of the support structure. A summary of the test program is tabulated in Table II.

3.4 Reduction of Measured Data

Response data from all accelerometers and microphones were recorded on 14 channels of FM tape. The overall instrumentation requirements are shown in Figure 24. Appropriate quick-look devices were employed to plot the test levels in one-third octave bands during the tests. All data were analyzed to obtain PSD's. The presentation of all measured data is contained in Appendix A.

A summary of the test results is shown in Figures 25 through 28. Figure 25 shows the measured sound pressure levels (SPL) within the reverberation room, at the control microphone location. It was concluded that the acoustic environment was in good agreement during all six tests. The average sound pressure levels measured by the four microphones installed near the surface of the aluminum cylinder are shown in Figure 26. The effect of pressure doubling at the test specimen surface over most of the frequency range can be clearly seen by comparing the levels in Figures 25 and 26.

Figures 27 and 28 show the unloaded and loaded acceleration responses of the cylinder at the measurement locations. It was noticed during the tests that the loaded responses at four "P" locations behaved quite erratically. Such patterns might be attributed to the nonlinear effect of the thin panel (0.02 inch) under acoustic excitations.

4.0 COMPARISON AND DISCUSSION OF RESULTS

In this section, two examples are given of the computation of structural responses due to acoustic excitation employing the constant mass attenuation method and the impedance ratio method. The analytical results are compared with the measured responses obtained from the experimental program. Details of the results are presented in the following paragraphs.

4.1 Response by Impedance Ratio Method

4.1.1 Structural Impedance. — The specimen used in the experimental program consisted of a basic cylindrical shell with longitudinal stringers and ring frames. Overall dimensions of the cylindrical structure are listed in Table III.

The computations of static stiffnesses, Z_r and Z_f, for the primary structure components have been evaluated previously, as shown in Figures 4 through 9. The impedance computations for the configuration with ring frames and stringers are shown in Figures 29 and 30. In the computation, it was assumed that these two rings act like end bulkheads with high structural rigidity so that the effective length of the cylinder becomes the length of the middle segment, which is equal to six inches. In Figure 30, the impedance for one stringer is plotted based on the values obtained from Figures 5 and 6. Similarly, the impedance curve representing the unstiffened cylindrical shell is plotted in Figure 31, in which the impedance representing the stringer is also shown. In Figures 30 and 31, the plotting scale is 100 times the current value as indicated by the scale factor = 0.01. Based on the procedure involving the LSC charts described in Section 2.2.1, the impedance of the stiffened shell, which is equal to the linear summation of these two component impedances, is obtained and is shown in Figure 31. Figure 32 shows the measured impedance data from reference 3, along with the computed impedance for comparison. Generally speaking, the comparison is considered quite satisfactory in the frequency range of interest. Test data obtained between 40 Hz and 100 Hz appear to be low in amplitude, which was caused by the low acceleration output of the impedance head and was considered to be invalid. Some discrepancies can be observed in the high frequency region. Such discrepancies are attributed to the errors incurred in summing the impedances of the stringers. Further refinements to this prediction technique, to achieve a higher degree of accuracy in this frequency range, are needed. However, it may be concluded that the equations and guidelines outlined in Section 2.2.1 are adequate for determining the structural impedances for design purposes.

The impedance of the component package was estimated and is presented in Figures 33 and 34. The predicted impedances for the stiffened cylinder at locations "R" and "S" are also shown in these two figures, respectively. The two impedance curves shown are summed to form the combined impedance curve according to the procedure described in Section 2.2.1. The curve shown on the bottom of these two figures represents the length difference between the component impedance and the combined impedance at any frequency point. The resulting curve given is the impedance ratio term in the computation of the loaded response spectrum.

TABLE III. SUMMARY OF DIMENSIONS, STIFFNESS AND MASS PROPERTIES OF CYLINDER AND ITS COMPONENTS

Property	Dimension	Structural Items		
		Ring	Stringer	Shell
Mean Radius, R	(in.)	16.0	---	18.0
Overall Length, ℓ	(in.)	100.53	36.0	36.0
Shell Skin Thickness, h	(in.)	---	---	0.02
Cross-section Area, A	($in.^2$)	0.467	0.049	---
Moment of Inertia, I	($in.^4$)	0.995	0.00051	---
Weight per Unit Volume, ρg	($lb/in.^3$)	0.1	0.1	0.1
Modulus of Elasticity, E	($lb/in.^2$)	10^7	10^7	10^7
Weight per Stiffener*	(lb)	4.695	0.1764	8.143
Total Weight of Structure	(lb)	---	---	45.00
Weight for Unit Surface	($lb/in.^2$)	---	---	0.011

*The cylinder consisted of five rings spaced at 6' in the longitudinal direction and 24 stringers spaced at 4.75" in the circumferential direction.

4.1.2 Blocked Sound Pressure. — The ambient sound pressure levels measured within the reverberation room and at the surface of the cylinder are shown in Figures 25 and 26. Figure 26 represents the blocked sound pressure levels measured during the tests, with the test specimen installed.

The ambient sound pressure is again plotted in the computation chart shown in Figure 35, along with the $\sqrt{\beta}$ -coefficient curve. The $\sqrt{\beta}$ -curve of the cylinder, with a diameter of 36 inches, is obtained by shifting the fD scale by a factor of 36 to the left from the theoretical curve as shown in Figure 28. The analytical prediction of the blocked pressure spectrum is then obtained by adding the $\sqrt{\beta}$ -length values at each frequency point to the ambient (or free-field) sound pressure. Figure 36 shows the comparison between analytical prediction and experimentally measured data. Excellent agreement between these two plots can be observed.

4.1.3 Structural Responses. — To obtain structural responses from the blocked sound pressure, the acoustic mobility is required. For an aluminum cylinder with $D = 36$ inches, $Q = 10$, and $(m/D)^2 = 1 \times 10^{-7}$ lb/in^3., the normalized acoustic mobility curve, shown in Figure 13, is converted to $|\alpha^2|$ versus frequency format by shifting the abscissa scale by a factor of 36 to the left and shifting the ordinate scale upward by 7 decades. The resulting curve is shown in Figure 37, along with the measured data from reference 3. In comparing these two results, a significant discrepancy was observed in the low frequency range. This discrepancy is due to the way in which the empirical curves for acoustic mobility were derived. Because considerable scatter exists between the various acoustic mobility experimental measurements, the empirical curve can only represent the general trend of the structural response. By overlaying the blocked pressure spectrum in Figure 35 and the acoustic mobility in Figure 37, the unloaded velocity response spectrum is the vector sum of these two curves, and is shown in Figure 38.

Based on the impedance ratios shown in Figures 33 and 34, the unloaded response spectrum of Figure 38 can be converted into the loaded response spectrum by summing these two individual curves. The final computation was performed and is shown in Figure 39; the resulting test criteria is shown by the dashed line. Note that this figure can also be used as the conversion chart to convert the acceleration PSD into velocity PSD and vice versa. The velocity response is read-off from the vertical scale at the left-hand side and the acceleration response is read-off from the right-hand side.

4.2 Response by Constant Mass Attenuation Method

The equation for predicting the unloaded response environment, G_n, of the cylinder structure is described in Section 2.1. Thus:

$$G_n = G_r \left(\frac{p_n}{p_r} \right)^2 \left(\frac{\rho_r h_r}{\rho_n h_n} \right)^2 F \qquad (11)$$

in which these parameters were obtained as follows:

G_r = the known vibration response as shown in Figure 2

h_r = 0.19 in.

ρ_r = 0.1 lb/in.^{3}

p_r = 0.156 psi

h_n = 0.02 in.

ρ_n = 0.1 lb/in.^{3}

p_n = the free-field sound pressure as shown in Figure 35

F = a factor which takes into account the effect of component loading. For unloaded structures, the factor is considered as unity.

Substituting the calculated values into Equation (11) results in:

$$G_n = 3708.5\ \rho_n^2\ G_r \tag{12}$$

The equation for predicting the loaded response, G_c, of a component on the cylinder is as follows:

$$G_c = G_n \left(\frac{W_n}{W_n + W_c} \right) \tag{13}$$

in which these parameters were obtained as follows:

W_n = 45 lb

W_c = 3.81 lb

Therefore,

$$G_c = 0.92\ G_n \tag{14}$$

Now, the resultant response environments, G_n and G_c, can be obtained by multiplying the ratios, as indicated by $3708.5\ \rho_n^2$ and 0.92, by the reference environments, respectively. The entire computation to obtain the unloaded and loaded response spectra was carried out in Table IV.

4.3 Comparison of Structural Responses

Computations via the constant mass attenuation method and the impedance ratio method are compared with the measured data in Figures 40 and 41. As can be seen from Figure 40, the predicted response obtained from the constant mass attenuation method is much too low in the high frequency range (300 ~ 2,000 Hz), and provides reasonable accuracy in predicting the response only in the intermediate frequency range.

The results obtained from the impedance ratio method were slightly high in the frequency range of 300 ~ 2,000 Hz, but were judged to be acceptable since the predicted results provide the more conservative estimate for design evaluation. The peak and valley responses shown in the frequency region of 400 Hz represent the primary resonant responses of the cylindrical structure. The analytical predictions obtained from the impedance ratio method can only be used to estimate the average curve that passes through the points of inflection of the response data. At frequencies below 300 Hz, a significant discrepancy between the predicted and measured responses is observed in these two figures. Such over-prediction of response is due to the inaccuracy of the acoustic mobility curve at lower frequencies, as discussed previously.

TABLE IV. COMPUTATION OF RESPONSE ENVIRONMENT UTILIZING CONSTANT MASS ATTENUATION METHOD

Frequency (Hz)	Acoustic Pressure P_n(psi)	Conversion Factor 3708.5 P_n^2	Reference* Environment $G_r(g^2/Hz)$	Unloaded Response Spectra $G_n(g^2/Hz)$	Loaded Response Spectra $G_n(g^2/Hz)$
20.00	0.0002	0.0001	0.0010	0.0000	0.0000
25.00	0.0004	0.0006	0.0090	0.0000	0.0000
31.50	0.0009	0.0033	0.0140	0.0000	0.0000
40.00	0.0016	0.0100	0.0230	0.0002	0.0002
50.00	0.0025	0.0241	0.0340	0.0008	0.0008
63.00	0.0037	0.0499	0.0540	0.0027	0.0025
80.00	0.0047	0.0823	0.0820	0.0067	0.0064
100.00	0.0054	0.1073	0.1250	0.0134	0.0127
125.00	0.0055	0.1114	0.2000	0.0223	0.0210
160.00	0.0050	0.0927	0.3100	0.0287	0.0271
200.00	0.0041	0.0629	0.4800	0.0302	0.0285
250.00	0.0033	0.0406	0.4800	0.0195	0.0184
315.00	0.0024	0.0223	0.4800	0.0107	0.0101
400.00	0.0018	0.0123	0.4800	0.0059	0.0056
500.00	0.0014	0.0078	0.4800	0.0037	0.0035
630.00	0.0010	0.0041	0.4800	0.0020	0.0019
800.00	0.0007	0.0021	0.2300	0.0005	0.0005
1000.00	0.0005	0.0009	0.1100	0.0001	0.0001
1250.00	0.0004	0.0006	0.1100	0.0001	0.0001
1600.00	0.0003	0.0003	0.1100	0.0000	0.0000
2000.00	0.0002	0.0001	0.1100	0.0000	0.0000

*Tabulated values are obtained from Figure 2.

5.0 SUMMARY AND CONCLUSIONS

5.1 Summary

During this study, the constant mass attenuation method has been investigated and utilized to predict the responses of a cylindrical shell to reverberant sound pressure environments. This method is based upon the fact that similar structures have similar response characteristics and is valid for all materials. Equation (1) is used to predict localized vibratory environments. But it should be recognized that the frequency characteristics of structures is not included in the computation.

The major advantages of this method are that it is simple to apply in predicting vibro-acoustic responses for both simple and complex structures.

The limitations of this method are as follows:

- This technique requires only the information of thickness, and density of new structures to be used in the prediction. It has been shown that responses of structures subjected to acoustic excitations are dependent on other dimensional parameters, such as diameter and length. Consequently, the accuracy of this method may be impaired by the omission of such dimensional parameters as stated above.

- Damping os structures is neglected in the computations. The vibration response of a structural system is highly dependent on the damping property of the structure. The omission of damping in the analysis will also introduce errors in predicted results.

- The mass attenuation factor was defined as a function of ratio of masses of component and support structures. This condition is applicable to a primary structure with sufficiently high impedance than that of the component; and does not apply to general cases.

- The method was formulated based on the measured vibration responses of a reference vehicle structure with a typical skin thickness and vehicle diameter. For wide application, more measured data for different vehicle specimens are needed in order to provide more accurate predictions.

The impedance ratio method has been used to predict the unloaded and loaded response spectra of a component and its support structure (cylindrical structure) which is subjected to broadband acoustic excitations. The method was derived from a one-dimensional impedance model, and the computation is performed by means of nomograms and design charts.

The major advantages of the impedance ratio method are as follows:

- The simplified computation method, as presented, has been shown to be accurate and conservative within current acceptable tolerance limits within certain frequency ranges. The computation process requires minimum manual effort and no computer assistance is required.

- The method does include effects of component/primary structure coupling and provide frequency characteristics of the structure. Hence the predicted results provide more realistic estimates of the structural responses.

- The dynamic magnification factor, Q which is related to structural damping may be incorporated in the computation.

- This technique will permit satisfactory environmental estimates of highly complex structures with a minimum amount of manual computation.

The chief limitations of the impedance ratio method are:

- A knowledge of the computation sequence and some engineering judgment in estimating structural impedance on the part of the user are required to perform the predictions.

- The predicted responses are slightly high in some cases, but are considered to be acceptable, since the results provide a more conservative estimate for use in design.

- The accuracy of the predicted response is highly dependent upon the assumed damping characteristics of the structural systems. For aerospace structures, the dynamic magnification factor, Q, is estimated to be around 10 to 20 over much of the frequency range, and the resulting structural response discrepancy is about a half decade.

5.2 Conclusions

The following conclusion can be drawn from the results of this study:

(A) Prediction of Unloaded Structural Responses

- The results presented in Section 4.0 have shown that, in terms of the prediction accuracy, both analytical methods cannot be considered entirely satisfactory over the complete frequency range of interest (20 - 2000 Hz).

For a typical structure excited by a random acoustic pressure field, the predicted response obtained from the constant mass attenuation method shows reasonable accuracy in the frequency range from 100 Hz to 300 Hz, and the responses predicted by the impedance ratio method provides acceptable results in the frequency range from 300 Hz to 2000 Hz.

- Both methods, when used to predict the structural responses, are highly dependent on the reference data curves. The constant mass attenuation method is based on a fixed data base derived from a reference structure. Therefore, its applicability to different types of structures would be limited. On the other hand, the impedance ratio method was derived from the empirical acoustic mobility curves which were obtained from a wide range of measured vibration data. It has been observed that considerable scatter exists between the various experimental measured responses to broadband acoustic excitations, and the acoustic mobility curves can only represent general trends in structural response. Further refinements are needed to obtain a better collapse of the experimental data, and achieve a higher degree of accuracy in the lower frequency range.

(B) Prediction of Loaded Structural Responses

- The constant mass attenuation method will generate higher response levels due to the omission of support structure/component coupling. This would lead to possible over testing in component qualification.

- The impedance ratio method allows reasonable accurate predictions on responses of a loaded structure based on given measured unloaded responses of the same structure. Thus this technique may provide more realistic component environment criteria for component qualification.

REFERENCES

1. Barrett, R.E.: "Techniques for Predicting Localized Vibratory Environments of Rocket Vehicles, NASA TN D-1836, October 1963.

2. Kao, G.C., and Sutherland, L.C.: "Development of Equivalent One-Dimensional Acoustic Force Spectra by Impedance Measurement Techniques," Wyle Laboratories Research Staff Report WR 69-11, May 1969.

3. Kao, G.C.: "Prediction of Force Spectra by Mechanical Impedance and Acoustic Mobility Measurement Techniques," Wyle Laboratories Research Staff Report WR 71-16, October 1971.

4. Chang, K.Y., Cockburn, J.C., and Kao, G.C.: "Prediction of Vibro-Acoustic Loading Criteria for Space Vehicle Components," Wyle Laboratories Research Staff Report WR 73-9, September 1973.

5. Chang, K.Y., and Kao, G.C.: "Development of Modified Vibration Test Criteria for Qualifying Space Vehicle Components," Wyle Laboratories Research Staff Report WR 74-6, September 1974.

6. Waterhouse, R.V., "Diffraction Effects in a Random Sound Field," JASA, vol. 35, October 1963, pp. 1610-1620.

7. Conticelli, V.M., "Evaluation of Blocked Pressure Spectra on Stiffened Cylindrical Shells," Wyle Laboratories Research Staff Technical Memorandum TM 71-1, September 1974.

FIGURES

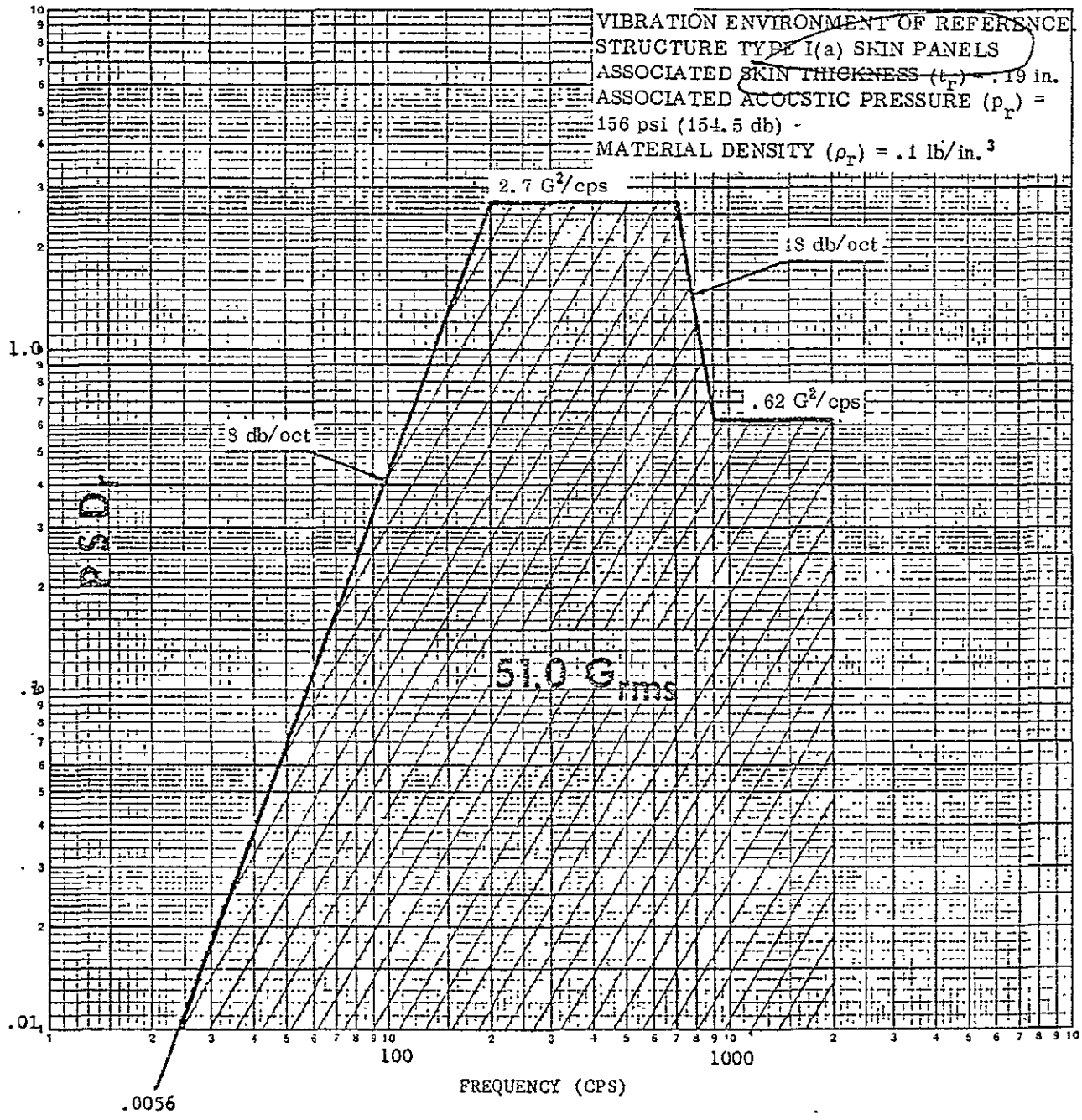

Figure 1. Random Reference Environment - Type I(a) Skin Panels (Reference 1)

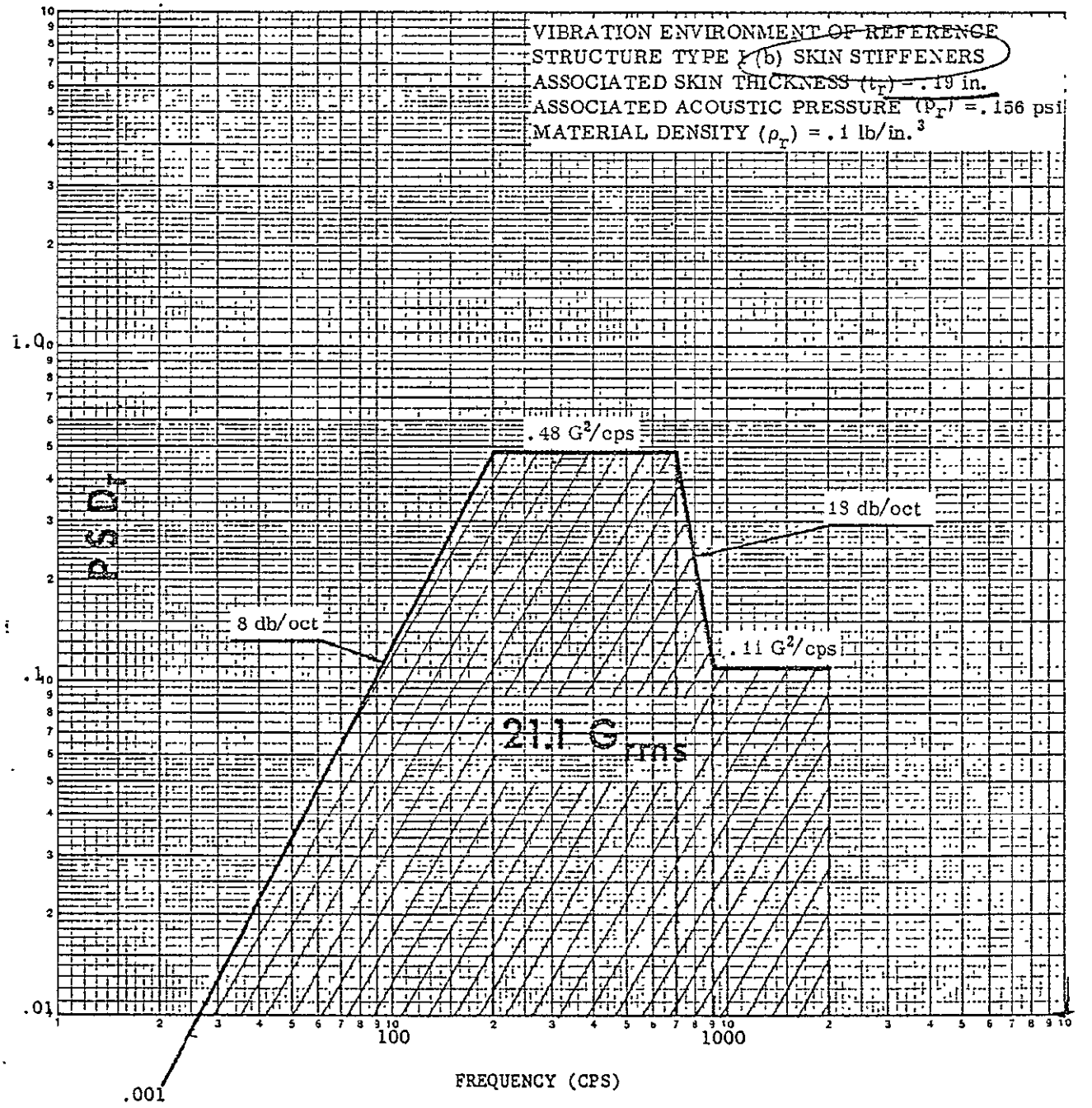

Figure 2. Random Reference Environment - Type I(b) Skin Stiffeners (Reference 1)

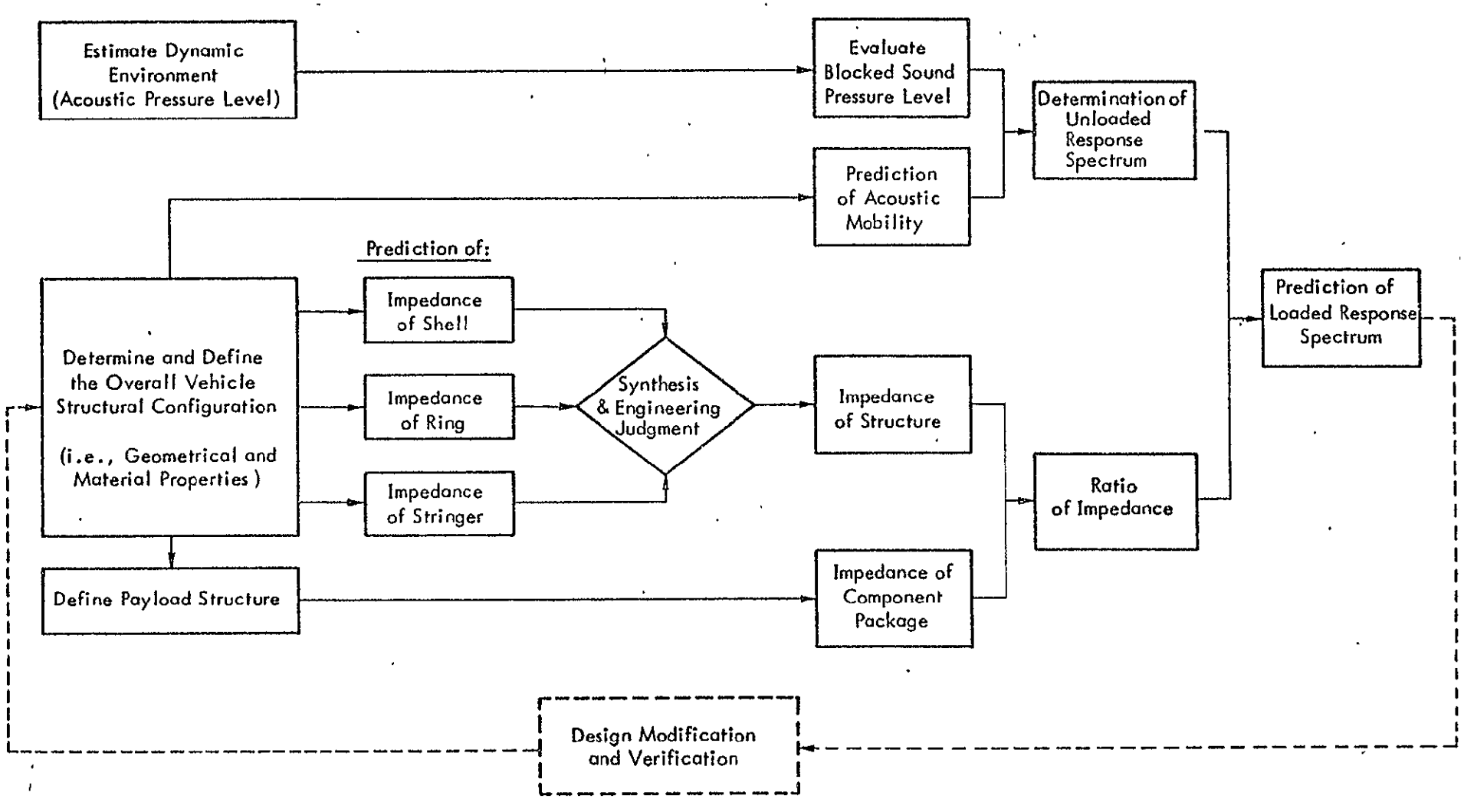

Figure 3. Flowchart for Predicting the Loaded Response Spectrum of Structures

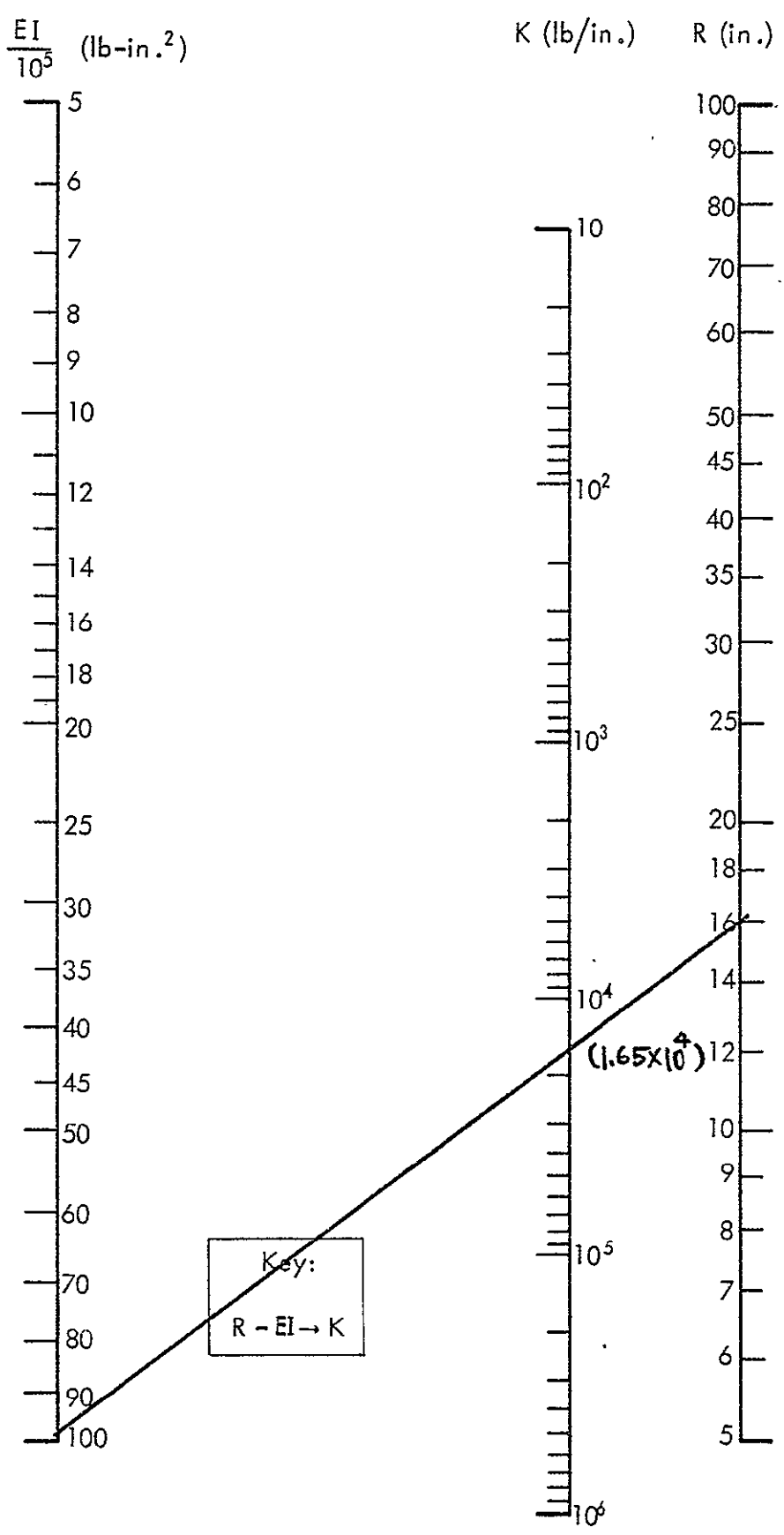

Figure 4. Nomograph for Determining Static Stiffness of Rings

$$K = \frac{EI}{0.15\ R^3} = 1.65 \times 10^4$$

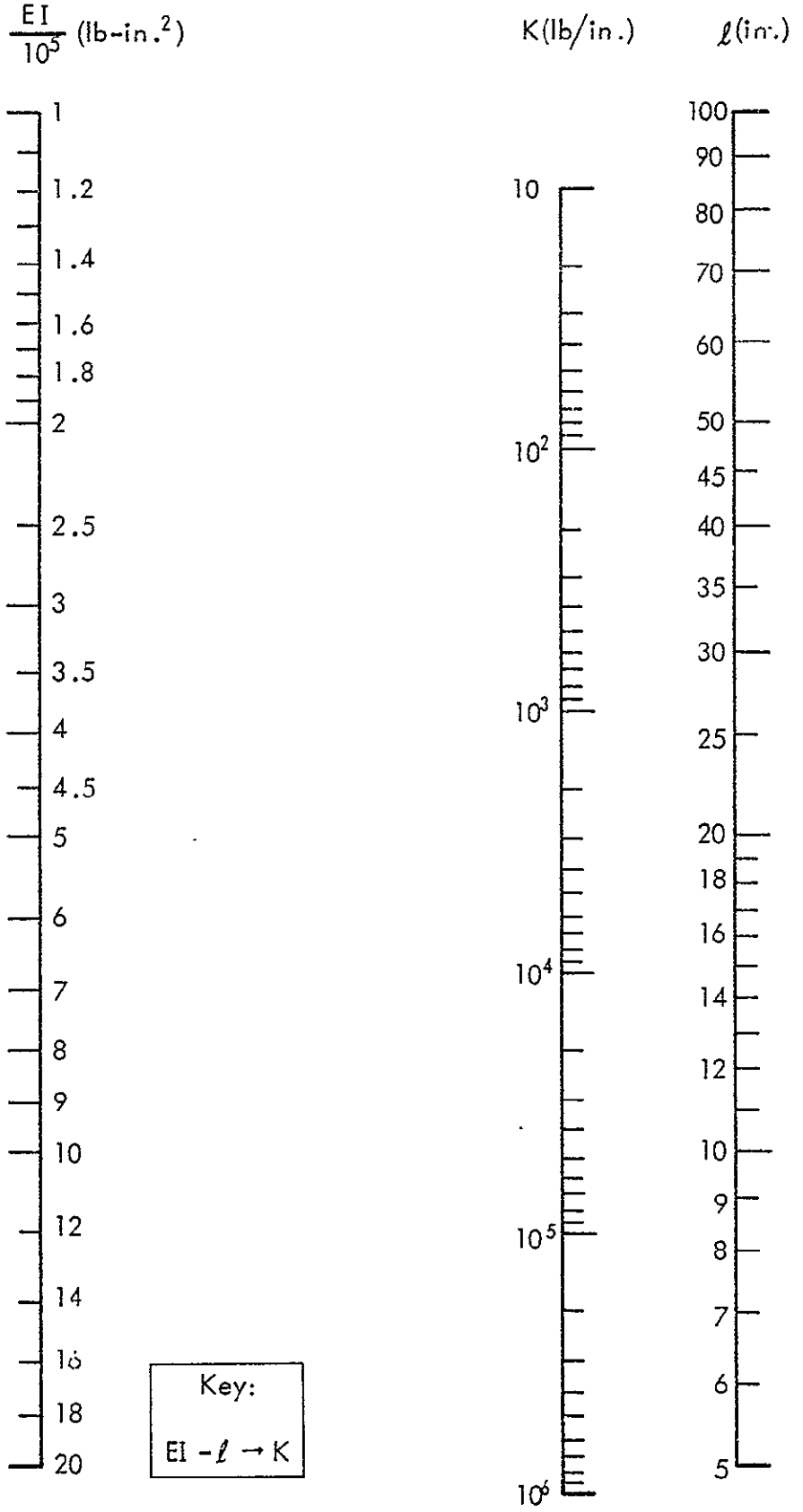

Figure 5. Nomograph for Determining Static Stiffness of Beams

$K = 48\ EI/\ell^3 = 1133.33$

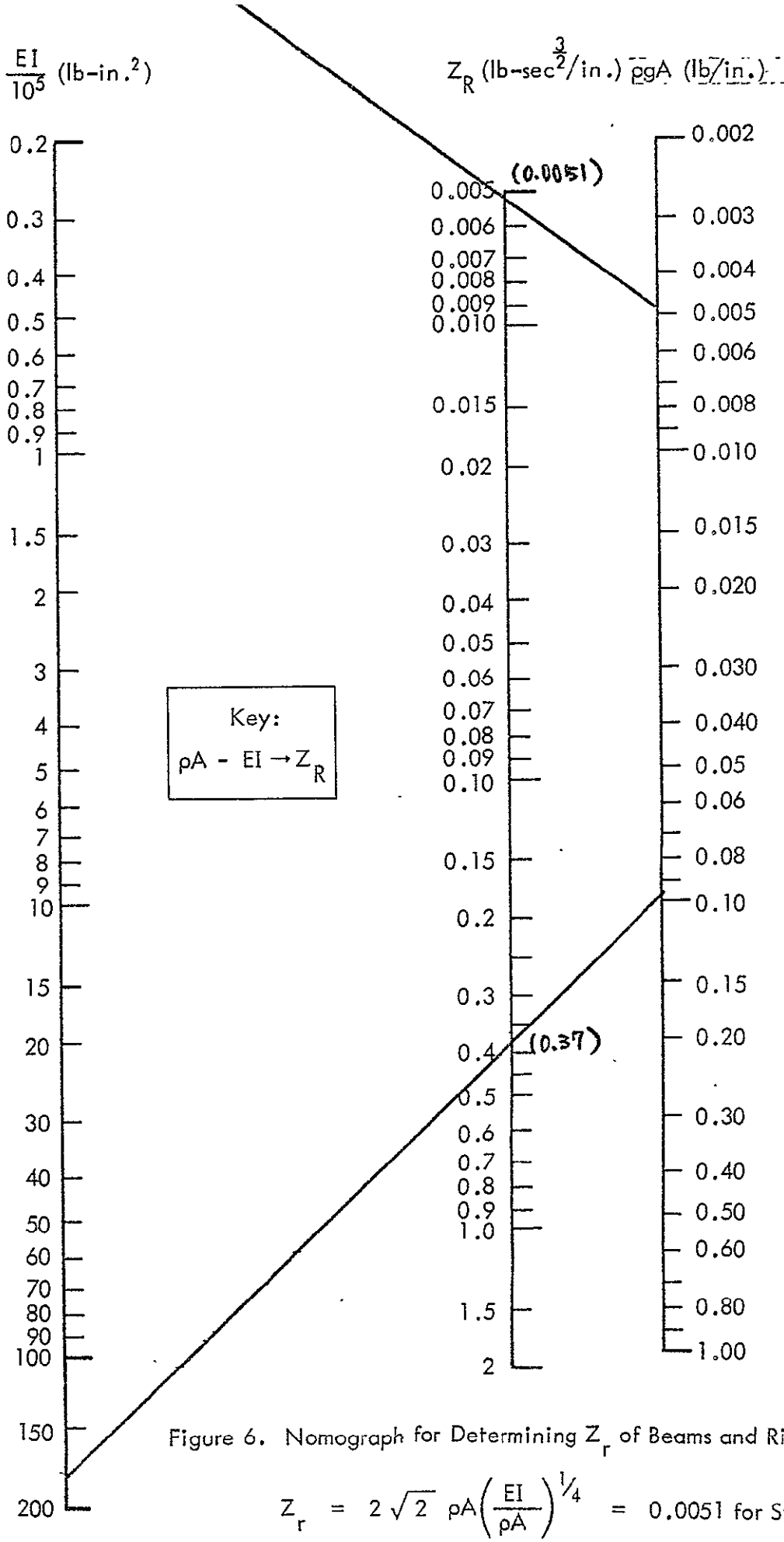

Figure 6. Nomograph for Determining Z_r of Beams and Rings

$$Z_r = 2\sqrt{2}\ \rho A\left(\frac{EI}{\rho A}\right)^{1/4} = 0.0051 \text{ for Stringer}$$

$$= 0.37 \text{ for Ring}$$

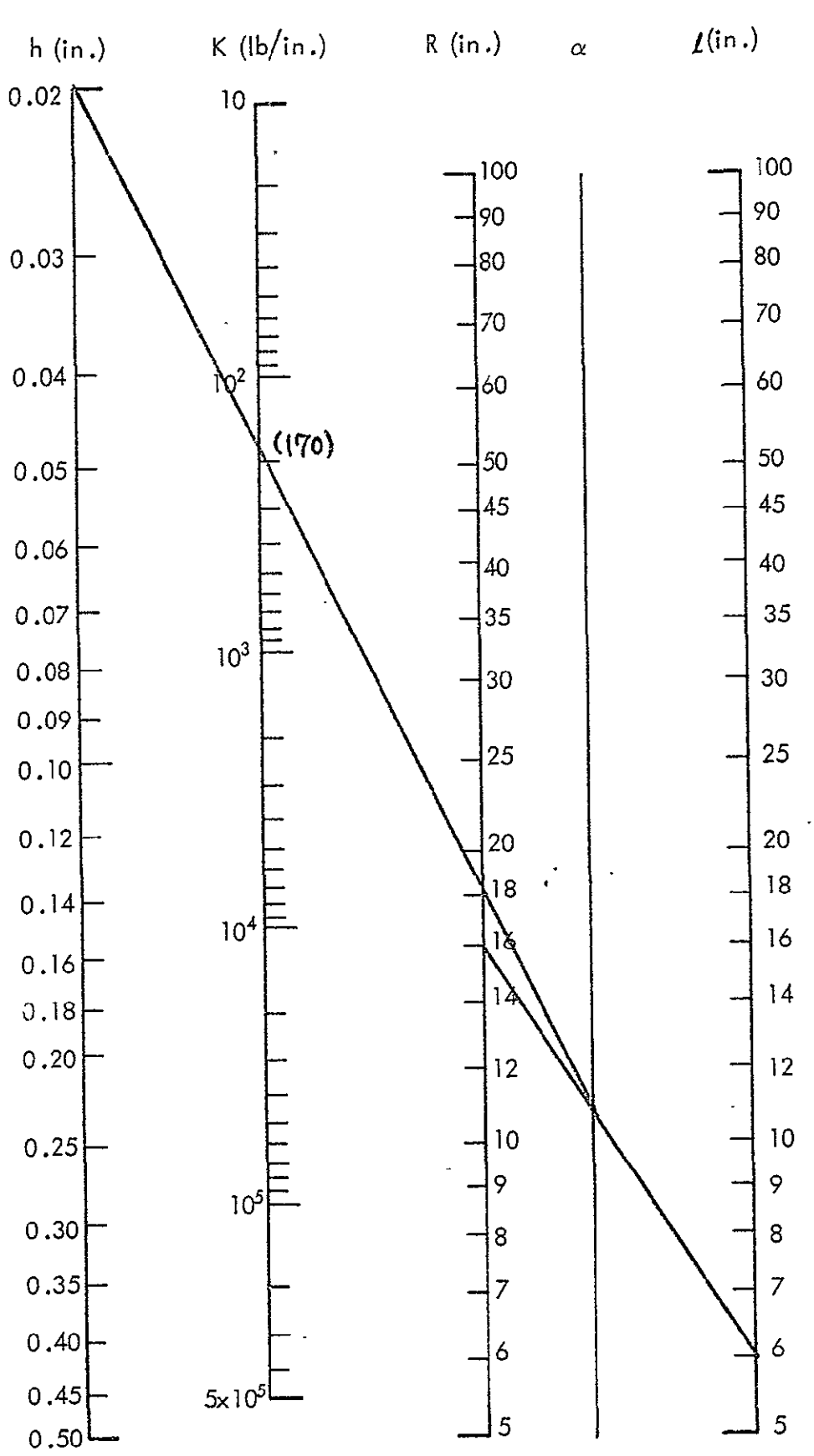

Figure 7. Nomograph for Evaluating Static Stiffness of Unstiffened Cylinder

$$K = 2.5\,Eh\left(\frac{R}{\ell}\right)^{1/2}\left(\frac{h}{R}\right)^{5/4}, \quad (E = 10^7 \text{ psi for Al})$$

$$= 170$$

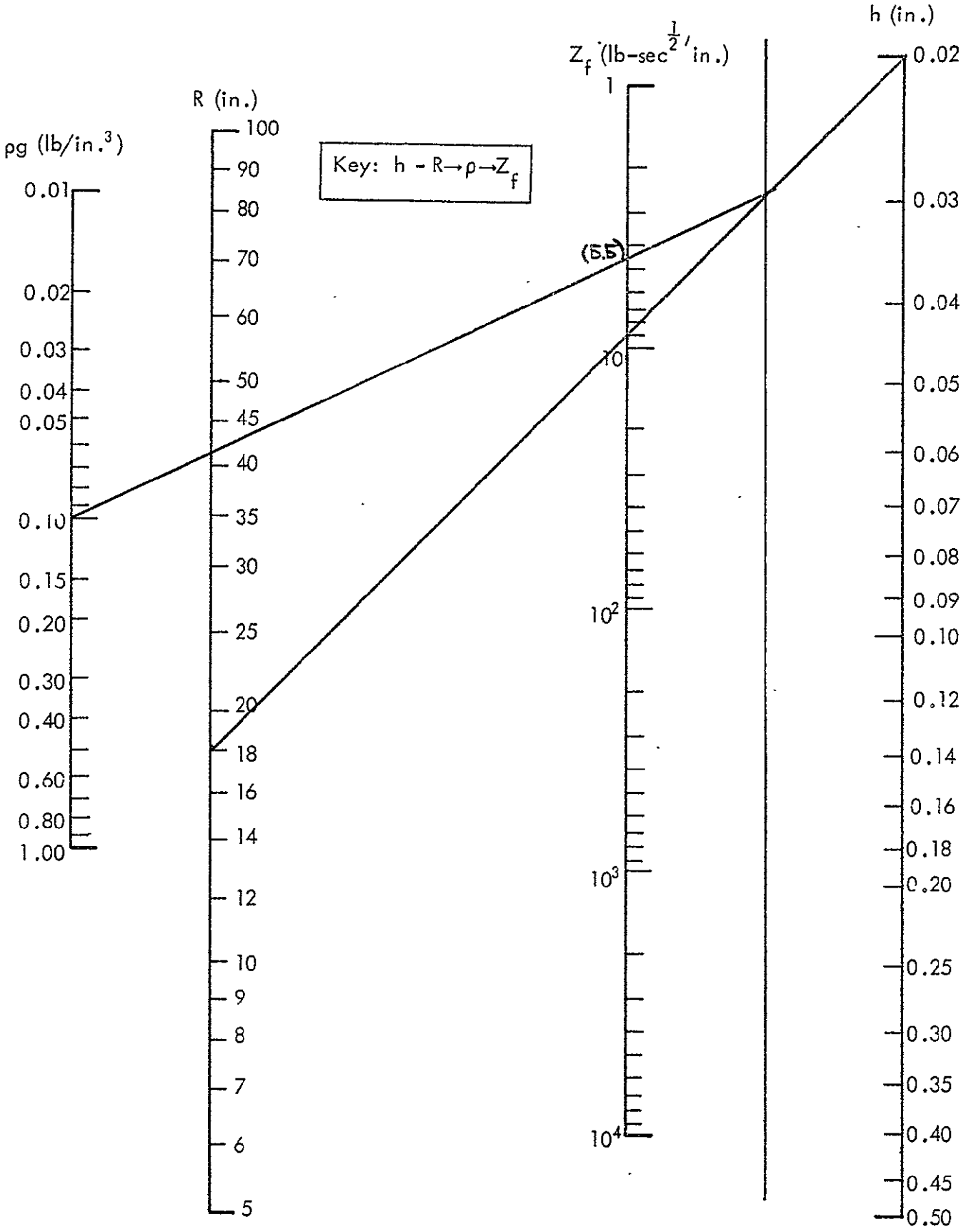

Figure 8. Nomograph for Determining Z_f of Unstiffened Cylinders

$$Z_f = \frac{4}{\sqrt{3}} \rho h^2 \sqrt{\frac{E}{\rho}} \left(\frac{E}{\rho R^2}\right)^{1/4}, \quad (E = 10^7 \text{ psi for Al})$$

$$= 5.5$$

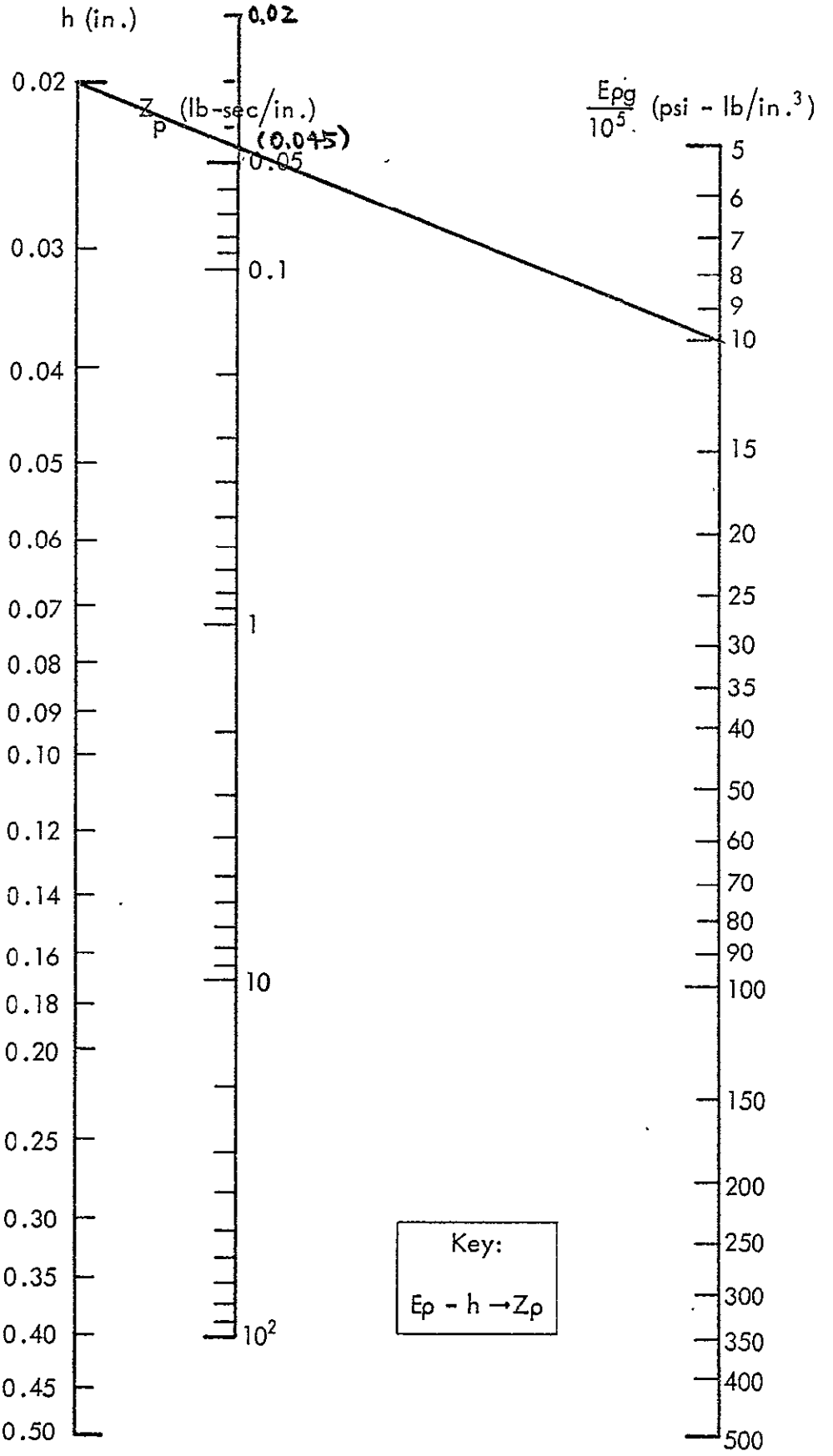

Figure 9. Nomograph for Evaluating Impedance of Infinite Plate

$$Z_p = \frac{4}{\sqrt{3}} h^2 \sqrt{E\rho} = 0.045$$

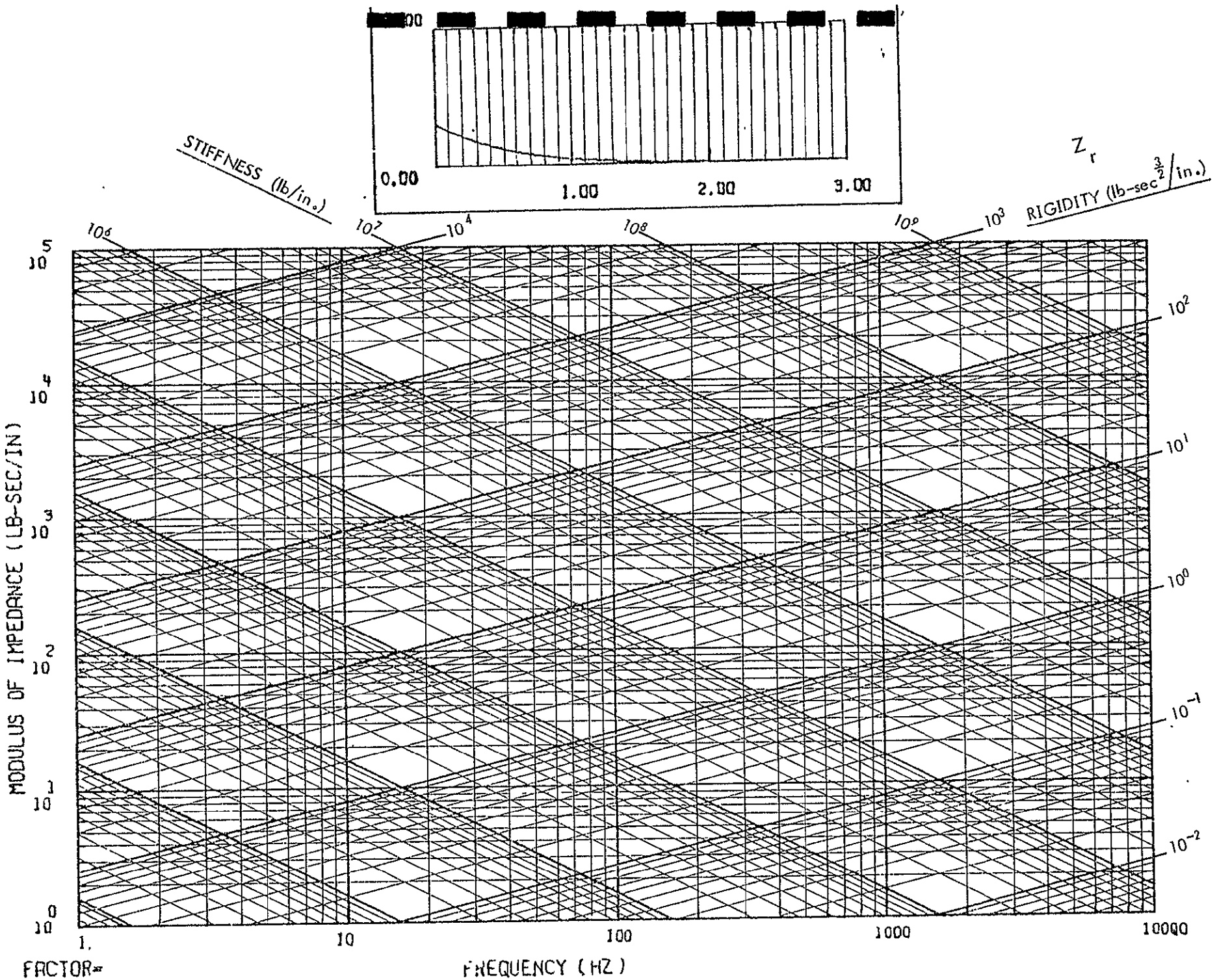

Figure 10. Impedance Chart for Stiffeners

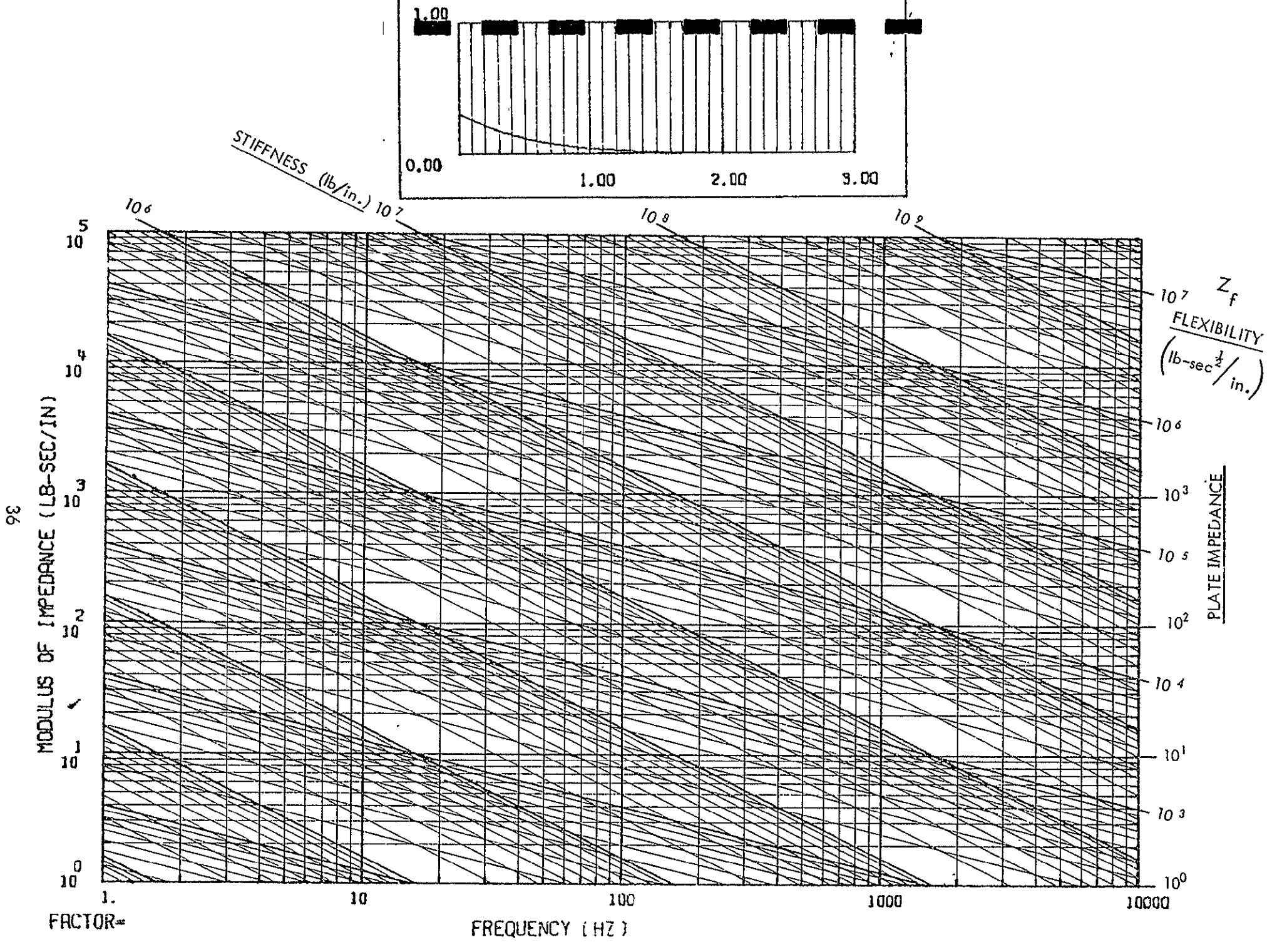

Figure 11. Impedance Chart for Cylindrical Shell

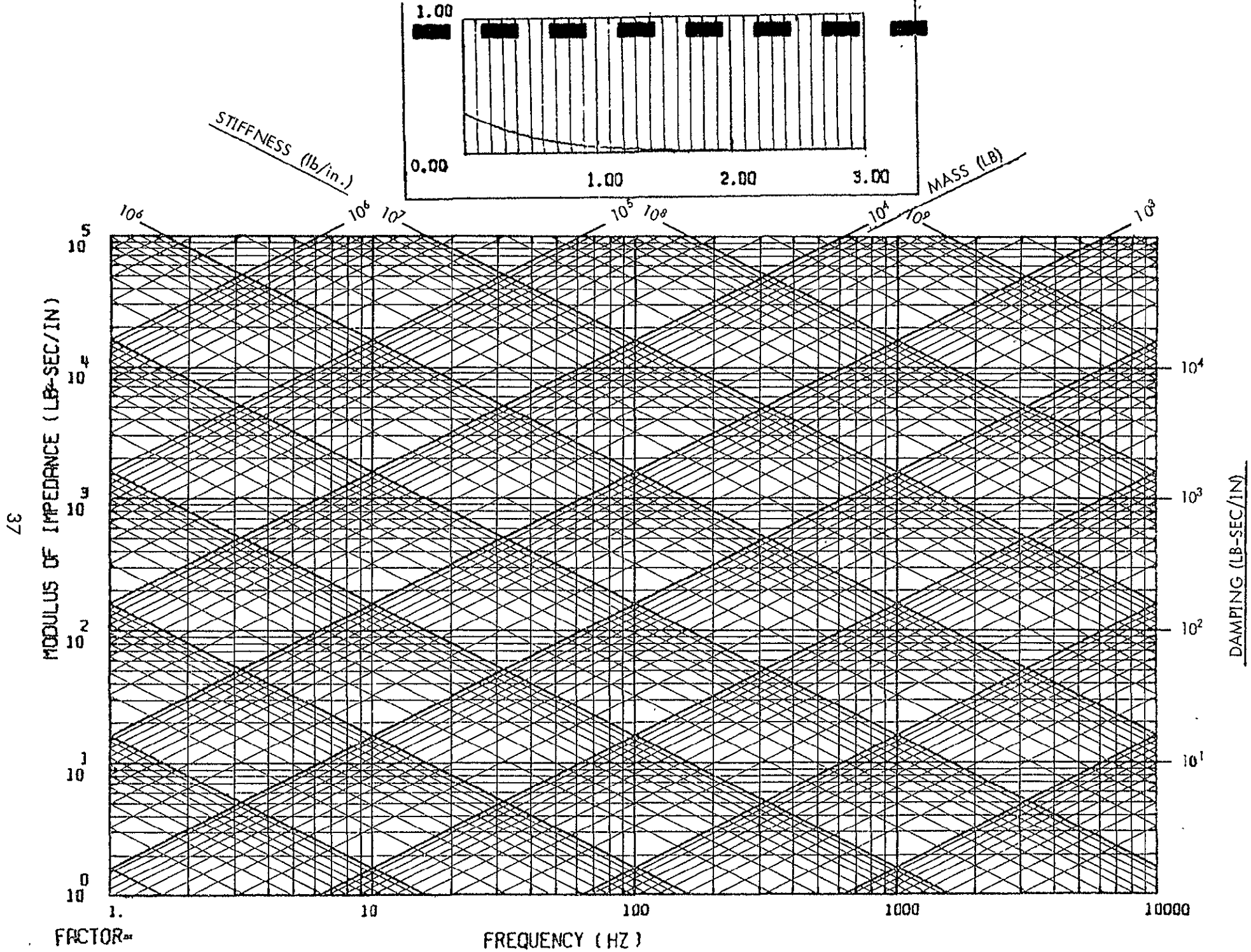

Figure 12. Impedance Chart for Component Package

α = Acoustic mobility (in./sec/psi)

m = Surface density (weight) (lb/in^2)

D = Diameter (in.)

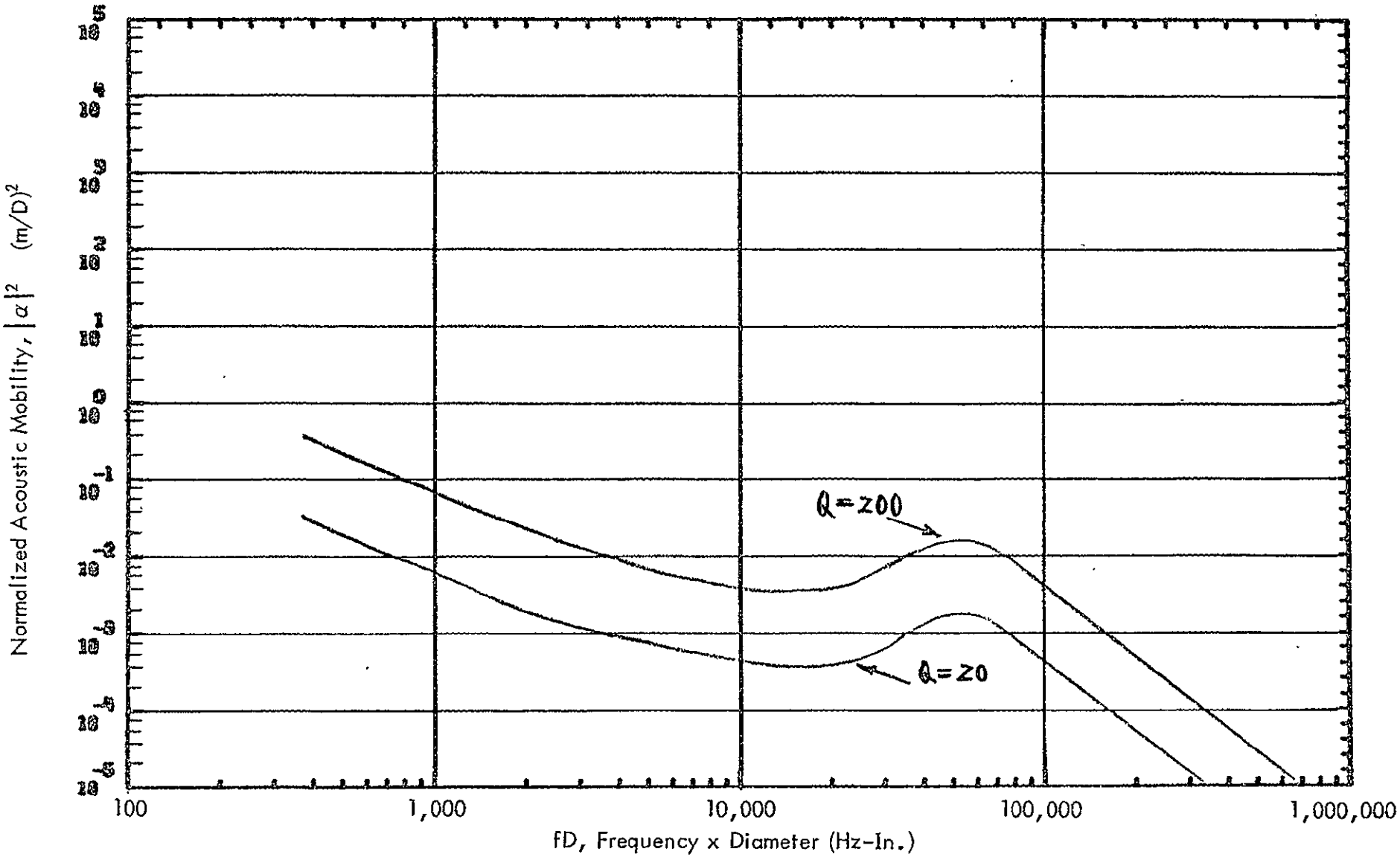

Figure 13. Velocity Mobility Levels for Cylindrical Structures

Figure 14. Theoretical $\sqrt{\beta}$-curve for a Cylinder in a Random Sound Field

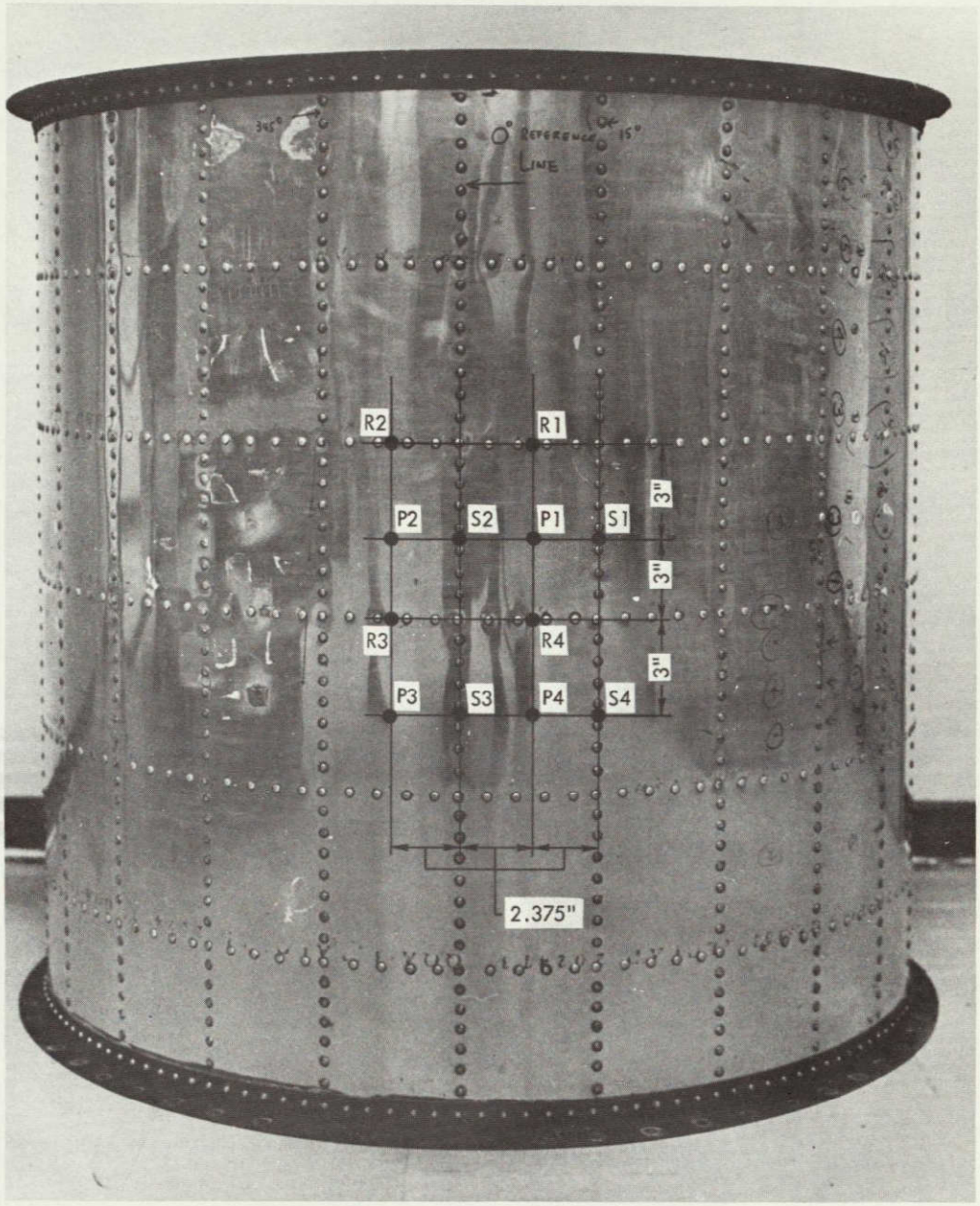

Figure 15. Stiffened Cylinder and Component Specimen Mounting Locations

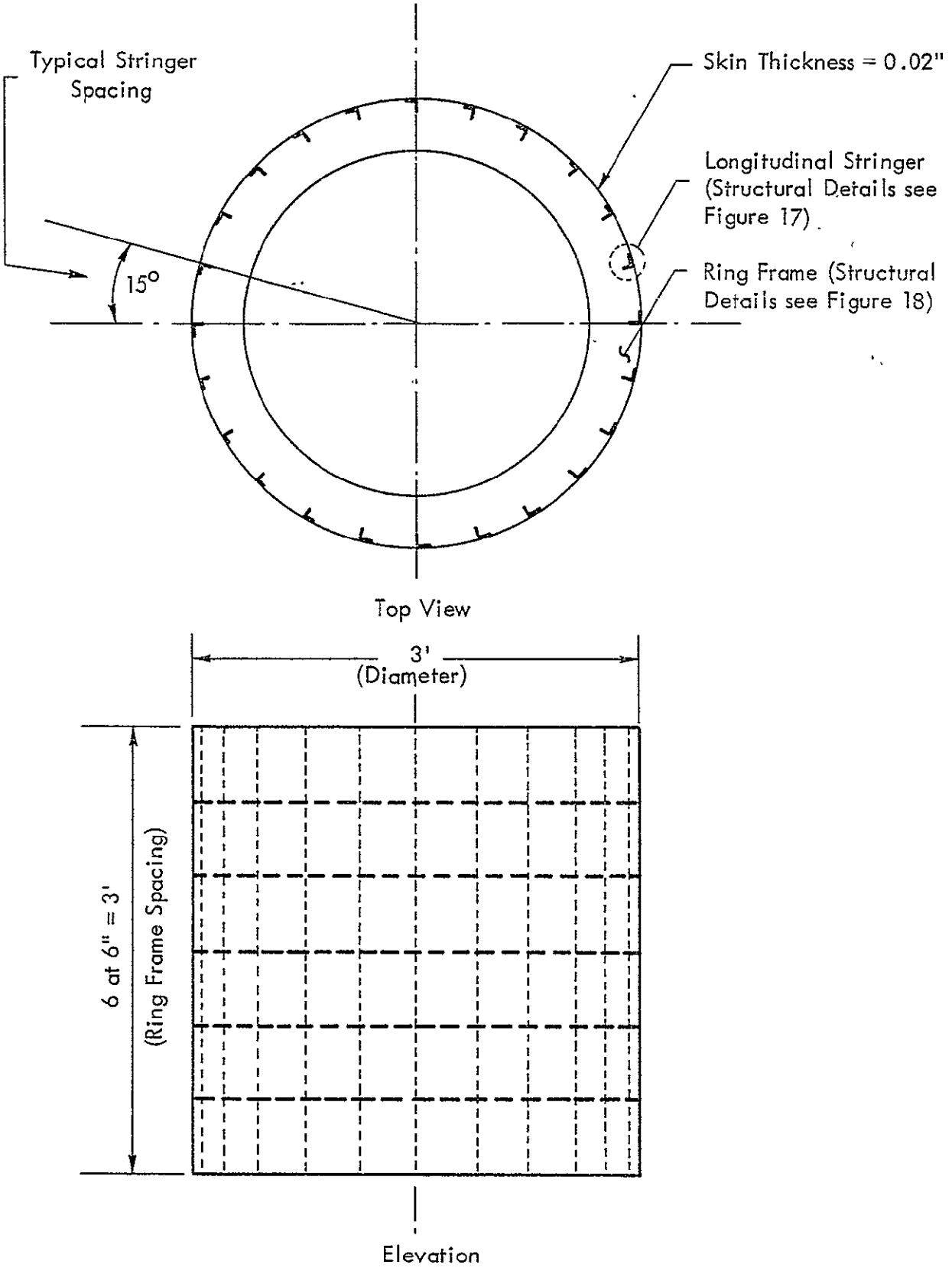

Figure 16. Structural Configuration of the Stiffened Aluminum Cylinder (End Rings and Bulkheads Not Shown)

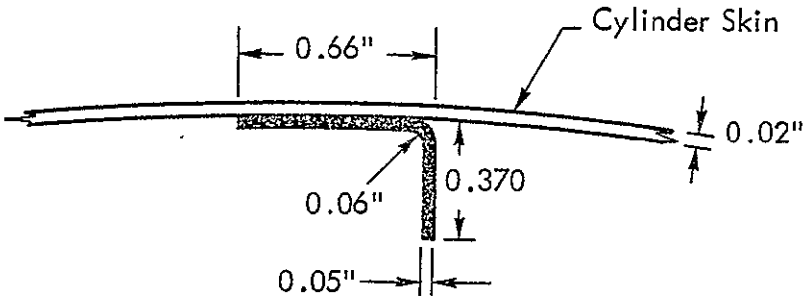

Figure 17. Structural Details of Longitudinal Stringer

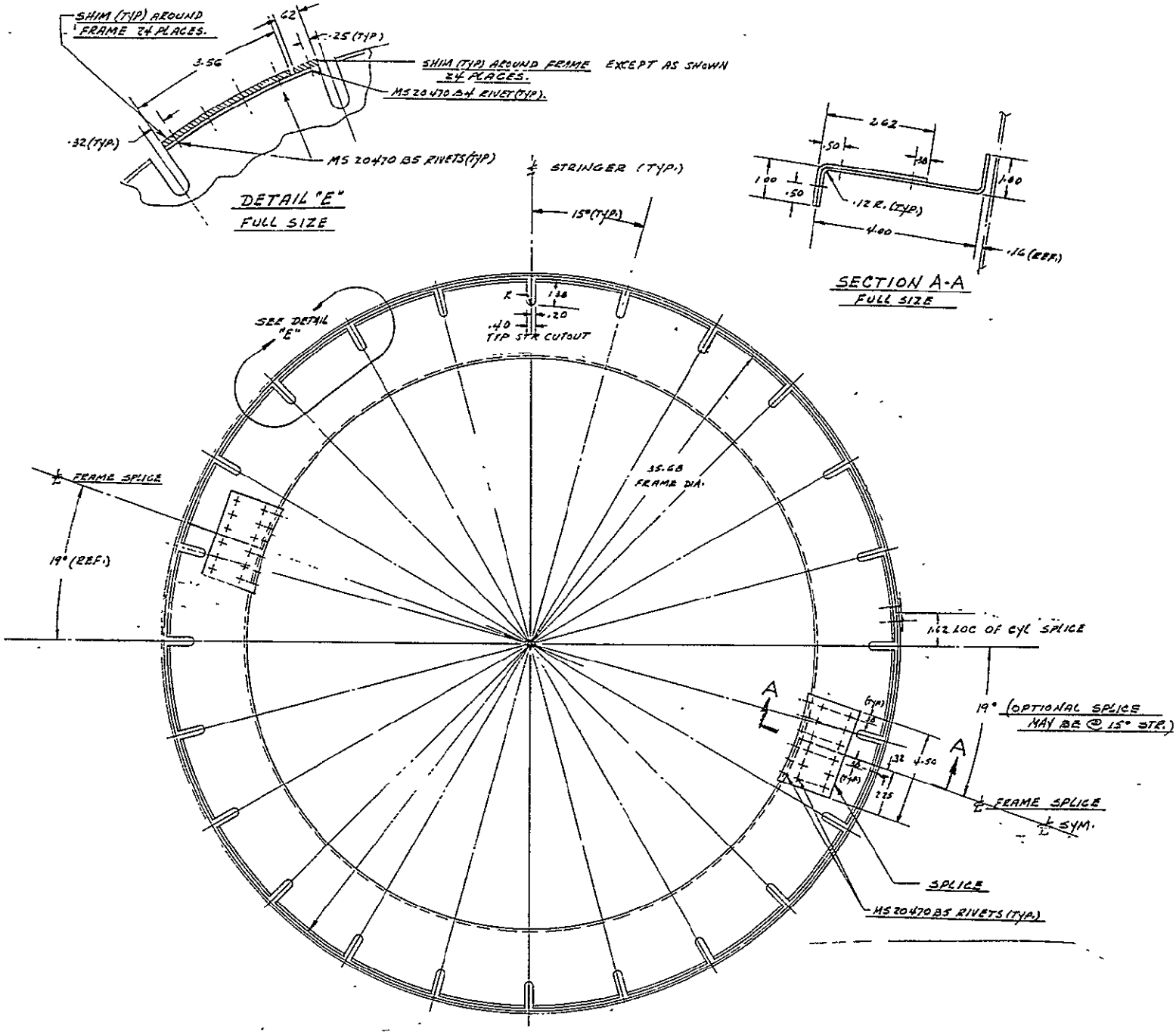

Figure 18. Structural Details of a Ring Frame

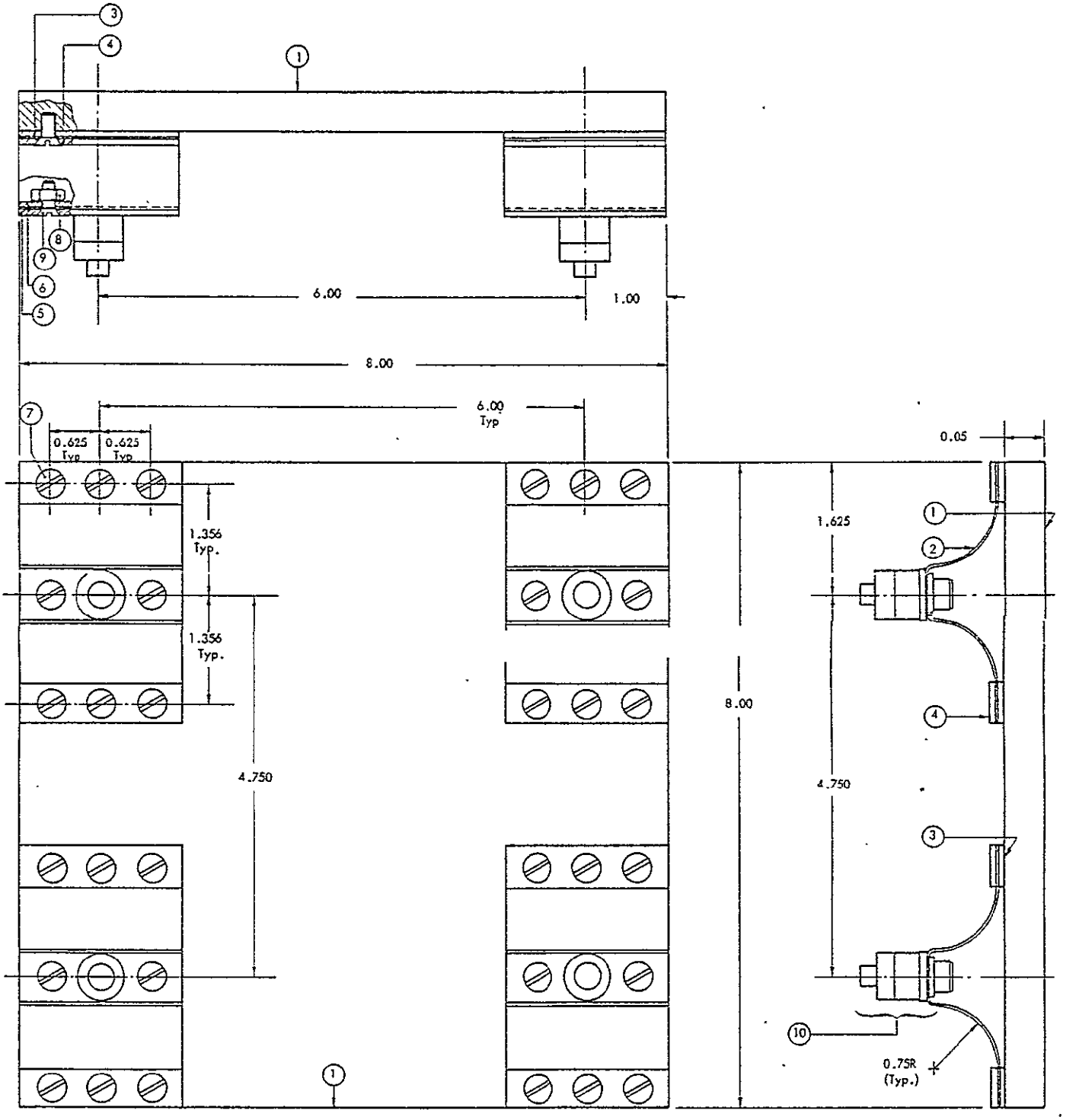

(1) 1/2" x 8" x 8" Plate
(2) 4 - 0.008 Steel Leave Springs
(3) 0.031 x 2.00 x 4.193 Strip
(4) 0.063 x 0.50 x 2.00 Strip
(5) 0.063 x 0.550 x 2.00 Strip
(6) 0.063 x 0.550 x 2.00 Strip
(7) No. 10-32 100° Flat Head Screw x 5/6" Lg.
(8) No. 10-32 Hex Nut
(9) No. 10-32 100° Flat Head Screw x 3/8" Lg.
(10) Mounting Assembly

NOTE: All parts, except Item No. 2, were made of Aluminum Alloy Type 6061-T6

Figure 19. Dimensions of the Simulated Component Package (All Dimensional Units are in Inches)

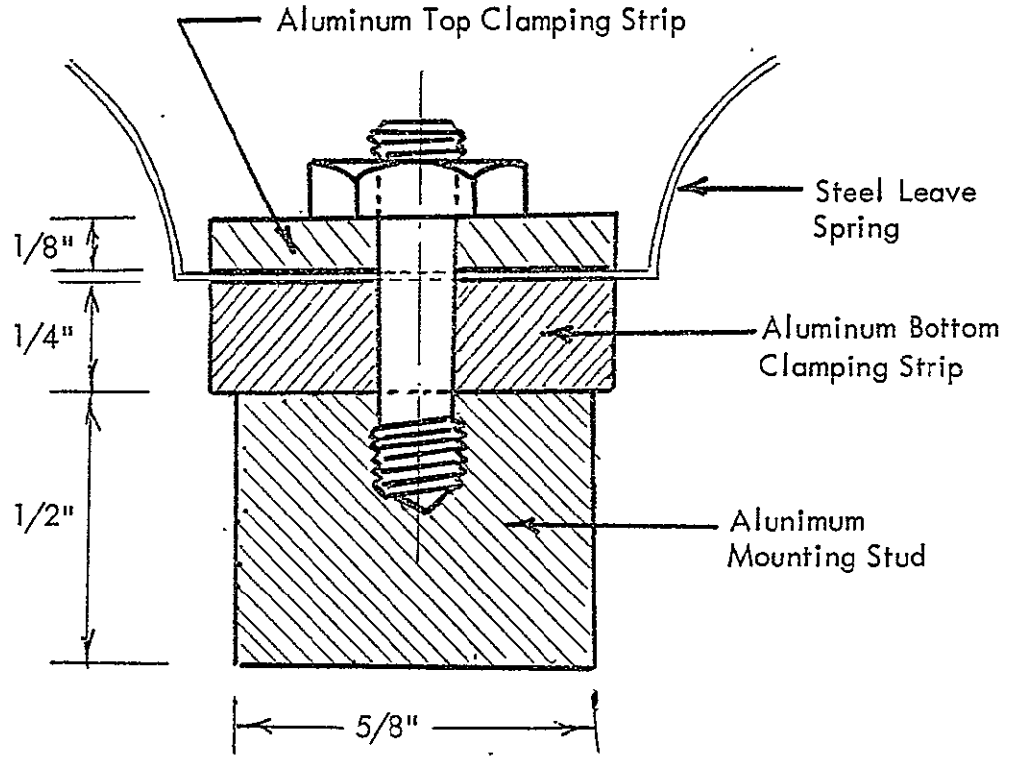

Figure 20. Details of Mounting Assembly

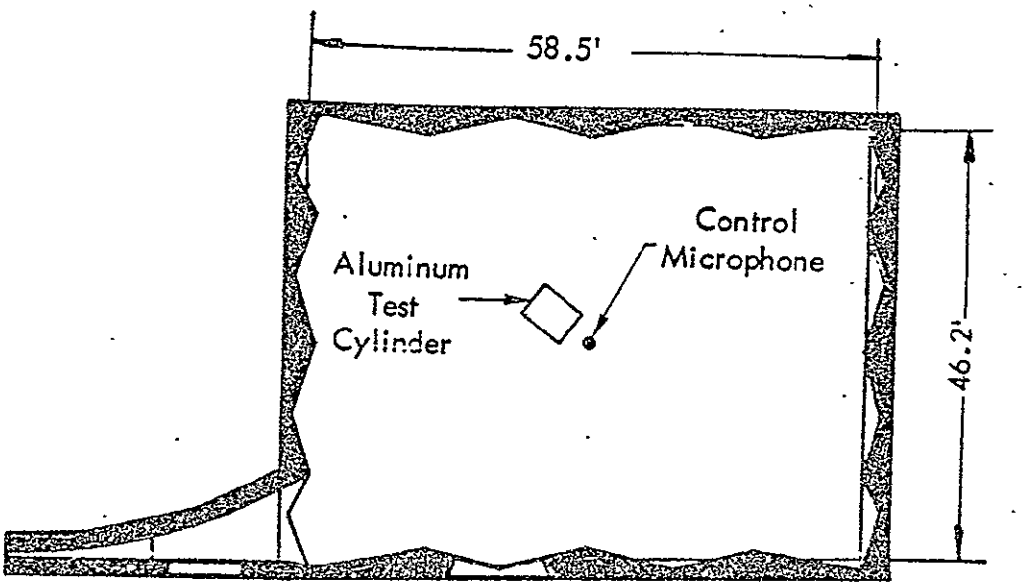

(Room Height 37.0')

Figure 21. Plan View Showing Set-up of Test Specimen in the Reverberation Room

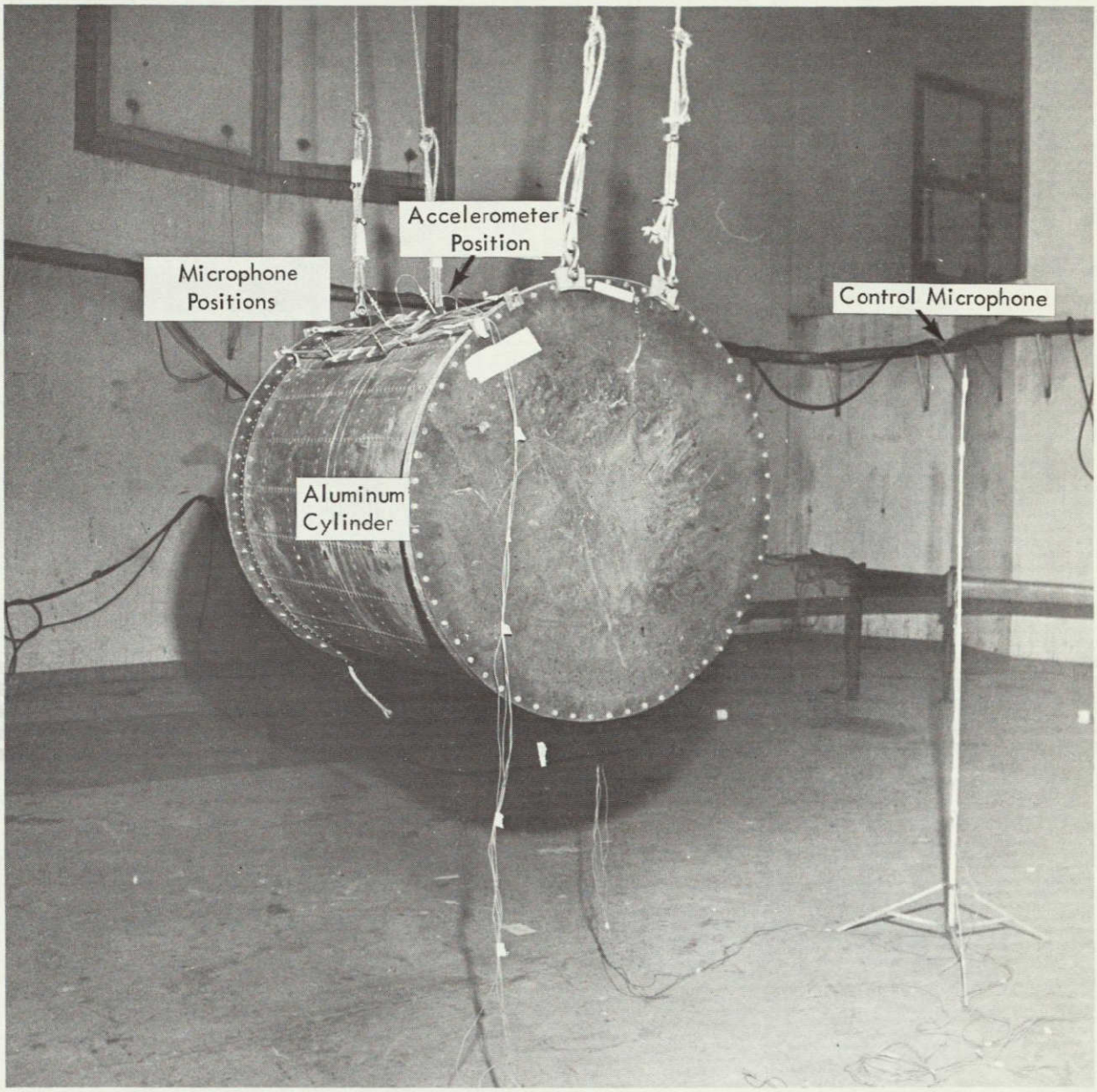

Figure 22. Relative Positions of Test Cylinder, Microphones and Accelerometer in the Reverberation Room

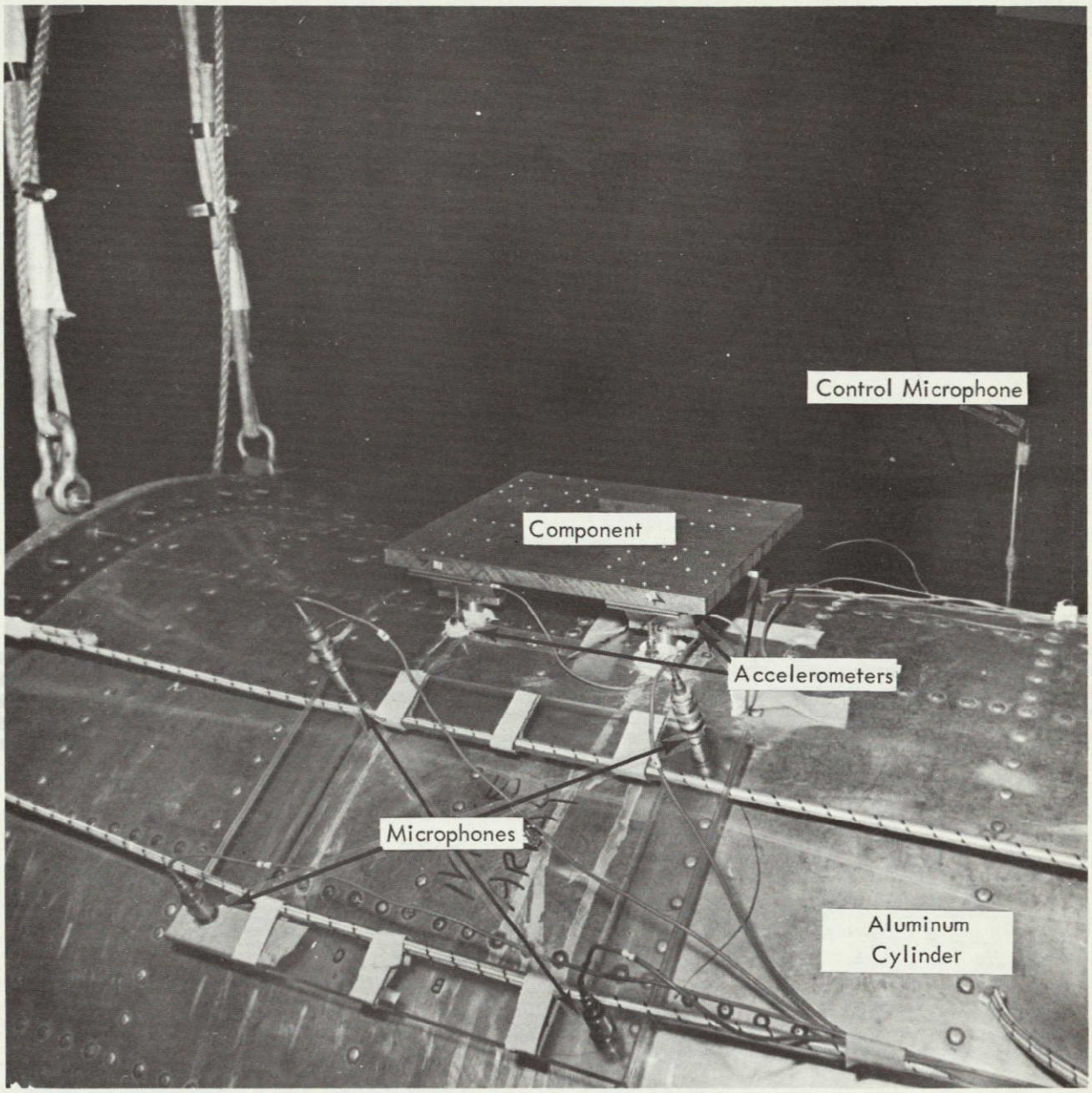

Figure 23. Measurement of Loaded Structural Responses

LEGEND:

ACC	—	Accelerometer
MK	—	Microphone
CA	—	Charge Amplifier
BA	—	Buffer Amplifier
MA	—	Microphone Amplifier

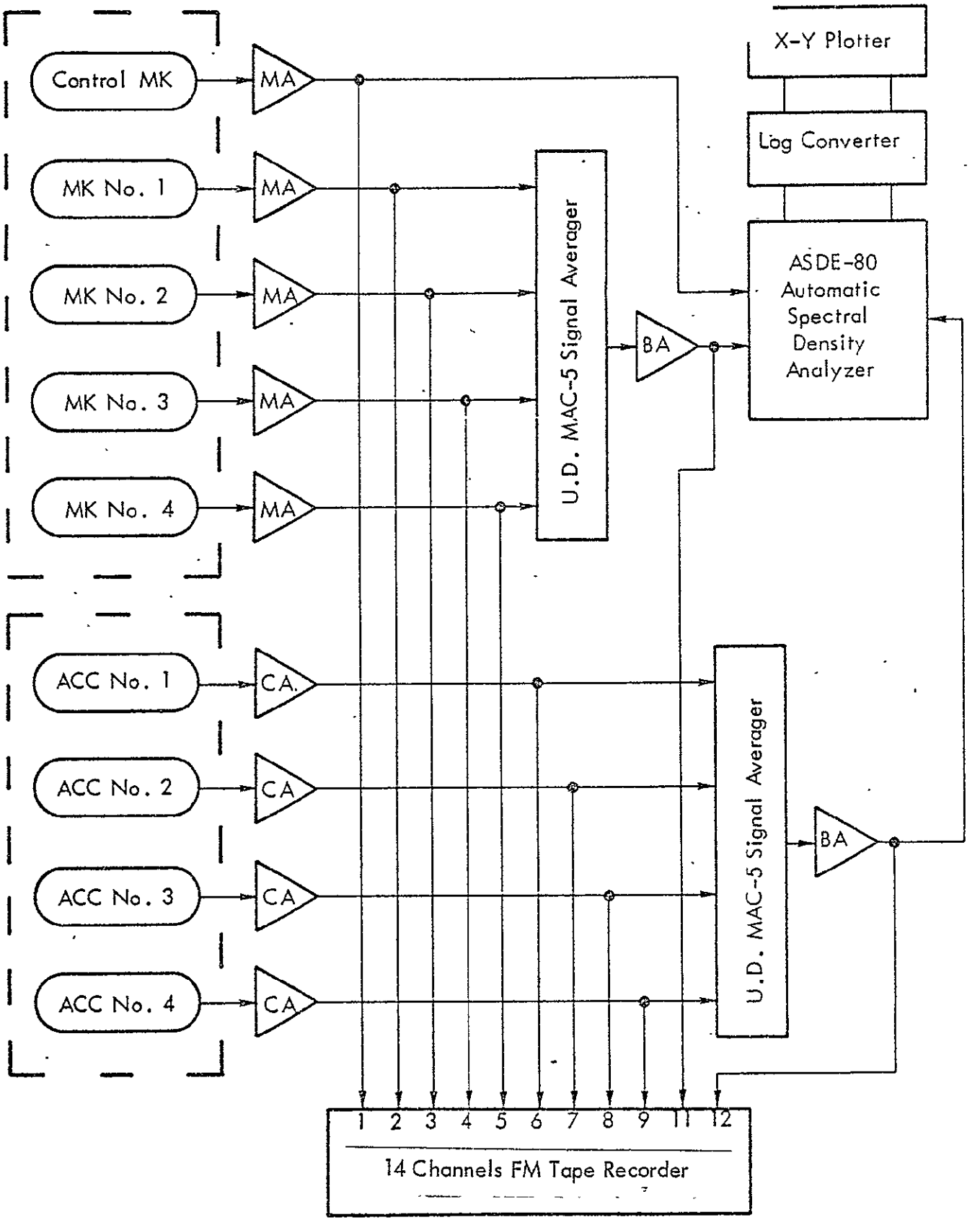

Figure 24. Instrumentation Block Diagram for Vibro-Acoustic Experiments

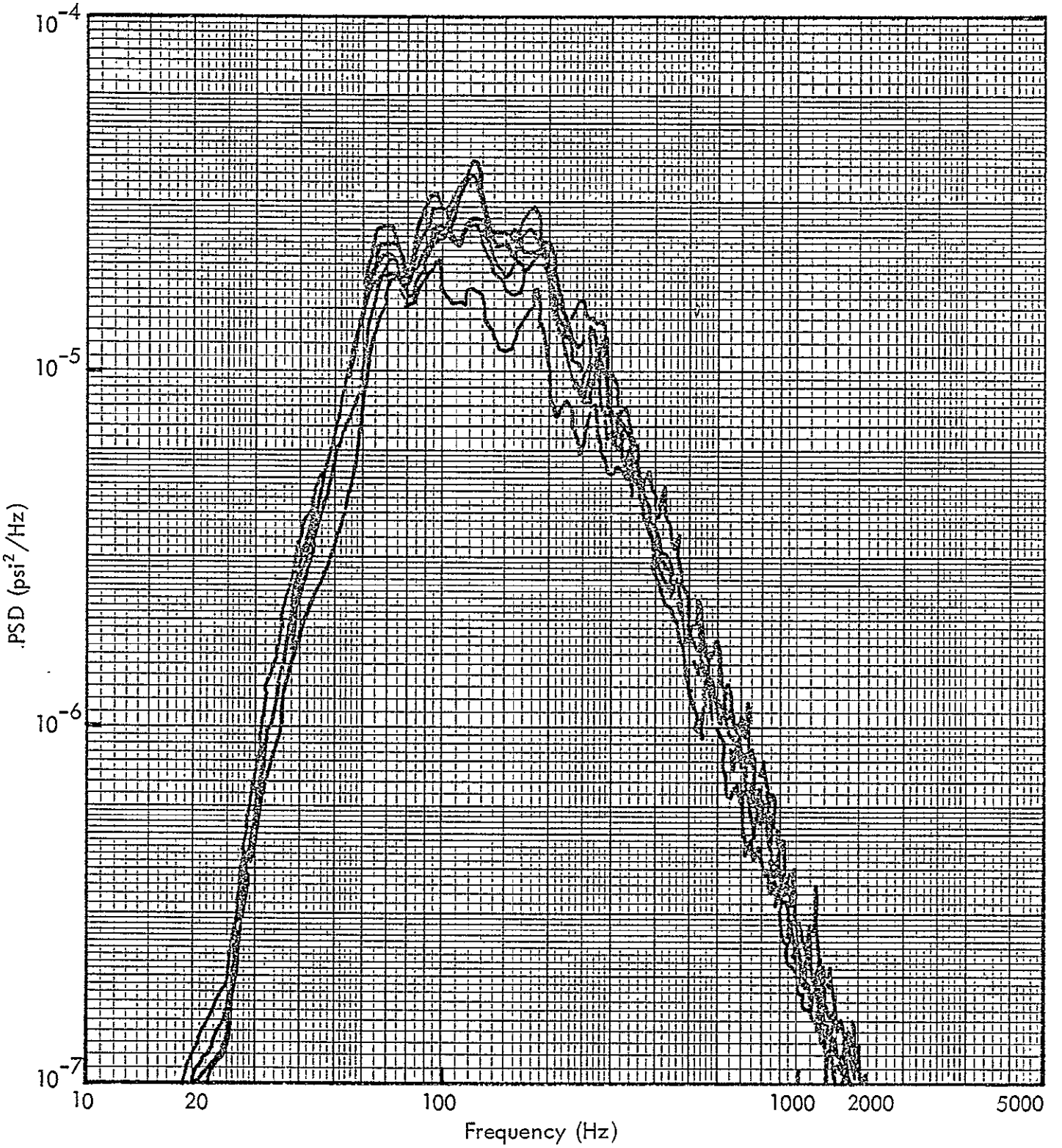

Figure 25. Free-Field Sound Pressure Levels

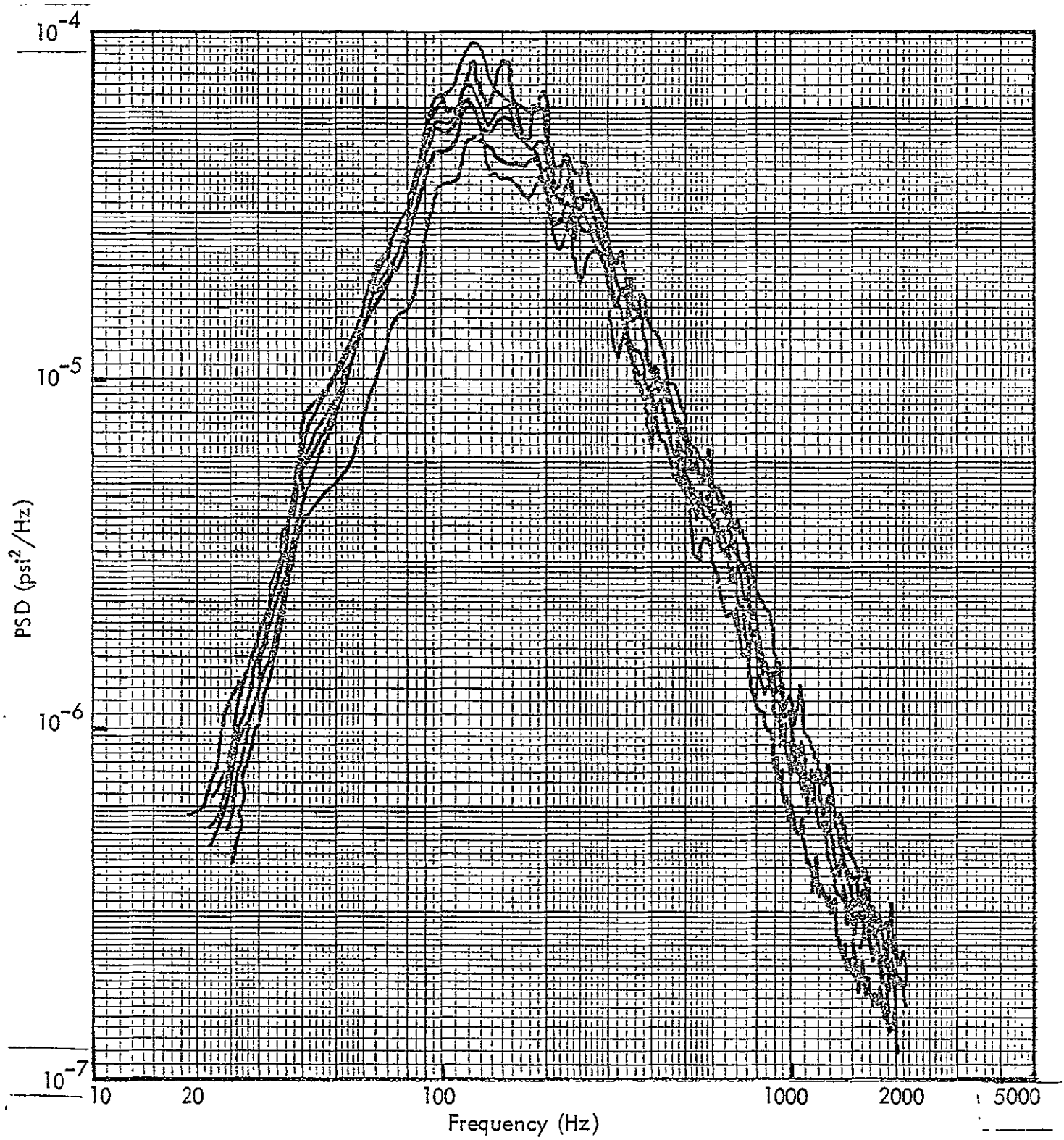

Figure 26. Surface Sound Pressure Levels

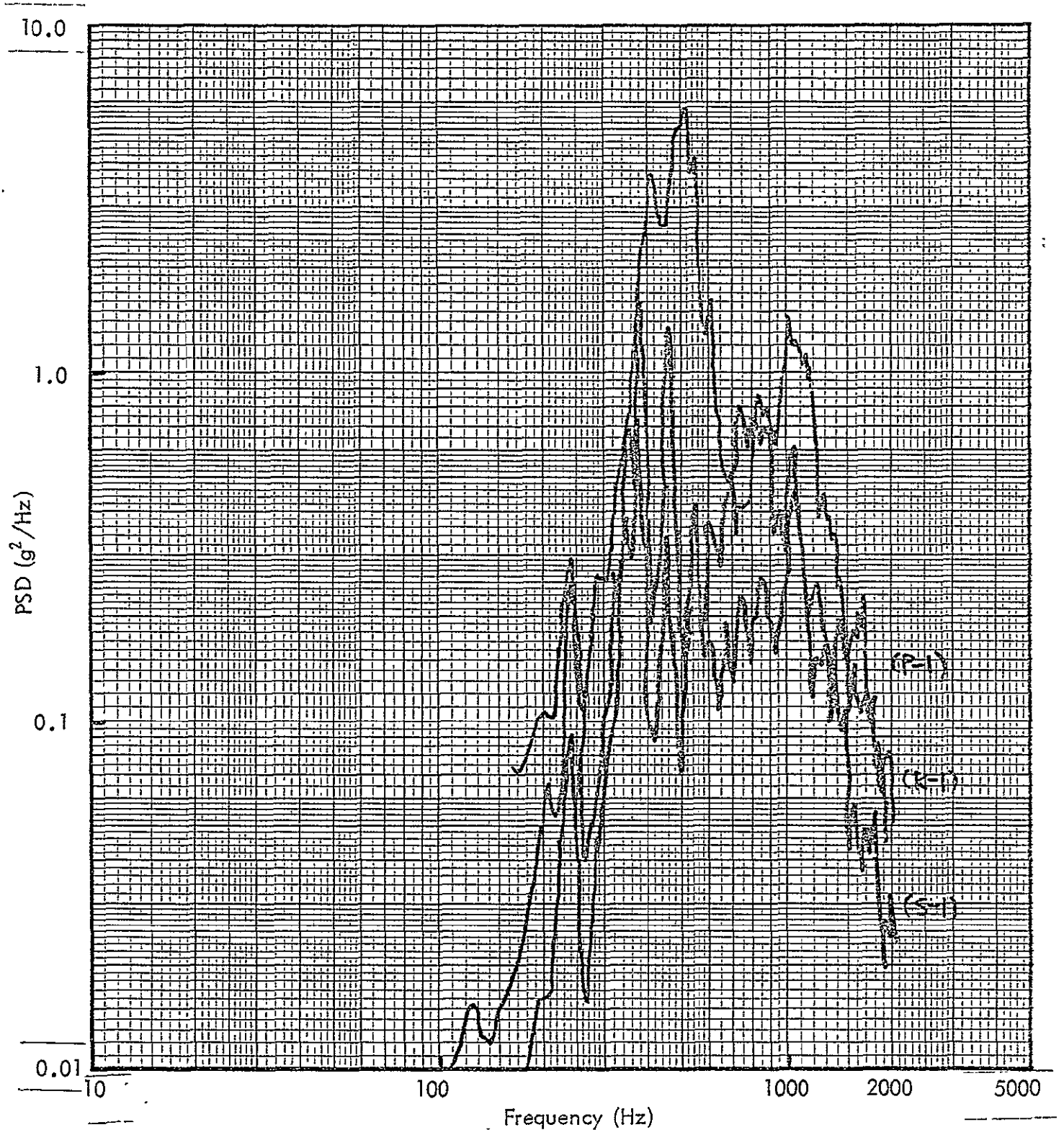

Figure 27. Measured Cylinder Responses Without Component Attached

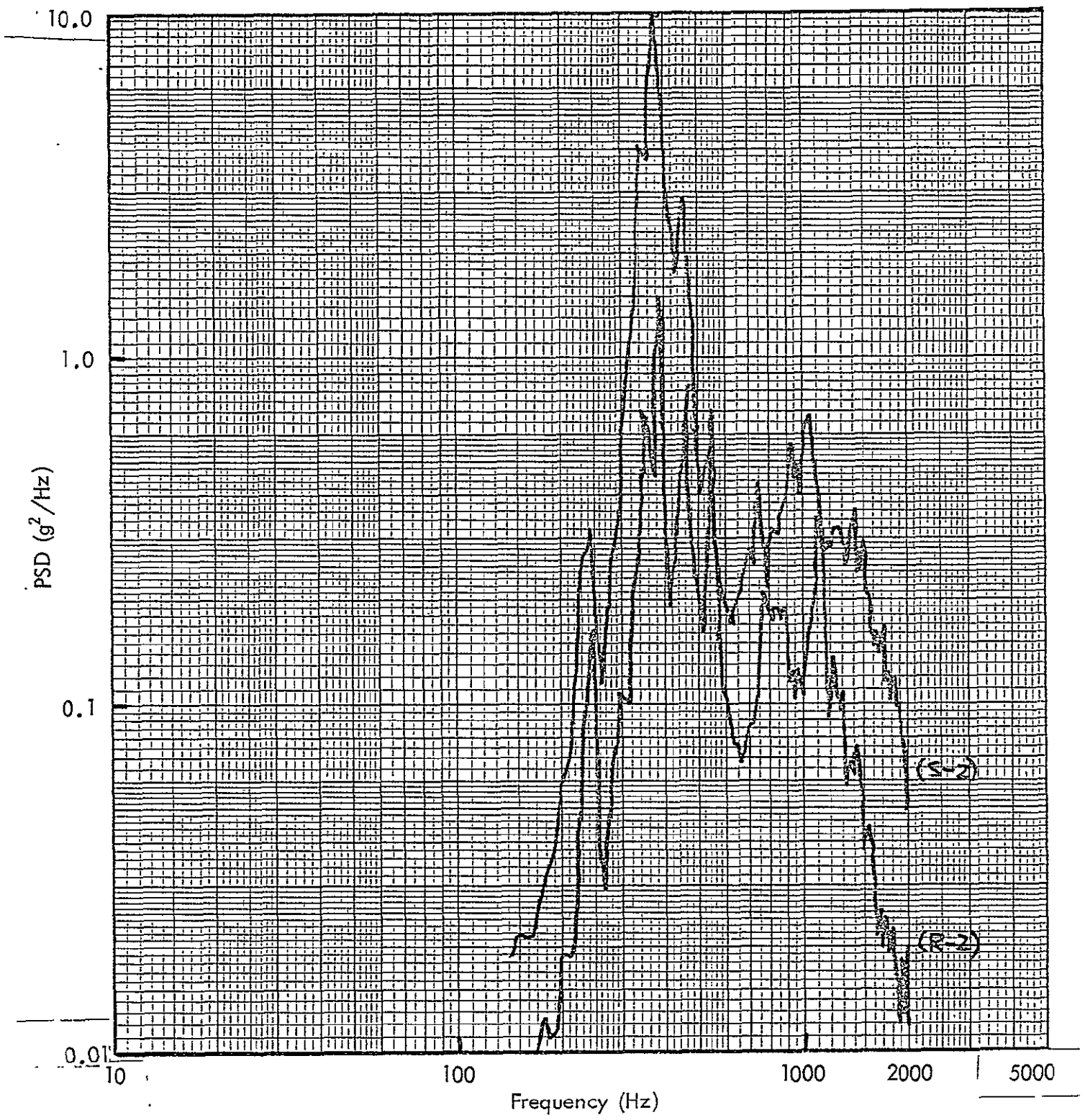

Figure 28. Measured Cylinder Responses With Component Attached

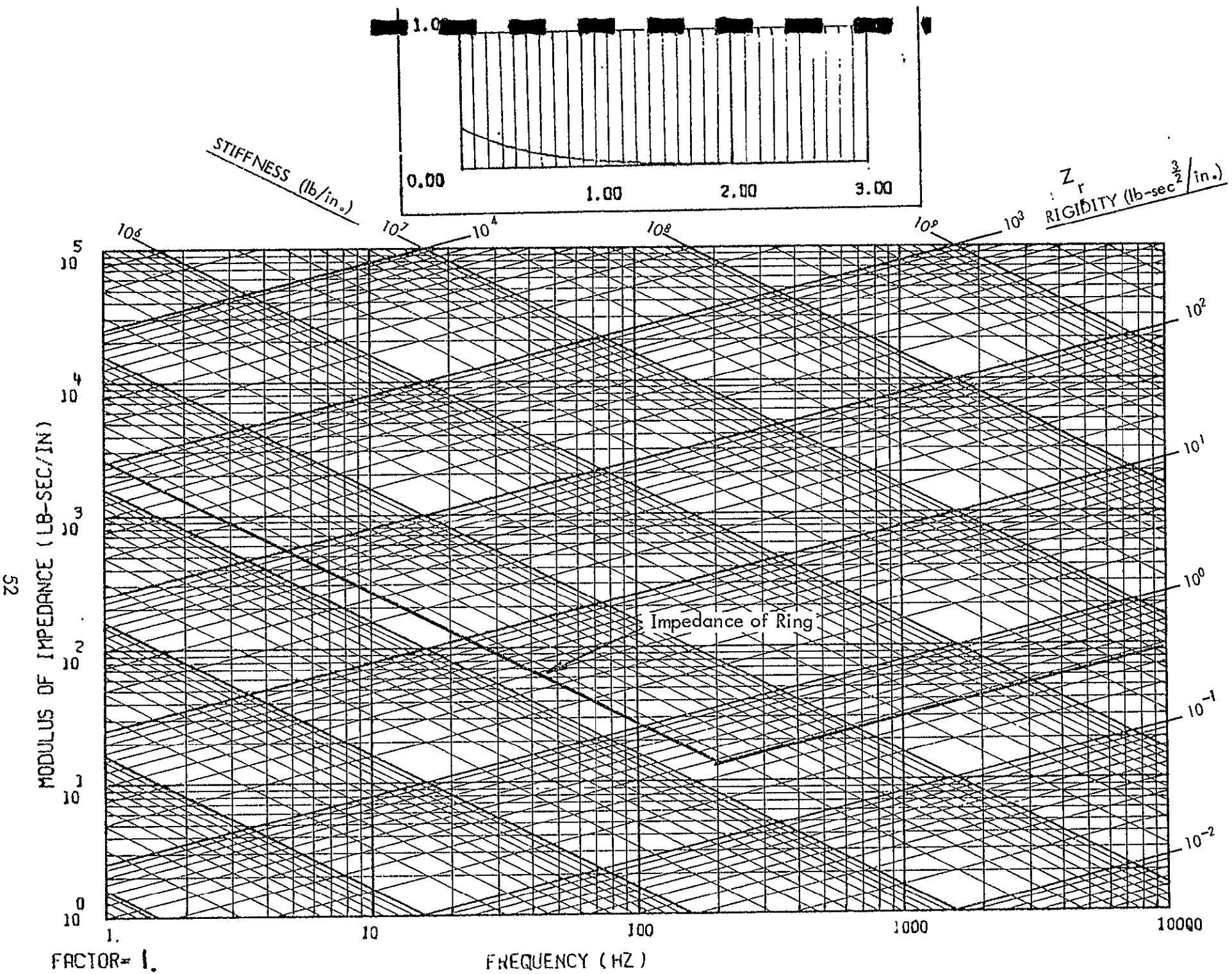

Figure 29. Impedance of Rings (at Location R)

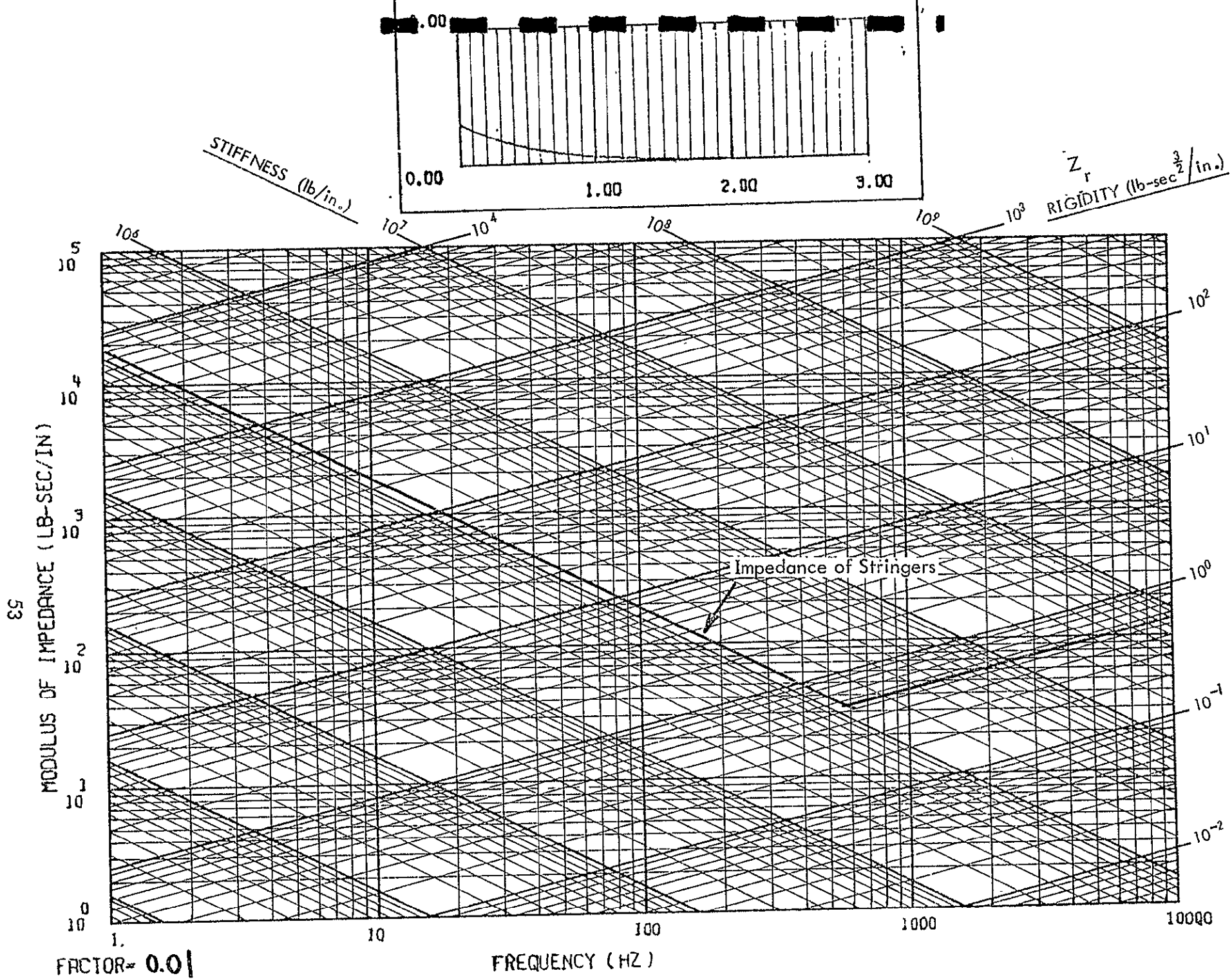

Figure 30. Impedance of Stringers

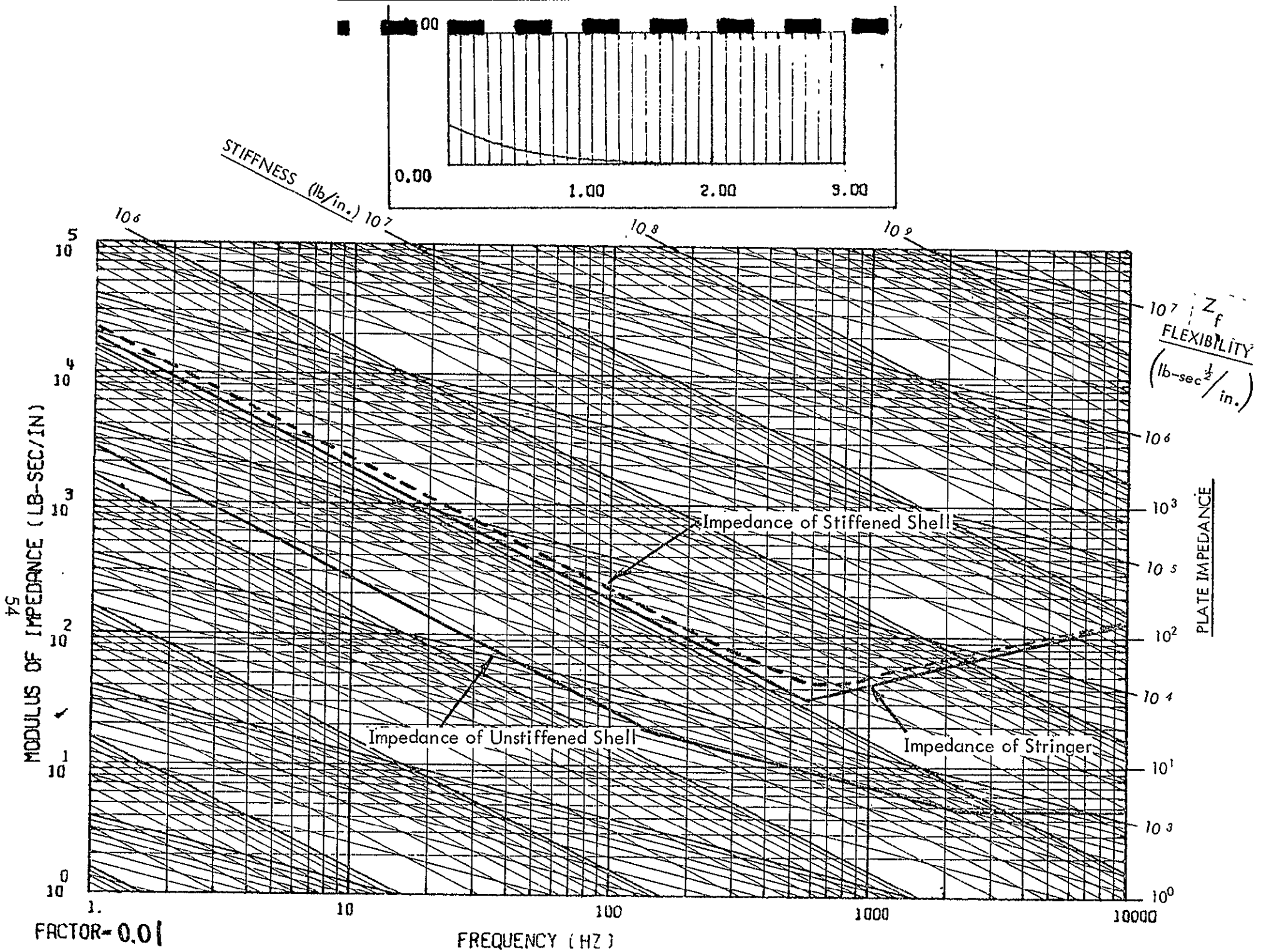

Figure 31. Impedance of Stiffened Shells (Impedance at Location S)

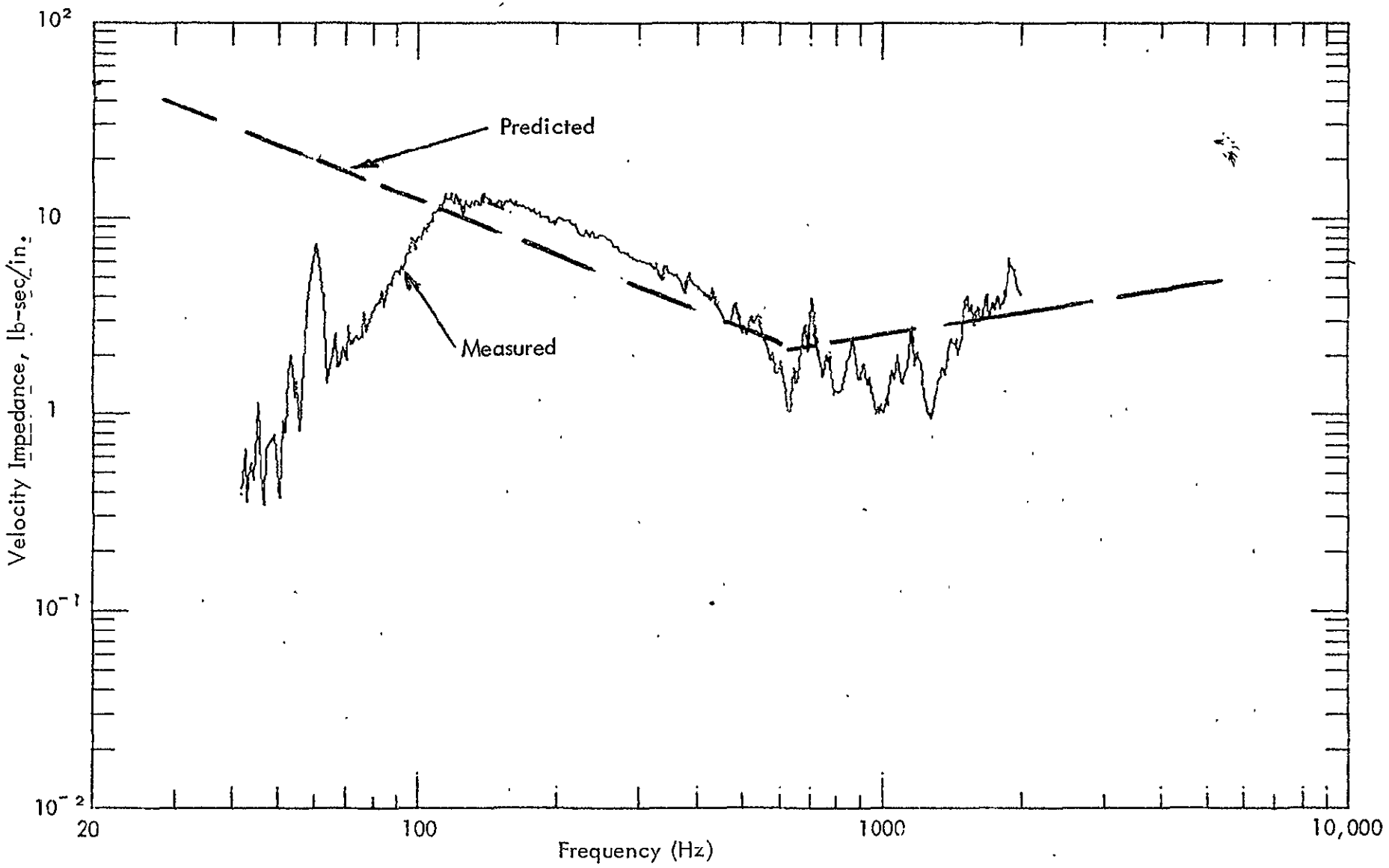

Figure 32. Summed Impedance at Location S (Ref. 3)

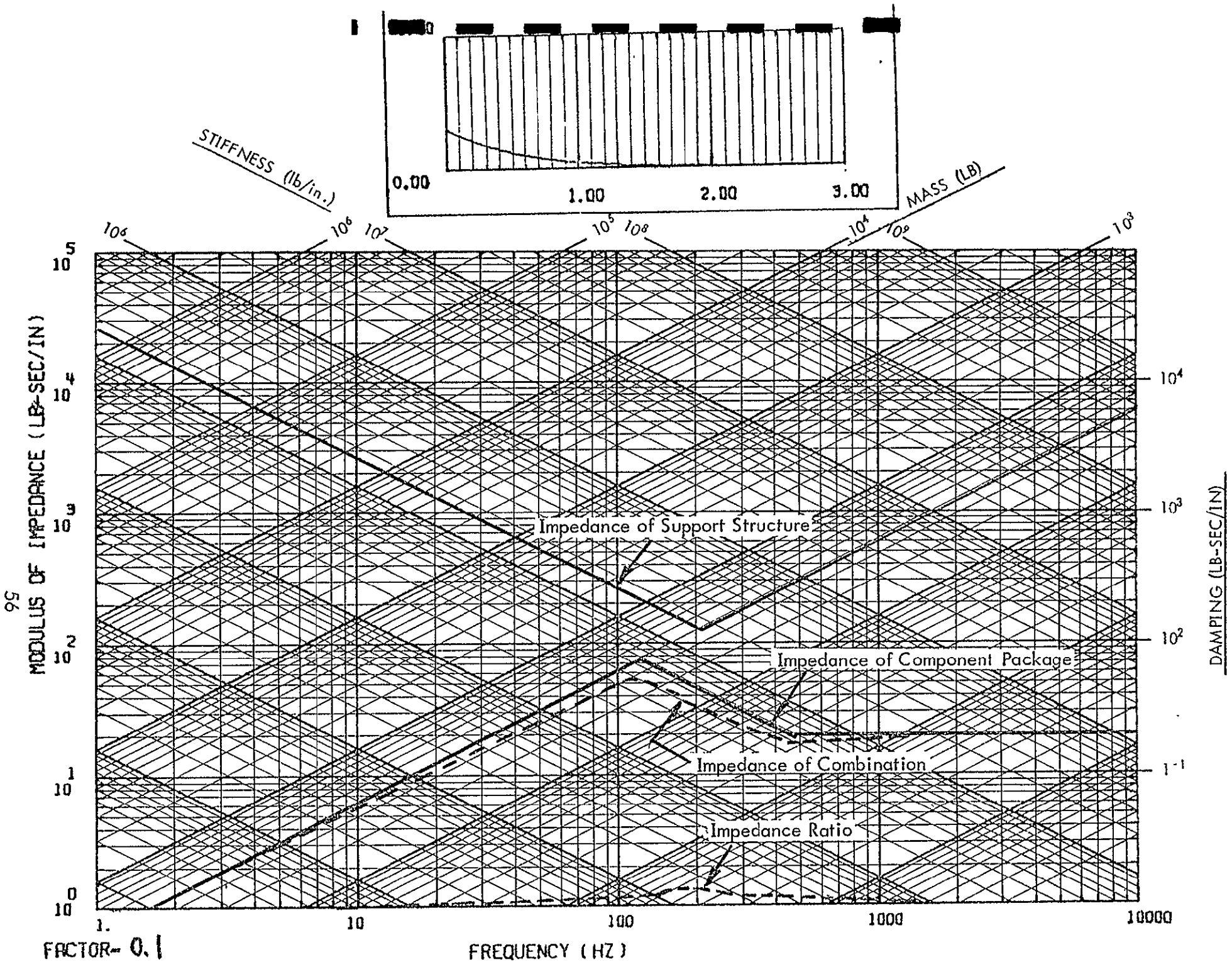

Figure 33. Impedance Ratio at Location R

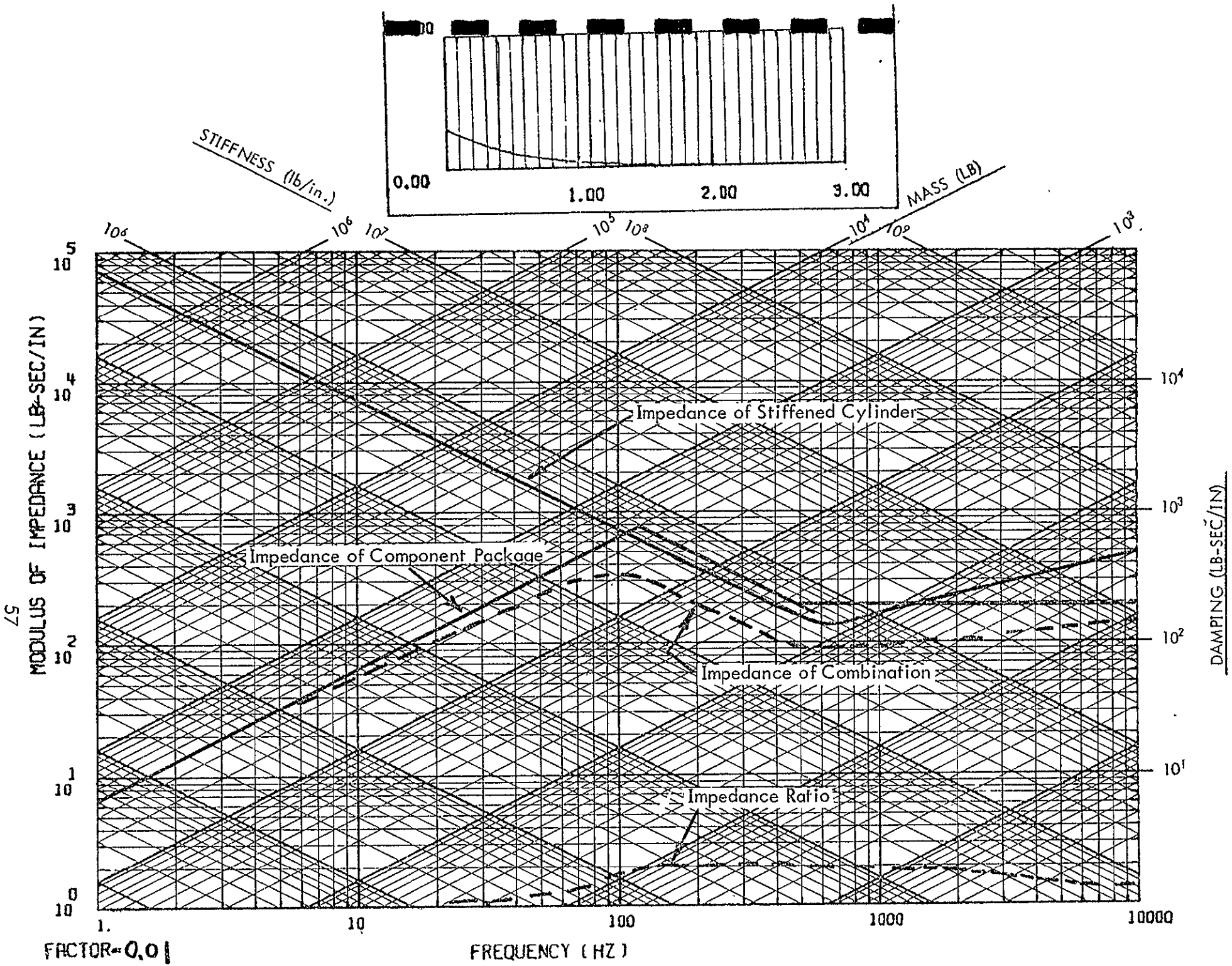

Figure 34. Impedance Ratio at Location S

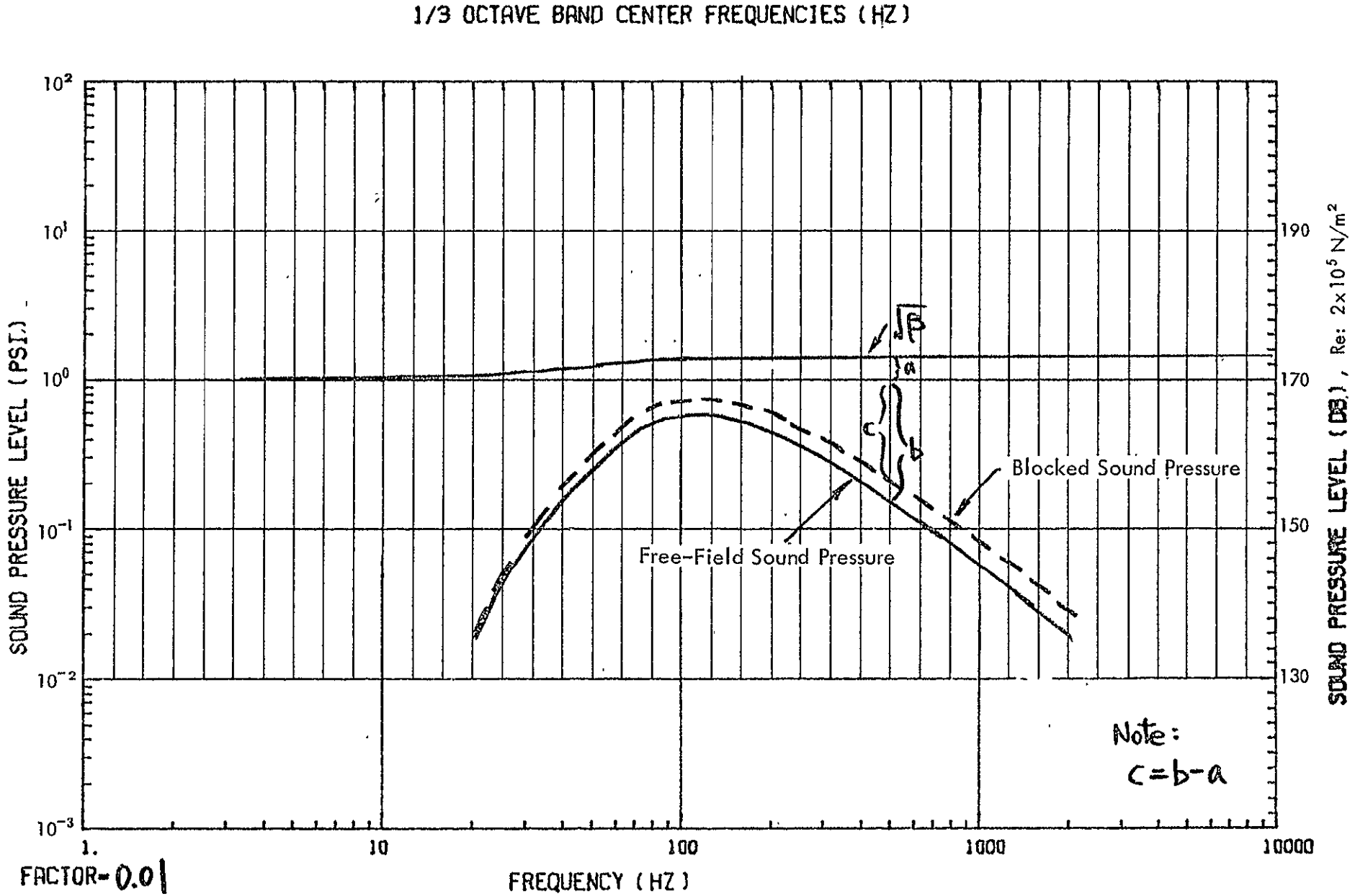

Figure 35. Determination of Blocked Sound Pressure Level

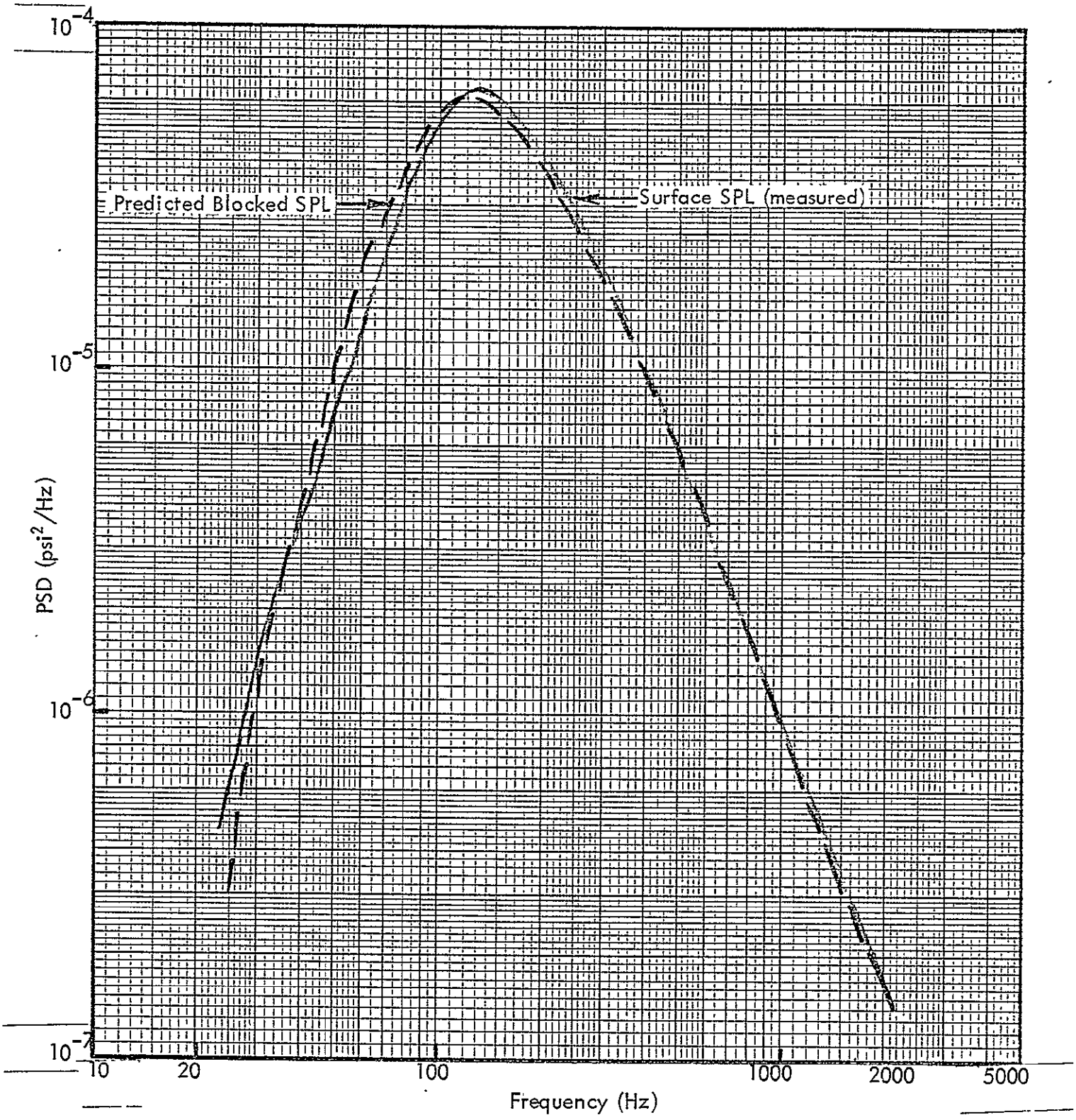

Figure 36. Blocked Sound Pressure Levels (SPL)

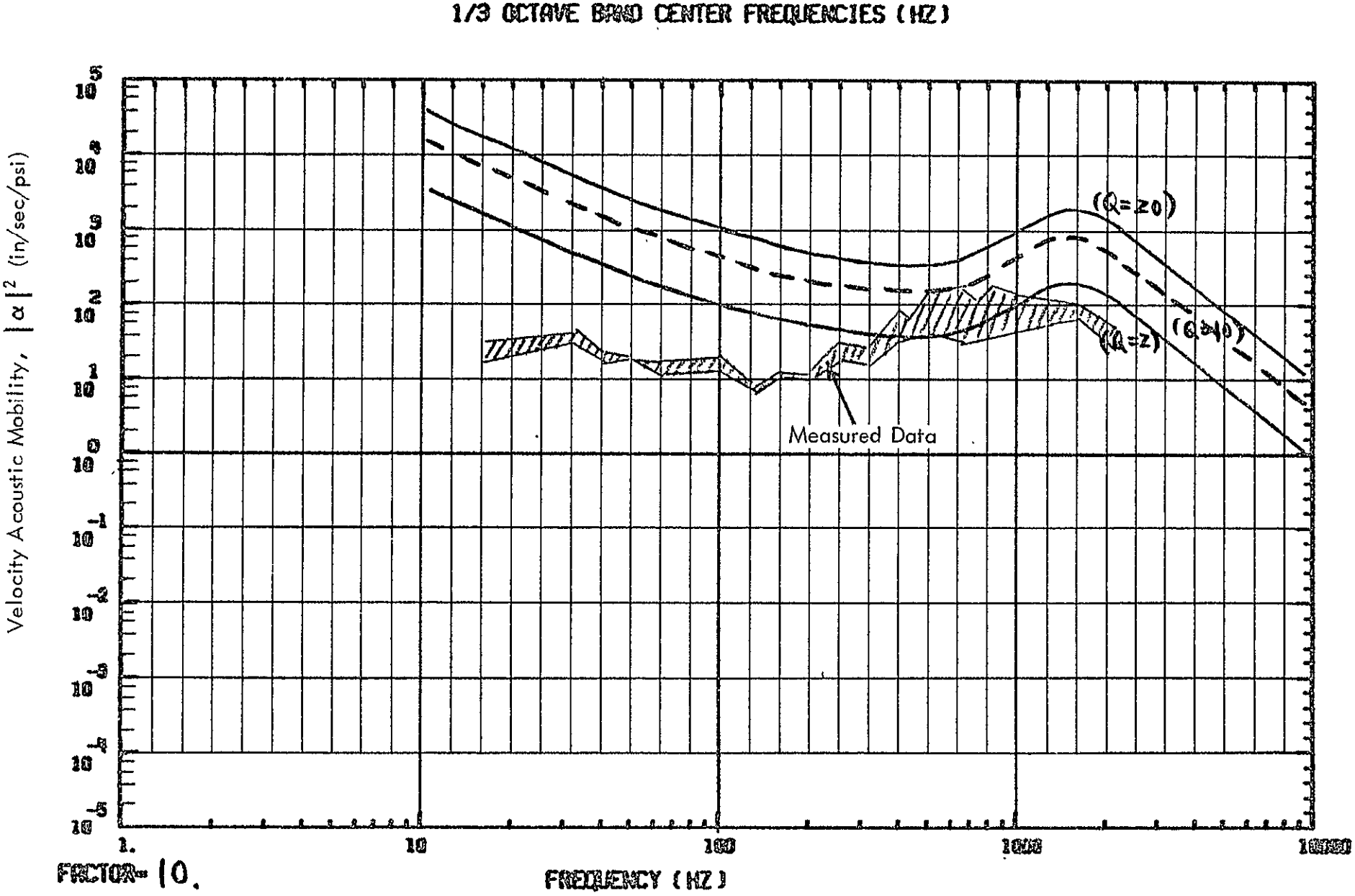

Figure 37. Velocity Acoustic Mobility of Cylinder

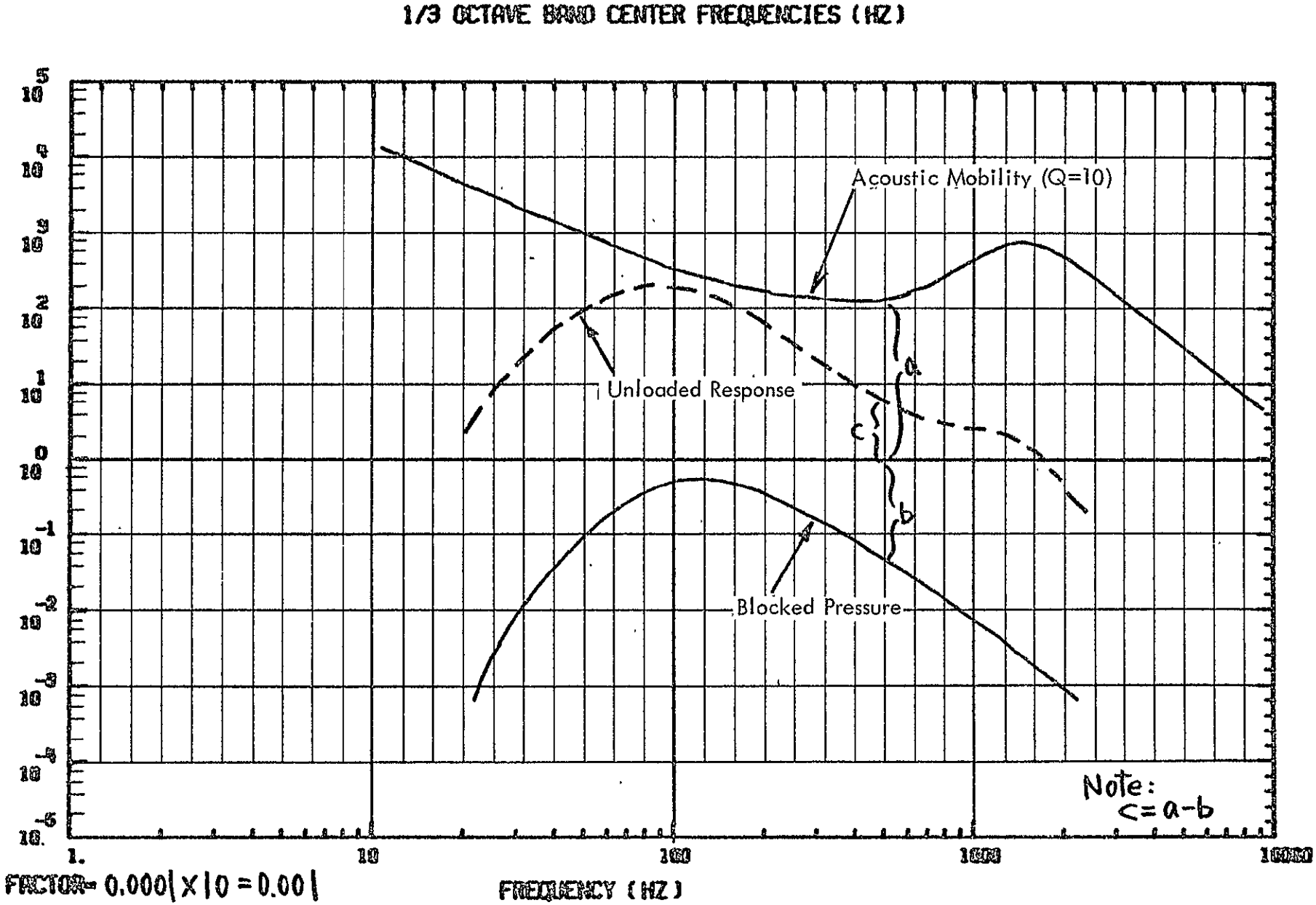

Figure 38. Determination of Unloaded Structural Response

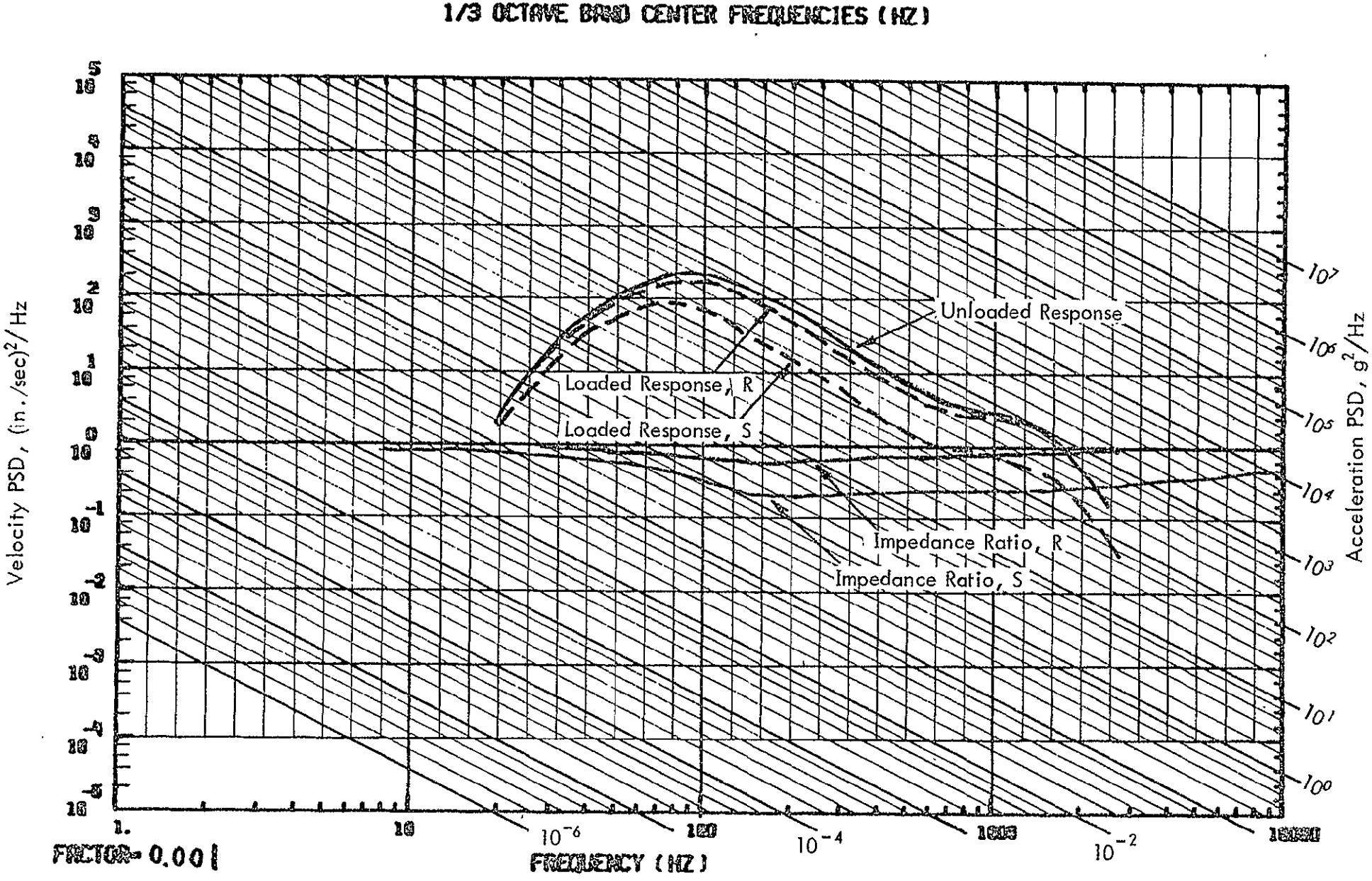

Figure 39. Prediction of Loaded Response Spectrum

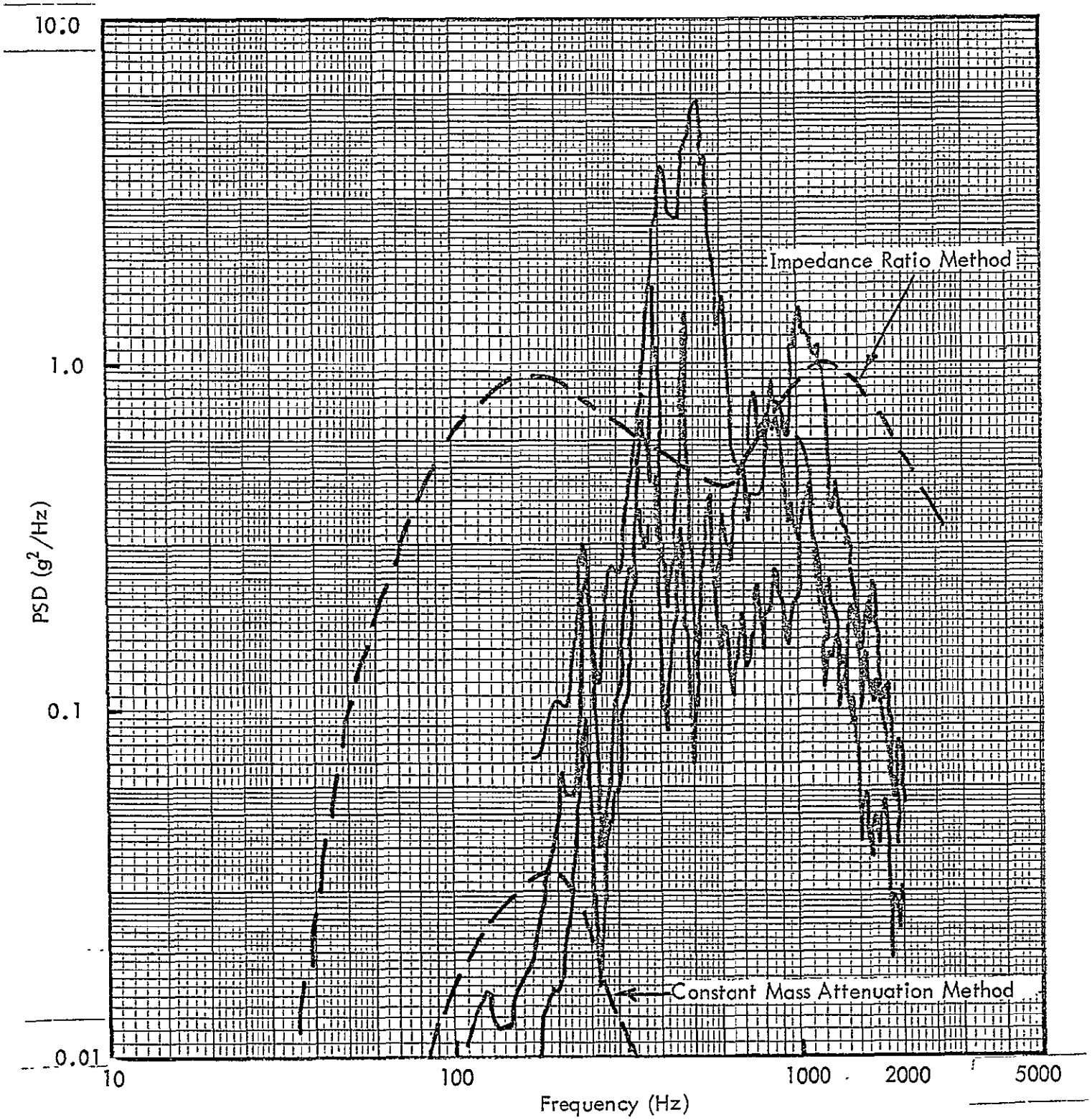

Figure 40. Measured, Unloaded Structural Acceleration Response

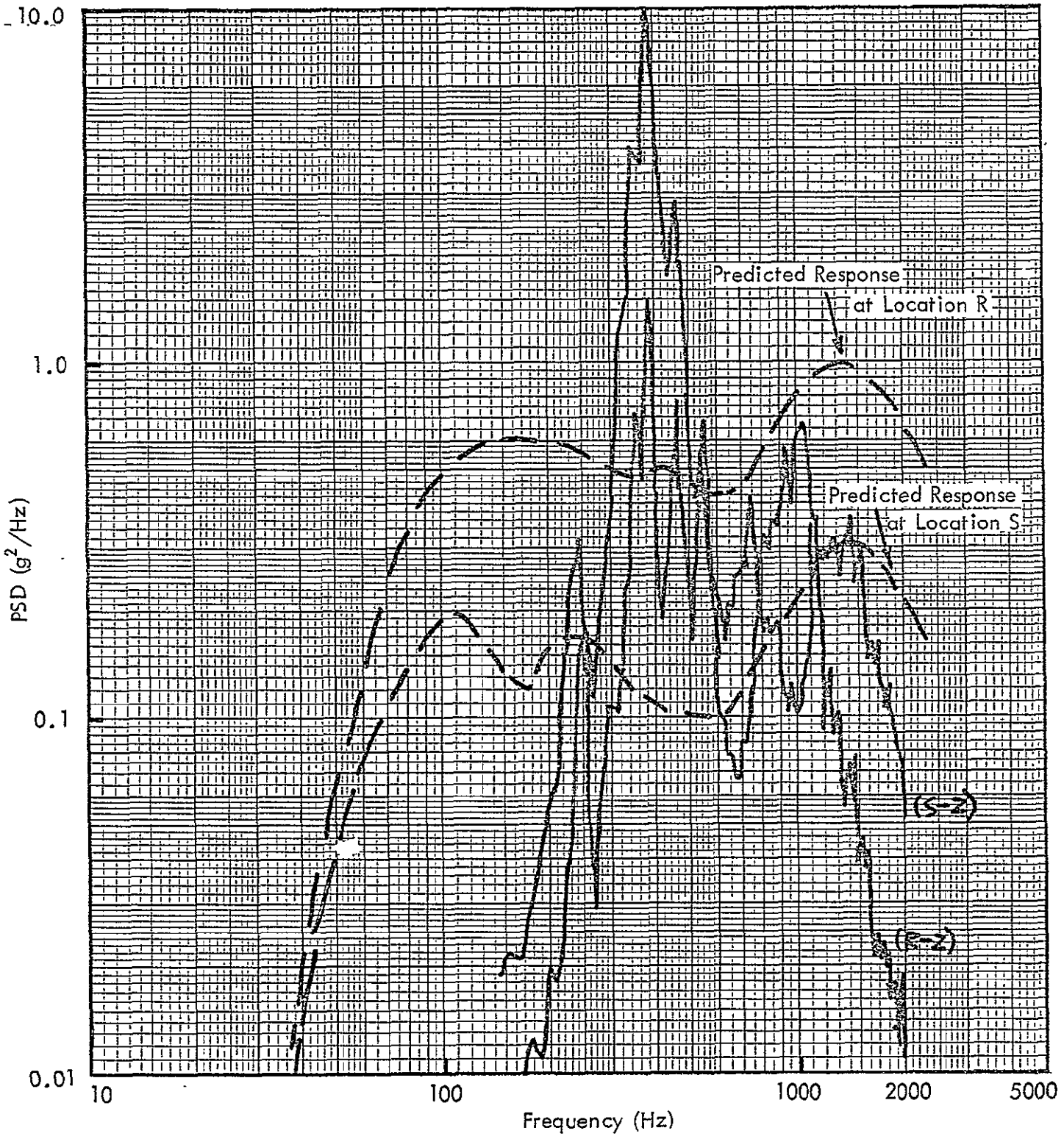

Figure 41. Measured, Loaded Structural Acceleration Response

APPENDIX A

VIBRO-ACOUSTIC DATA

APPENDIX A

VIBRO-ACOUSTIC DATA

In this appendix, the vibro-acoustic data obtained during the experimental program is presented in the form of:

- One-third octave band sound pressure levels (SPL)
- One-third octave band acceleration response levels
- Power spectral densities of SPL
- Power spectral densities of acceleration response

These measurements are presented in graphical form; the locations of the transducers have been defined in the main text.

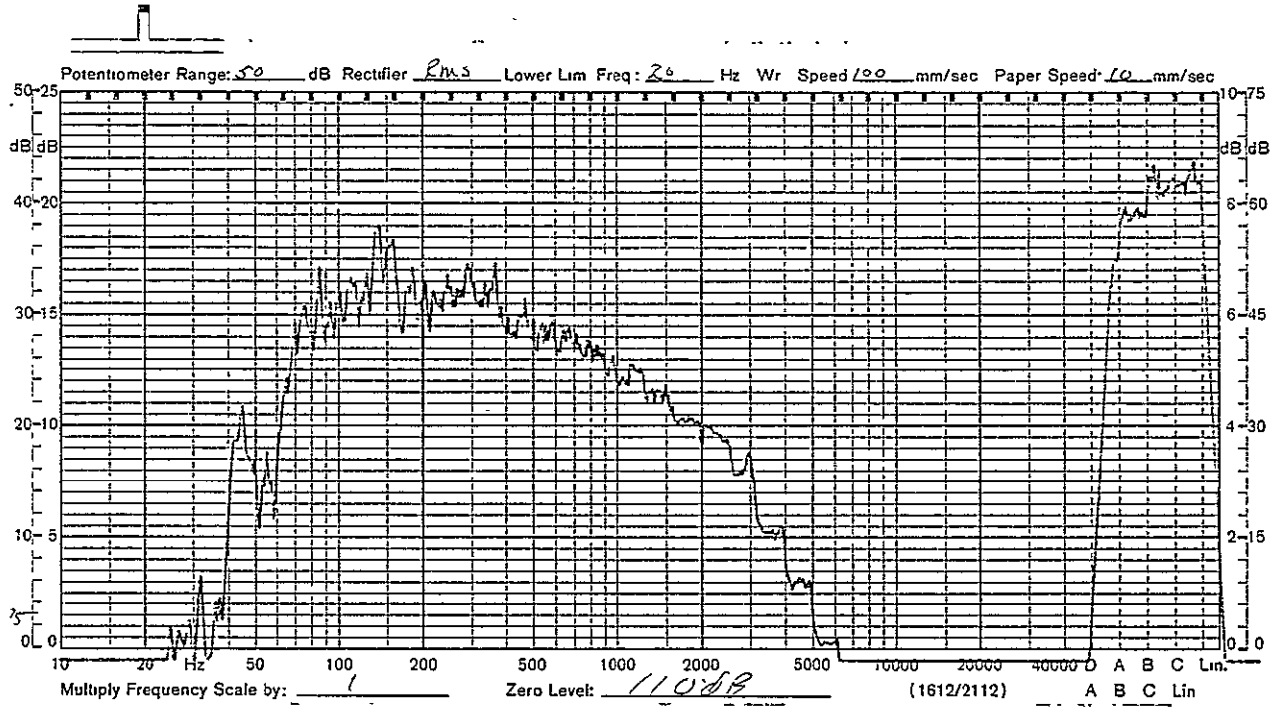

(a) Microphone M1

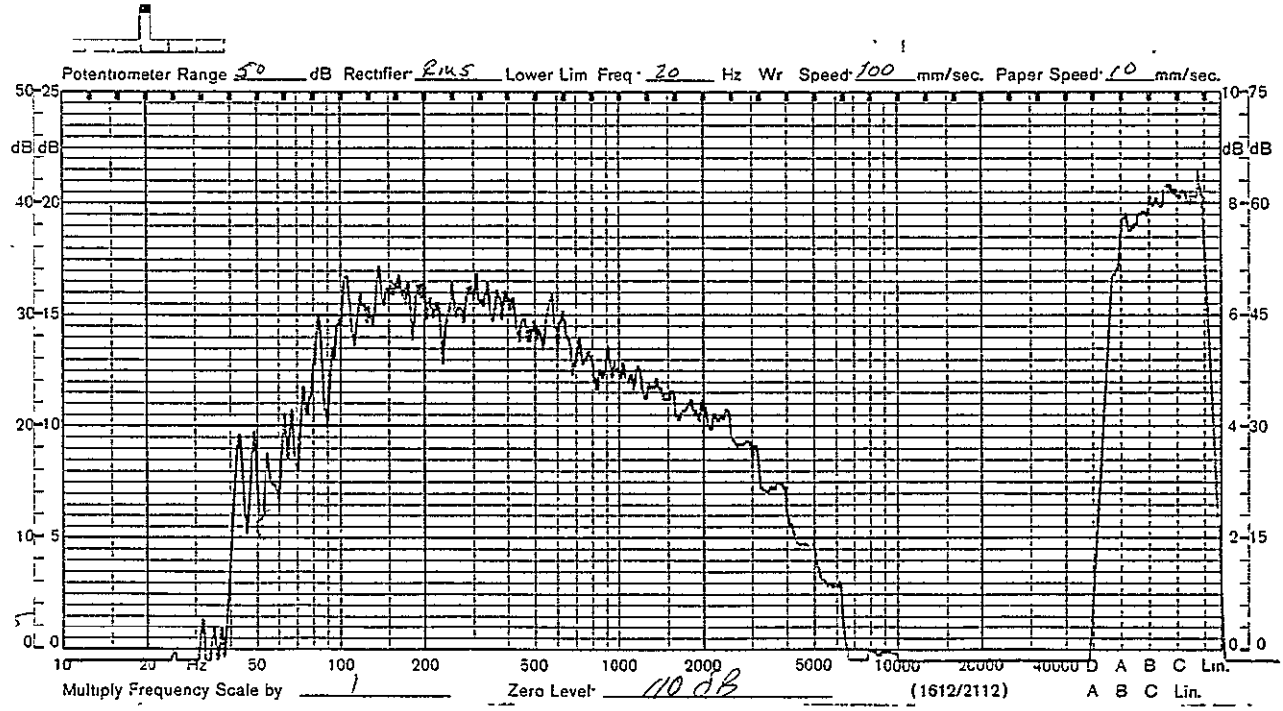

(b) Microphone M2

Figure A-1. Measured 1/3-Octave Sound Pressure Levels During Test Run P-1

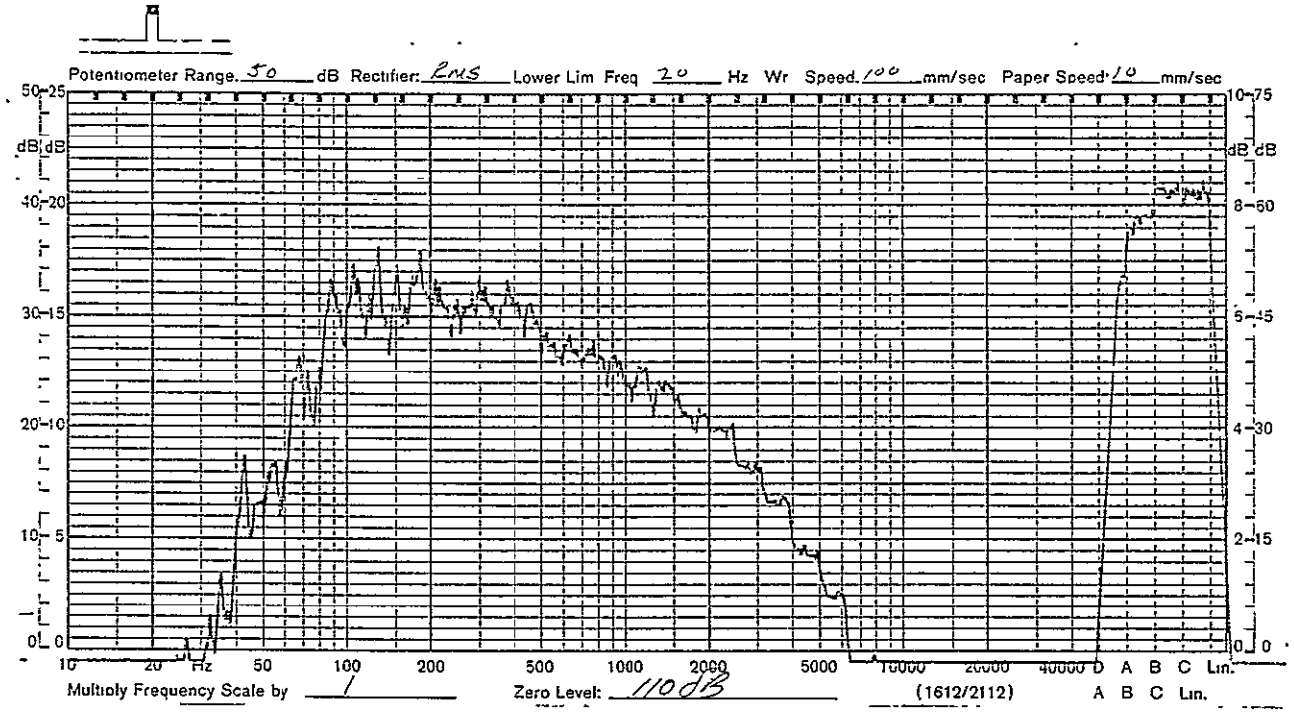

(c) Microphone M3

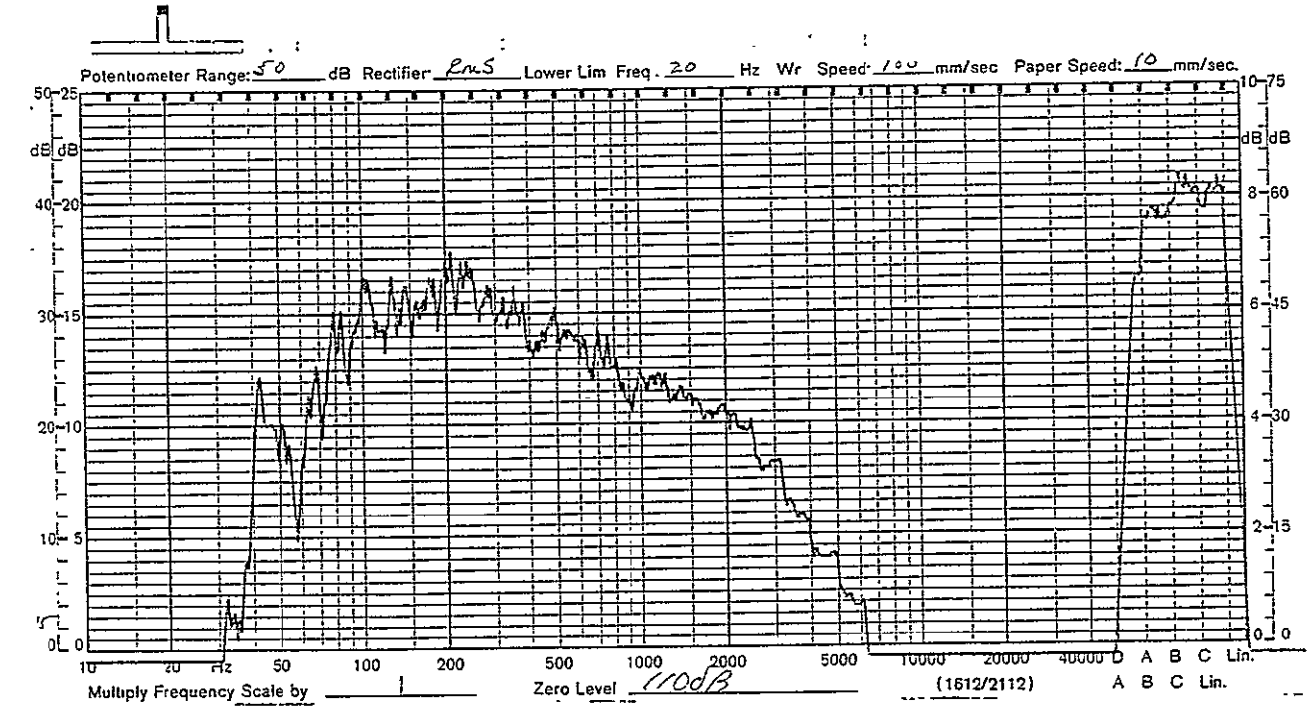

(d) Microphone M4

Figure A-1. (Concluded)

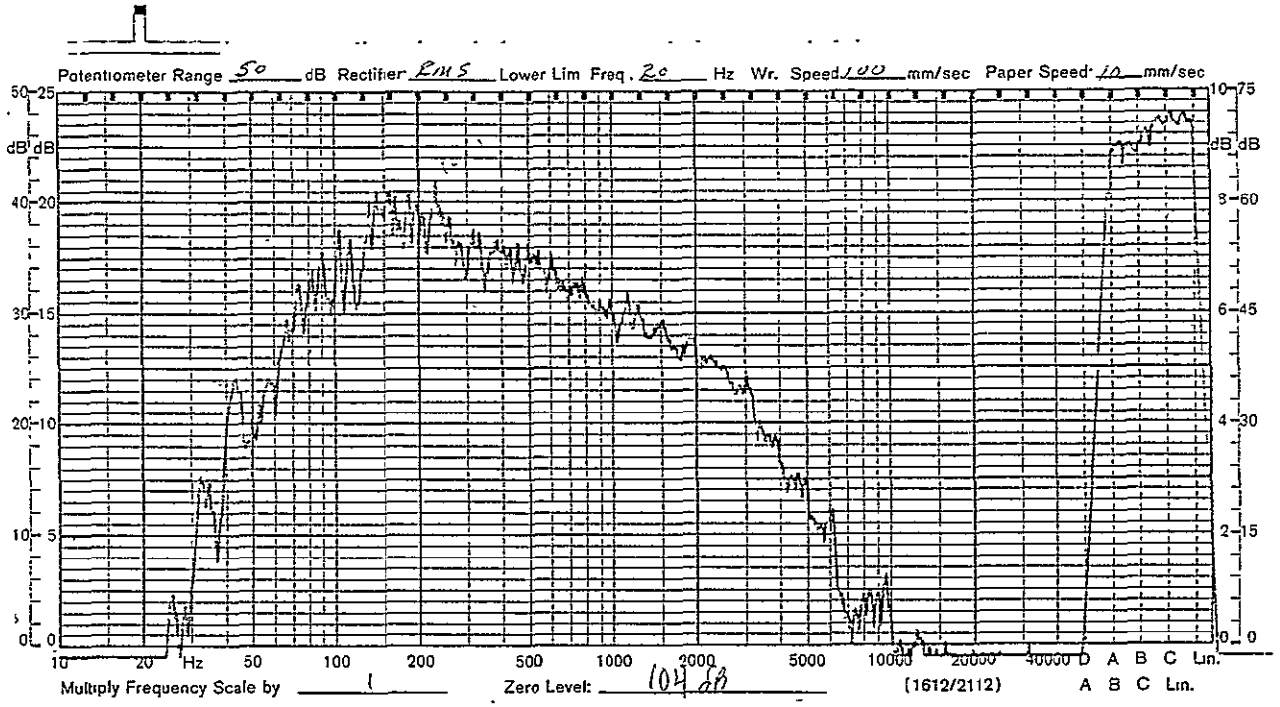

Figure A-2. Averaged 1/3-Octave Sound Pressure During Test Run P-1

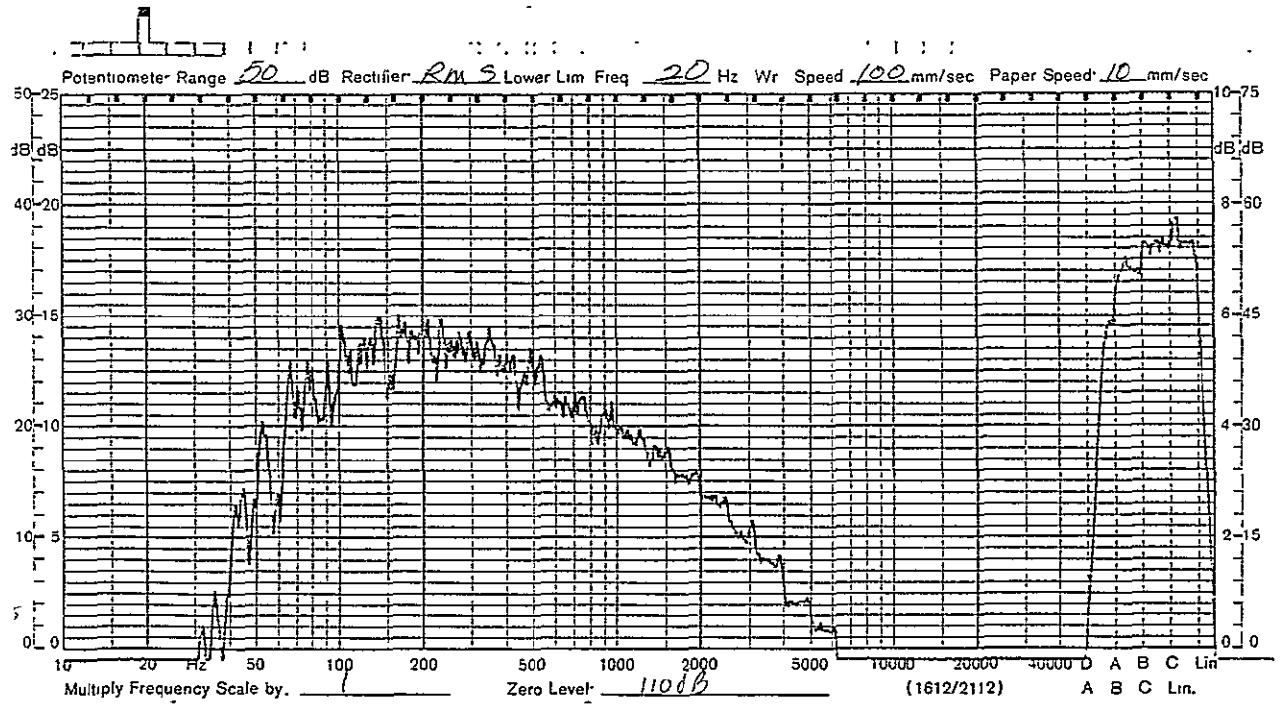

Figure A-3. Measured 1/3-Octave Sound Pressure of Control Microphone M5 During Test Run P-1

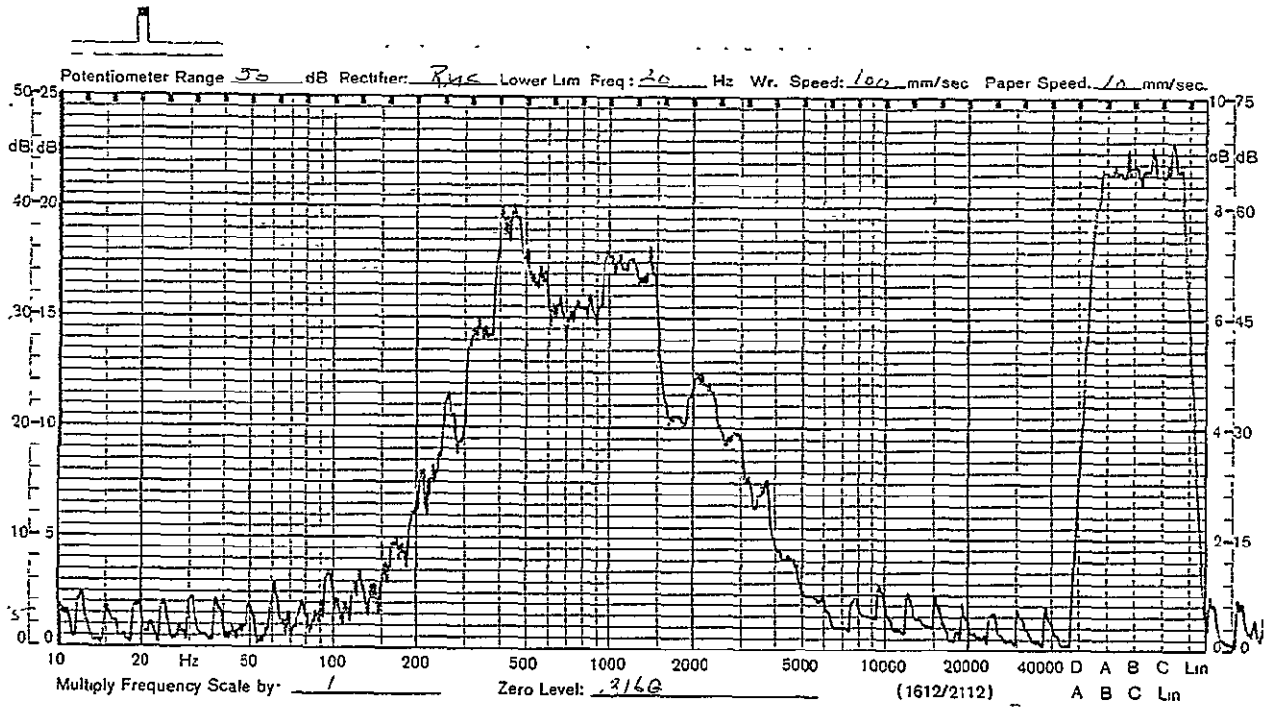

(a) Accelerometer A1

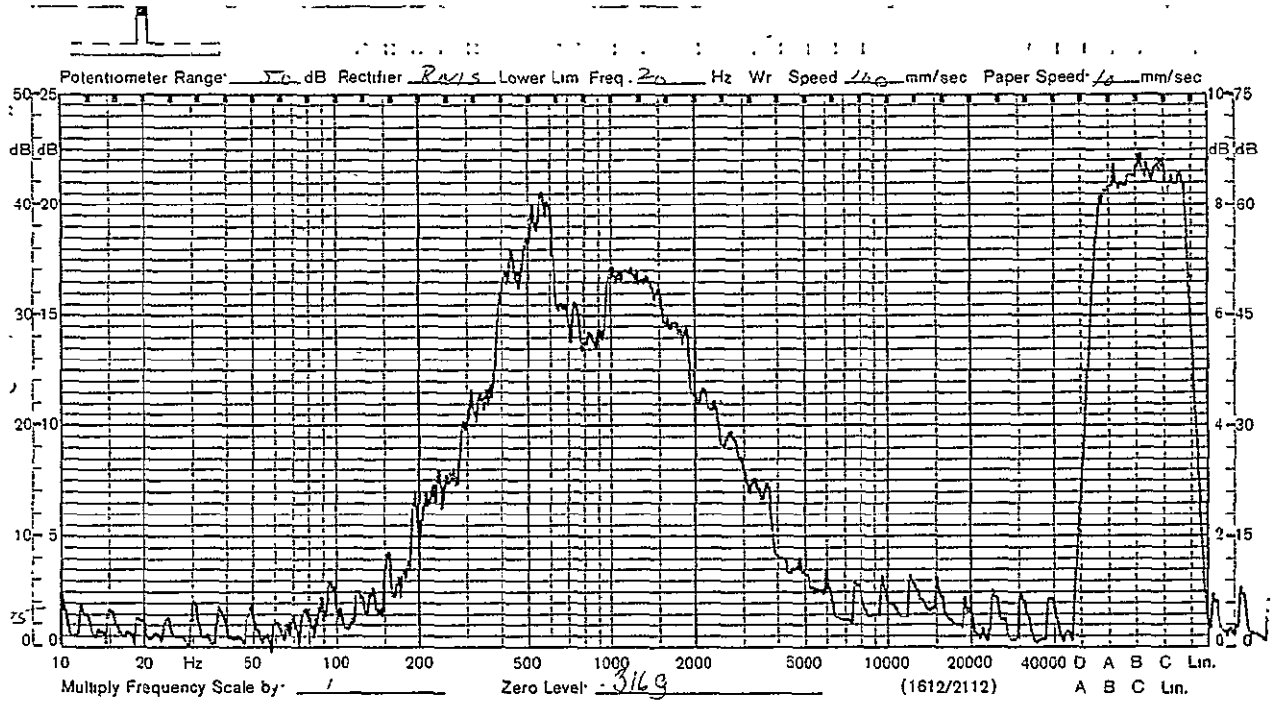

(b) Accelerometer A2

Figure A-4. Measured 1/3-Octave Acceleration Response Levels During Test Run P-1

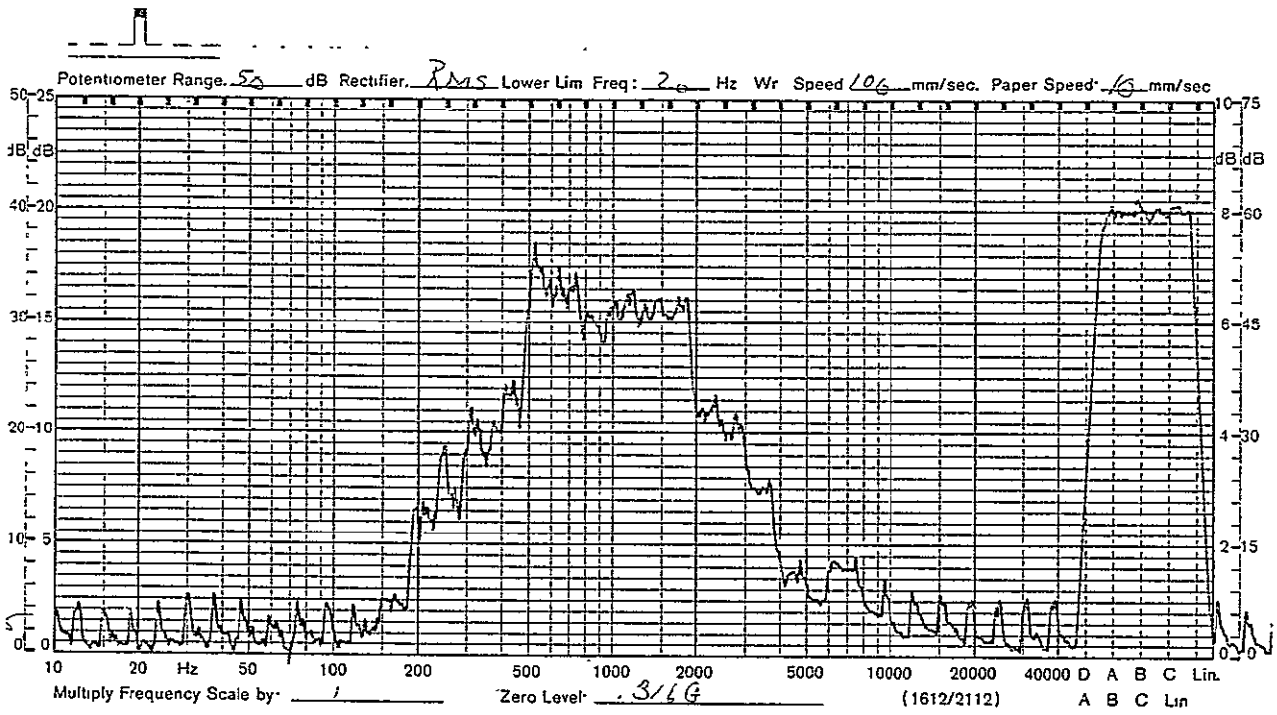

(c) Accelerometer A3

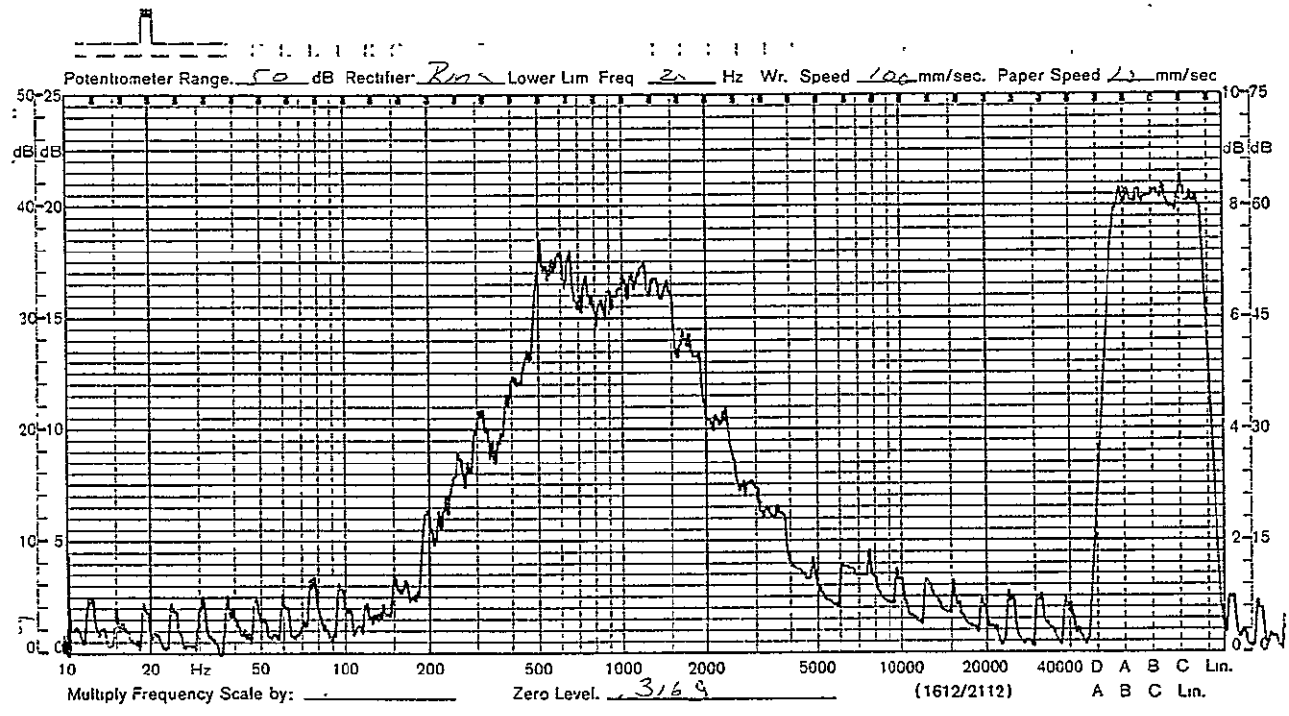

(d) Accelerometer A4

Figure A-4. (Concluded)

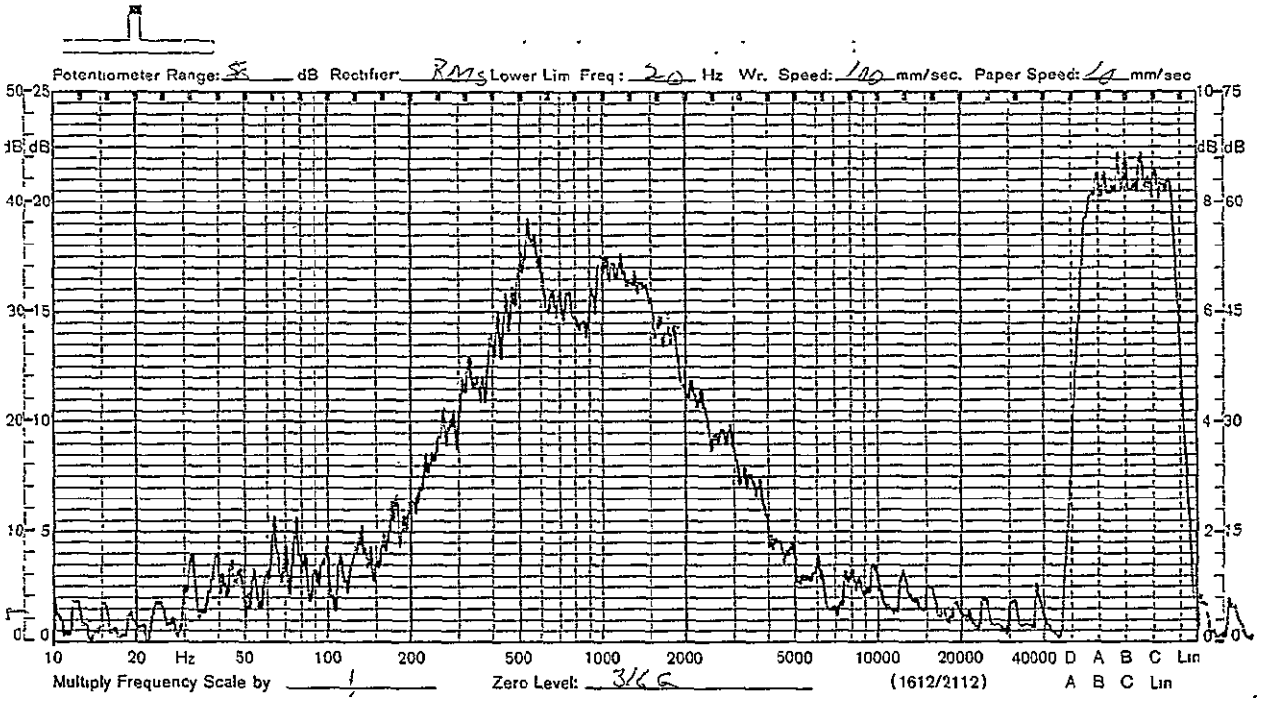

Figure A-5. Averaged 1/3-Octave Acceleration Response During Test Run P-1

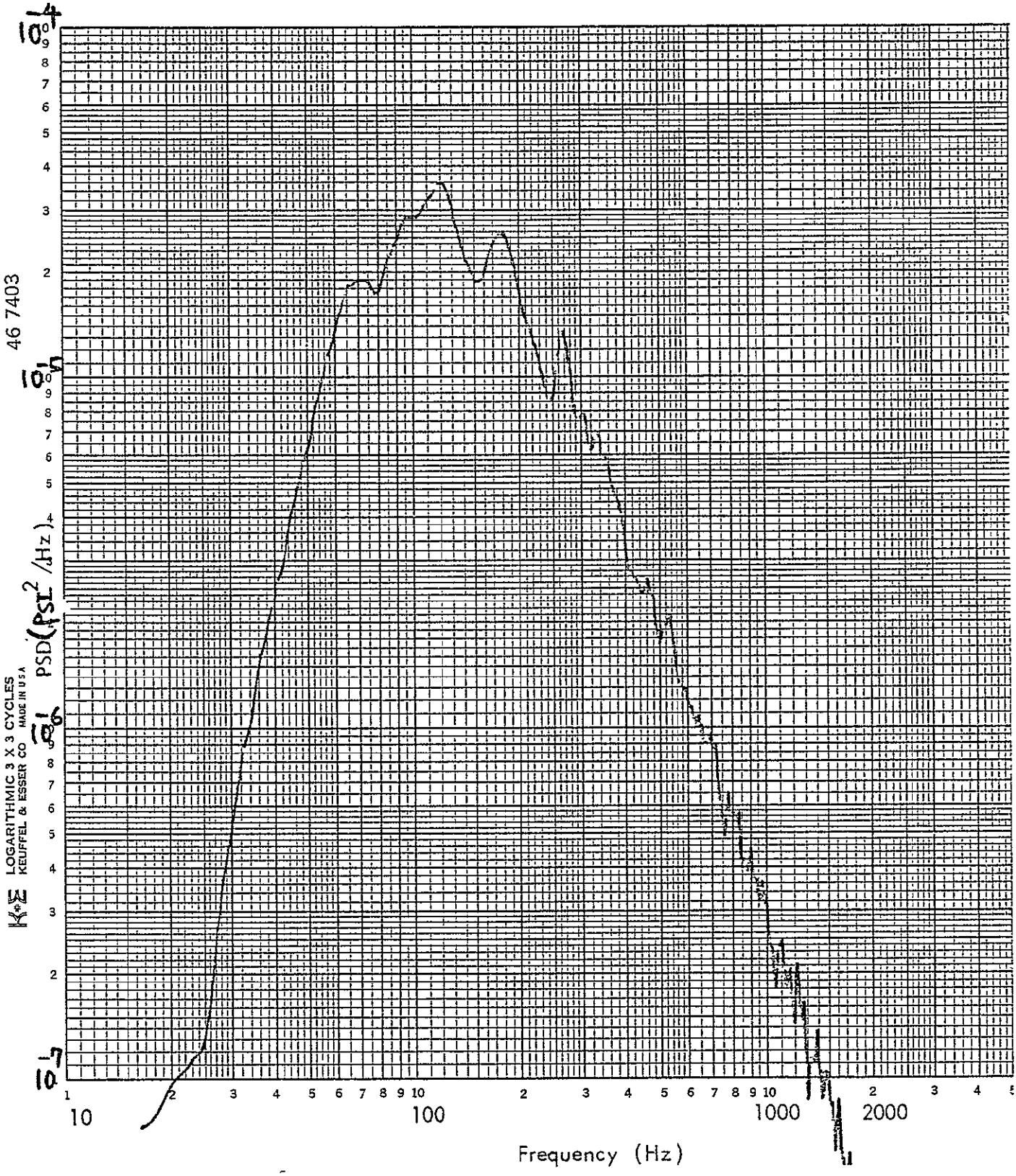

Figure A-6. Power Spectral Density (PSD) of Microphone M5, Test Run P-1

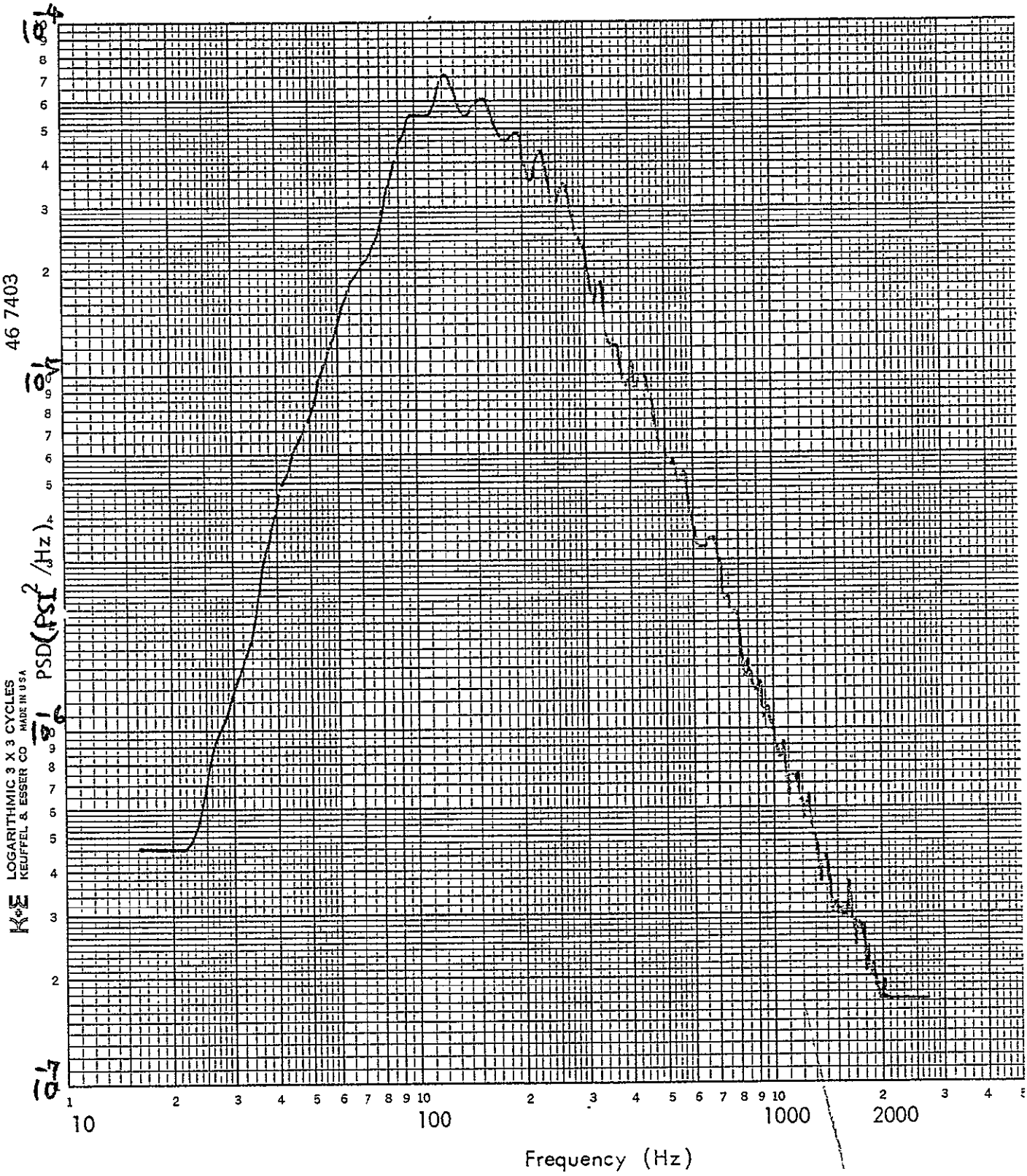

Figure A-7. PSD of Averaged Sound Pressure Levels, Test Run P-1

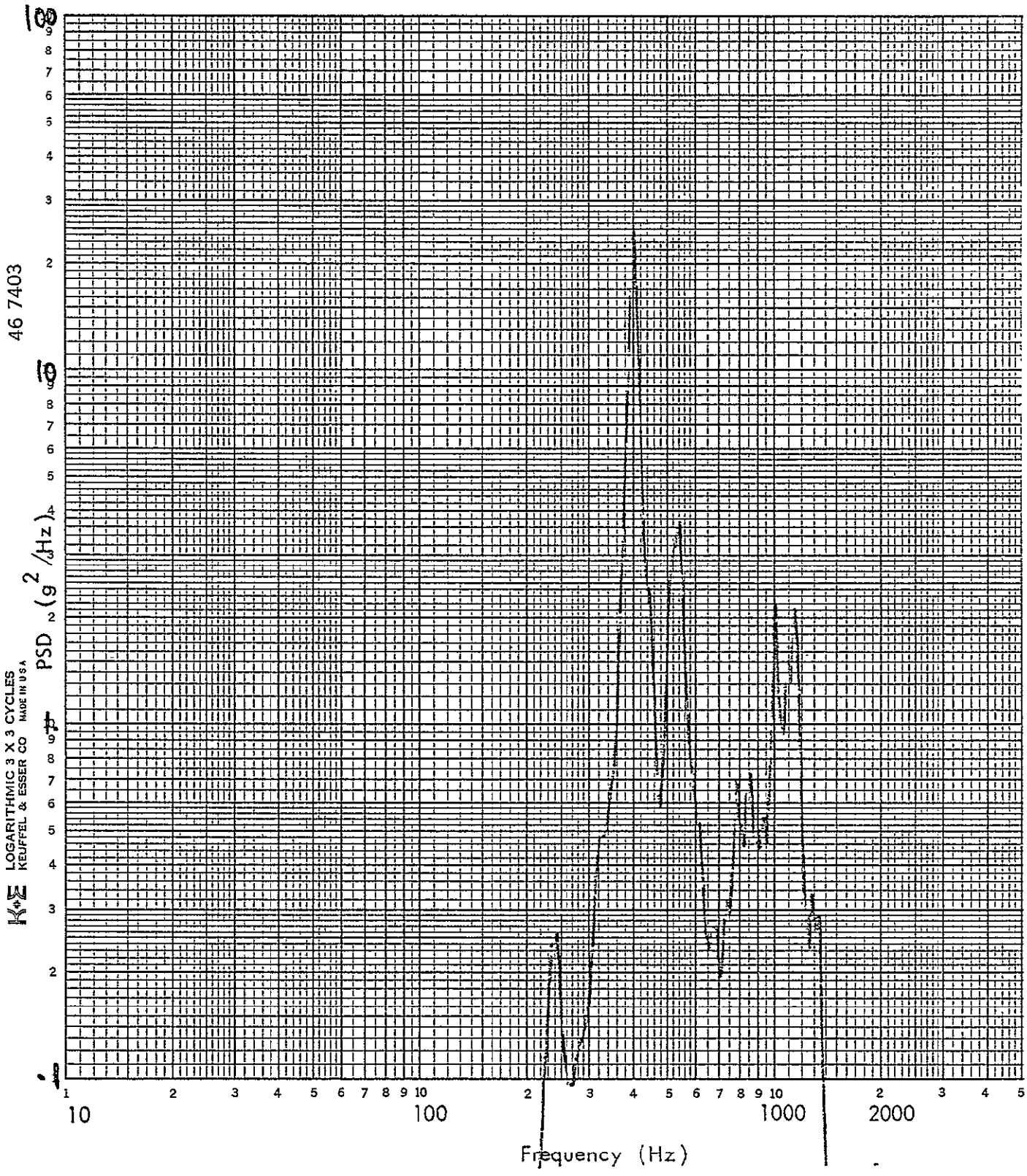

Figure A-8. PSD of Accelerometer A1, Test Run P-1

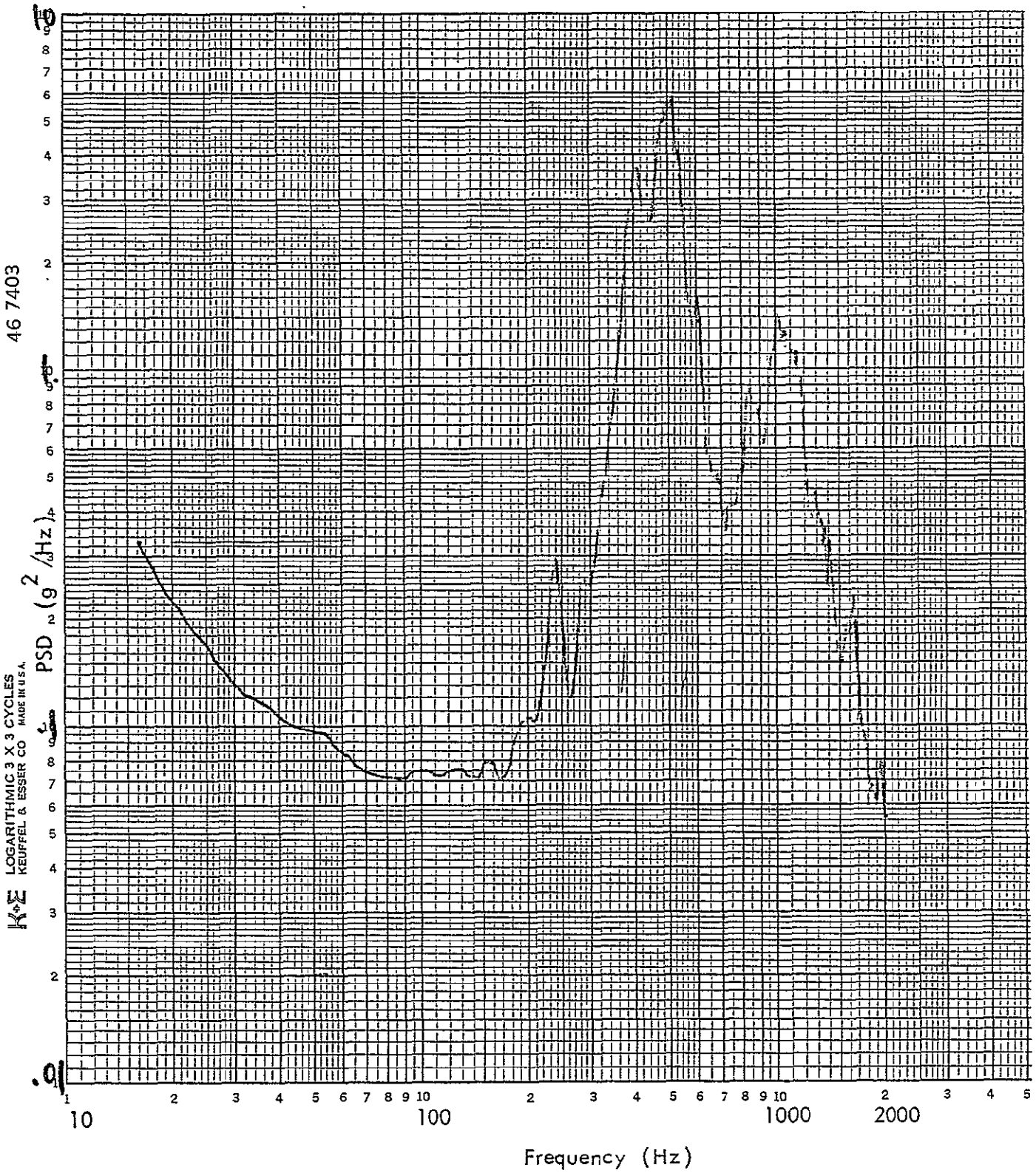

Figure A-9. PSD of Averaged Acceleration Responses, Test Run P-1

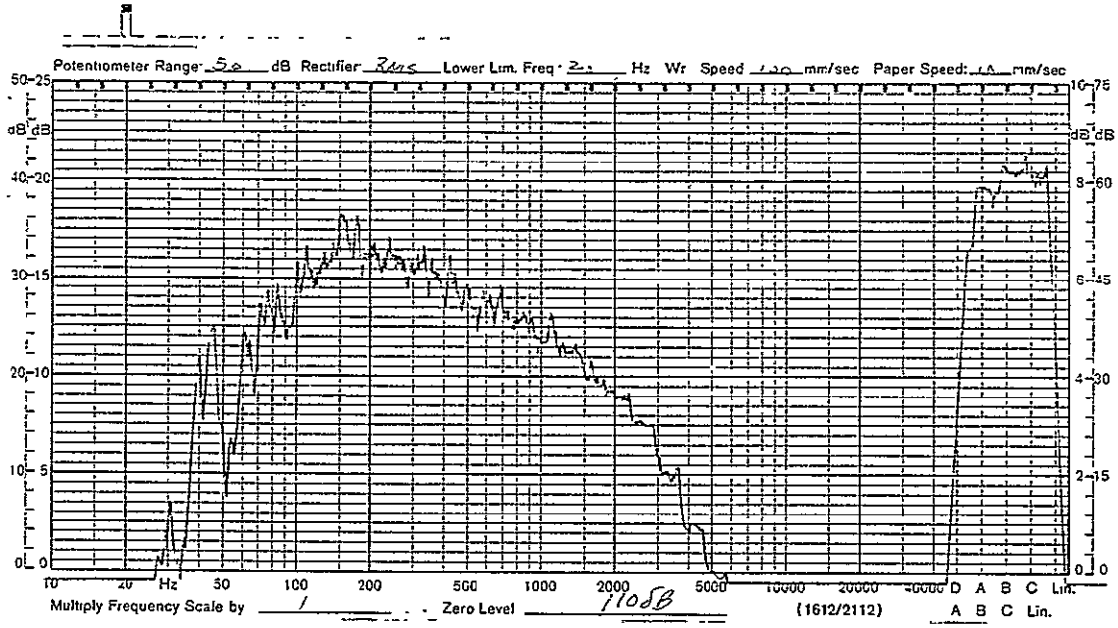

(a) Microphone M1

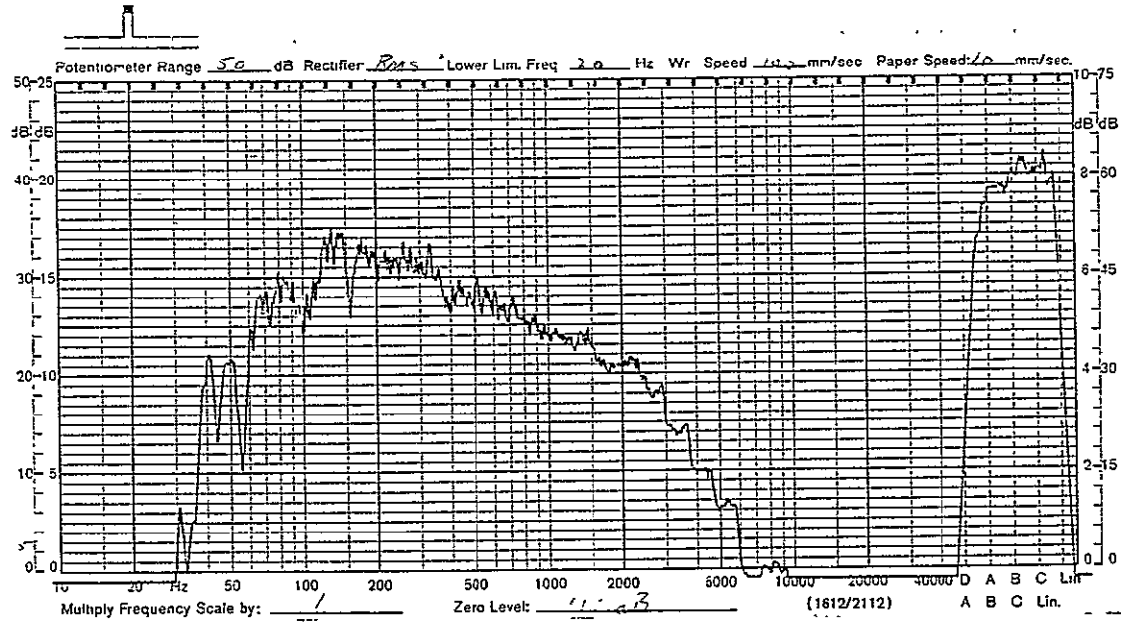

(b) Microphone M2

Figure A-10. Measured 1/3-Octave Sound Pressure Levels During Test Run R-1

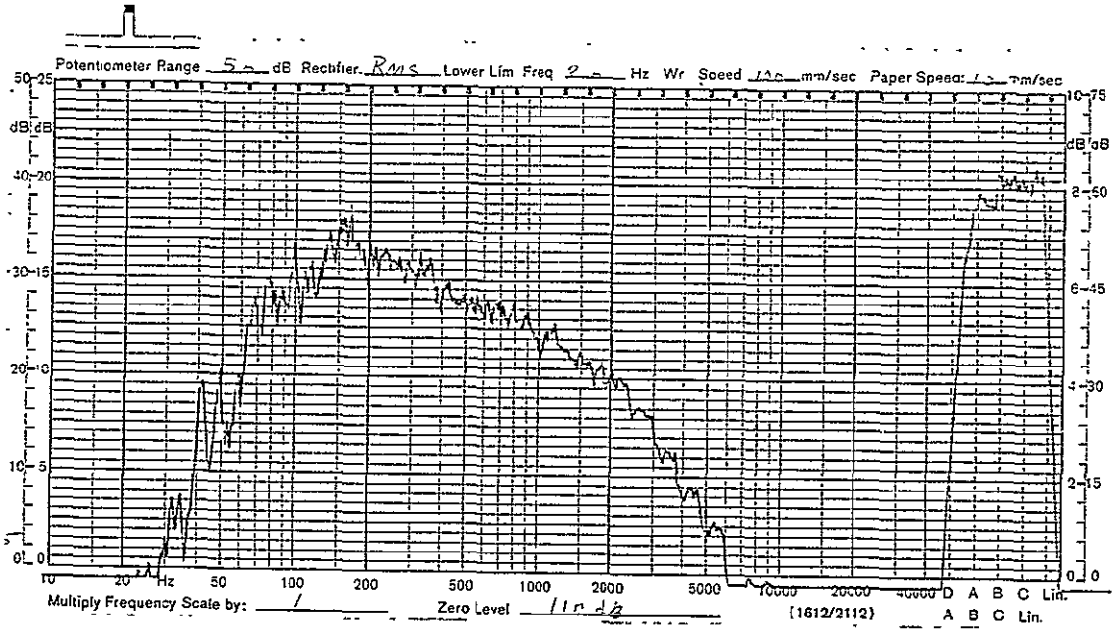

(c) Microphone M3

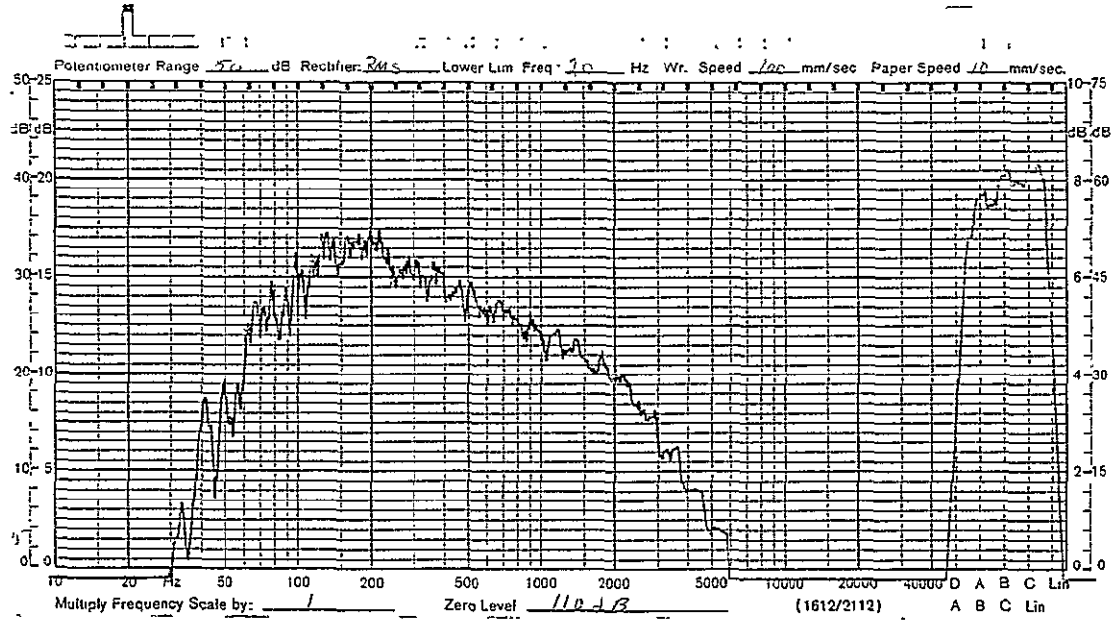

(d) Microphone M4

Figure A-10. (Concluded)

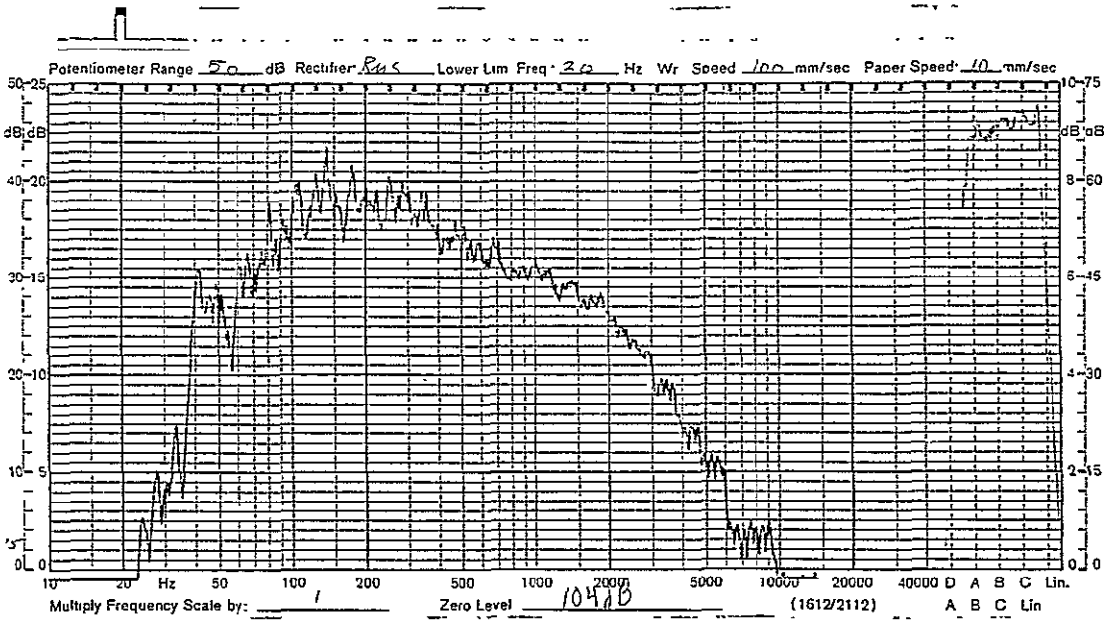

Figure A-11. Averaged 1/3-Octave Sound Pressure During Test Run R-1

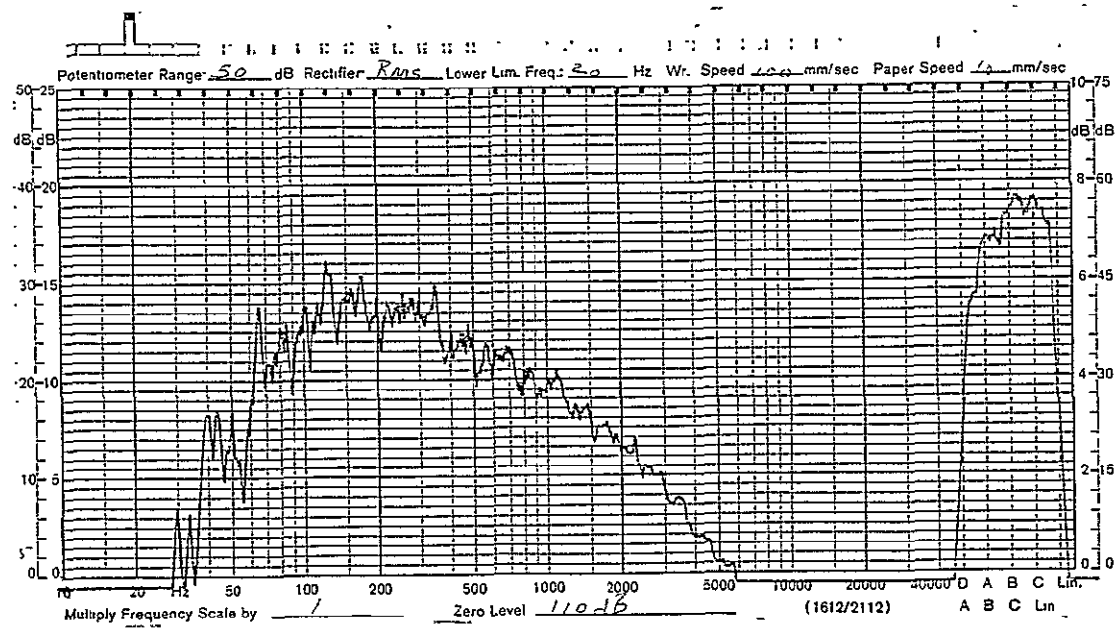

Figure A-12. Measured 1/3-Octave Sound Pressure of Control Microphone M5 During Test Run R-1

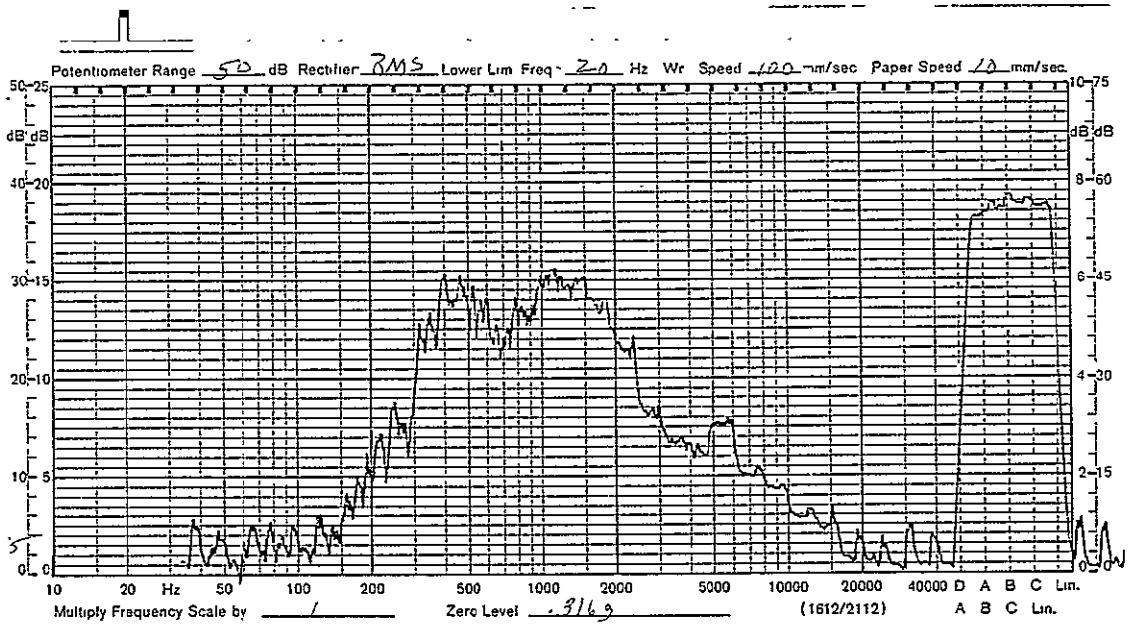

(a) Accelerometer A1

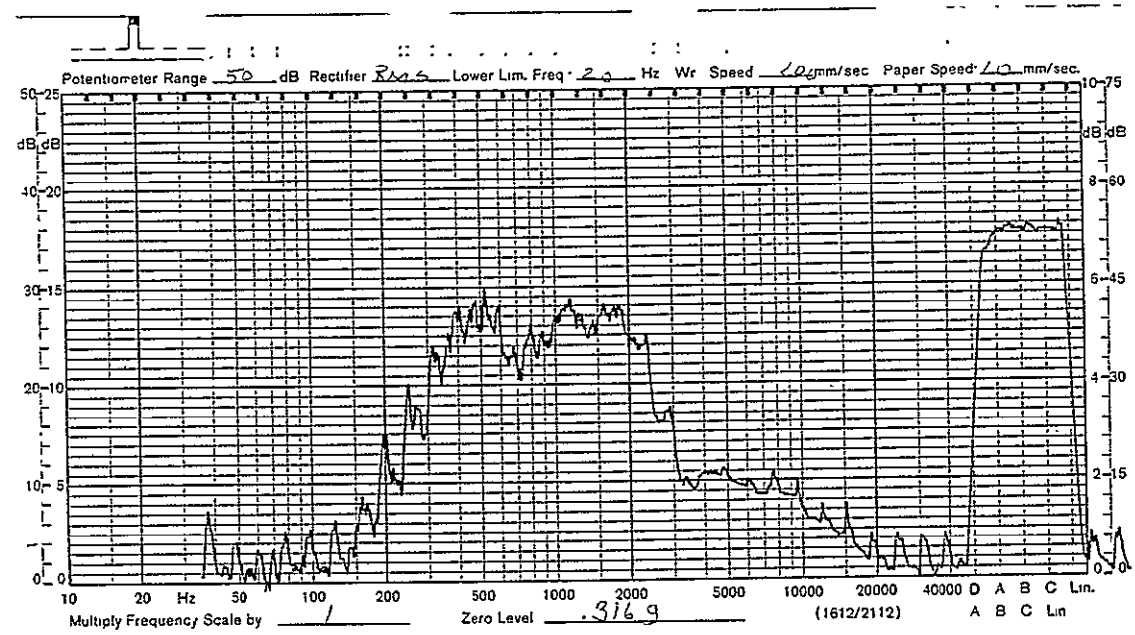

(b) Accelerometer A2

Figure A-13. Measured 1/3-Octave Acceleration Response Levels During Test Run R-1

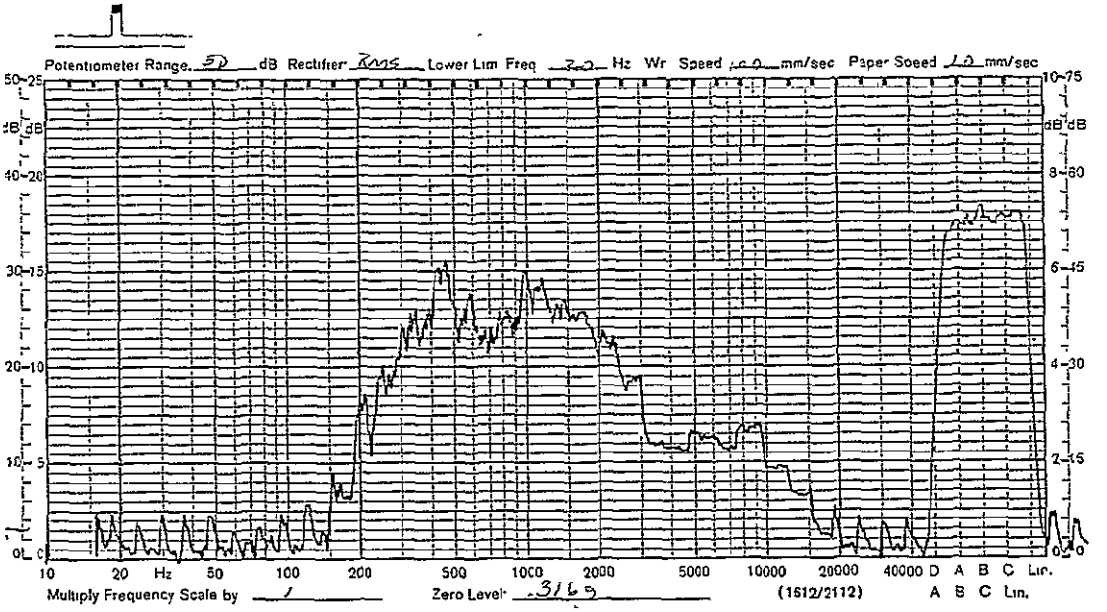

(c) Accelerometer A3

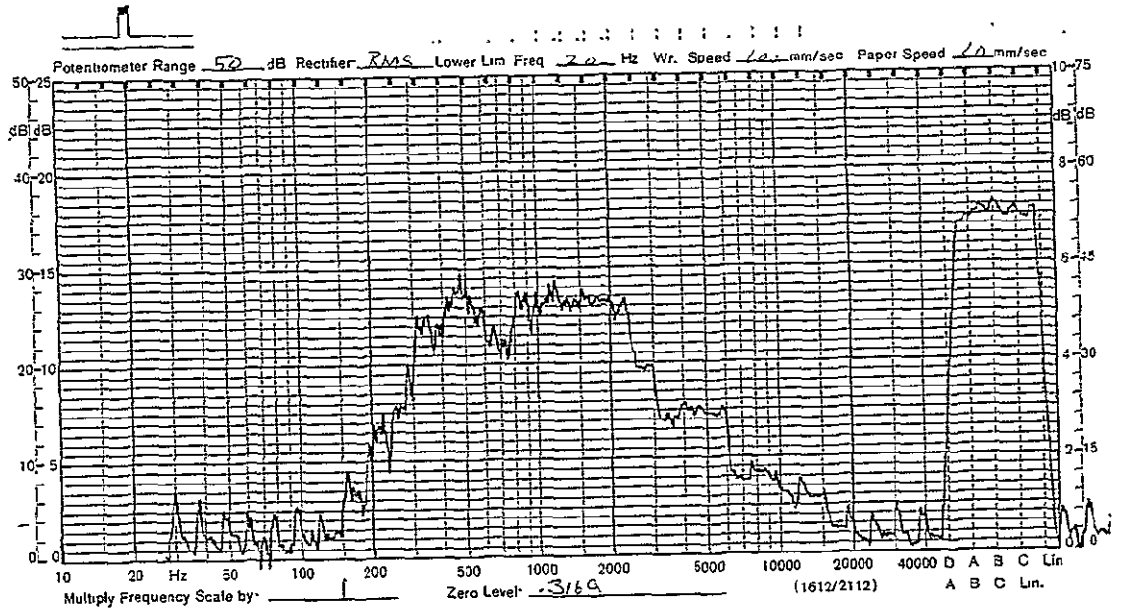

(d) Accelerometer A4

Figure A-13. (Concluded)

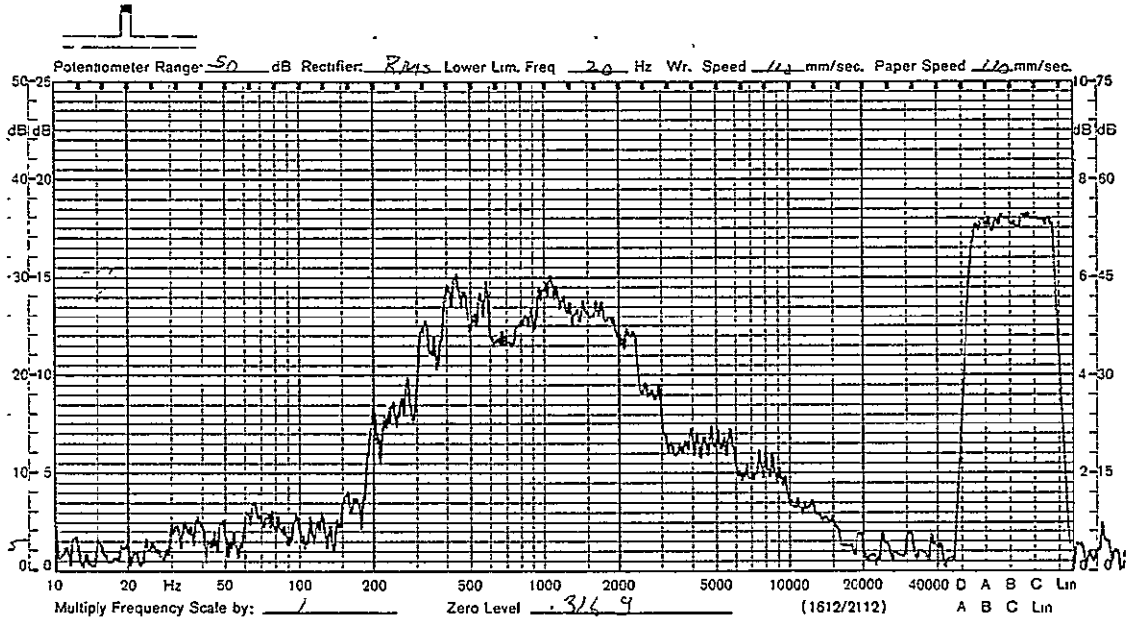

Figure A-14. Averaged 1/3-Octave Acceleration Response During Test Run R-1

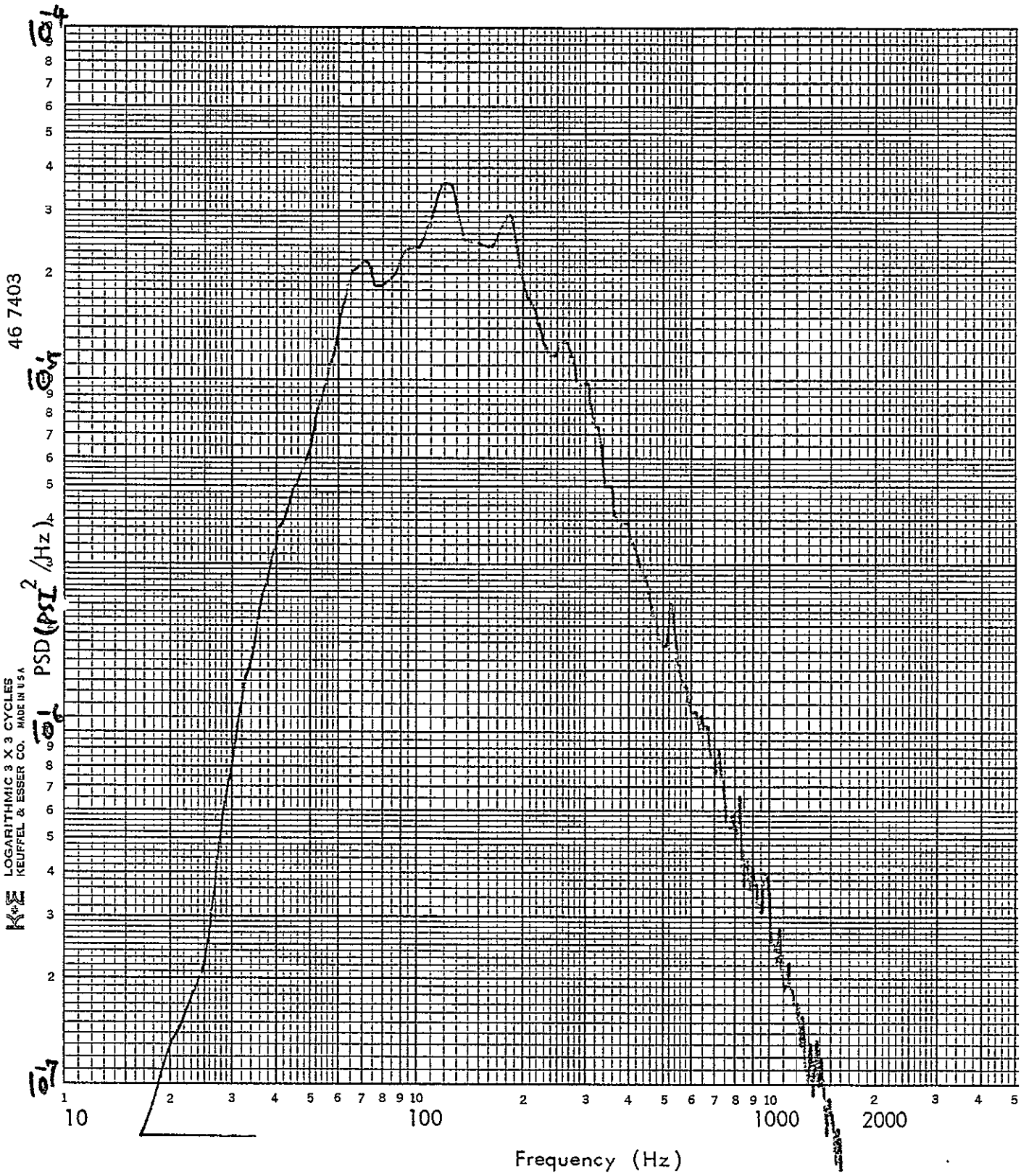

Figure A-15. PSD of Microphone M5, Test Run R-1

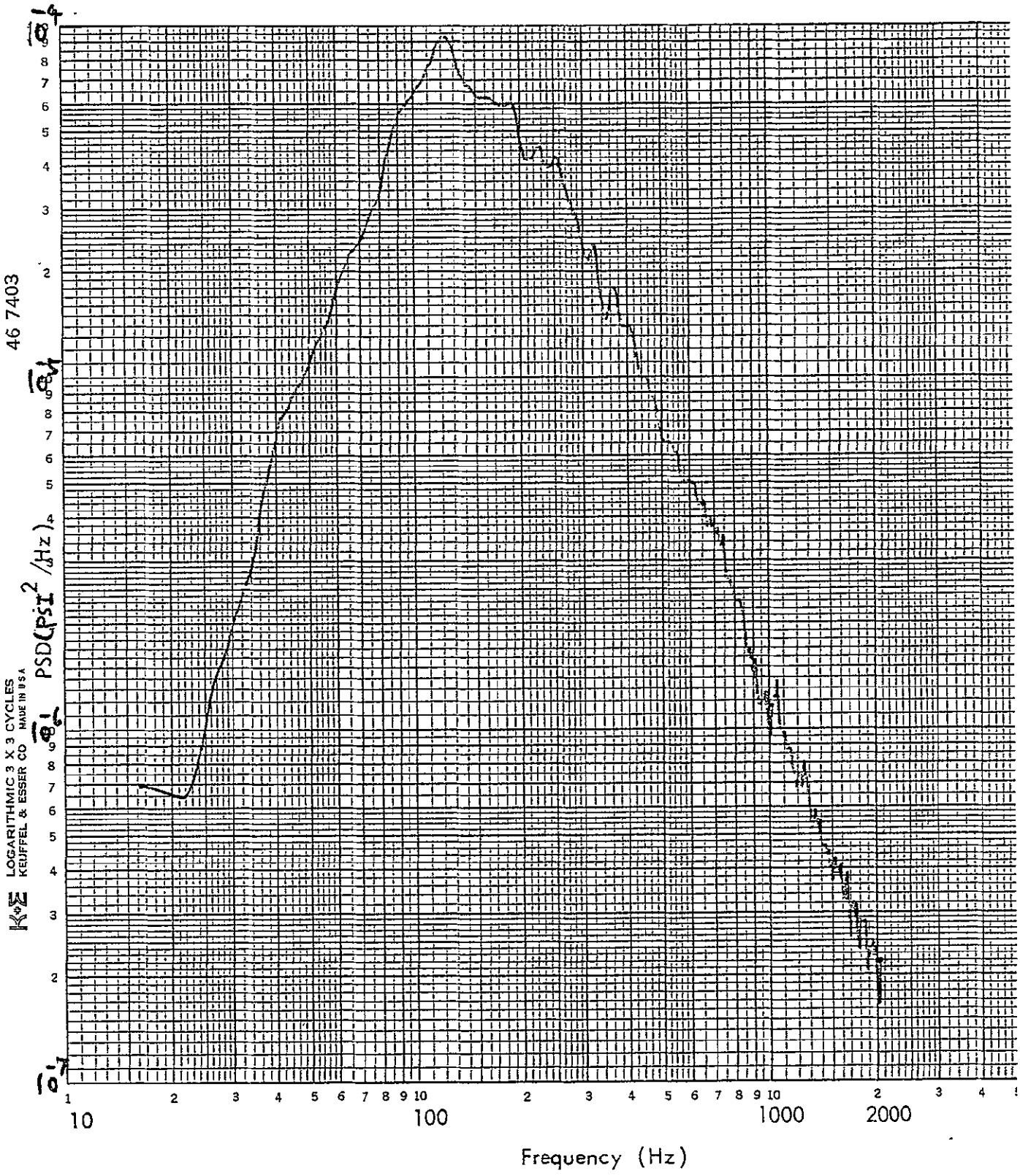

Figure A-16. PSD of Averaged Sound Pressure Levels, Test Run R-1

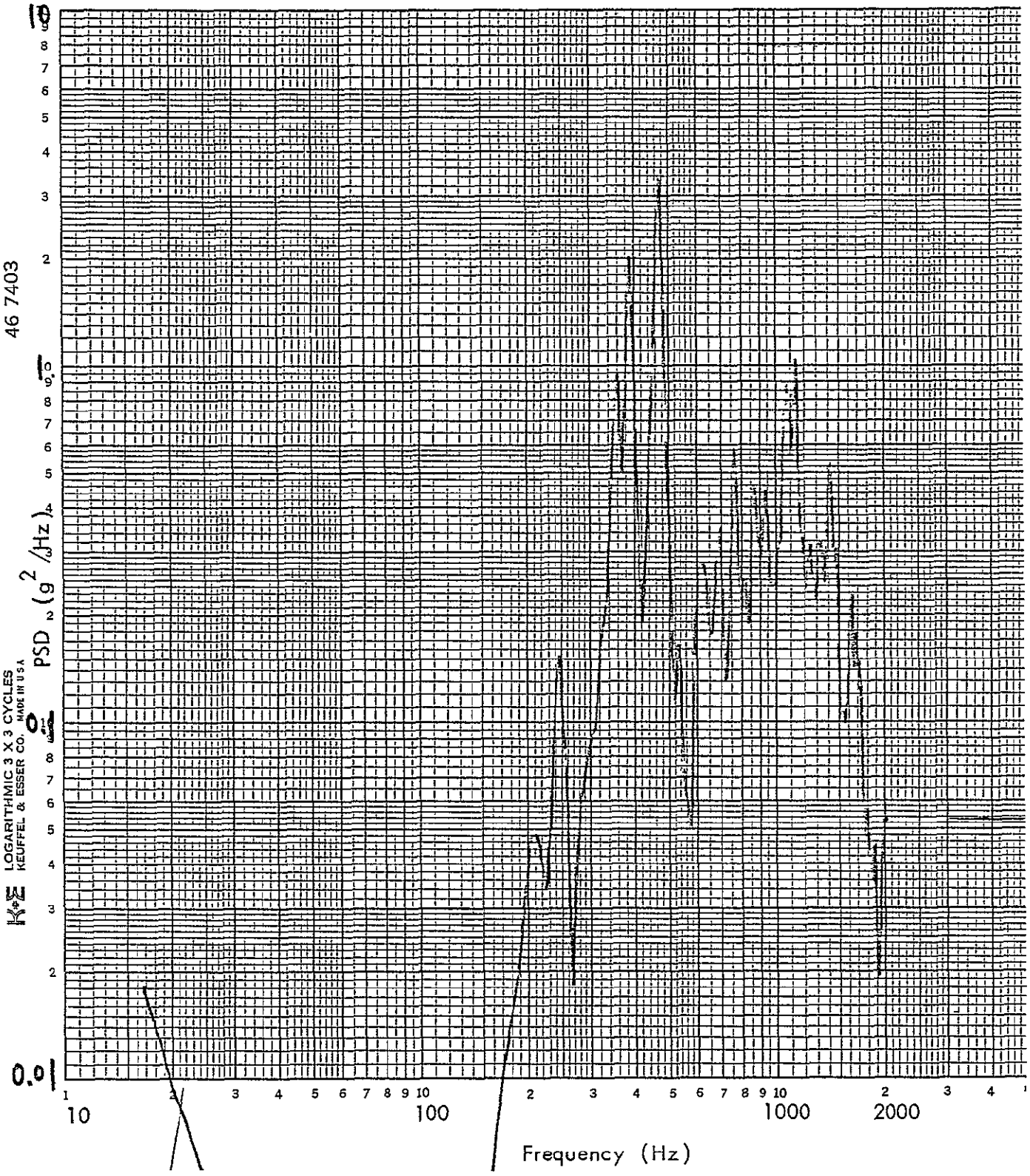

Figure A-17. PSD of Accelerometer A1, Test Run R-1

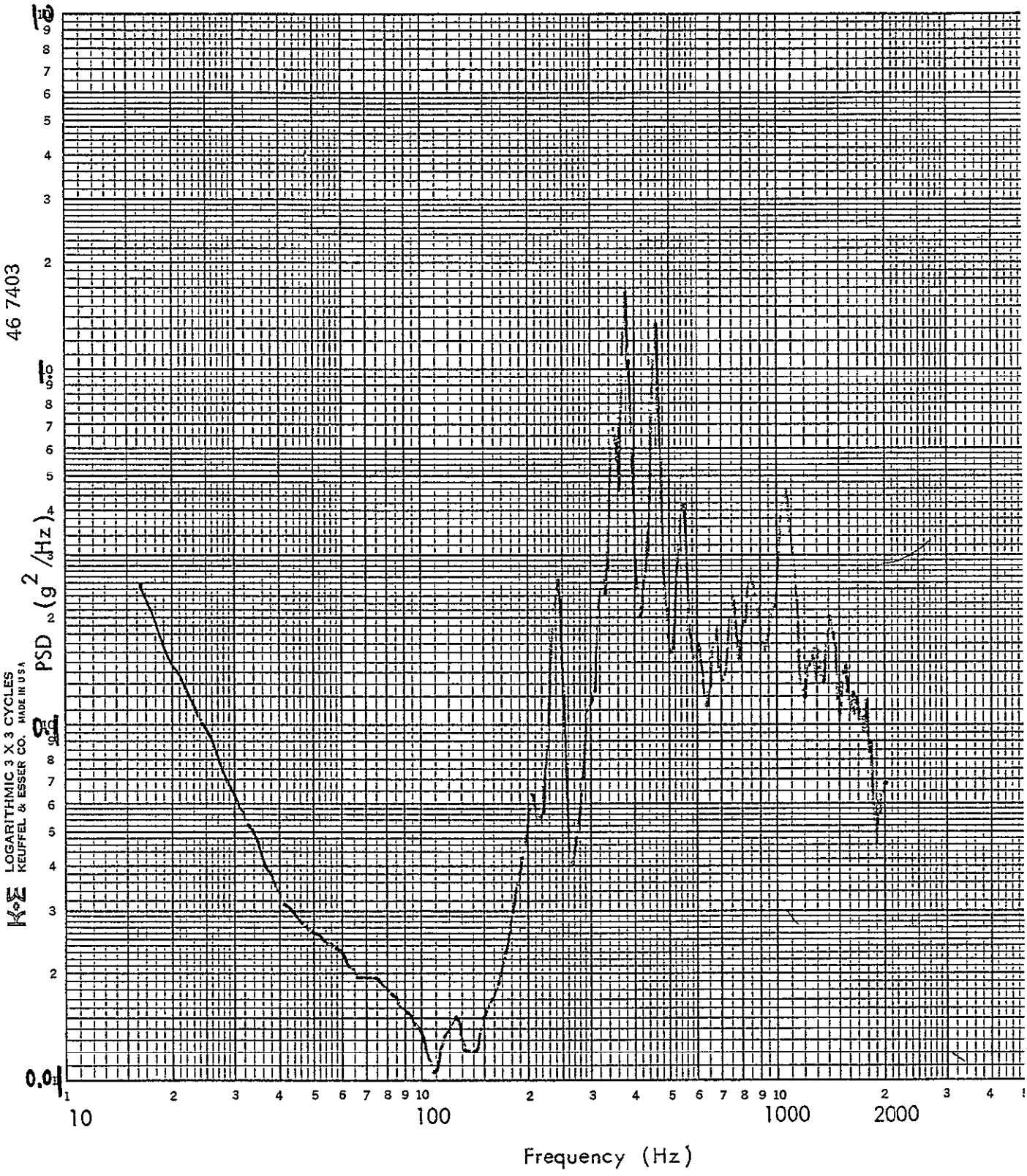

Figure A-18. PSD of Averaged Acceleration Responses, Rest Run R-1

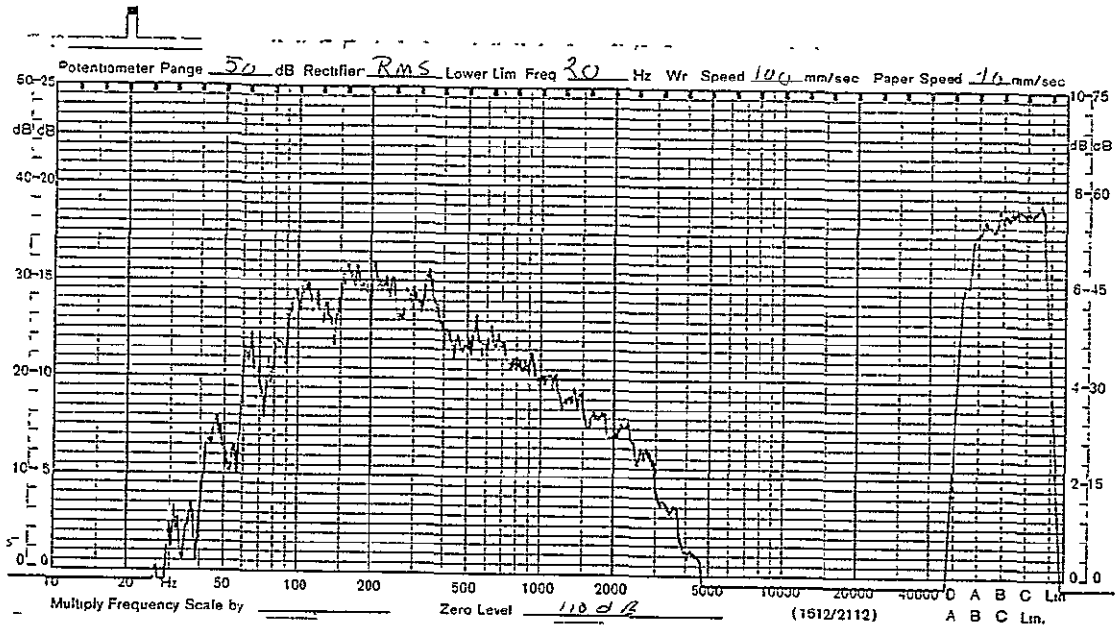

(a) Microphone M1

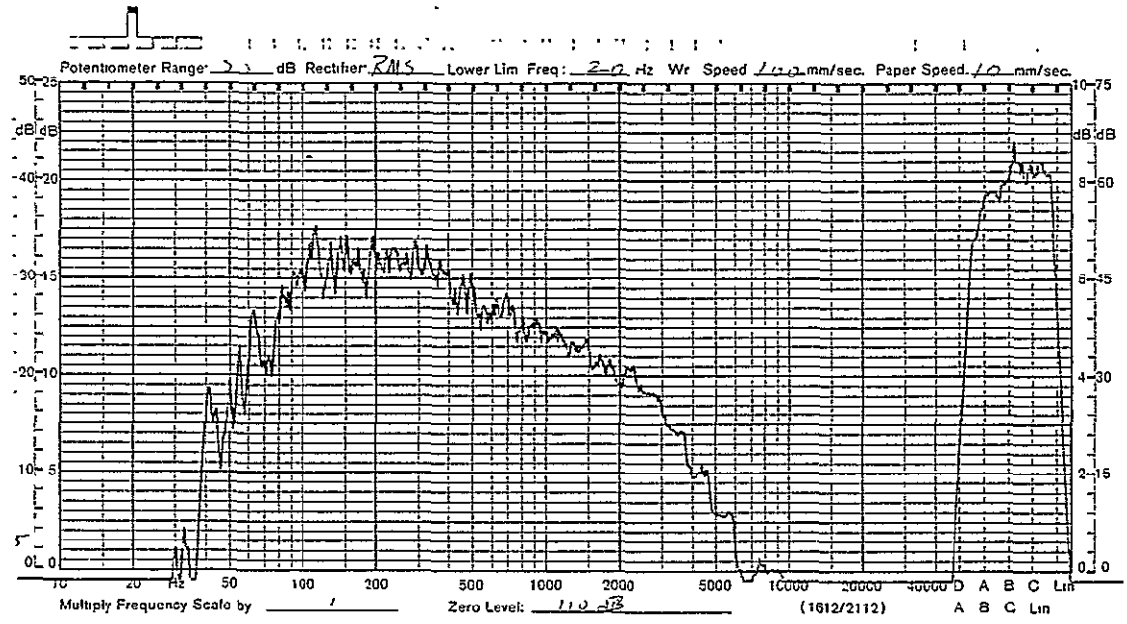

(b) Microphone M2

Figure A-19. Measured 1/3-Octave Sound Pressure Levels During Test Run S-1

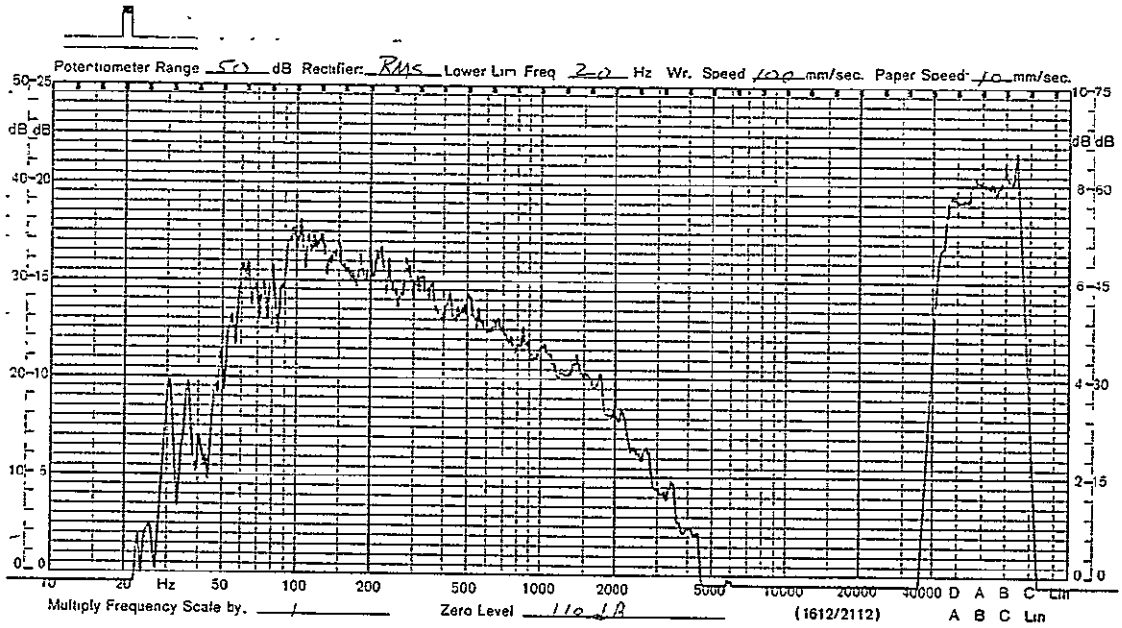

(c) Microphone M3

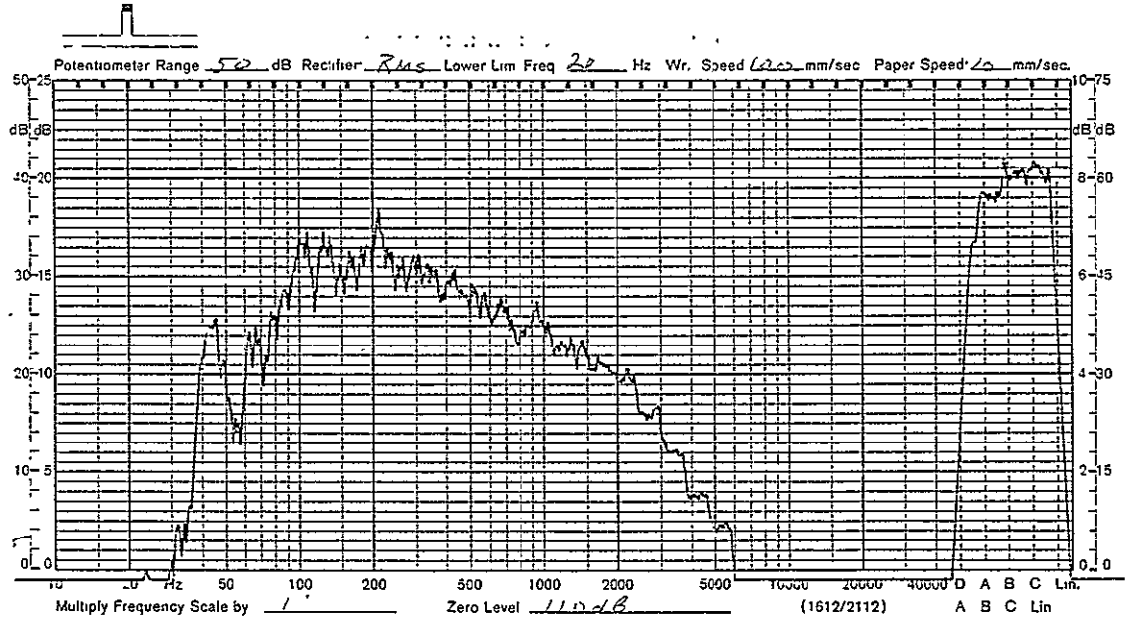

(d) Microphone M4

Figure A-19. (Concluded)

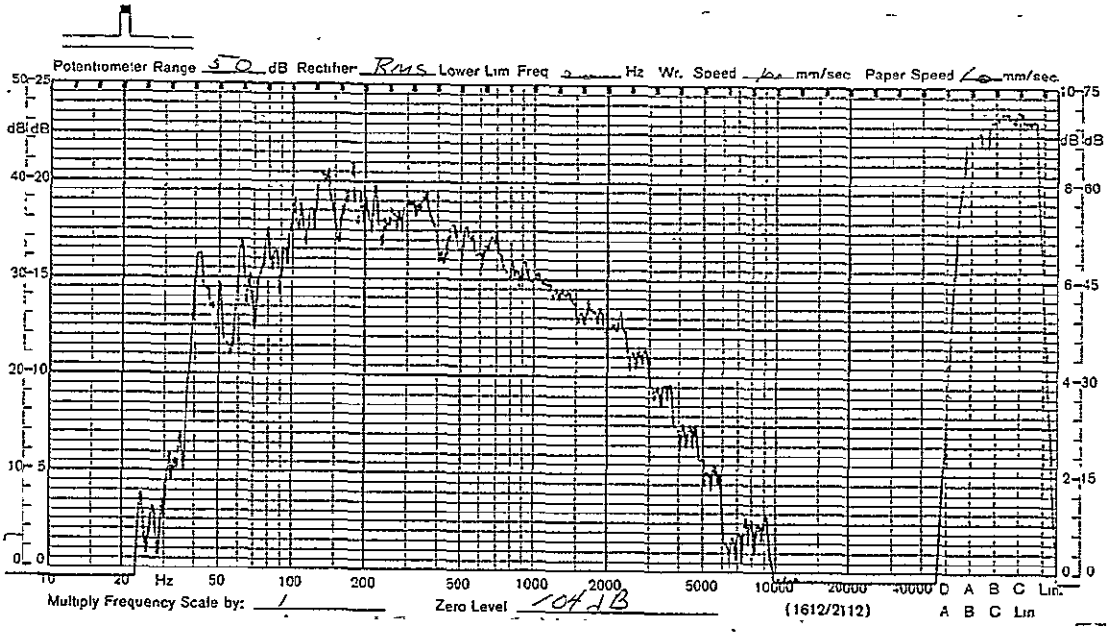

Figure A-20. Averaged 1/3-Octave Sound Pressure During Test Run S-1

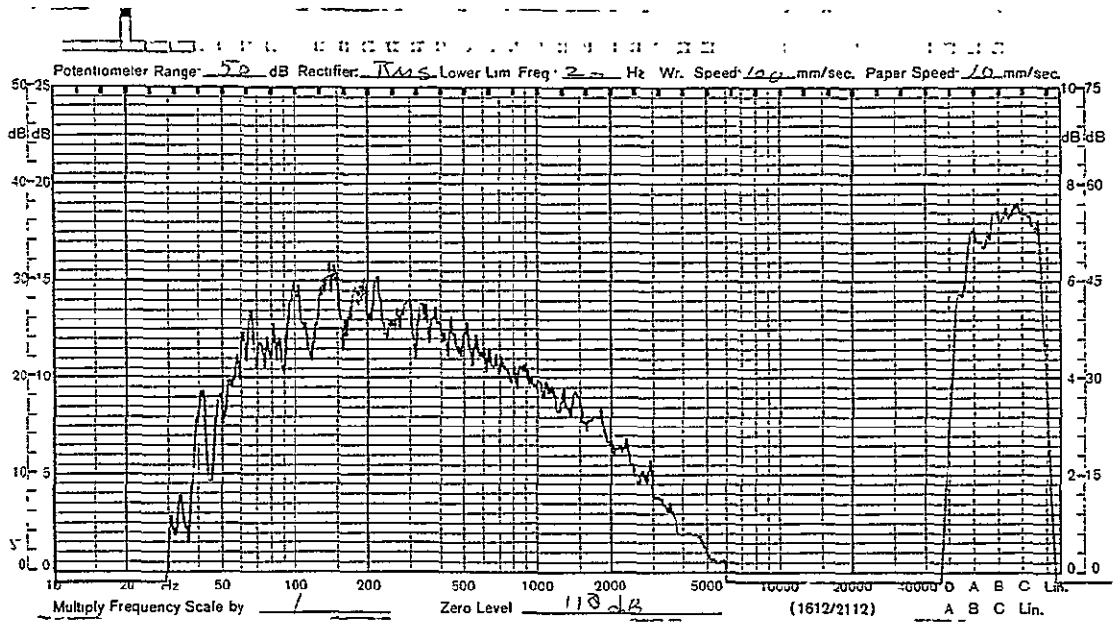

Figure A-21. Measured 1/3-Octave Sound Pressure of Control Microphone M5 During Test Run S-1

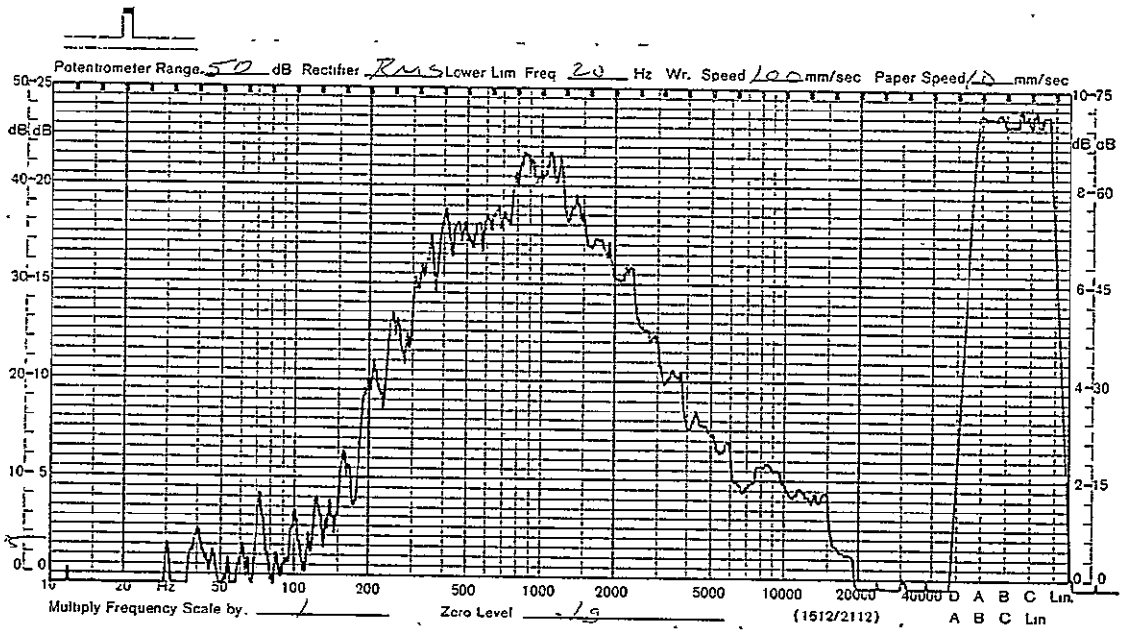

(a) Accelerometer A1

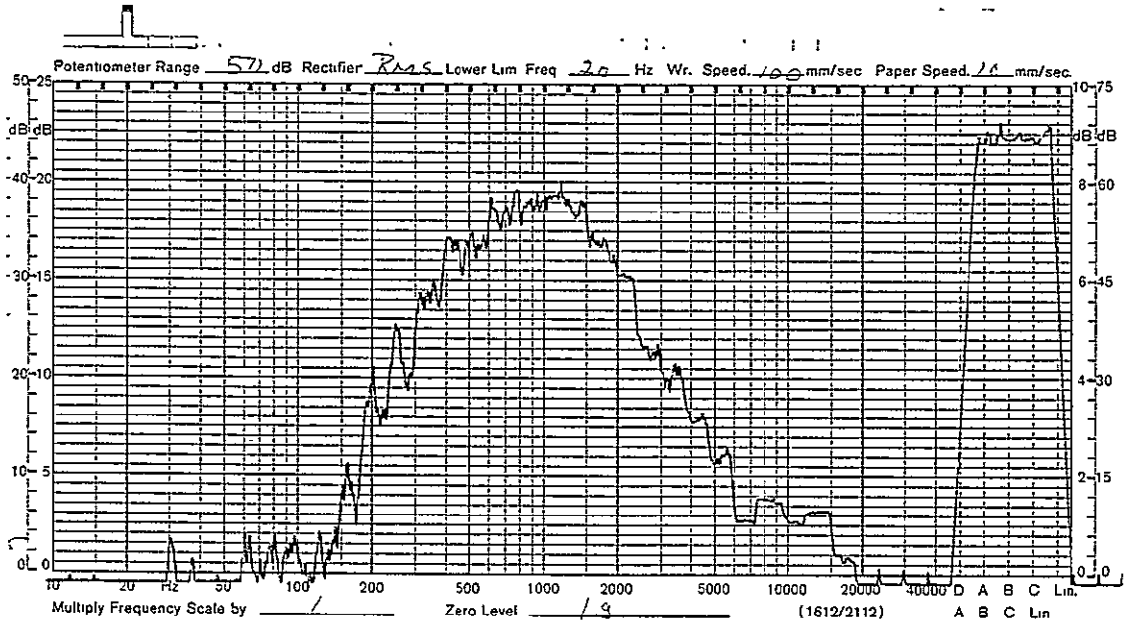

(b) Accelerometer A2

Figure A-22. Measured 1/3-Octave Acceleration Response Levels During Test Run S-1

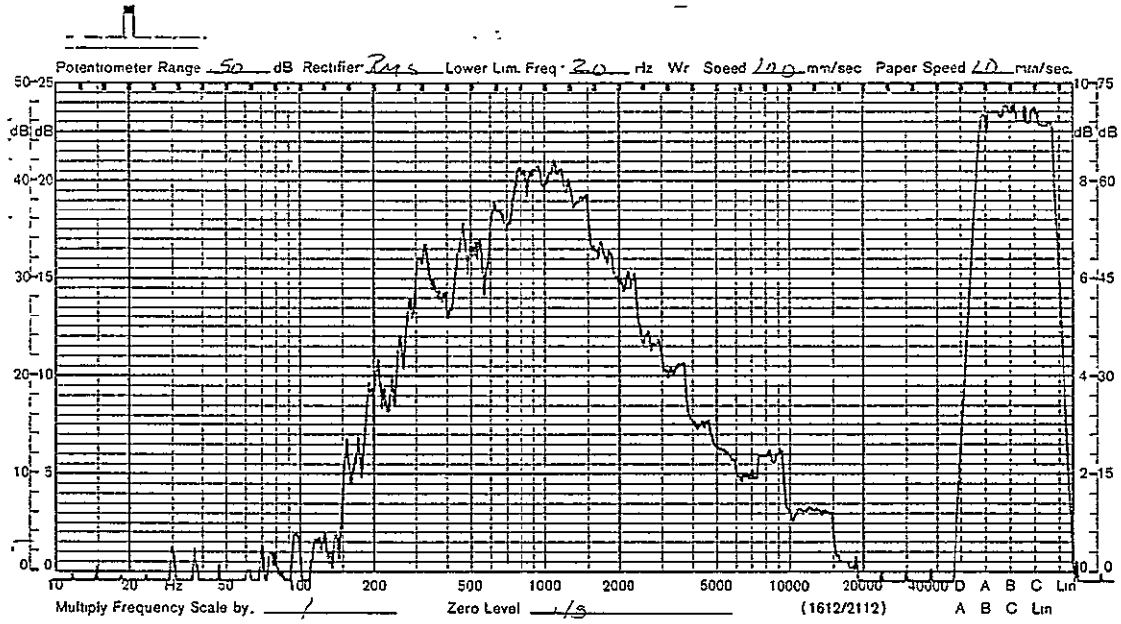

(c) Accelerometer A3

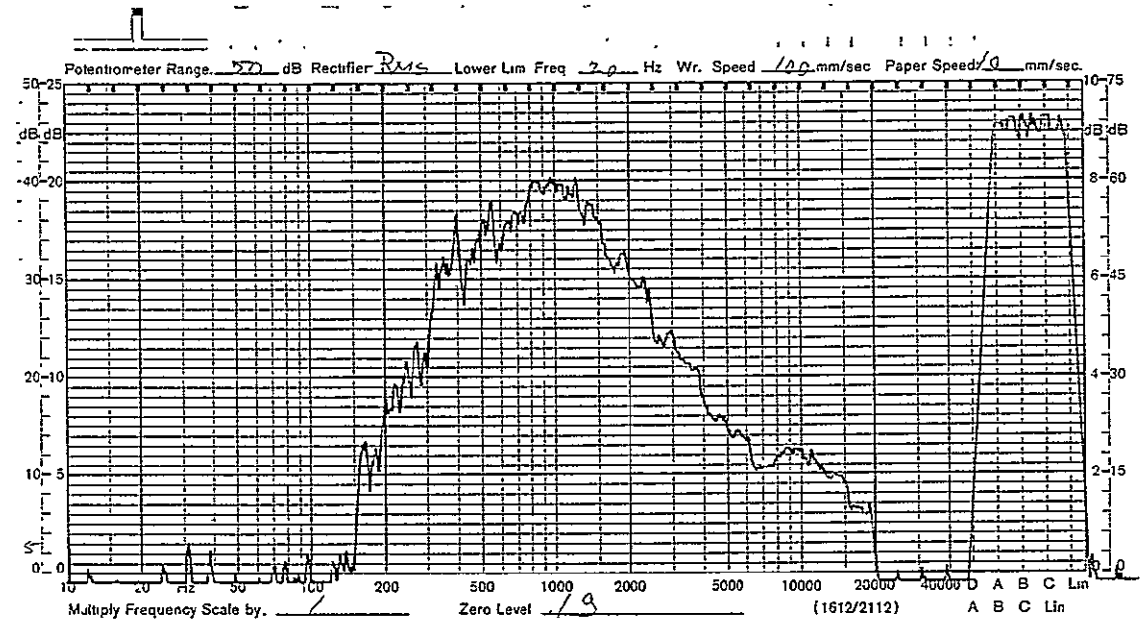

(d) Accelerometer A4

Figure A-22. (Concluded)

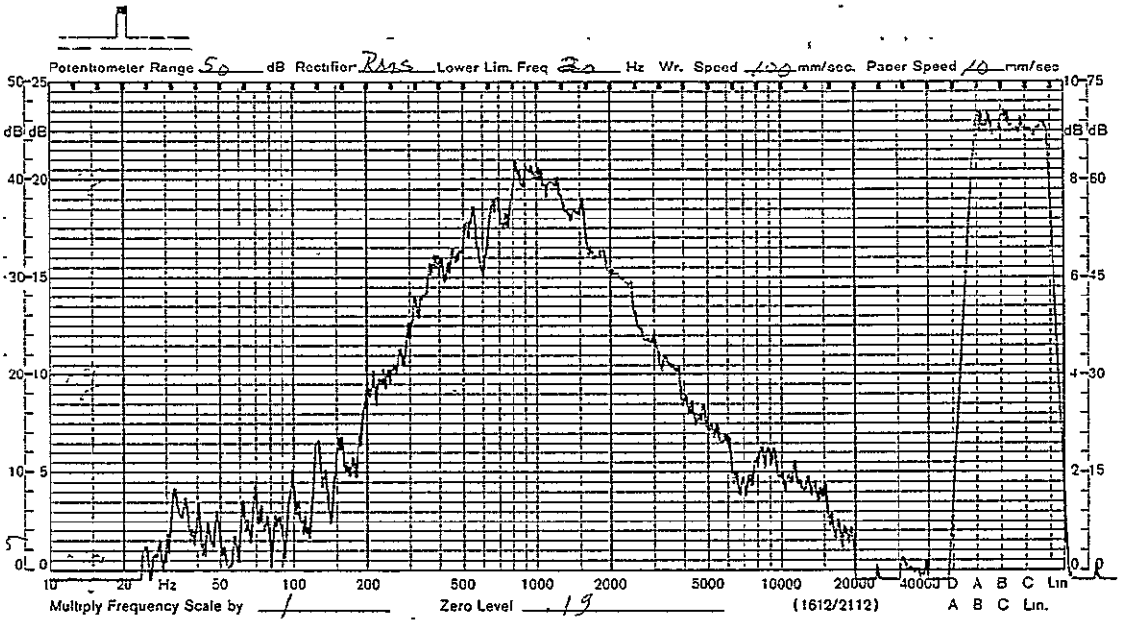

Figure A-23. Averaged 1/3-Octave Acceleration Response During Test Run S-1

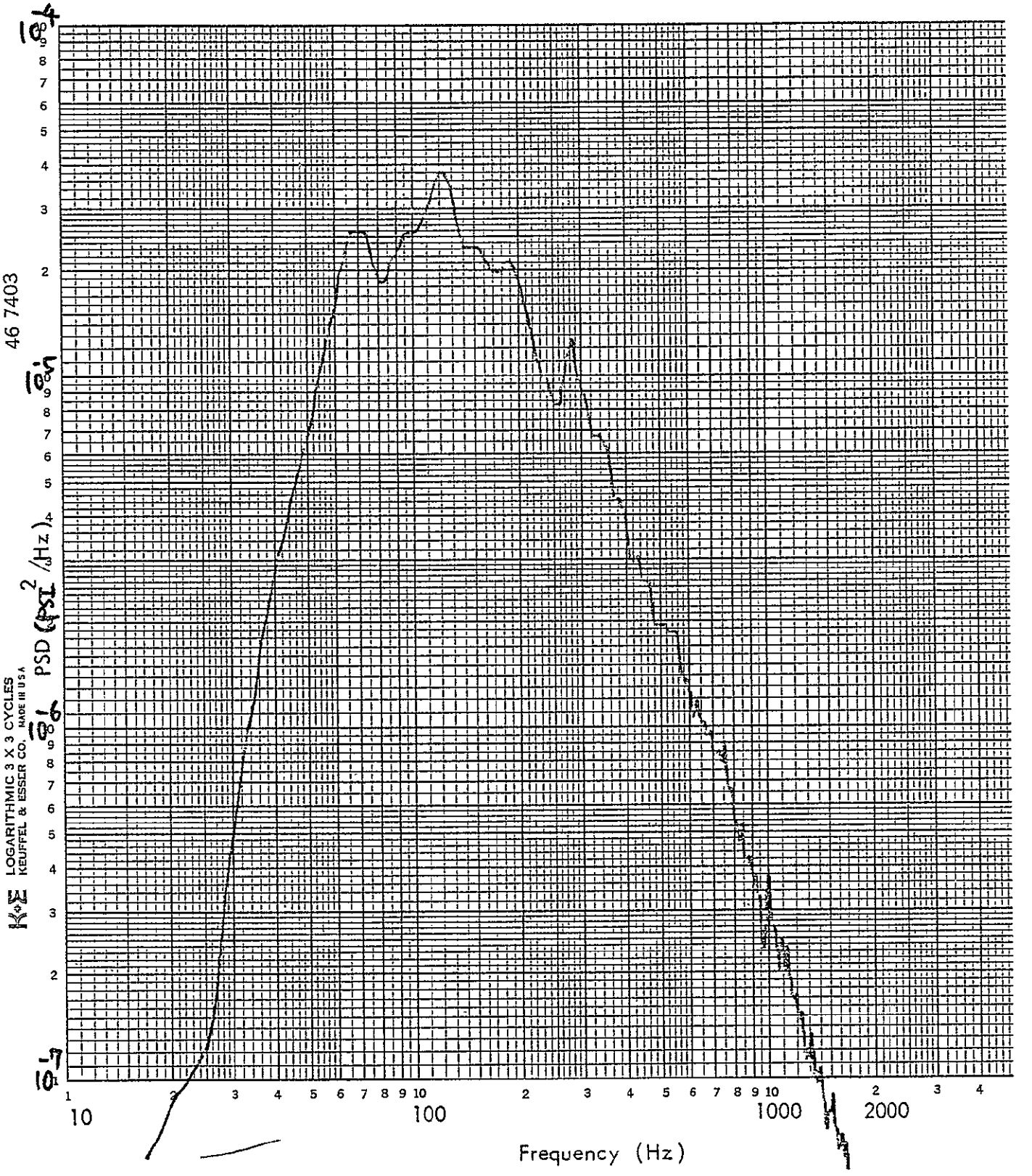

Figure A-24. PSD of Microphone M5, Test Run S-1

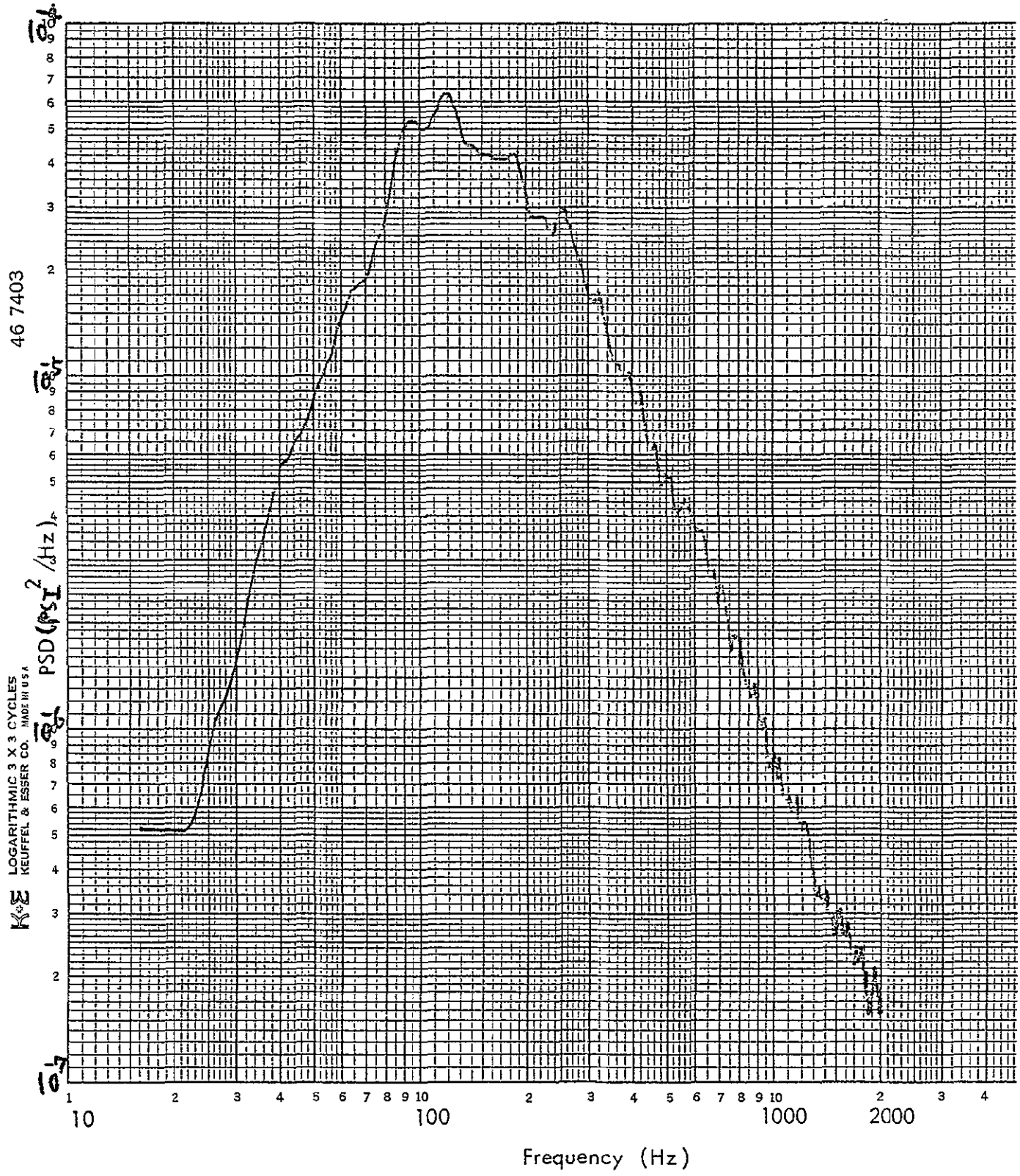

Figure A-25. PSD of Averaged Sound Pressure Levels, Test Run S-1

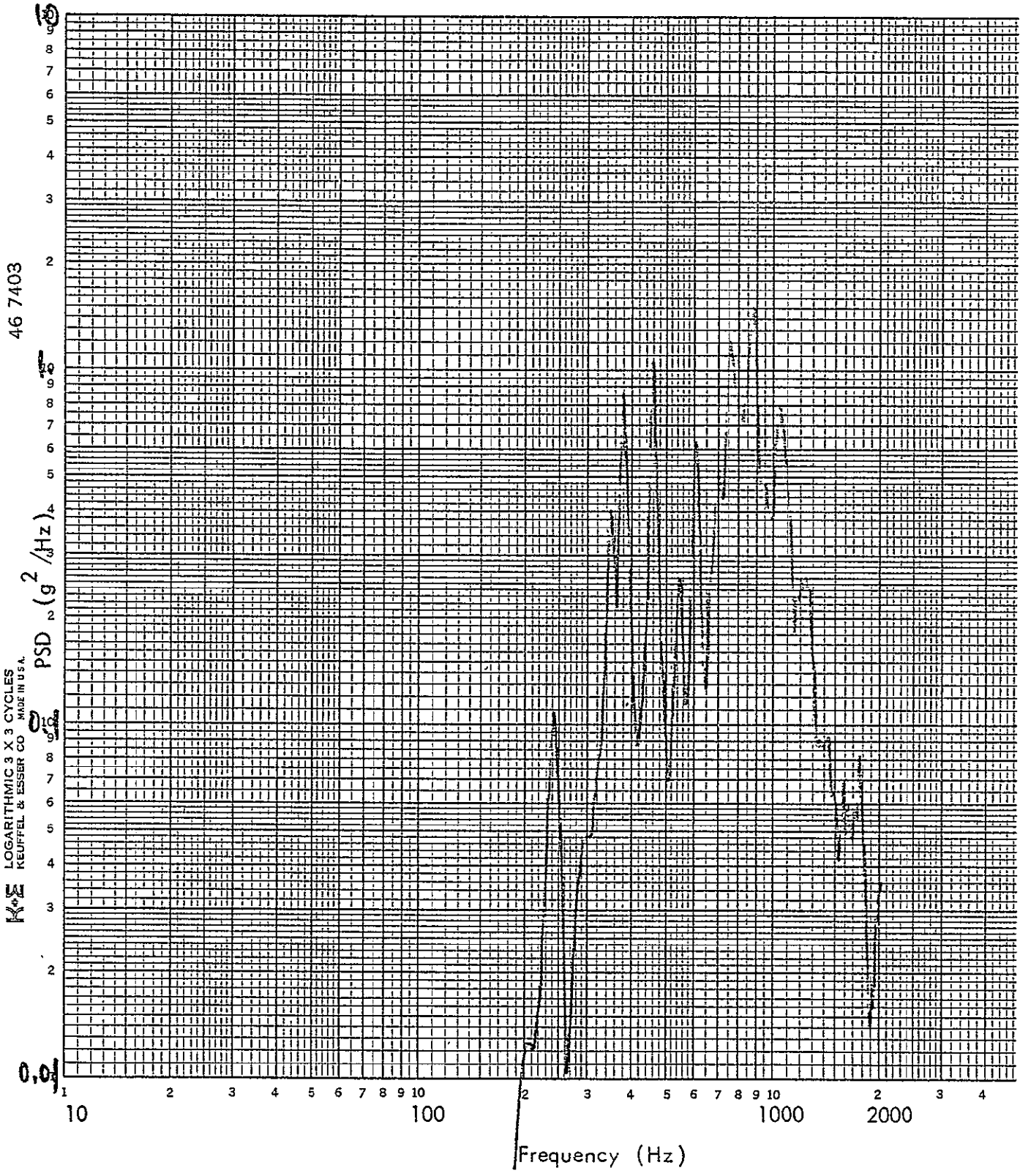

Figure A-26. PSD of Accelerometer A1, Test Run S-1

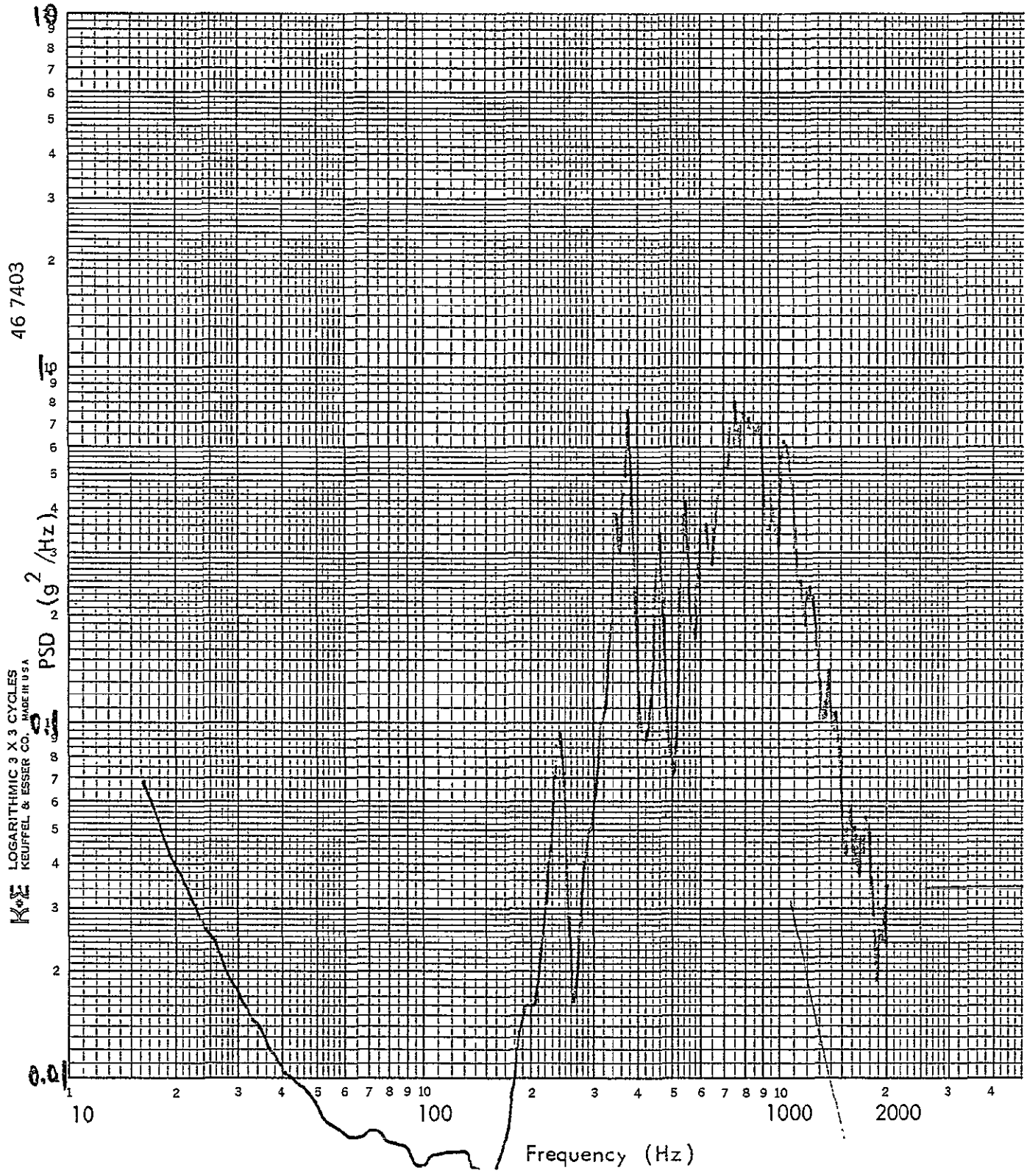

Figure A-27. PSD of Averaged Acceleration Responses, Test Run S-1

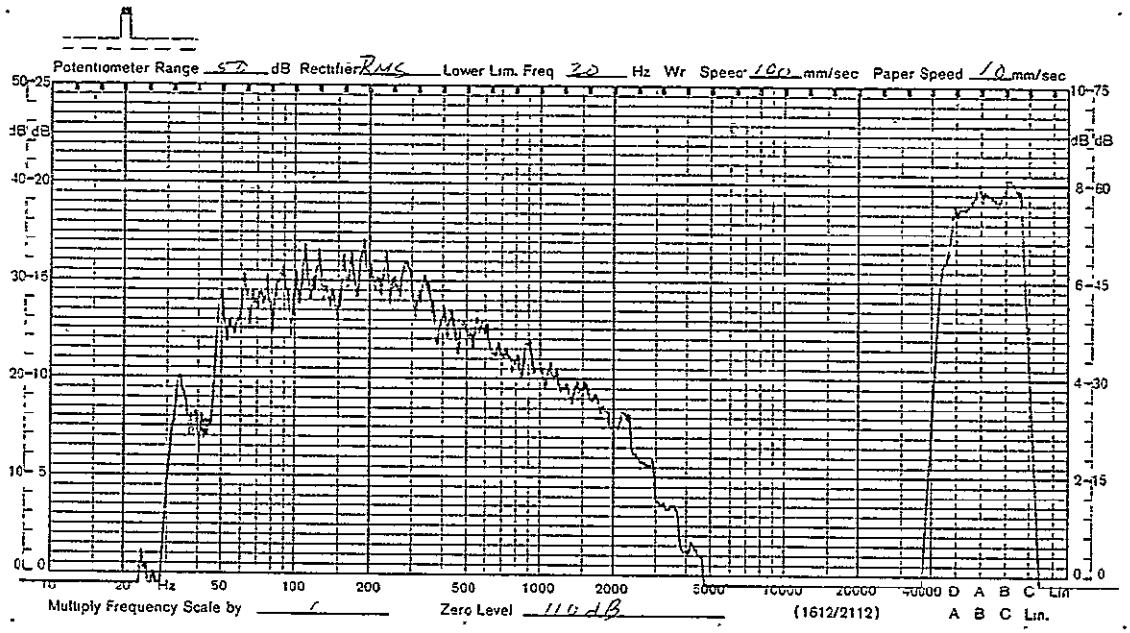

(a) Microphone M1

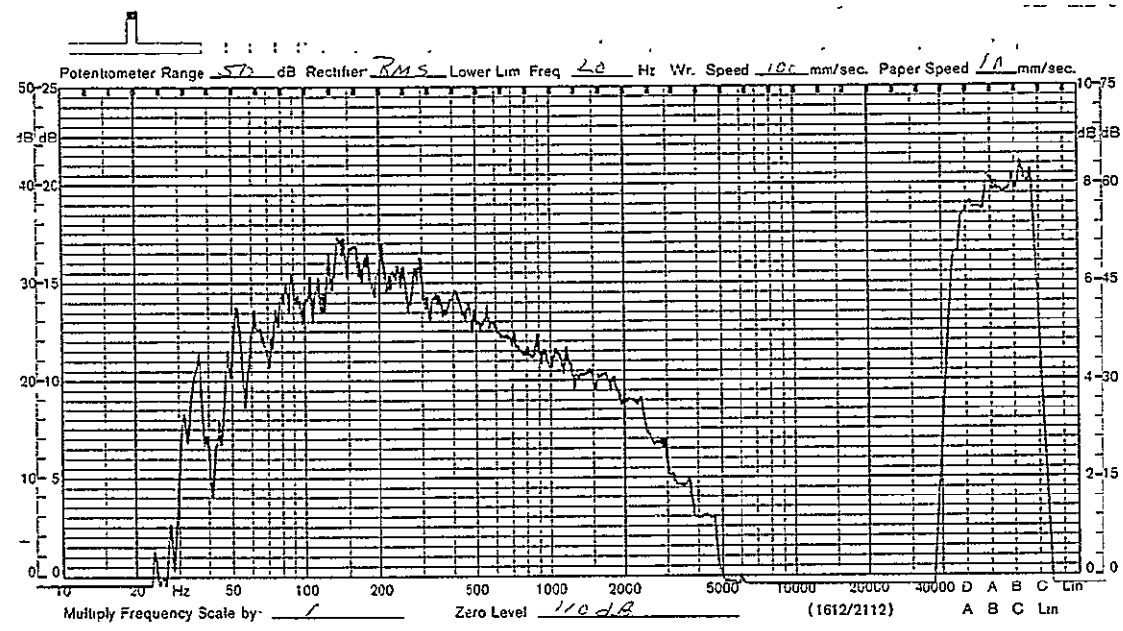

(b) Microphone M2

Figure A-28. Measured 1/3-Octave Sound Pressure Levels During Test Run P-2

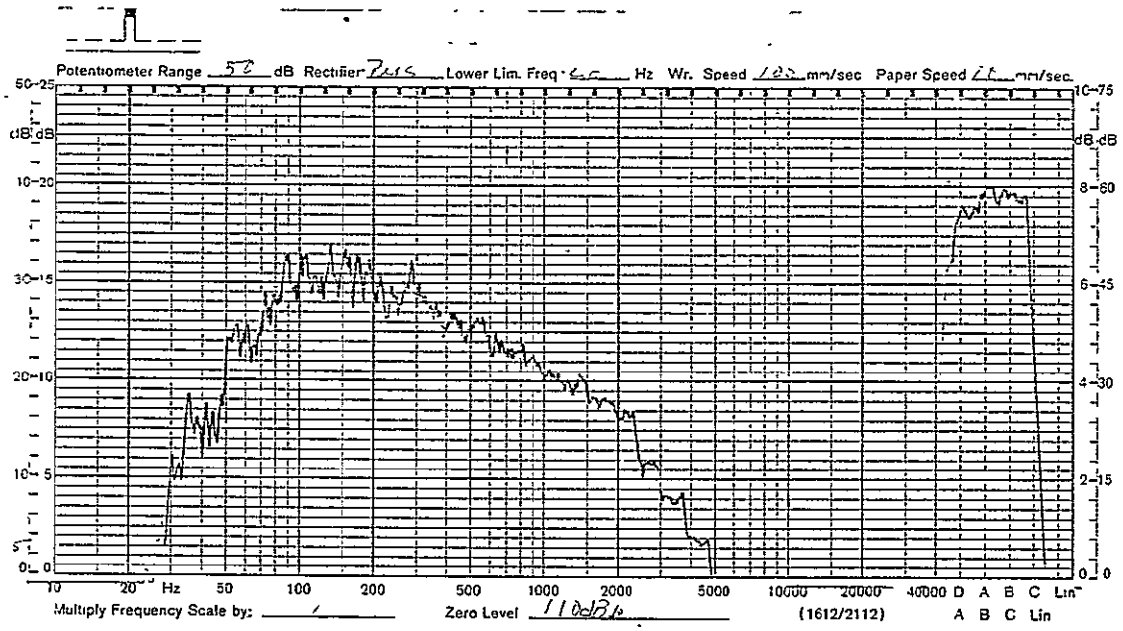

(c) Microphone M3

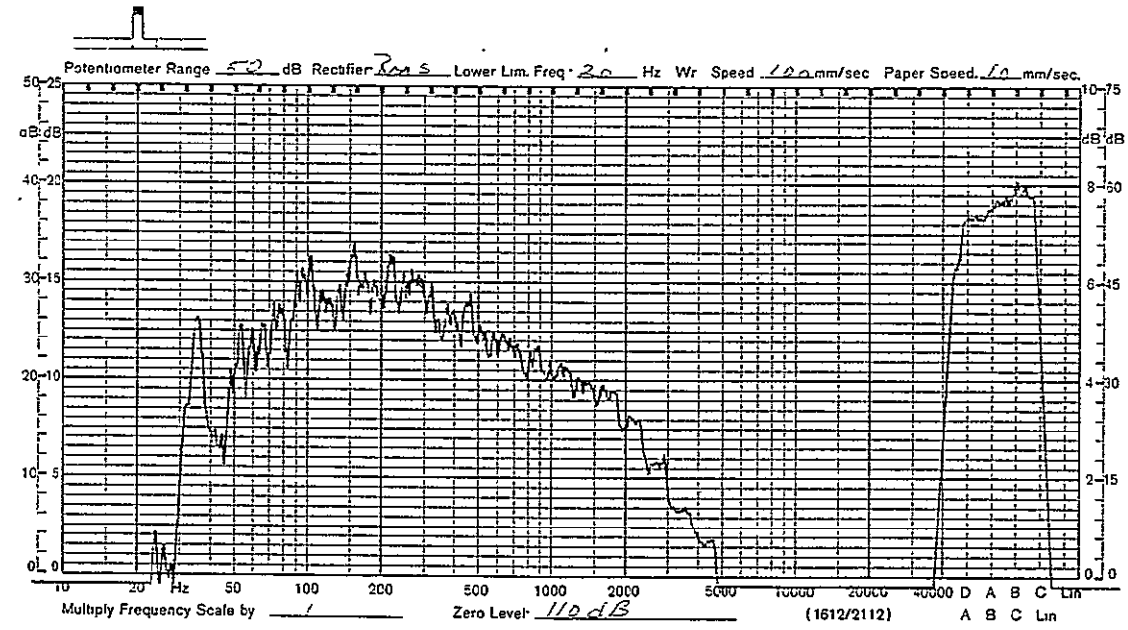

(d) Microphone M4

Figure A-28. (Concluded)

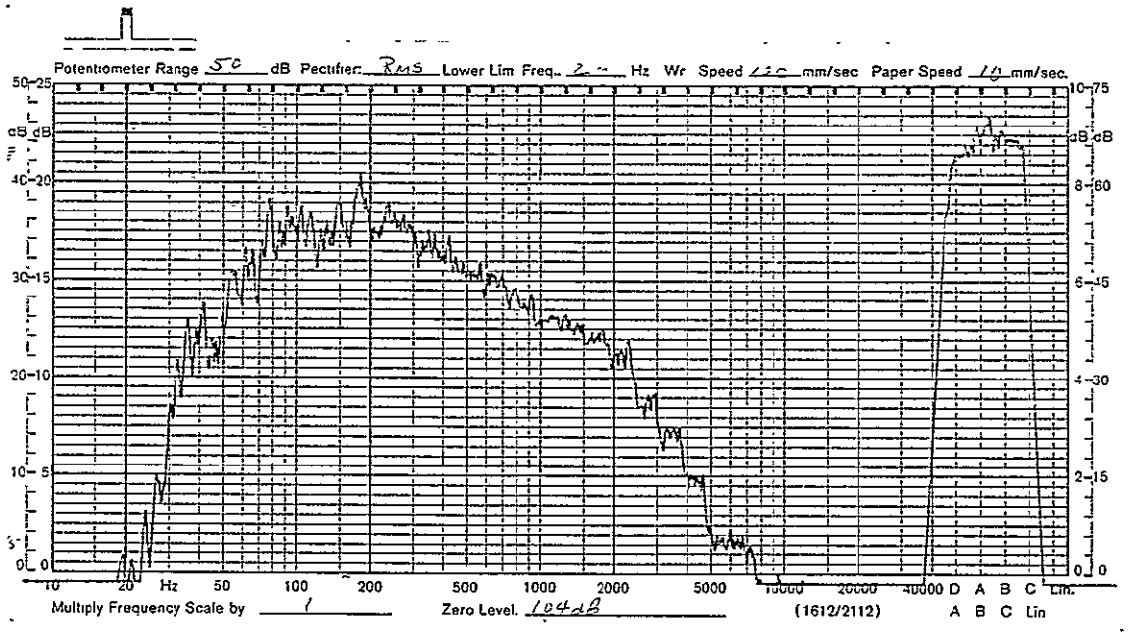

Figure A-29. Averaged 1/3-Octave Sound Pressure During Test Run P-2

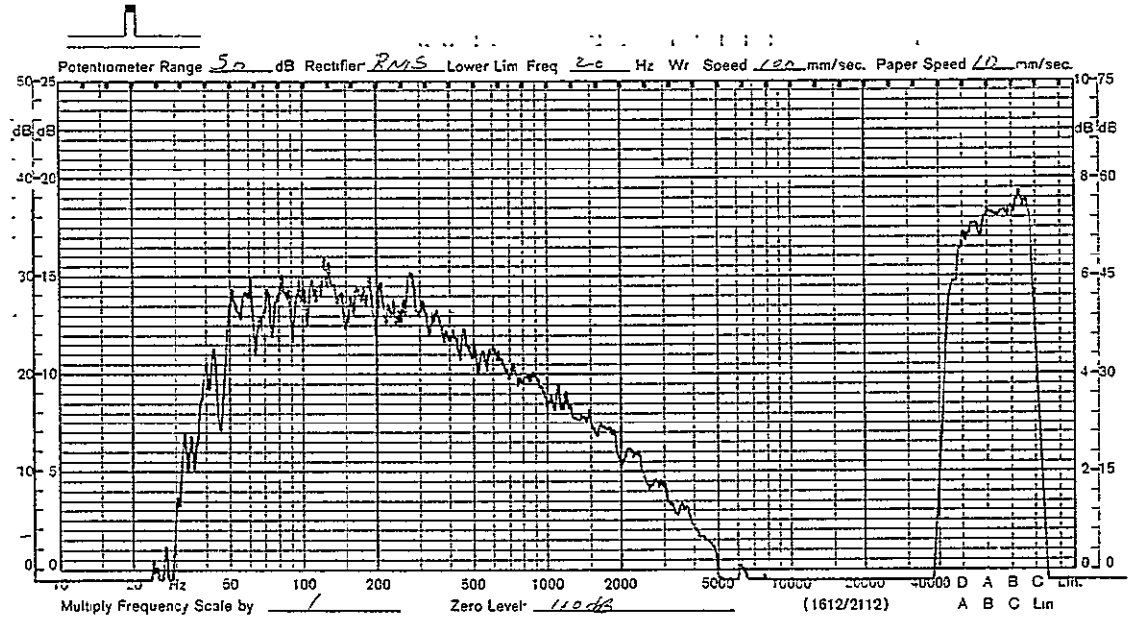

Figure A-30. Measured 1/3-Octave Sound Pressure of Control Microphone M5 During Test Run P-2

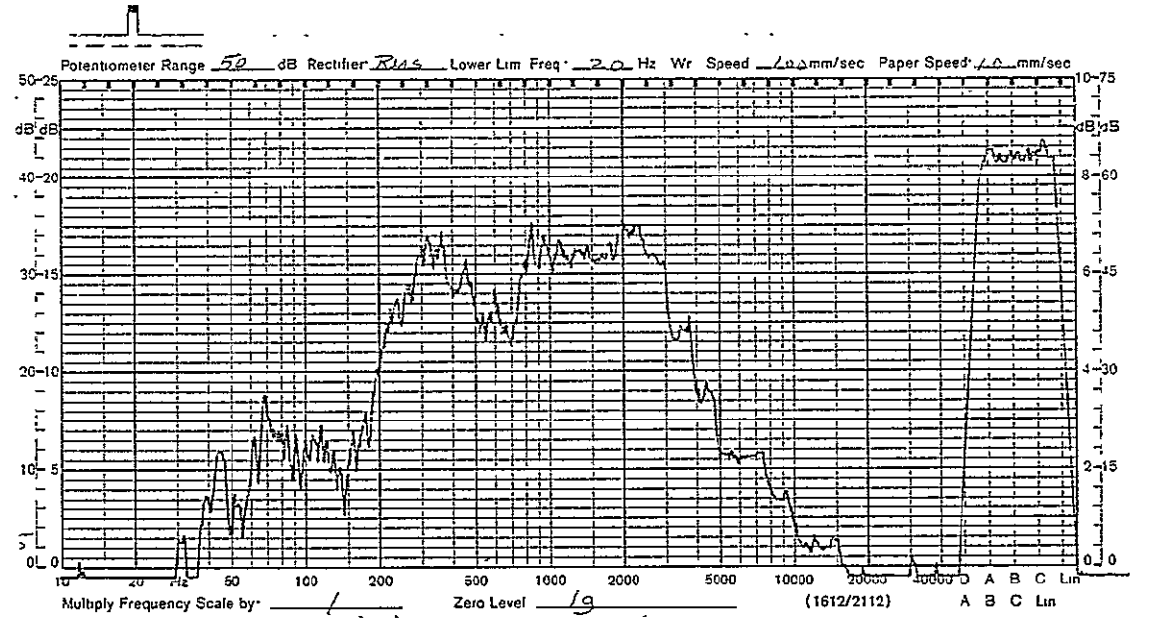

(a) Accelerometer A1

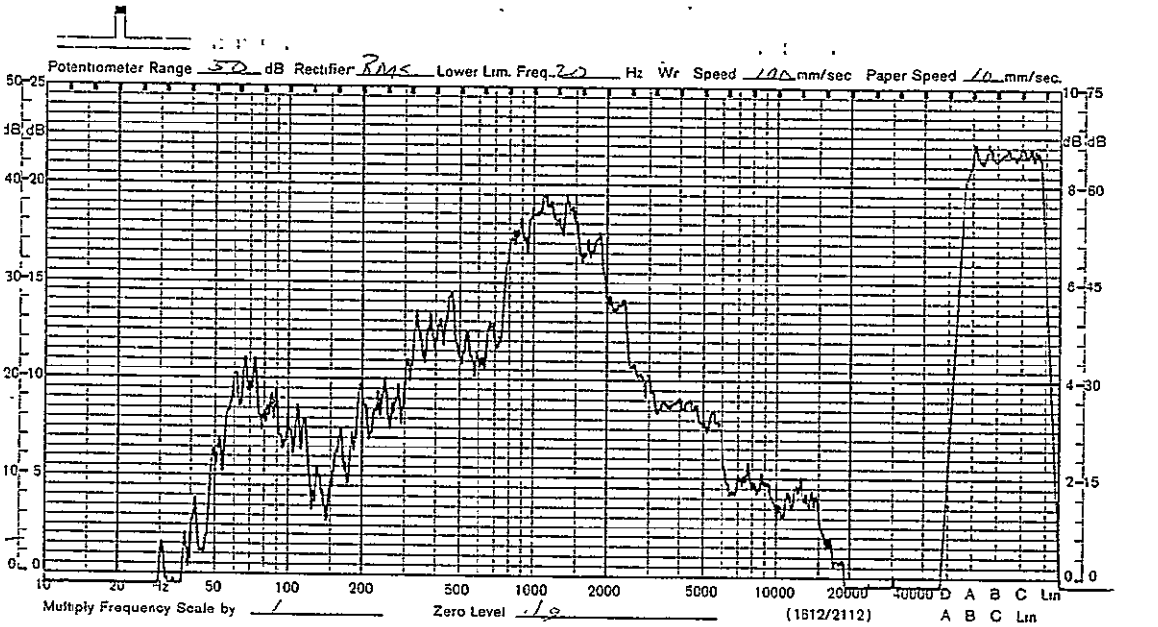

(b) Accelerometer A2

Figure A-31. Measured 1/3-Octave Acceleration Response Levels During Test Run P-2

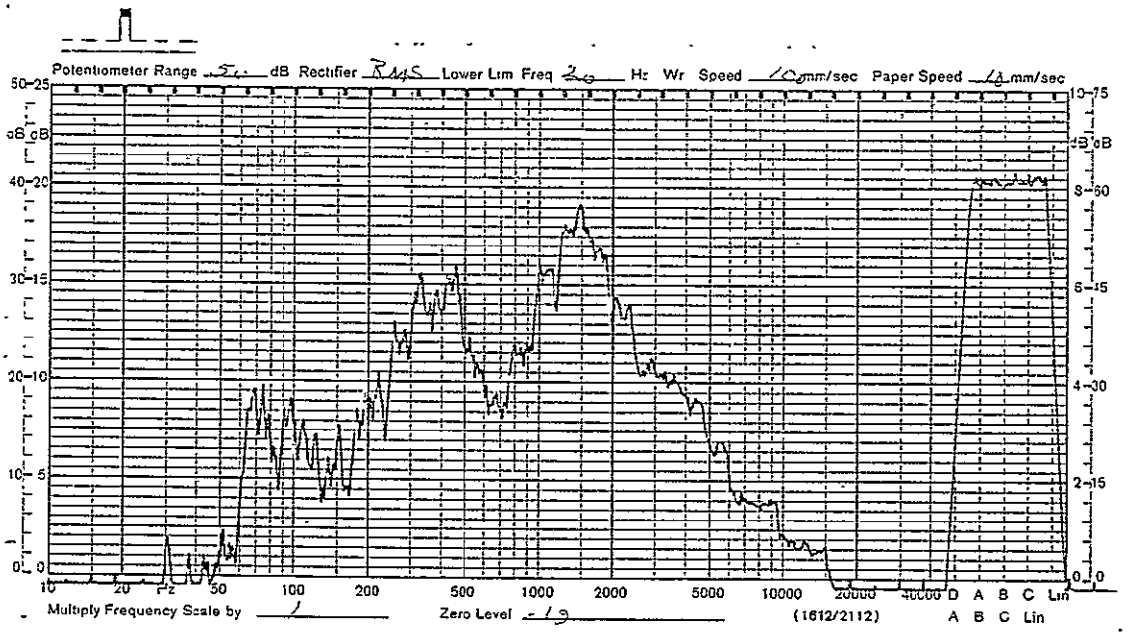

(c) Accelerometer A3

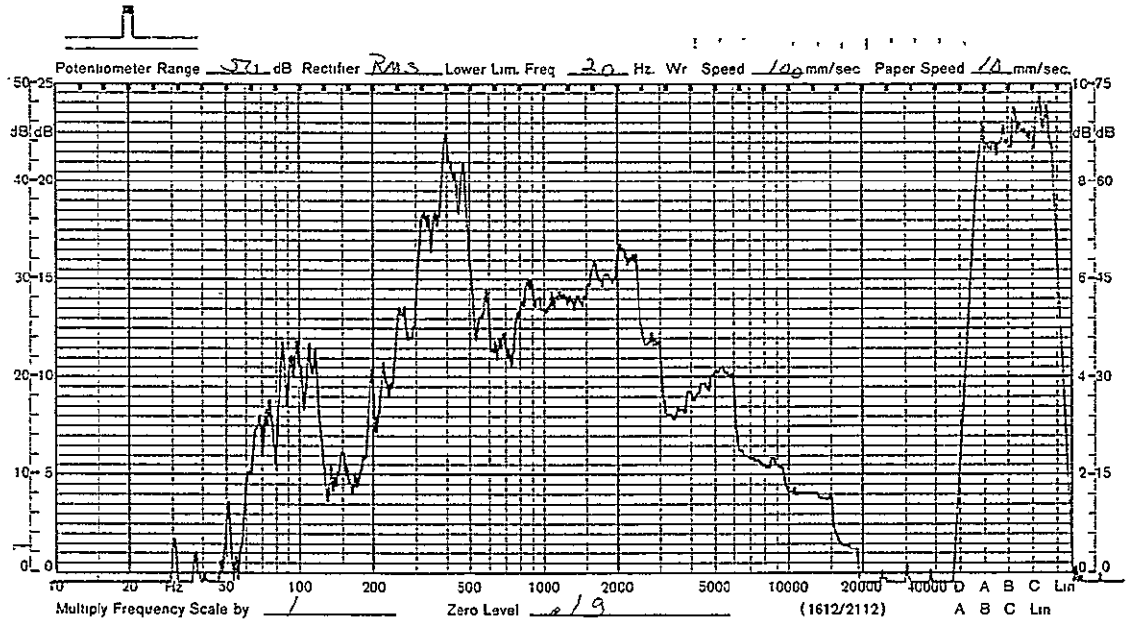

(d) Accelerometer A4

Figure A-31. (Concluded)

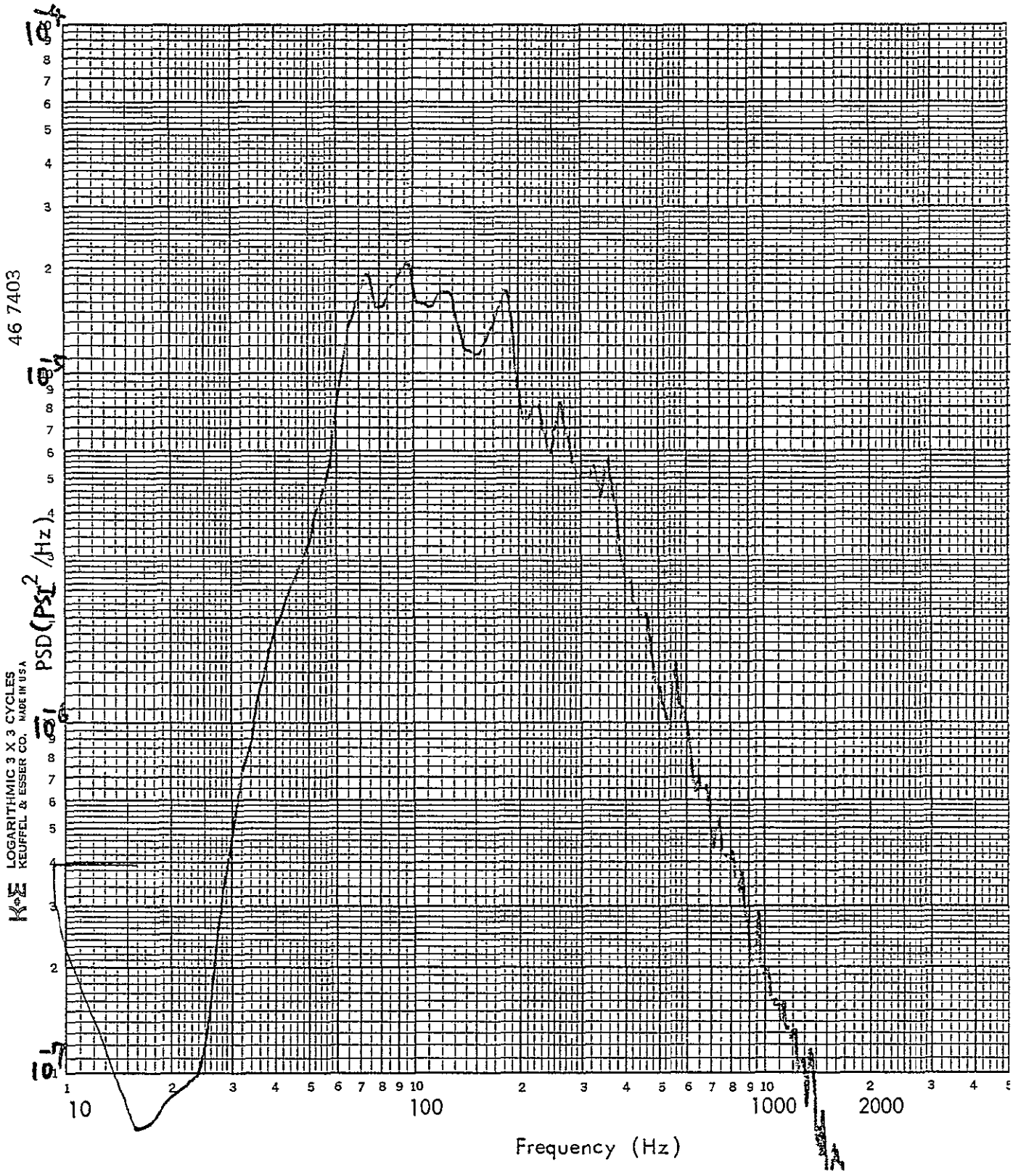

Figure A-32. PSD of Microphone M5, Test Run P-2

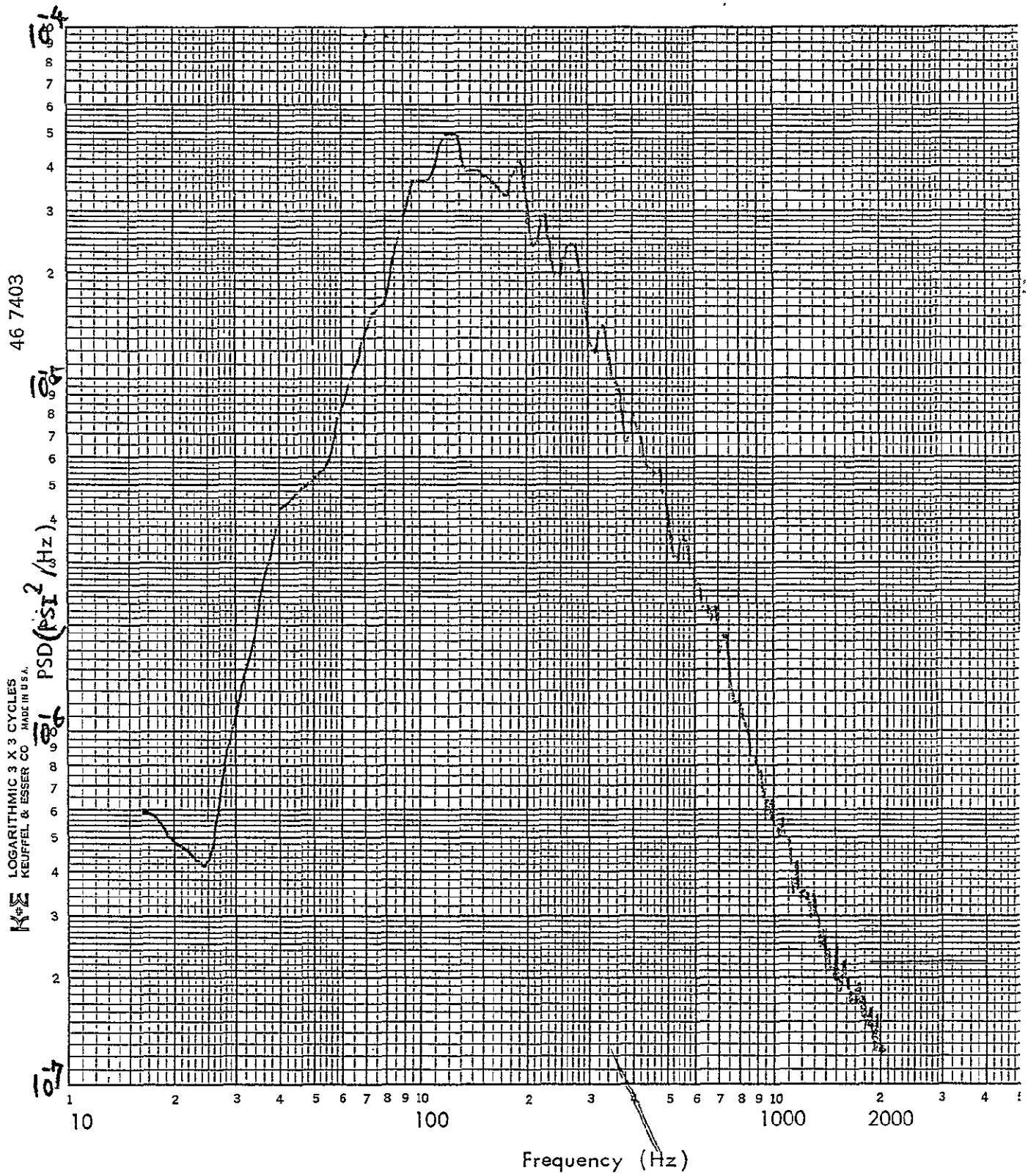

Figure A-33. PSD of Averaged Sound Pressure Levels, Test Run P-2

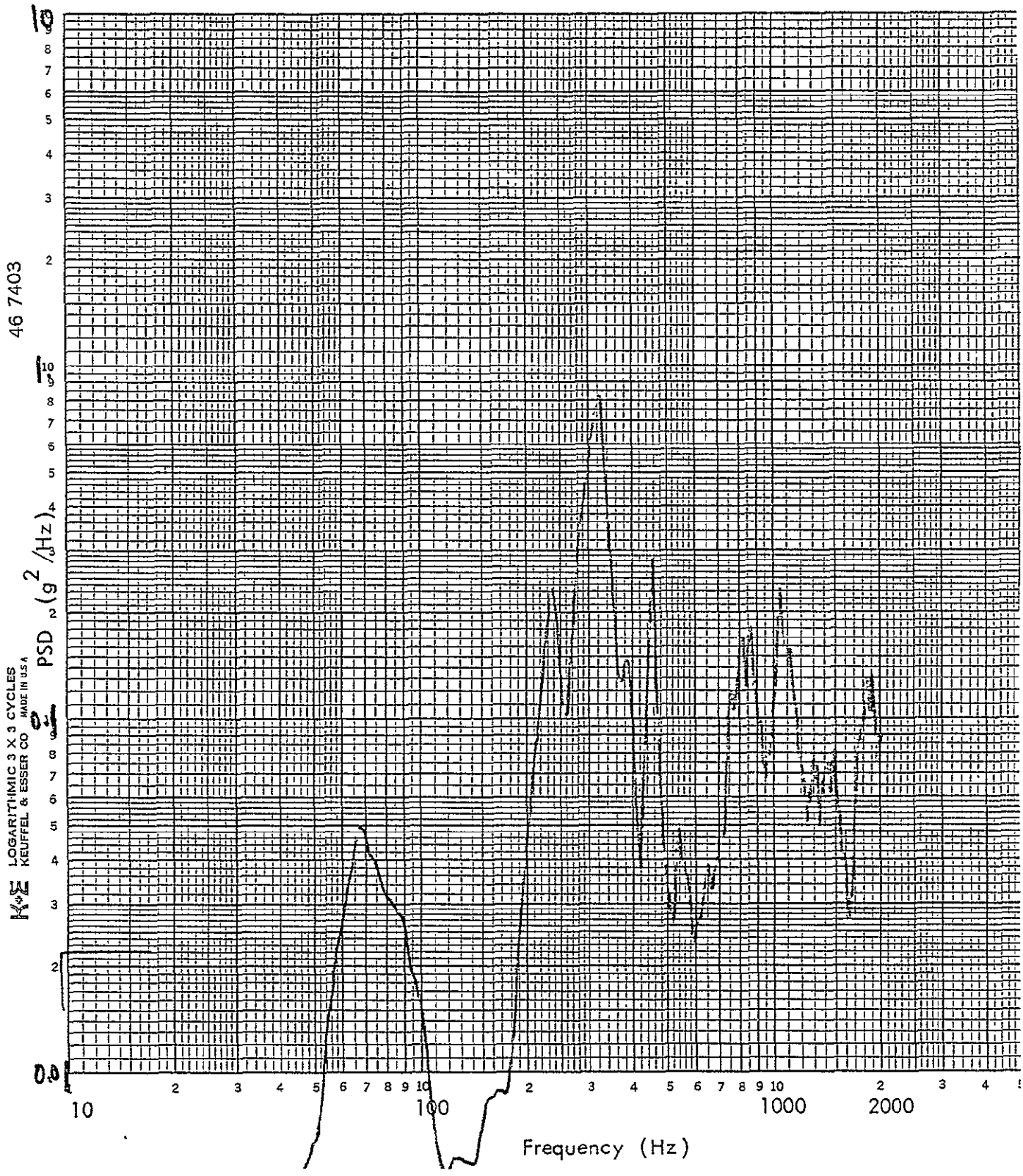

Figure A-34. PSD of Accelerometer A1, Test Run P-2

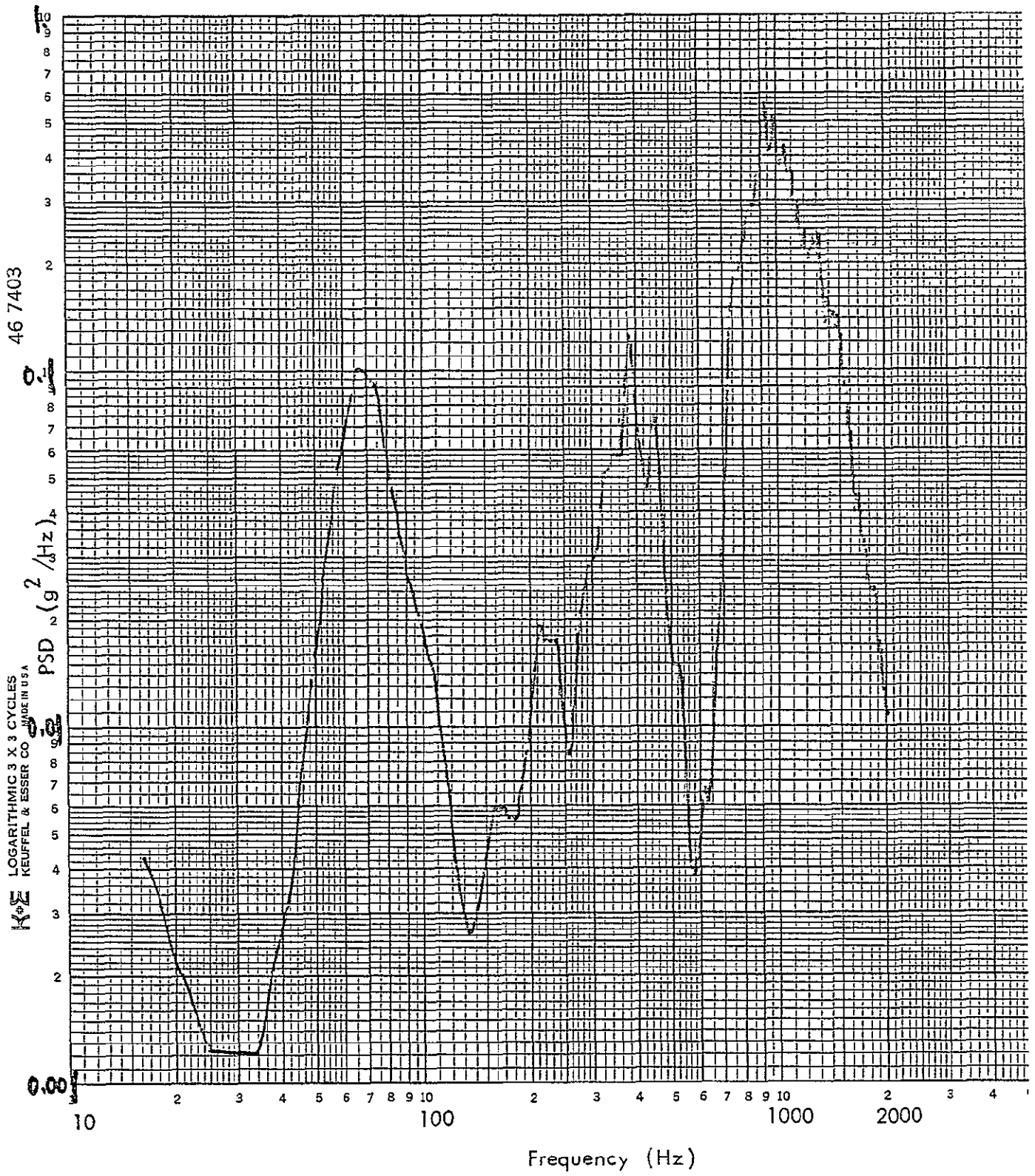

Figure A-35. PSD of Accelerometer A2, Test Run P-2

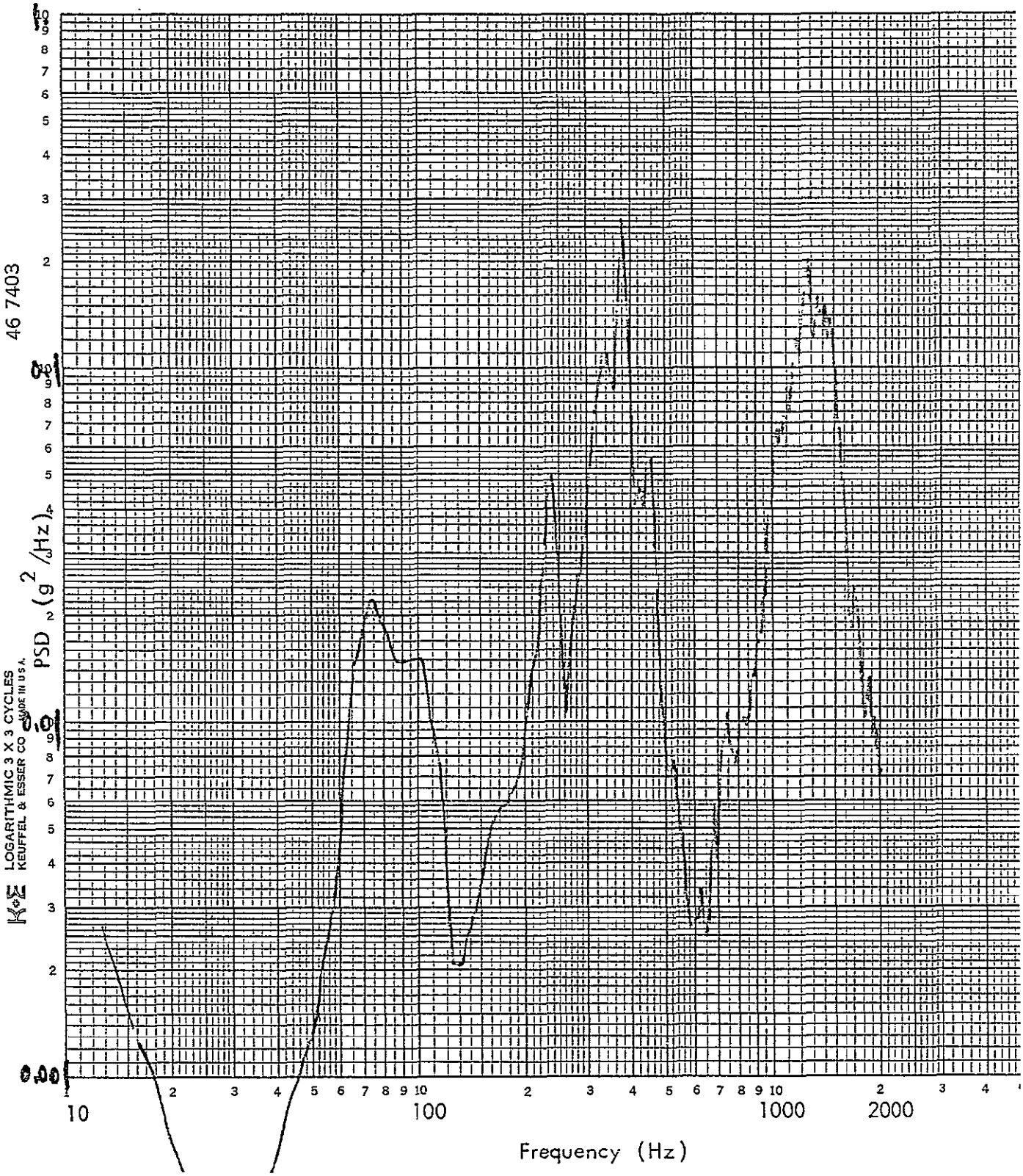

Figure A-36. PSD of Accelerometer A3, Test Run P-2

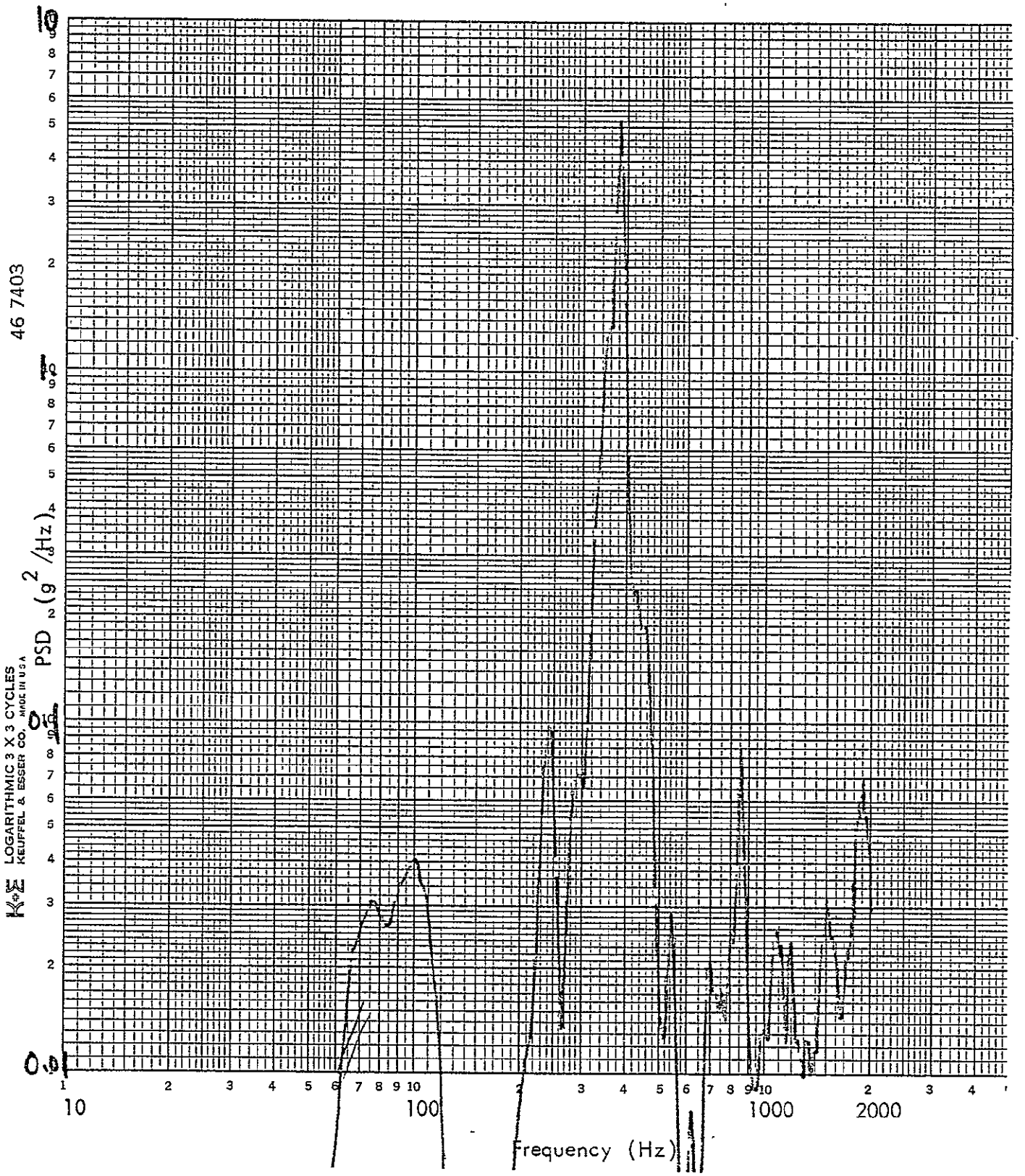

Figure A-37. PSD of Accelerometer A4, Test Run P-2

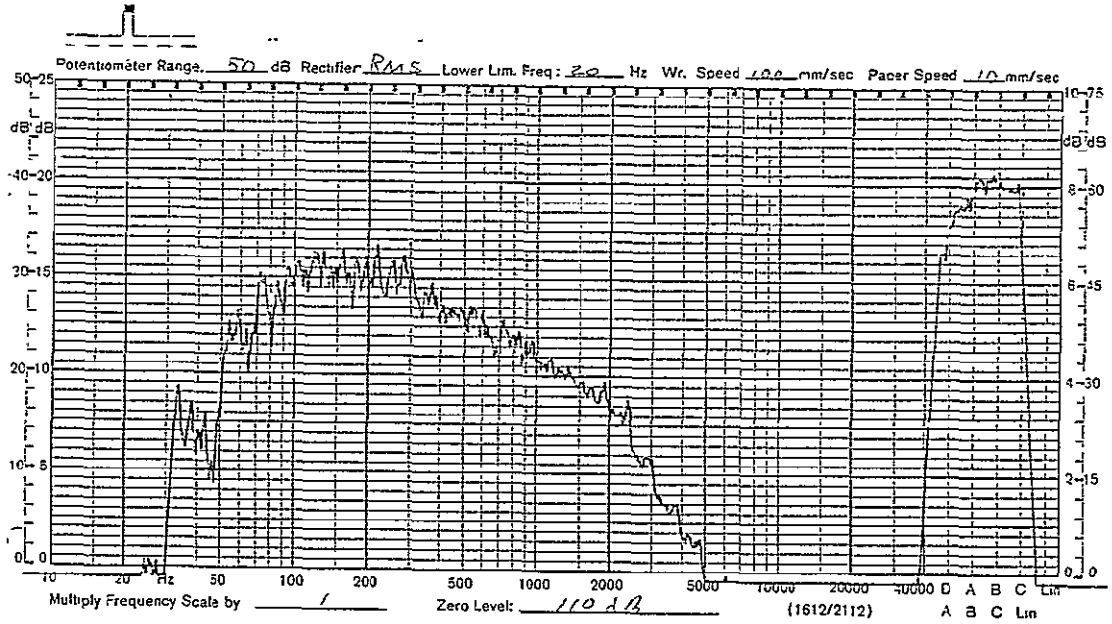

(a) Microphone M1

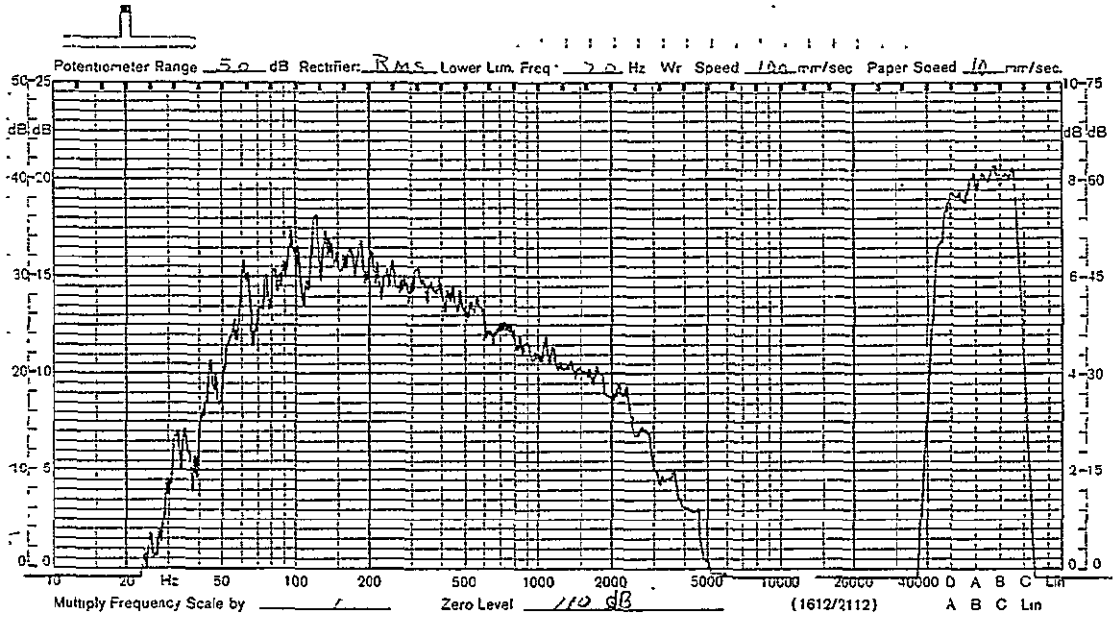

(b) Microphone M2

Figure A-38. Measured 1/3-Octave Sound Pressure Levels During Test Run R-2

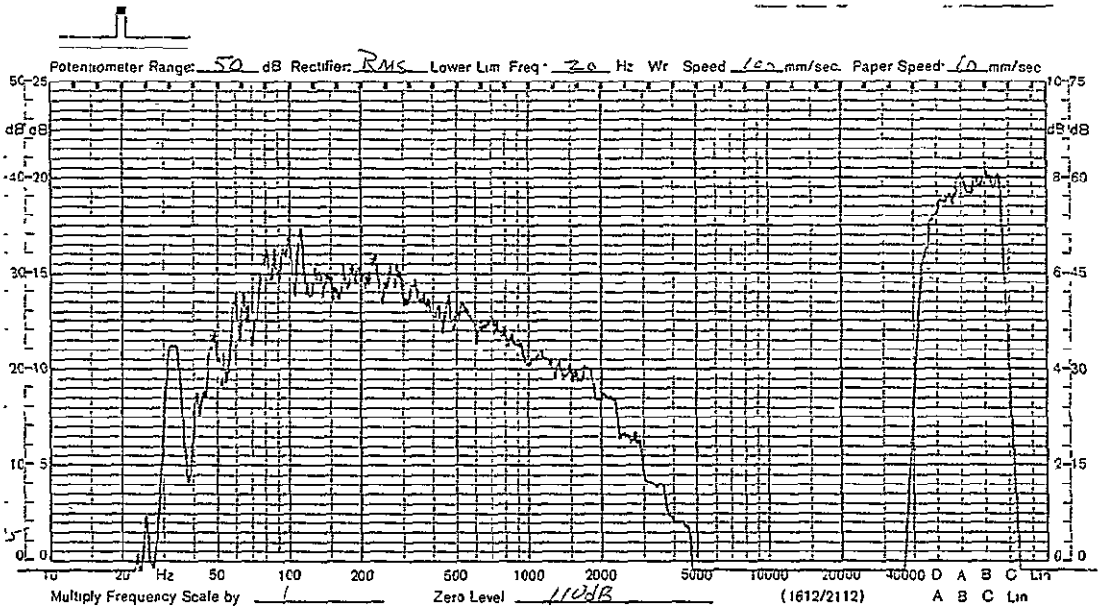

(c) Microphone 3

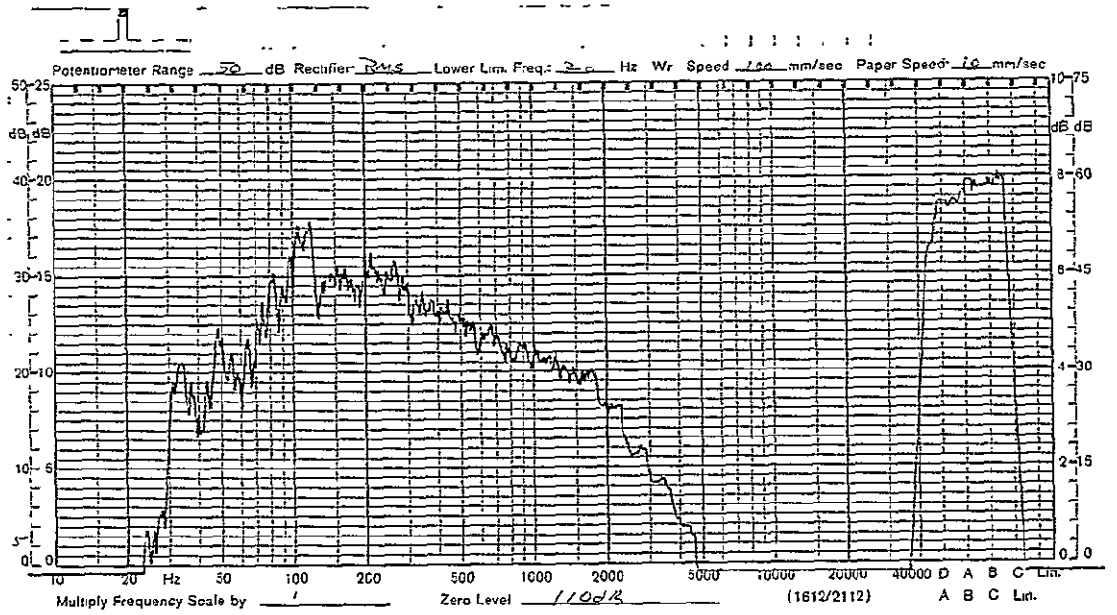

(d) Microphone M4

Figure A-38. (Concluded)

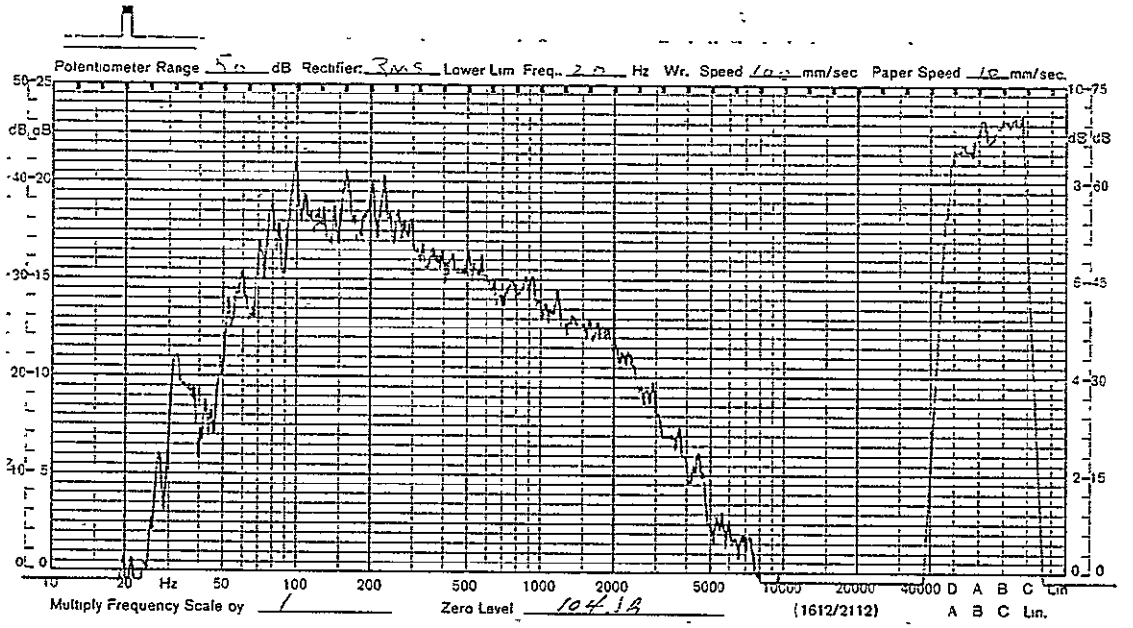

Figure A-39. Averaged 1/3-Octave Sound Pressure During Test Run R-2

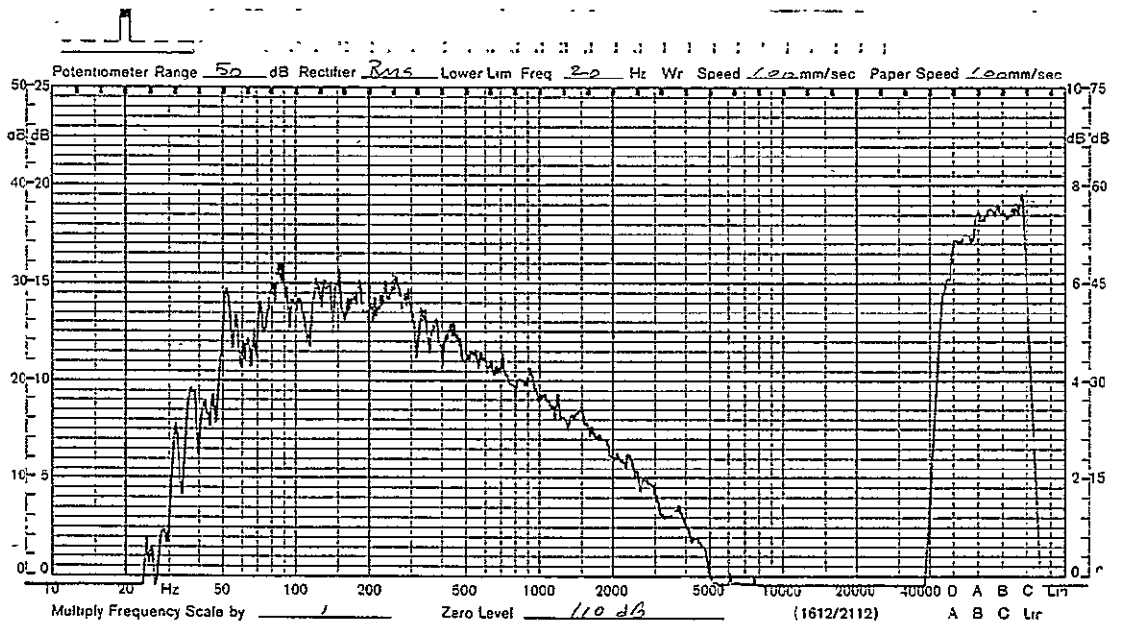

Figure A-40. Measured 1/3-Octave Sound Pressure of Control Microphone M5 During Test Run R-2

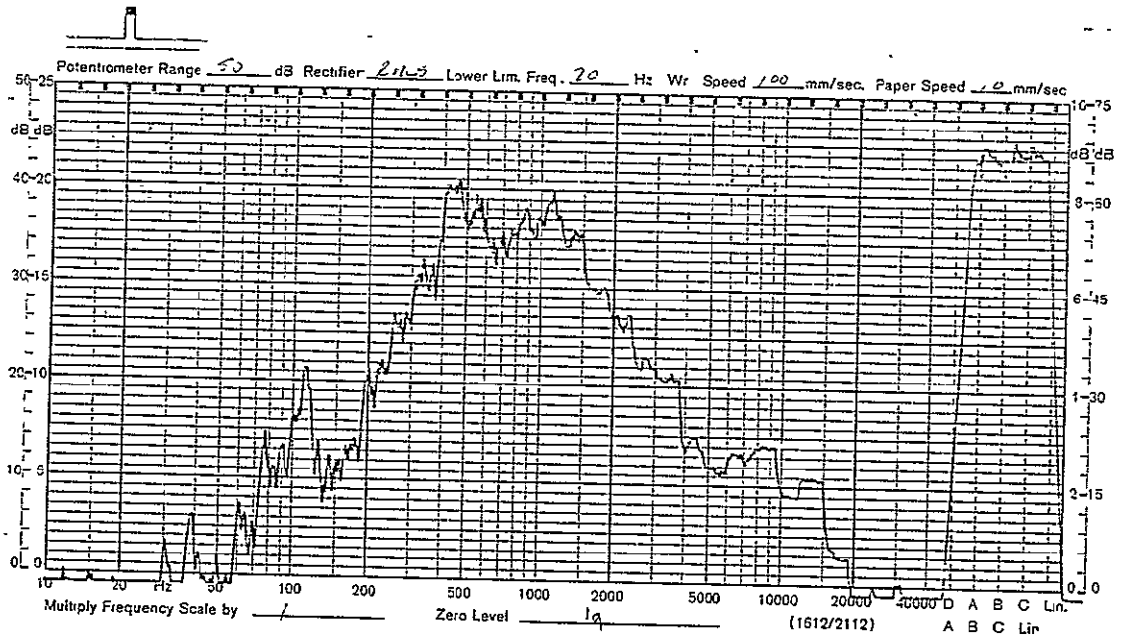

(a) Accelerometer A1

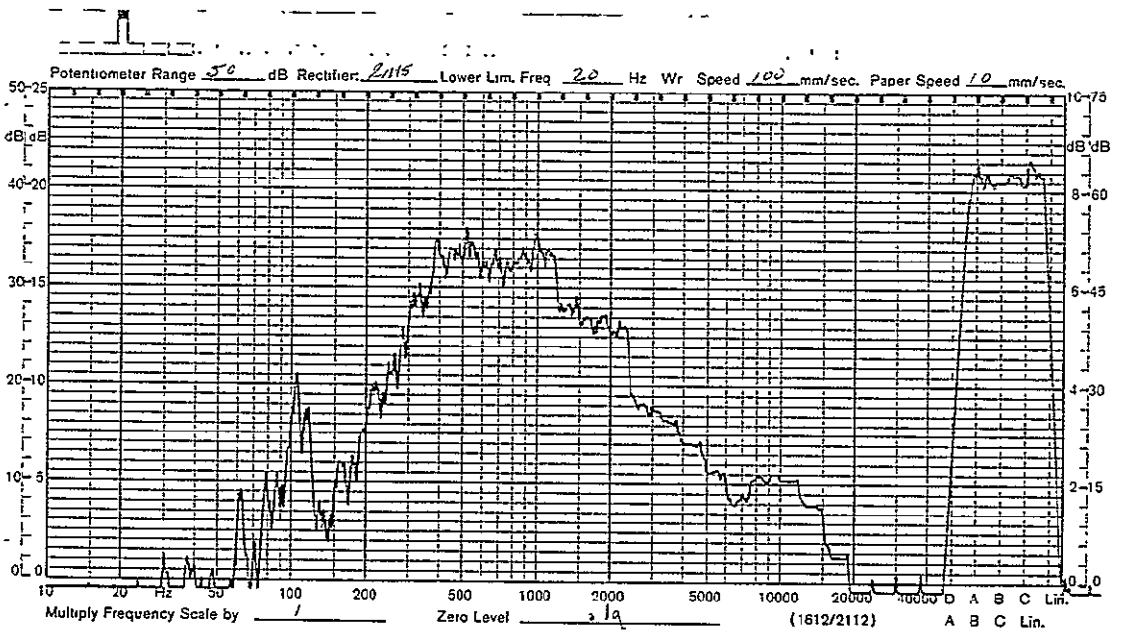

(b) Accelerometer A2

Figure A-41. Measured 1/3-Octave Acceleration Response Levels During Test Run R-2

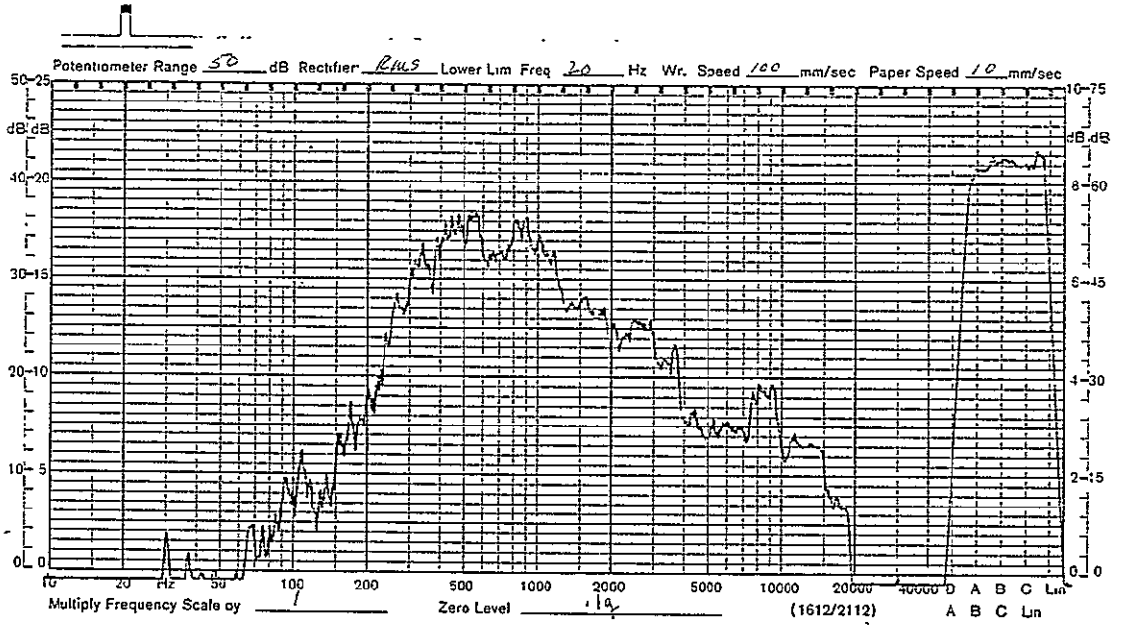

(c) Accelerometer A3

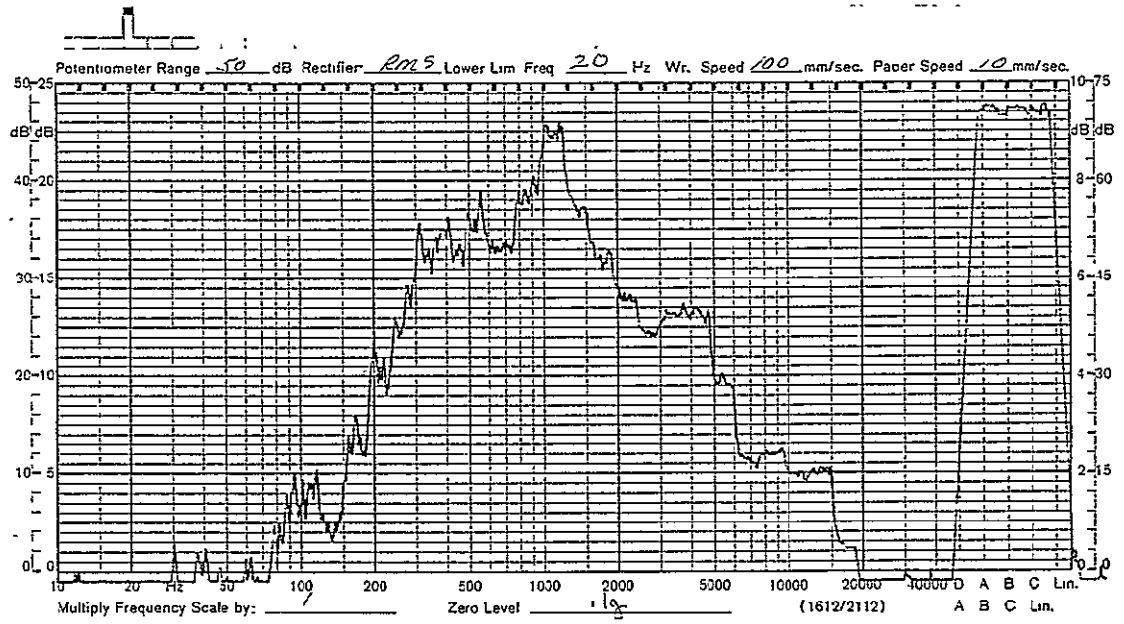

(d) Accelerometer A4

Figure A-41. (Concluded)

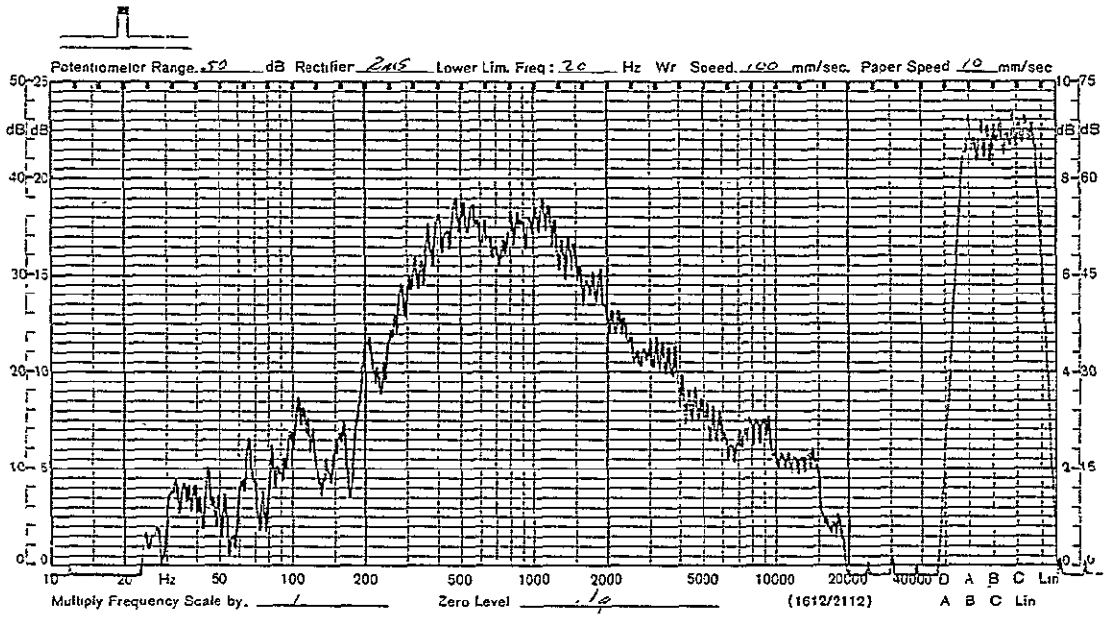

Figure A-42. Averaged 1/3-Octave Acceleration Response During Test Run R-2

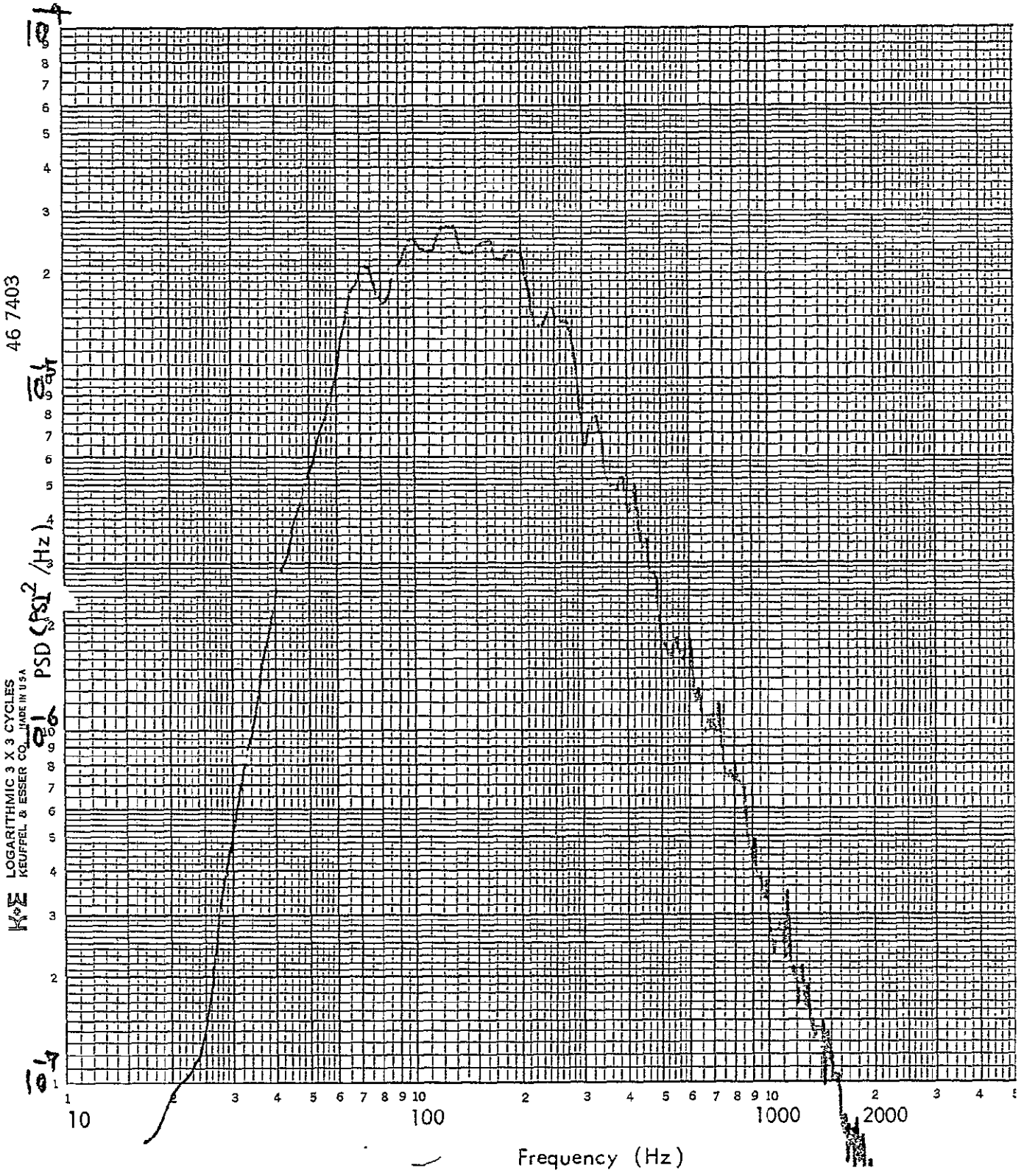

Figure A-43. PSD of Microphone M5, Test Run R-2

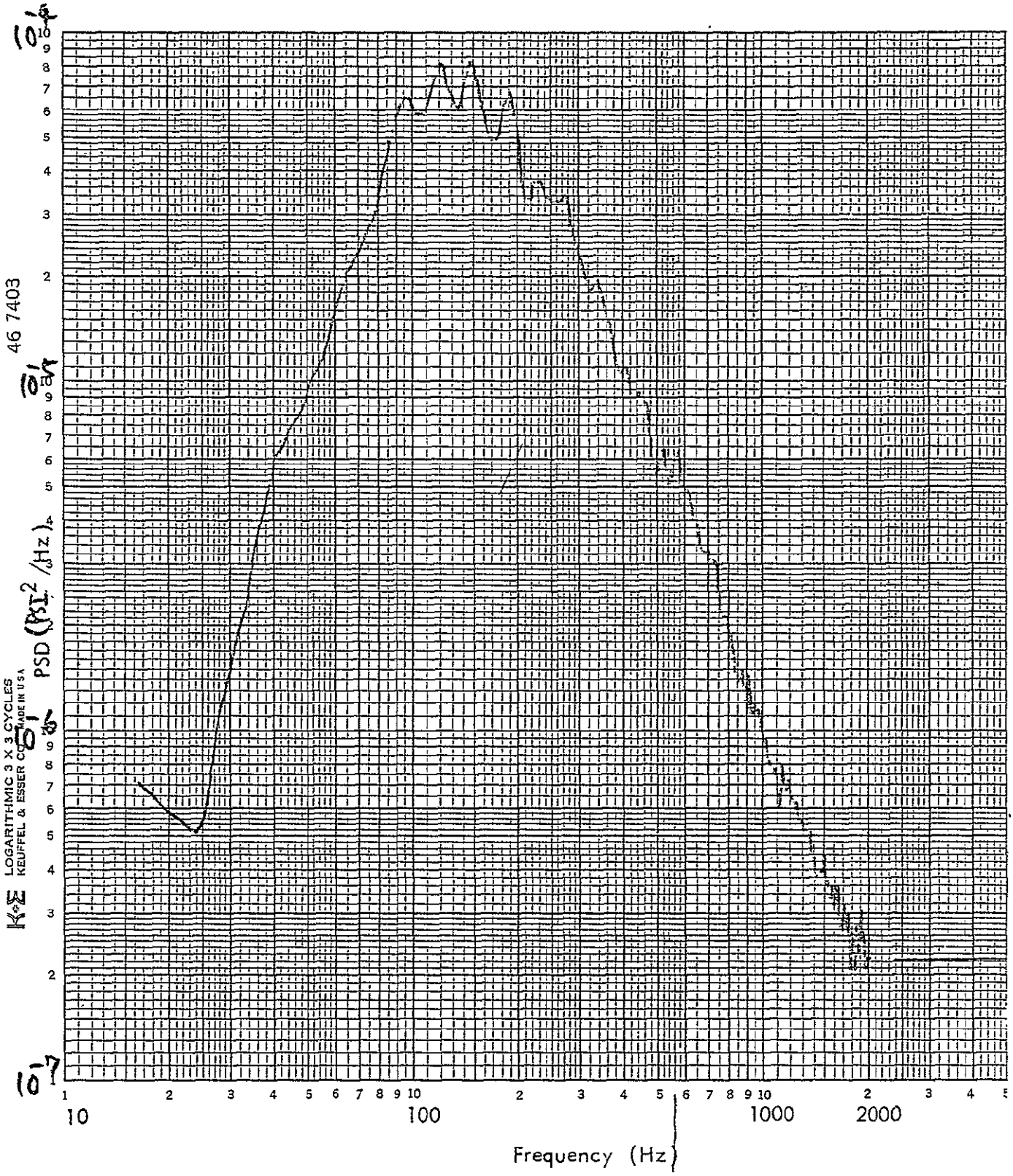

Figure A-44. PSD of Averaged Sound Pressure Levels, Test Run R-2

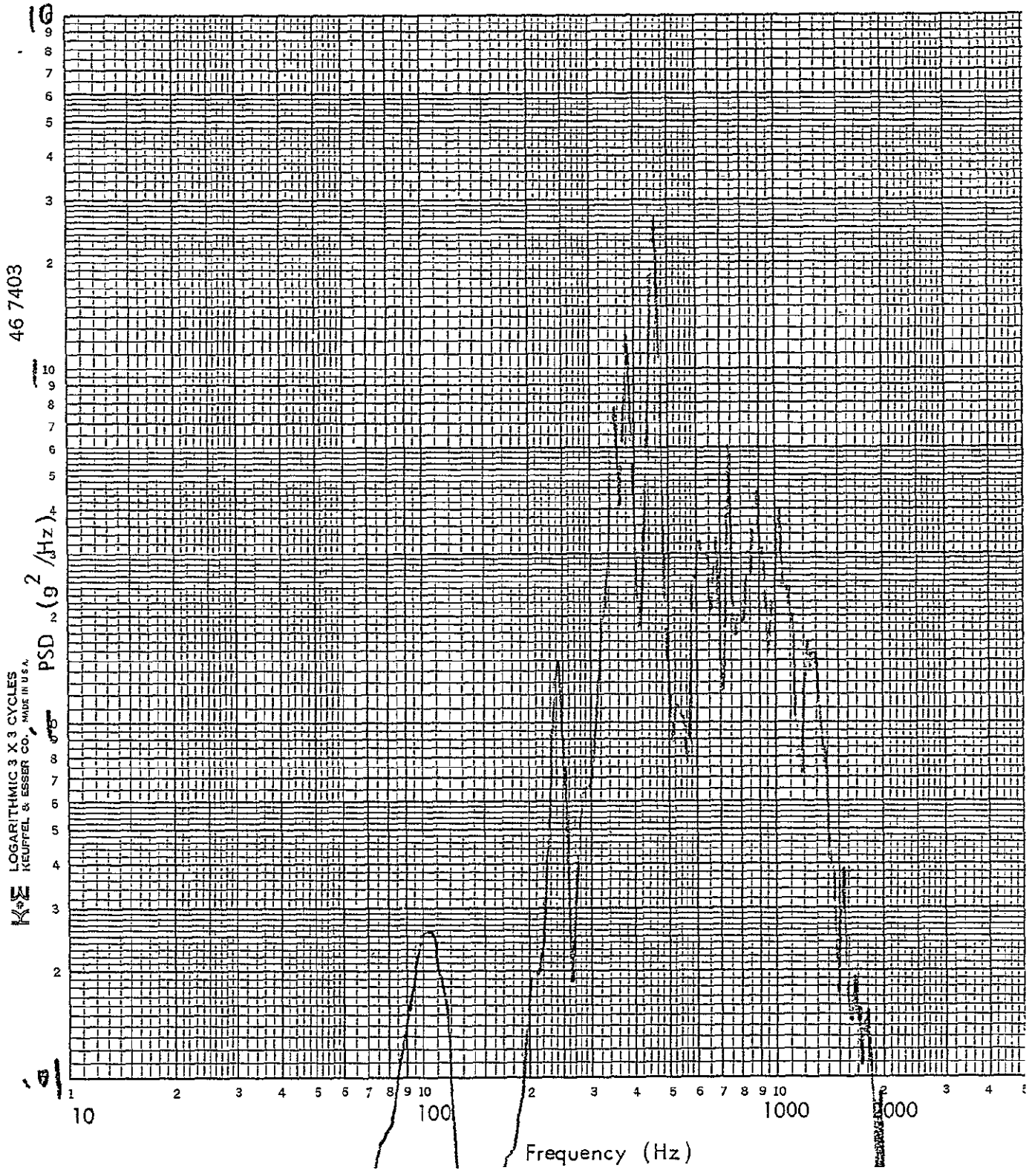

Figure A-45. PSD of Accelerometer A1, Test Run R-2

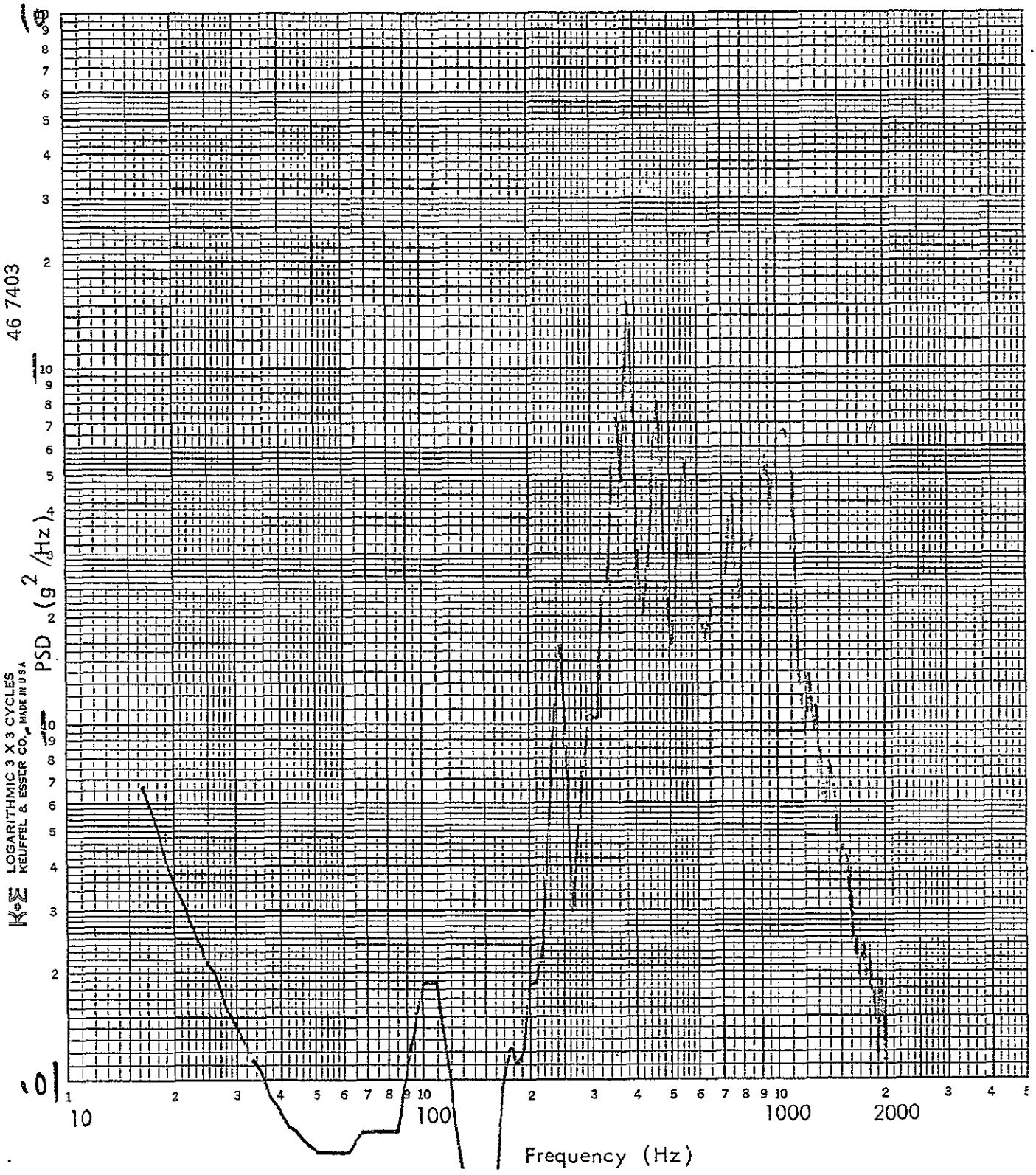

Figure A-46. PSD of Averaged Acceleration Responses, Test Run R-2

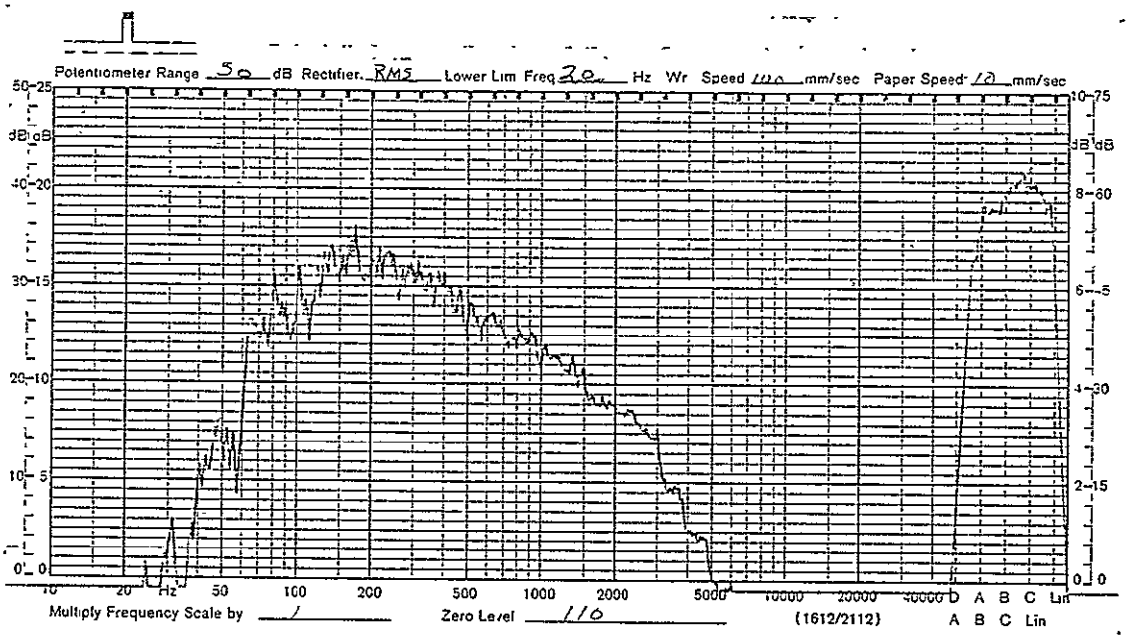

(a) Microphone M1

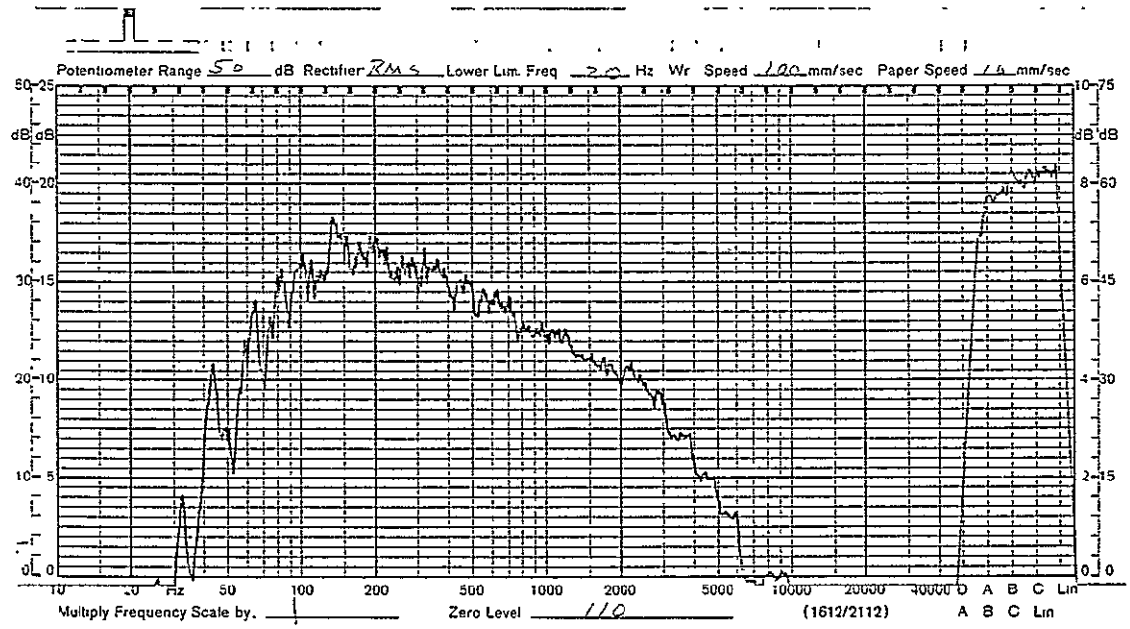

(b) Microphone M2

Figure A-47. Measured 1/3-Octave Sound Pressure Levels During Test Run S-2

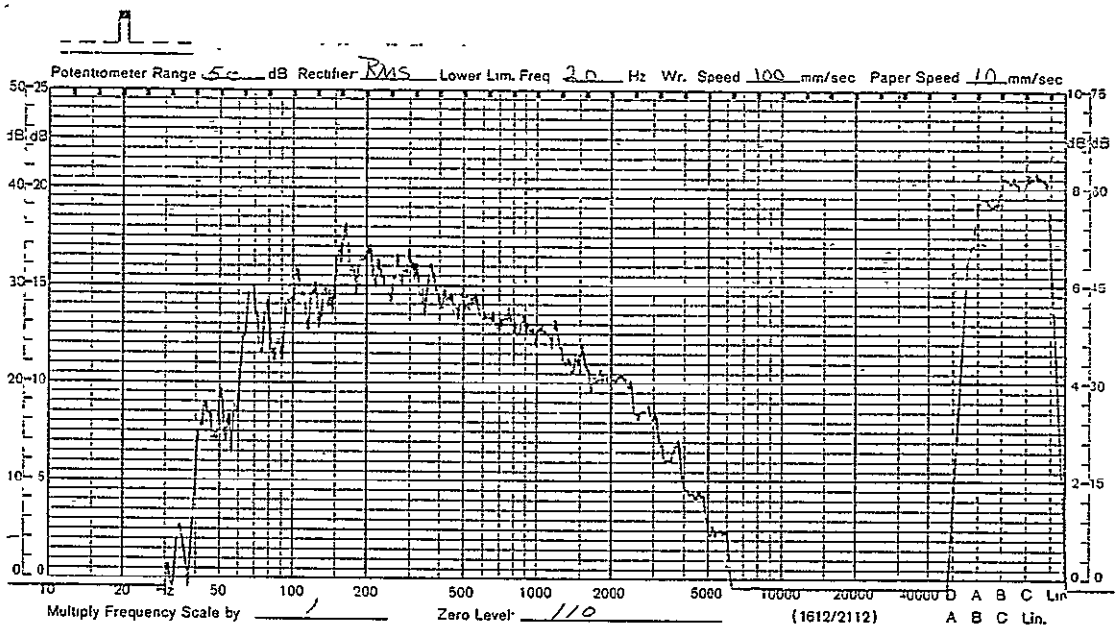

(c) Microphone M3

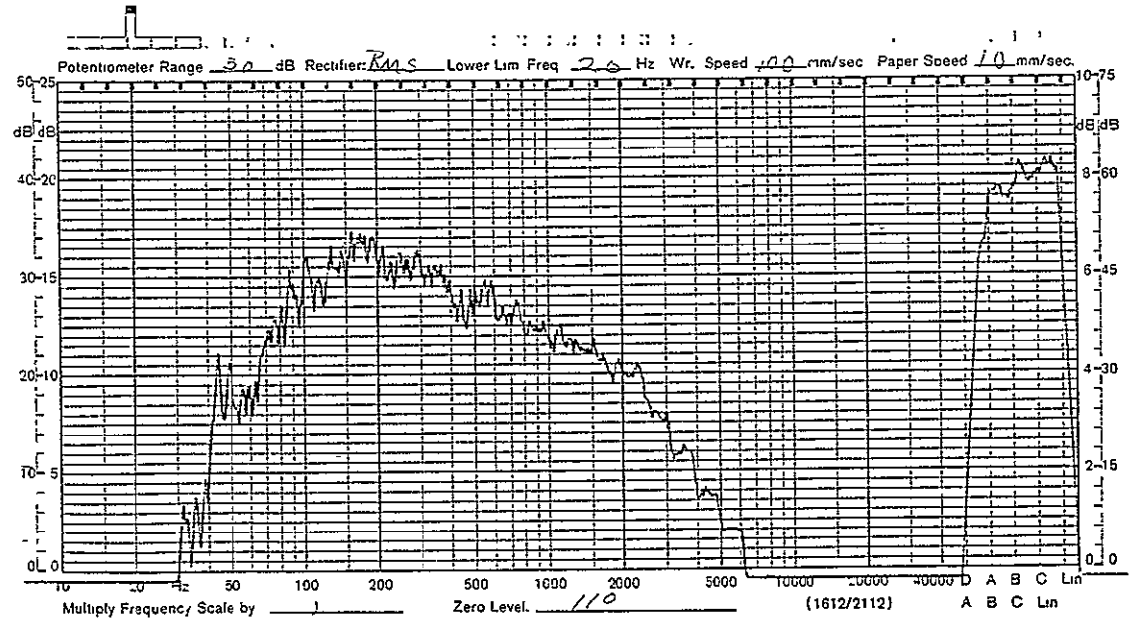

(d) Microphone M4

Figure A-47. (Concluded)

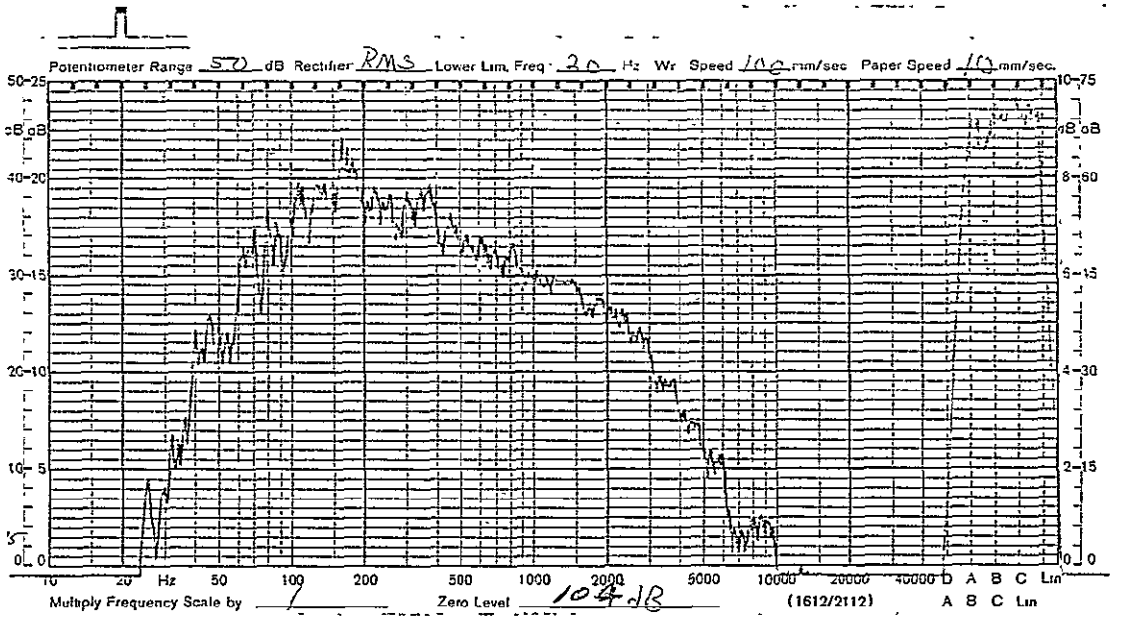

Figure A-48. Averaged 1/3-Octave Sound Pressure During Test Run S-2

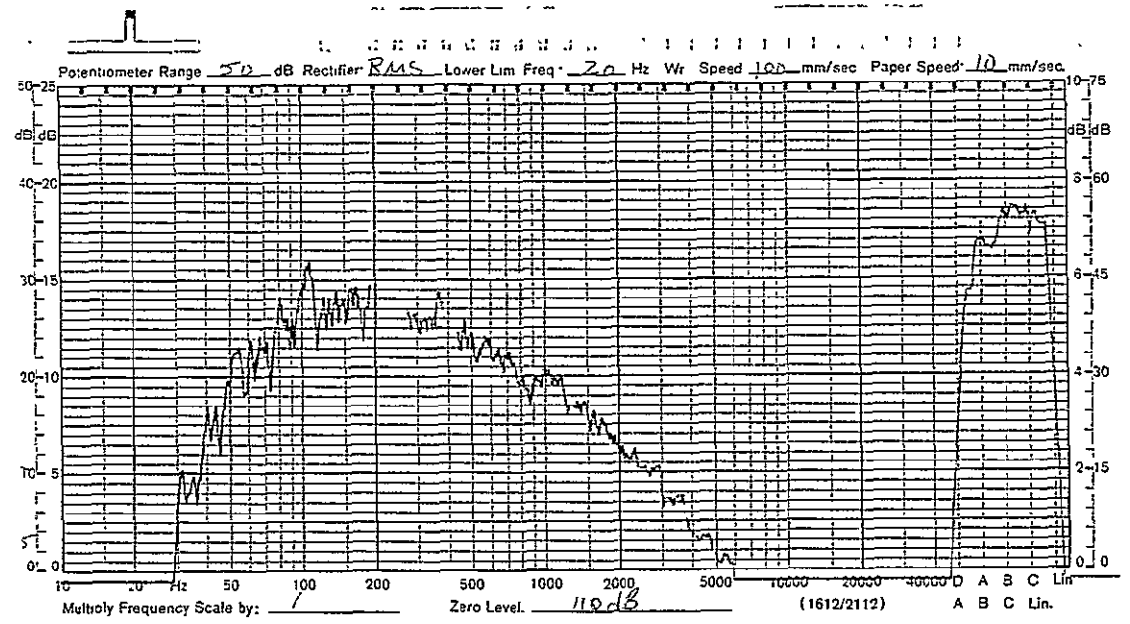

Figure A-49. Measured 1/3-Octave Sound Pressure of Control Microphone M5 During Test Run S-2

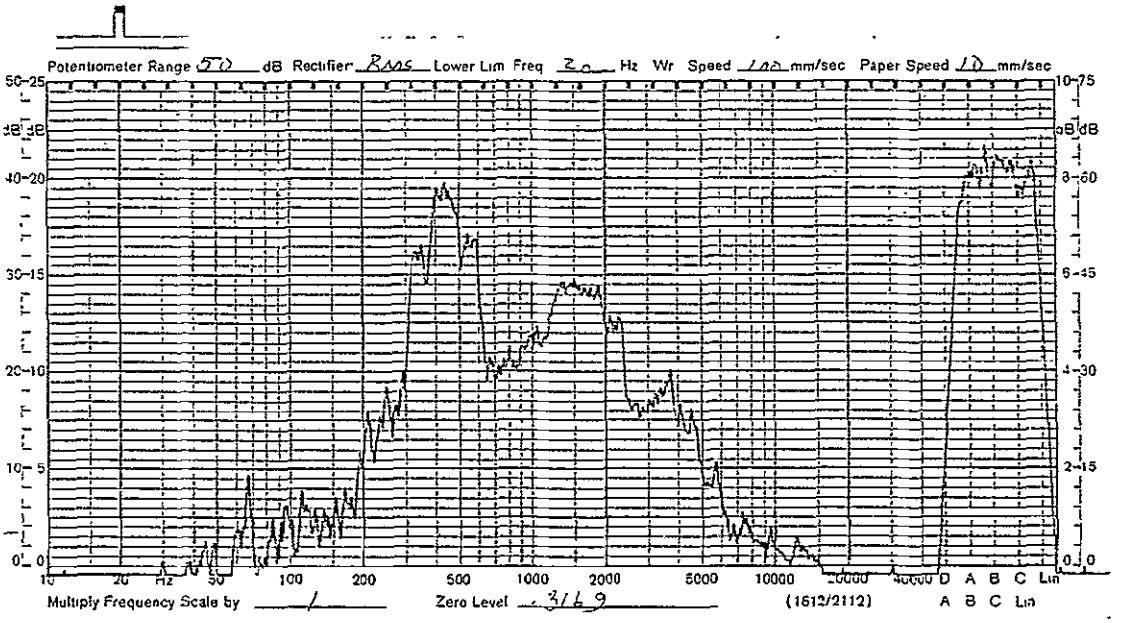

(a) Accelerometer A1

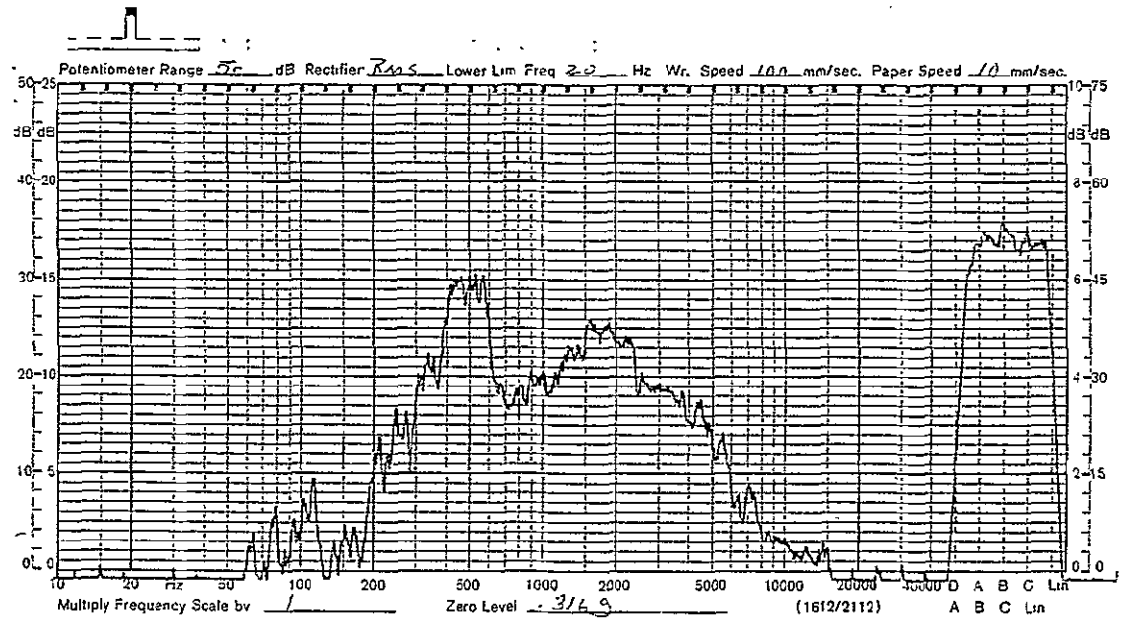

(b) Accelerometer A2

Figure A-50. Measured 1/3-Octave Acceleration Response Levels During Test Run S-2

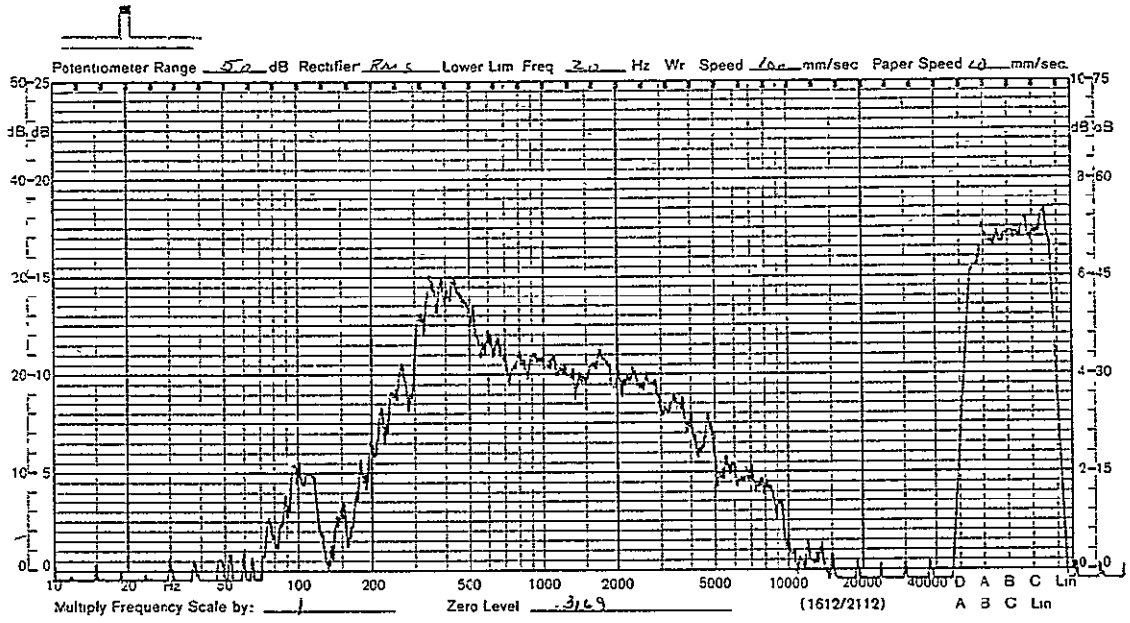

(c) Accelerometer A3

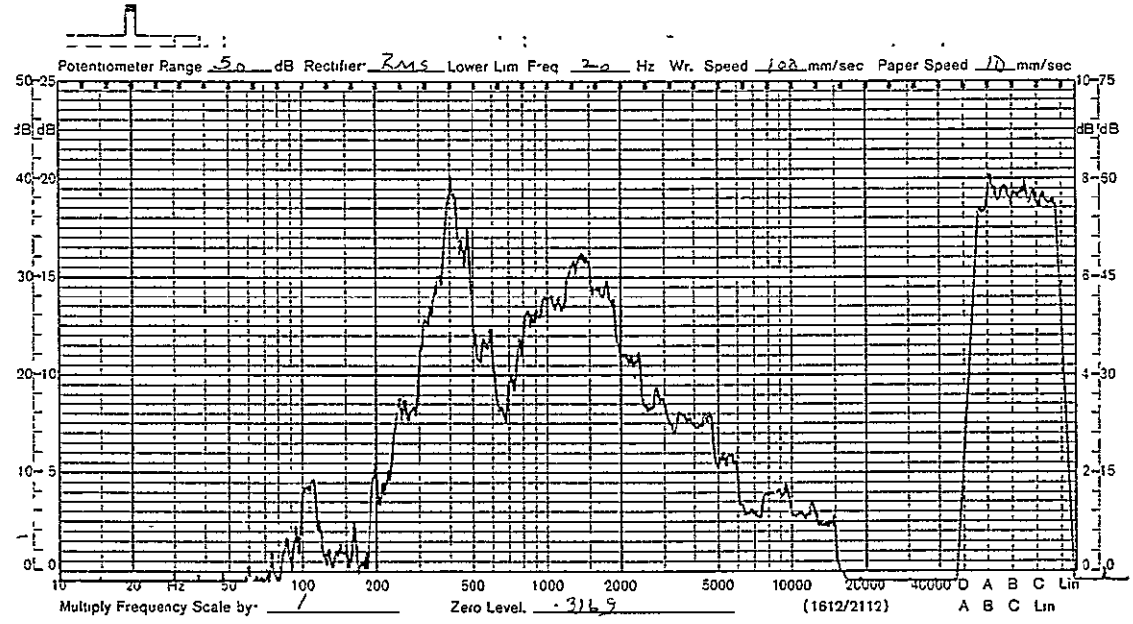

(d) Accelerometer A4

Figure A-50. (Concluded)

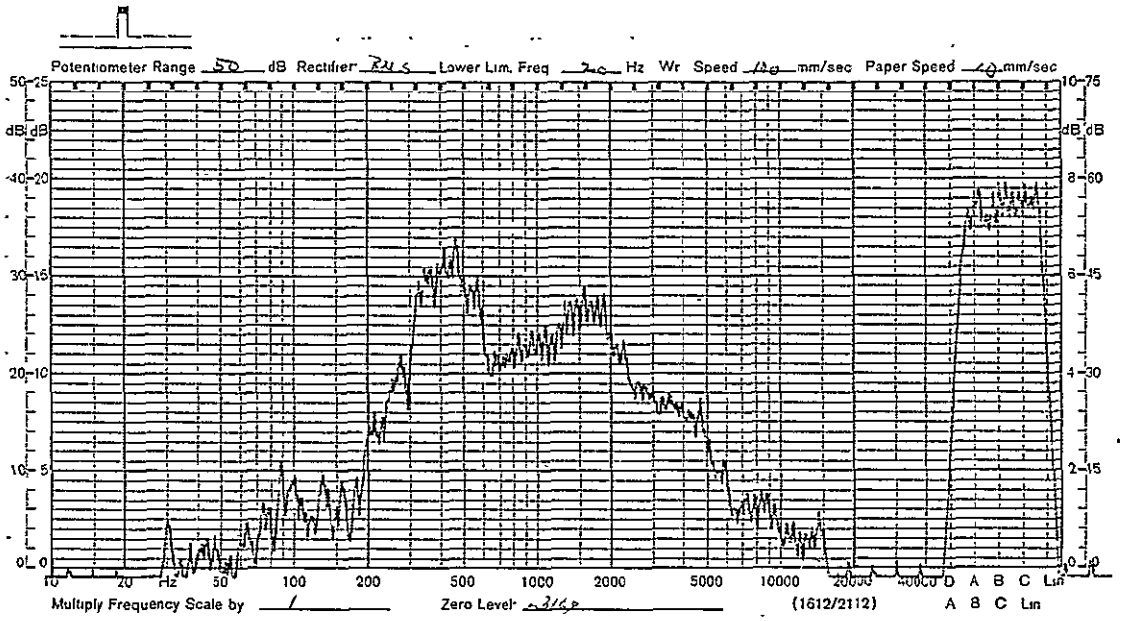

Figure A-51. Averaged 1/3-Octave Acceleration Response During Test Run S-2

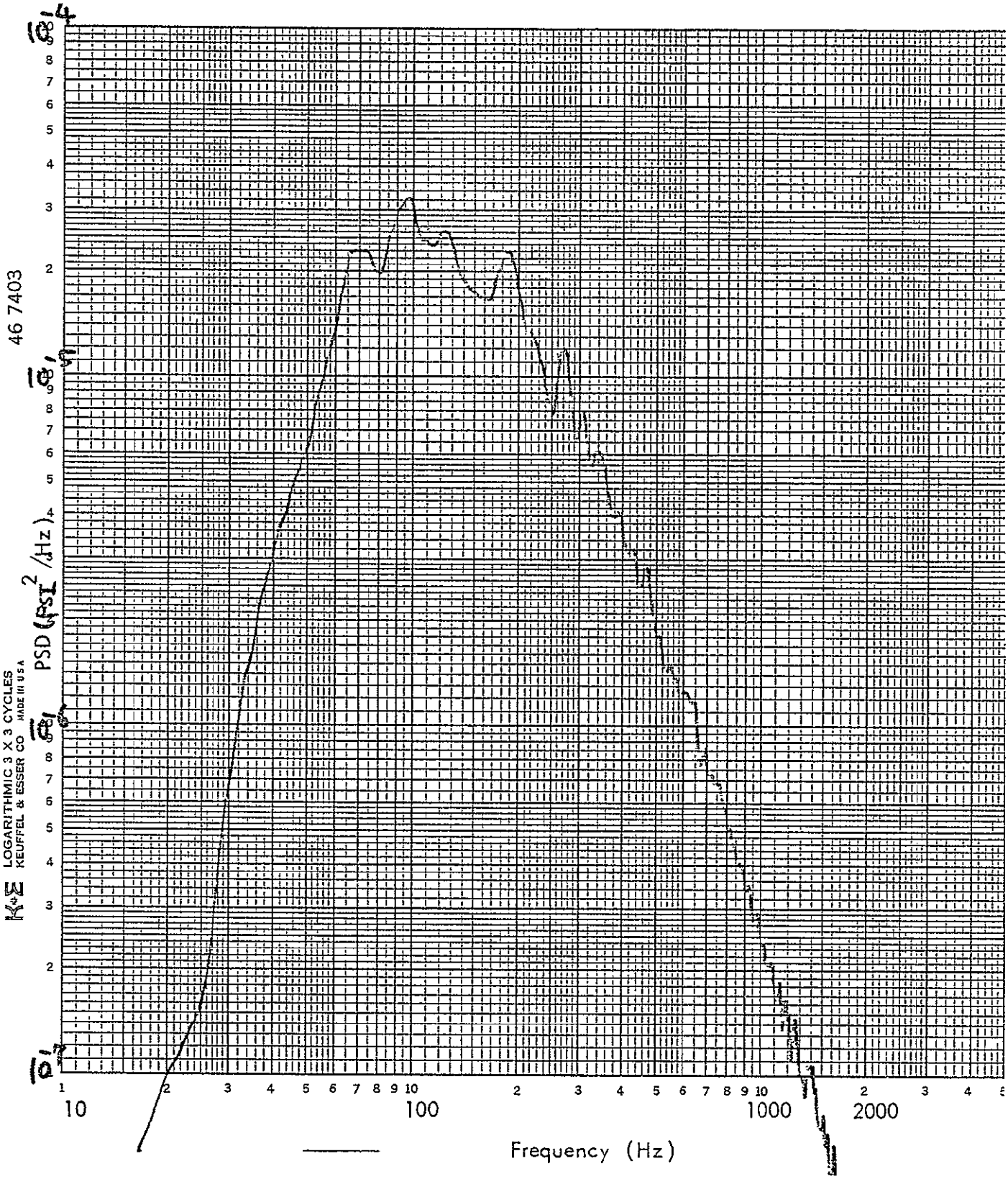

Figure A-52. PSD of Microphone M5, Test Run S-2

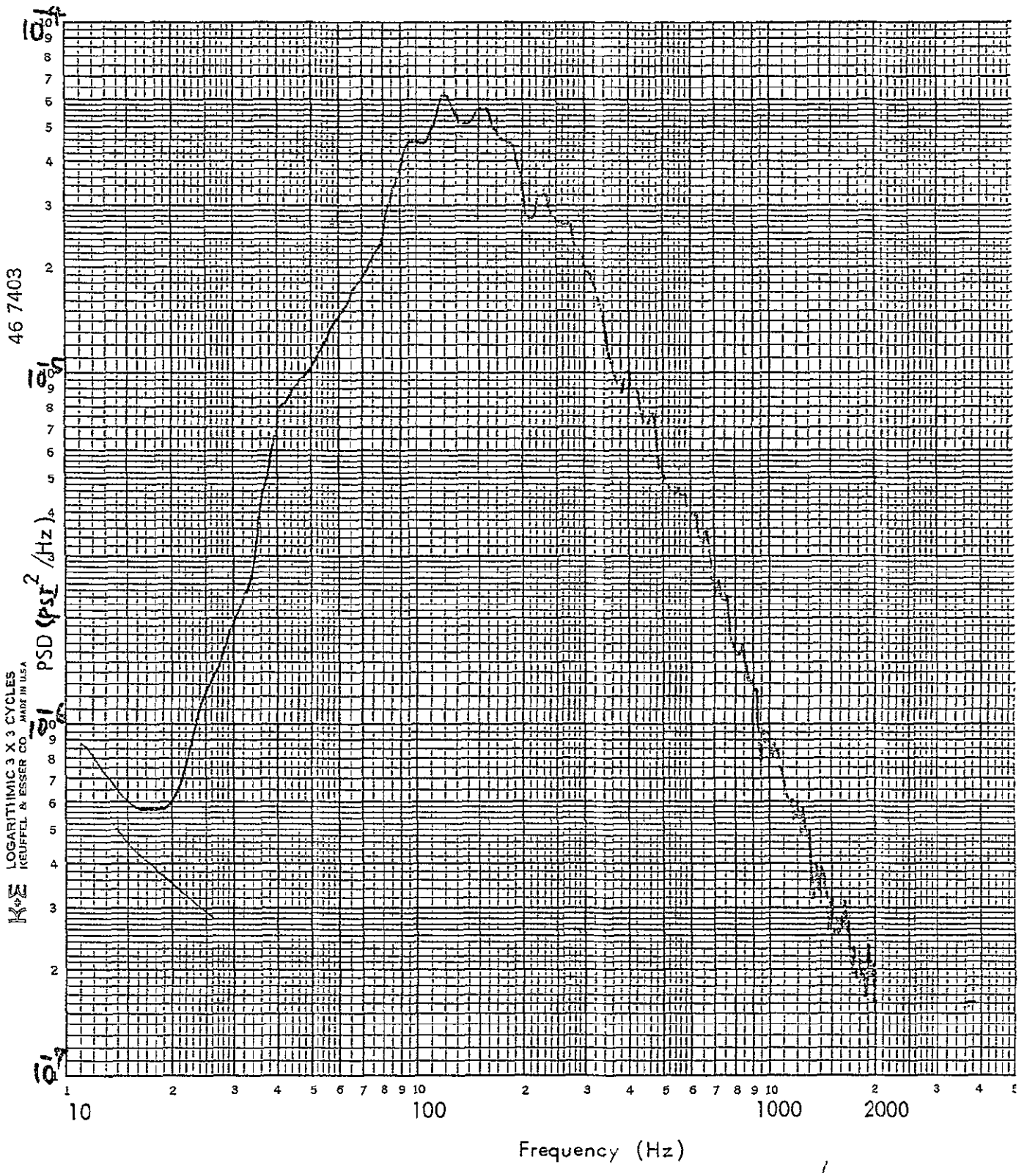

Figure A-53. PSD of Averaged Sound Pressure Levels, Test Run S-2

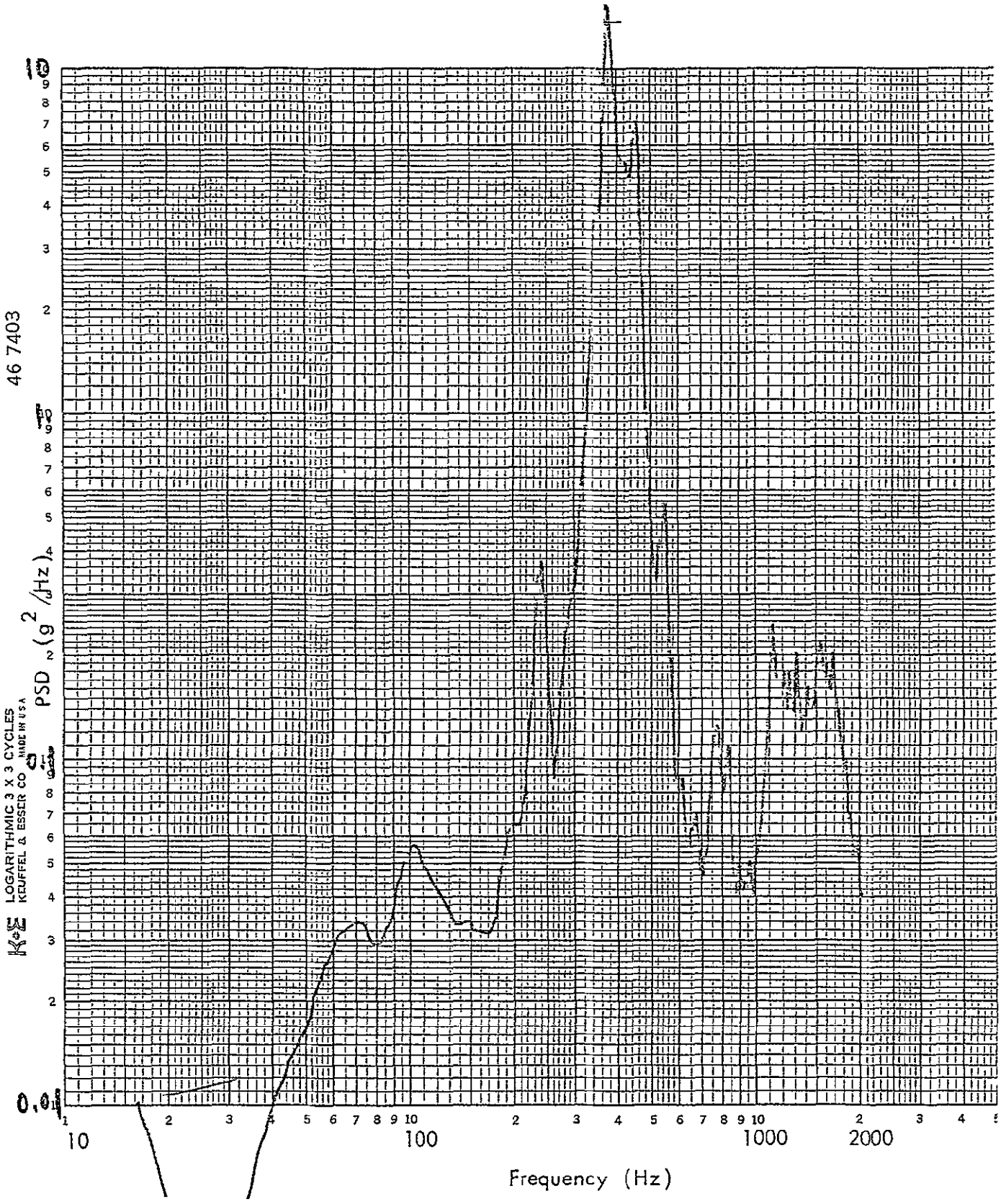

Figure A-54. PSD of Accelerometer A1, Test Run S-2

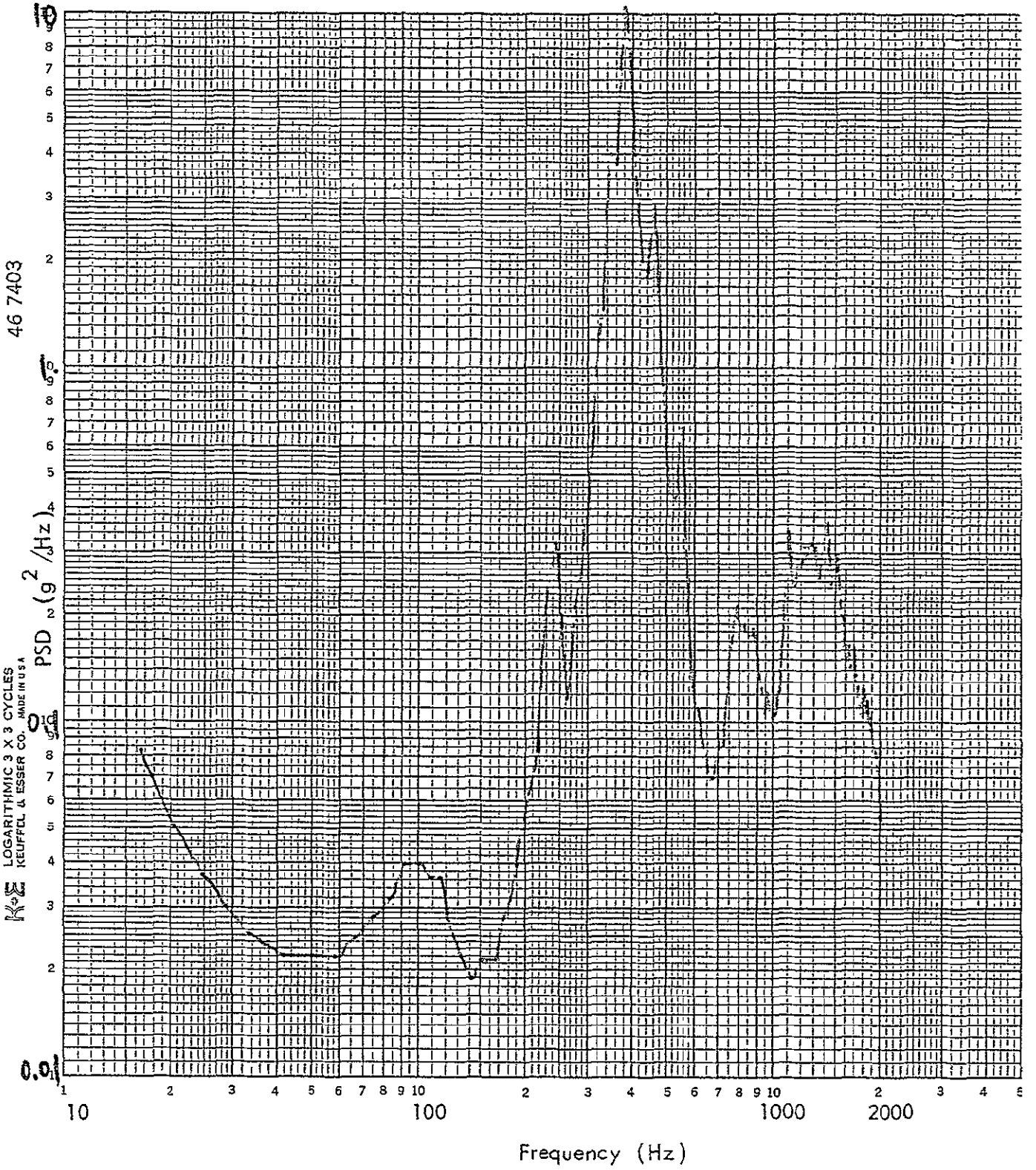

Figure A-55. PSD of Averaged Acceleration Responses, Test Run S-2

WR 76-4

DEVELOPMENT OF MODIFIED VIBRATION TEST CRITERIA FOR QUALIFYING SPACE VEHICLE COMPONENTS

K.Y. Chang and G.C. Kao
May 1976
Wyle Laboratories, Research Staff, Huntsville, Alabama

This report presents the results of the evaluation of two response prediction methods relating to the prediction of structural responses of stiffened shell structures with or without attached components, subjected to broadband acoustic excitations. The methods under evaluation were the constant mass attenuation method and the impedance ratio method. Example problems were used to illustrate the application procedures of these two methods and to compare their predicted results with the experimentally measured data. It was found that more realistic estimates of the structural response can be obtained by the impedance ratio method.

I. K.Y. CHANG
G.C. KAO

II. WR 76-4

III. P.O. No. NAS8-31414

1. Mechanical Impedance
2. Acoustic Mobility
3. Blocked Pressure
4. Nomograms
5. Stiffened Shells
6. Test Criteria
7. Computation Techniques
8. Experiments

WR 76-4

DEVELOPMENT OF MODIFIED VIBRATION TEST CRITERIA FOR QUALIFYING SPACE VEHICLE COMPONENTS

K.Y. Chang and G.C. Kao
May 1976
Wyle Laboratories, Research Staff, Huntsville, Alabama

This report presents the results of the evaluation of two response prediction methods relating to the prediction of structural responses of stiffened shell structures with or without attached components, subjected to broadband acoustic excitations. The methods under evaluation were the constant mass attenuation method and the impedance ratio method. Example problems were used to illustrate the application procedures of these two methods and to compare their predicted results with the experimentally measured data. It was found that more realistic estimates of the structural response can be obtained by the impedance ratio method.

I. K.Y. CHANG
G.C. KAO

II. WR 76-4

III. P.O. No. NAS8-31414

1. Mechanical Impedance
2. Acoustic Mobility
3. Blocked Pressure
4. Nomograms
5. Stiffened Shells
6. Test Criteria
7. Computation Techniques
8. Experiments

WR 76-4

DEVELOPMENT OF MODIFIED VIBRATION TEST CRITERIA FOR QUALIFYING SPACE VEHICLE COMPONENTS

K.Y. Chang and G.C. Kao
May 1976
Wyle Laboratories, Research Staff, Huntsville, Alabama

This report presents the results of the evaluation of two response prediction methods relating to the prediction of structural responses of stiffened shell structures with or without attached components, subjected to broadband acoustic excitations. The methods under evaluation were the constant mass attenuation method and the impedance ratio method. Example problems were used to illustrate the application procedures of these two methods and to compare their predicted results with the experimentally measured data. It was found that more realistic estimates of the structural response can be obtained by the impedance ratio method.

I. K.Y. CHANG
G.C. KAO

II. WR 76-4

III. P.O. No. NAS8-31414

1. Mechanical Impedance
2. Acoustic Mobility
3. Blocked Pressure
4. Nomograms
5. Stiffened Shells
6. Test Criteria
7. Computation Techniques
8. Experiments

WR 76-4

DEVELOPMENT OF MODIFIED VIBRATION TEST CRITERIA FOR QUALIFYING SPACE VEHICLE COMPONENTS

K.Y. Chang and G.C. Kao
May 1976
Wyle Laboratories, Research Staff, Huntsville, Alabama

This report presents the results of the evaluation of two response prediction methods relating to the prediction of structural responses of stiffened shell structures with or without attached components, subjected to broadband acoustic excitations. The methods under evaluation were the constant mass attenuation method and the impedance ratio method. Example problems were used to illustrate the application procedures of these two methods and to compare their predicted results with the experimentally measured data. It was found that more realistic estimates of the structural response can be obtained by the impedance ratio method.

I. K.Y. CHANG
G.C. KAO

II. WR 76-4

III. P.O. No. NAS8-31414

1. Mechanical Impedance
2. Acoustic Mobility
3. Blocked Pressure
4. Nomograms
5. Stiffened Shells
6. Test Criteria
7. Computation Techniques
8. Experiments

WR 76-4

DEVELOPMENT OF MODIFIED VIBRATION TEST CRITERIA FOR QUALIFYING SPACE VEHICLE COMPONENTS

K.Y. Chang and G.C. Kao
May 1976
Wyle Laboratories, Research Staff, Huntsville, Alabama

This report presents the results of the evaluation of two response prediction methods relating to the prediction of structural responses of stiffened shell structures with or without attached components, subjected to broadband acoustic excitations. The methods under evaluation were the constant mass attenuation method and the impedance ratio method. Example problems were used to illustrate the application procedures of these two methods and to compare their predicted results with the experimentally measured data. It was found that more realistic estimates of the structural response can be obtained by the impedance ratio method.

I. K.Y. CHANG
G.C. KAO

II. WR 76-4

III. P.O. No. NAS8-31414

1. Mechanical Impedance
2. Acoustic Mobility
3. Blocked Pressure
4. Nomograms
5. Stiffened Shells
6. Test Criteria
7. Computation Techniques
8. Experiments

WR 76-4

DEVELOPMENT OF MODIFIED VIBRATION TEST CRITERIA FOR QUALIFYING SPACE VEHICLE COMPONENTS

K.Y. Chang and G.C. Kao
May 1976
Wyle Laboratories, Research Staff, Huntsville, Alabama

This report presents the results of the evaluation of two response prediction methods relating to the prediction of structural responses of stiffened shell structures with or without attached components, subjected to broadband acoustic excitations. The methods under evaluation were the constant mass attenuation method and the impedance ratio method. Example problems were used to illustrate the application procedures of these two methods and to compare their predicted results with the experimentally measured data. It was found that more realistic estimates of the structural response can be obtained by the impedance ratio method.

I. K.Y. CHANG
G.C. KAO

II. WR 76-4

III. P.O. No. NAS8-31414

1. Mechanical Impedance
2. Acoustic Mobility
3. Blocked Pressure
4. Nomograms
5. Stiffened Shells
6. Test Criteria
7. Computation Techniques
8. Experiments

WR 76-4

DEVELOPMENT OF MODIFIED VIBRATION TEST CRITERIA FOR QUALIFYING SPACE VEHICLE COMPONENTS

K.Y. Chang and G.C. Kao
May 1976
Wyle Laboratories, Research Staff, Huntsville, Alabama

This report presents the results of the evaluation of two response prediction methods relating to the prediction of structural responses of stiffened shell structures with or without attached components, subjected to broadband acoustic excitations. The methods under evaluation were the constant mass attenuation method and the impedance ratio method. Example problems were used to illustrate the application procedures of these two methods and to compare their predicted results with the experimentally measured data. It was found that more realistic estimates of the structural response can be obtained by the impedance ratio method.

I. K.Y. CHANG
G.C. KAO

II. WR 76-4

III. P.O. No. NAS8-31414

1. Mechanical Impedance
2. Acoustic Mobility
3. Blocked Pressure
4. Nomograms
5. Stiffened Shells
6. Test Criteria
7. Computation Techniques
8. Experiments

WR 76-4

DEVELOPMENT OF MODIFIED VIBRATION TEST CRITERIA FOR QUALIFYING SPACE VEHICLE COMPONENTS

K.Y. Chang and G.C. Kao
May 1976
Wyle Laboratories, Research Staff, Huntsville, Alabama

This report presents the results of the evaluation of two response prediction methods relating to the prediction of structural responses of stiffened shell structures with or without attached components, subjected to broadband acoustic excitations. The methods under evaluation were the constant mass attenuation method and the impedance ratio method. Example problems were used to illustrate the application procedures of these two methods and to compare their predicted results with the experimentally measured data. It was found that more realistic estimates of the structural response can be obtained by the impedance ratio method.

I. K.Y. CHANG
G.C. KAO

II. WR 76-4

III. P.O. No. NAS8-31414

1. Mechanical Impedance
2. Acoustic Mobility
3. Blocked Pressure
4. Nomograms
5. Stiffened Shells
6. Test Criteria
7. Computation Techniques
8. Experiments